UNIVERSIDADE FEDERAL DO CEARÁ

CENTRO DE TECNOLOGIA

DEPARTAMENTO DE ENGENHARIA QUÍMICA

PROGRAMA DE PÓS-GRADUAÇÃO EM ENGENHARIA QUÍMICA

ALIREZA BIK DELI

SEQUENTIONAL EXPLICIT AND IMPLICIT COUPLING OF 3D COMPOSITIONAL RESERVOIR, WELLS AND SURFACR FACILITY

FORTALEZA

2021

ALIREZA BIK DELI

SEQUENTIONAL EXPLICIT AND IMPLICIT COUPLING OF 3D COMPOSITIONAL RESERVOIR, WELLS AND SURFACR FACILITY

Tese apresentada ao Programa de Pós-Graduação em Engenharia Química da Universidade Federal do Ceará, como requisito parcial à obtenção do título de doutorado em Engenharia Química. Área de concentração: Processos Químicos e Bioquímicos.

Orientador:
Prof. Dr. Francisco Marcondes
Coorientador:
Prof. Dr. Kamy Sepehrnoori

FORTALEZA

2021

Dados Internacionais de Catalogação na Publicação
Universidade Federal do Ceará
Biblioteca Universitária
Gerada automaticamente pelo módulo Catalog, mediante os dados fornecidos pelo(a) autor(a)

B47s Bik Deli, Alireza.
Sequential Explicit and Implicit Coupling of 3D Compositional Reservoir, Wells and Surface Facility / Alireza Bik Deli. – 2021.
231 f. : il. color.

Tese (doutorado) – Universidade Federal do Ceará, Centro de Tecnologia, Programa de Pós-Graduação em Engenharia Química, Fortaleza, 2021.
Orientação: Prof. Dr. Francisco Marcondes.
Coorientação: Prof. Dr. Kamy Sepehrnoori.

1. Simulação Composicional de Reservatórios. 2. Tabelas de Fluxo. 3. Equipamento de Superfície. I. Título.
CDD 660

ALIREZA BIK DELI

SEQUENTIONAL EXPLICIT AND IMPLICIT COUPLING OF 3D COMPOSITIONAL RESERVOIR, WELLS AND SURFACR FACILITY

Thesis presented to the Graduate Program in Chemical Engineering of the Federal University of Ceará as a partial requirement for obtaining the Doctor of Philosophy degree in Chemical Engineering. Concentration area: Chemical Processes.

Aprovada em: 15/11/2021

BANCA EXAMINADORA

_____

Prof. Dr. Francisco Marcondes (Orientador)
Federal University of Ceará (UFC)

_____

Prof. Dr. Kamy Sepehrnoori (Coorientador)
University of Texas at Austin (UT)

_____

Prof. Dr. Sebastião Mardônio Pereira de Lucena
Federal University of Ceará (UFC)

_____

Prof. Dr. Denis José Schiozer
University of Campinas (UNICAMP)

_____

Prof. Dr. Luis Glauber Rodrigues
Federal University of Ceará (UFC)

_____

Dr. Daniel Nunes de Miranda Filho
PETROBRAS

Dedicated to Ahmad Saryar for all of the concerns that he had about me and my education at the most critical stage of my life.

Dedicated to Majid Dezfully, my high school calculus teacher, who died because of chemical weapons that were used in the Iran-Iraq war. He was the most dedicated man I have ever seen in my life. He was the first person who encouraged me by giving a mathematical modeling assignment about oil droplet, when realized I was interested in petroleum engineering. He died at age 63, while writing his master thesis. He never had a chance to accomplish his work. This Ph.D. thesis holds his name by wishing to put an end to his indefatigable efforts. Mr. Dezfully, I have made it, I never put down the flag of science as you requested.

Acknowledgments

I would like to firstly thank Allah for his blessing. I do strongly believe that the most important outcome of this Ph.D. thesis is the relationship that I found with God. I felt his existence in every single aspect of my life during my studies. I found Allah by knowing the people who joined and helped me on this journey. I was lost, I was alone and Allah guided me, even in those days that I did not call him.

Second, I want to express my great appreciation to my Ph.D. supervisor Prof. Dr. Francisco Marcondes. He is a mentor who taught and introduced me to the great world of computational science. I have learned too many wonderful lessons from my supervising professor. However, I do believe, the most important lesson was how a great father he is. I cannot mention the number of discussions that we had throughout the course of this work. I had a keen interest in research and a Ph.D. degree seemed like a golden opportunity, that Prof. Marcondes provided for me.

Third, I would like to sincerely express my acknowledgment to my co-supervising professor, Prof. Dr. Kamy Sepehrnoori, who gave me a chance and showed me his countless support and love. I would like to repeat what I said earlier in my Master's thesis; realizing him to be the best event of my life. It was only because of Prof. Sepehrnoori that I did not give up, both in my academic and personal life.

Fourth, I would like to thank Ivens Lima, for helping me with the enormous difficulties that I encountered in my studies. He is a brother that science gave to me. He taught me thousands of tips about working with the UTCOMPRS simulator and programming. He was there every single time that I needed help. Also, I would like to thank Matheus Barroso for helping me and for the discussions that we had while running, debugging, validating and modifying my codes.

Fifth, I would like to thank my mother, Shahla Sardari, for showing me her countless love during my research. A great portion of the burden of this work was on her shoulders. I deeply appreciate her love, support and understanding, without which this work could not have been accomplished.

Sixth, I like to thank the faculty members of the chemical engineering department of the Federal University of Ceará, as follows: Prof. Luciana for teaching me to be kind, Prof. Hosiberto for teaching me to think profoundly, Prof. Moises for teaching me to be humble, Prof. Diana for teaching me to be supportive, and Prof. Glauber for teaching me to be a hardworking researcher. Also, I want to thank Dr. Daniel Miranda, not only as a

member of my committee, but as a kind industrial mentor, who taught and suggested me lots of modifications and improvements to my work. Also, I'd like to express my gratitude to Dr. Sebastião Mardônio Pereira de Lucena and Dr. Denis José Schiozer, not only as members of my committee, but also as researchers who contributed to many aspects of simulation studies.

Seventh, I sincerely acknowledge the financial support of the ASTEF Foundation, Petrobras Company, and Prof. Sepehrnoori for the last year of my studies. Also, I would like to express my appreciation to the Center of Petroleum and Geosystems Engineering of The University of Texas at Austin for providing the UTCOMPRS simulator and thank ESSS for the license of the Kraken package as post-processor of UTCOMPRS. Additionally, I want to express my gratitude to Victor Salazar from CMG, for providing me with significant information about the CoFlow simulator and Builder.

Last but not least, I want to thank Prof. Mohammad Reza Rasaei, from the University of Tehran, Iran. He taught me in his fractured reservoir course why I needed to get a Ph.D. degree, by telling me the story of Madam Marie Curie and the persistence she had in science. It was such an inspiring story that it showed me that I have to dedicate myself to science.

A. R. Bigdeli (KJ)
Fortaleza – CE – Brazil
Summer 2021
During Covid-19 Pandemic

“Allah does not impose on any soul a responsibility beyond its capacity. Every soul receives whatever it gains and is liable for whatever it does”.

Quran - Surah Al Baqarah - 286

- A quote that my father used to read a lot.

RESUMO

Os sistemas de produção de petróleo consistem em três elementos individuais que operam conjuntamente: reservatório, poços e equipamentos de superfície. O projeto, a construção e a manutenção de instalações de superfície para produção de hidrocarbonetos requerem estudos de simulação. Esses estudos se tornam muito mais realistas quando as instalações de poço e superfície são simuladas junto com o reservatório.

O principal objetivo desta tese é desenvolver uma estrutura de cálculo que possa ser empregada para estimar o escoamento composicional multifásico/multicomponente do reservatório, poços e equipamentos de superfície usando tabelas de fluxo para avaliar a perda de pressão através de poços e tubulações. A estrutura de cálculo será acoplada ao simulador composicional multifásico/multicomponente da The University of Texas at Austin denominado UTCOMPRS.

Duas estruturas foram desenvolvidas para UTCOMPRS. O primeiro é o acoplamento explícito sequencial e o segundo é o acoplamento implícito sequencial. Dentre as abordagens para o cálculo da queda de pressão ao longo da tubulação, incluindo o modelo homogêneo, o modelo de deslocamento e uso tabela pré-calculada; o foco principal deste trabalho se dará no último método. Para o acoplamento explícito sequencial, três classes de tabelas de fluxo foram desenvolvidas e validadas com um simulador comercial, que trabalha em conjunto com as equações de balanço do reservatório, resolvidas através da formulação IMPEC (Implicit Pressure Explicit Composition). Além disso, algumas ferramentas adicionais para controlar e relatar os modelos integrados são descritas. Diferentes estudos de caso neste trabalho demonstraram vários cenários de produção na estrutura desenvolvida para modelos de reservatório 2D e 3D. A precisão da estrutura desenvolvida é altamente dependente da interpolação da pressão do fundo do poço e da ativação da restrição do injetor, entre outros parâmetros operacionais. Uma nova ferramenta chamada tabelas de conexão foi desenvolvida para acoplamento implícito sequencial. Esta tabela processa os dados, recursos e mapa do equipamento de superfície. Com tantas incógnitas quanto o usuário precisar, a tabela de conexão pode ser consistente. A explicação matemática da tabela de conexão também é dada para a condição de cada segmento, seja uma equação de fluxo ou uma tabela de fluxo. O simulador pode gerar a configuração do equipamento de superfície sem o uso de um simulador de terceiros, uma vez que a tabela de conexão é fornecida a ele.

Palavras-chave: Simulação Composicional de Reservatórios; Tabelas de Fluxo; Equipamento de Superfície.

ABSTRACT

Petroleum production systems consist of three integrated individual elements: subsurface reservoir, wells, and surface facility. The design, construction, and maintenance of surface facility for hydrocarbon production require simulation studies. These studies become much more realistic when well and surface facility are simulated together with the subsurface reservoir.

The main objective of this thesis is to develop a framework to model the compositional multiphase/multicomponent fluid flow from reservoir, wells, and surface facility using flow tables to evaluate the pressure loss through wells and pipes. The framework is integrated to the multiphase/multicomponent compositional reservoir simulator called UTCOMPRS from the University of Texas at Austin.

Two new frameworks have been developed for UTCOMPRS. The first is sequential explicit coupling and the second is sequential implicit coupling. Among three approaches for pressure drop calculation along the tubing, including the homogenous model, drift flux model, and a pre-calculated table; the main focus here is concentrated on the last method. For sequential explicit coupling, three classes of flow tables were developed and validated with a commercial simulator, which works in conjunction with the IMPEC (Implicit Pressure Explicit Composition) reservoir formulation. Also, some additional tools for controlling, and reporting the integrated models are described. Different case studies of this work demonstrated various production scenarios on the developed framework for 2D and 3D reservoirs. The accuracy of the developed framework is highly dependent on the interpolation of the bottom hole pressure and the injector constraint activation, among other operational parameters. A new tool called connection tables has been developed for sequential implicit coupling. This table processes the data, features, and map of the surface facility. With as many unknowns as the user requires, the connection table can be consistent. The mathematical explanation of the connection table is also given for each segment's condition, whether it be a flow equation or a flow table. The simulator can generate the surface facility configuration without the use of a third-party simulator once the connection table is supplied to it.

Keywords: Compositional Reservoir Simulation; Flow Tables; Surface Facility.

LIST OF FIGURES

Figure 1 – Different stages of a theoretical production profile of an oilfield. From (Höök et al.; 2009)..... 35

Figure 2 – An example of a self-learning reservoir management workflow that shows the importance of monitoring individual oil, gas, water rates, and bottom hole pressures as the controlling parameters. From (SAPUTELLI et al., 2010)..... 37

Figure 3 – An example of analysis flow in the network for PPS 38

Figure 4 – Application of Nodal Analysis for floating production storage and offloading (FPSO) unit..... 39

Figure 5 – PPS that works with a choke, flowline, and a separator 40

Figure 6 – Effect of choke valve size on the liquid rate production. From Schiozer and Aziz (SCHIOZER;AZIZ;1992)..... 40

Figure 7 – Example of PPS that is connected to separator directly..... 41

Figure 8 – Comparison of accuracy vs computation effort for three different mathematical formulations..... 45

Figure 9 – The surface facility model of Puchyr (PUCHYR; 1991)..... 46

Figure 10 – The surface facility model used by Biswas (2006) to investigate the sensitivity analysis..... 47

Figure 11 – The surface facility configuration of the Alexis' report 47

Figure 12 – Different time scales and elements of PPS. From (SANKARAN et al.; 2017)..... 50

Figure 13 – Different onshore and offshore reservoirs and the corresponding surface facilities equipment. From (YOUTUBE)..... 66

Figure 14 – An example of integrated surface and subsurface for the onshore reservoir. From (YOUTUBE)..... 67

Figure 15 – Different water cut values can change the operational point of surface facility model coupled with the subsurface model. From (ARSALAN et al.; 2003)…… 68

Figure 16 – Different water cut values can change the operational point of surface facility model coupled with the subsurface model. From (ARSALAN et al.; 2003) 68

Figure 17 – Results of the cumulative coal bed methane production for different surface facility layout. From (ZHOU et al.; 2017)……..... 69

Figure 18 – The conceptual diagram of connections and nodes that can be used for surface facility modeling. From (CAO et al.;2015)……... 70

Figure 19 – Mathematical discretization of a horizontal pipeline which considers 1) pressure and temperature unknowns at the nodes (upper figure), and 2) flow rates at each node (lower figure)……...……..... 71

Figure 20 – Example of a pipeline, where rates are calculated at nodes for a black oil formulation. From (GAO, 2014)…… 72

Figure 21 – Different calculated values of BHP value as a function of inhibitors injections based on compositional modeling. From (OLIVARES,2015)…… 74

Figure 22 – Surface facility pipeline and tubing with 23 segments and 24 connections spanning. From (OILVARES, 2015) ……..……... 75

Figure 23 – The conceptual schematic of the surface facility network as an extension of the reservoir grid blocks. From (WATTS et. al., 2010) …….. 76

Figure 24 – Example of SurfNetTM Software, from Nexus simulator package that the surface facility nodes are solved as an extension of the reservoir model (NEXUSE® MANUAL)……... 76

Figure 25 – A simple surface facility network consisted of two wellheads that are connected at the manifold and separator. From (SHIRALKAR et al.; 2005)……... 77

Figure 26 – Global Jacobian matrix and its four sub-categories. From (JING, 2017)….. 81

Figure 27 – Global Jacobian matrix and its nine sub-categories ……..……... 82

Figure 28 – Modifications for the global Jacobian matrix and its seven sub-categories. From (OLIVARES, 2015) ……..... 83

Figure 29 – A single well connected to a separator and wellhead…….. 84

Figure 30 – Impact of the choke valve on PPS, when it is fully open or 75% open. From (STANKO,2021)……. 88

Figure 31 – The use of ESP to achieve a required specific flow rate. From (STANKO, 2021)…… 89

Figure 32 – Conceptual schematic of the choke value and its relation with up and downstream pressures. From (ECONOMIDES et al. 2013)…..……. 90

Figure 33 – Flow rate through a choke versus the ratio of the upstream to the downstream pressure. From (JANSEN; 2017)…… 91

Figure 34 – Details of a producing well, the location of FTHP, chock valve, manifold and separator. From (JAHN et al., 1998) ……... 93

Figure 35 – Coupling configuration where the coupling point is at the wellhead level. From(BARROUX et al., 2000)…… 94

Figure 36 – Coupling configuration where the coupling point is at the bottom hole level. From (BARROUX et al., 2000)…… 94

Figure 37 – Different wellbore boundary conditions. From (SHIRDEL, 2013)…… 96

Figure 38 – Boundary condition of a horizontal well as an extended model of vertical wells. From (TRINA, JOHANSEN, 2012)……. 96

Figure 39 – Tubing pressure calculator software of the builder Simulator ……..……. 99

Figure 40 – Example of a pre-calculated table generated by Builder ……100

Figure 41 – Different levels of the flow calculation in wellbore and surface facility. From (BYER, 2000) ……... 101

Figure 42 – The network facility configuration and its corresponding connection data. From (SHIRALKAR et al., 2005) …….. 102

Figure 43 – Surface network consisted of seven connections that uses only three sets of flow tables. From (MONCORGE, 2011) ……... 103

Figure 44 – Tubing intake curve for varying production rates. From (JANSEN, 2017)……... 104

Figure 45 – The different situations of IPR and Flow Table solutions. From (CAO et al., 2015) ……..... 105

Figure 46 – : Original IPR and tubing curves with different scenarios. (ISLAMOV et al., 2020)……..……... 105

Figure 47 – Example of detected dynamic well operating envelope. From (ISLAMOV et al., 2020).……. 106

Figure 48 – Example of the normalizing method of the flow table by Tnavigator simulator (TNAVIGATOR MANUAL,2020)..... 107

Figure 49 – Elements and different parts of integrated models ……..... 110

Figure 50 – New feature in the well section of the input file of the UTCOMPRS simulator …… 111

Figure 51 – Three functions to read, compare and print the information that is in association with option number -5 ……. 112

Figure 52 – Additional input and output files that are requested and provided with option number -5.……..…..... 112

Figure 53 – Different locations of coupling points and their impact on reading, comparing and printing functions of option number -5. …… 113

Figure 54 – Conceptual and example of SFTs…… 114

Figure 55 – Algorithm that was designed for implementation of SFT inside the UTCOMPRS ……..…… 115

Figure 56 – AFT algorithm, used for both WHP and BHP as coupling points …… 118

Figure 57 – Conceptual shape of the CFTs generated by a commercial simulator …….. 120

Figure 58 – General algorithm of commercial flow tables for the UTCOMPRS Simulator ……... 122

Figure 59 – Example of a commercial flow table to clarify how the bottomhole pressure values are selected ……..…… 123

Figure 60 – General structure of the surface facility option for UTCOMPRS, with dashed lined arrows indicating the newly added features……..... 125

Figure 61 – General geometric visualization of dependent (Y) and independent (X) variables for two given values (up and down) and a linear interpolated point between them …..…… 125

Figure 62 – Hypothetical case at standard condition demonstrated by Stackel and Brown (STACKEL, BROWN, 1981). The solid line shows the linear approximation at between two sets of bottomhole values……..……..… 127

Figure 63 – The calculated bottomhole at nonstandard condition (higher water cut condition)……... 127

Figure 64 – Algorithm of the multiple-well working with the flow table ……. 129

Figure 65 – Example of 2D and 3D reservoirs and how the 2D calculation can be extended for 3D models ……. 130

Figure 66 – Examples of new keywords developed for the Flow Table option…….. 131

Figure 67 – Example of a well that works with wellhead and a separator……. 132

Figure 68 – Flow rate between two nodes through a connection…… 133

Figure 69 – Two ways of mapping surface facility: on the left, the mapping increasing along the flow trajectory; and, on the right, pressure nodes are numbered first, and then connections…….. 135

Figure 70 – Example of table connection……... 136

Figure 71 – General workflow of sequential implicit coupling of the reservoir, well and surface facility……. 137

Figure 72 – Production curve of oil and gas of the first case with 3 components……. 143

Figure 73 – BHP and GOR overtime for the first case study with 3 componentss…… 143

Figure 74 – Different pressure profiles for 3 components fluid……. 144

Figure 75 – Production curve of oil and gas of case two for 100 days…….. 145

Figure 76 – BHP and GOR behavior of case two with a slight BHP increase of 55.6 kPa 145

Figure 77 – Different pressure changes of of 6 components fluid …….. 146

Figure 78 – BHP as a function of different interpolation parameters: (a) water cut; (b) gas-liquid ratio; (c) liquid rate; (d) WHP average from lower and higher indices; (e) WHP from the higher index; (f) WHP from the lower index: (g) pressure of the injector…… 148

Figure 79 – Oil production for high (top) and low (down) wellhead pressure constraints 151

Figure 80 – Gas production for high (top) and low (down) wellhead pressure constraints 152

Figure 81 – Comparison of wellhead pressures for different scenarios of production….. 153

Figure 82 – Interpolated BHP for high (top) and low (down) wellhead pressure constraints……154

Figure 83 – Injection pressure for high (top) and low (down) wellhead pressure constraints……. 156

Figure 84 – GOR results for high (top) and low (down) wellhead pressure constraints. 156

Figure 85 – Pressure profile at 359 days; UTCOMPRS (left) and commercial simulator (right)…….. 157

Figure 86 – Pressure profile at 8.999 days; UTCOMPRS (left) and commercial simulator (right)……... 157

Figure 87 – Oil saturation field at 2.499 days; UTCOMPRS (left) and commercial simulator (right)……. 157

Figure 88 – Oil saturation field at 8.499 days; UTCOMPRS (left) and commercial simulator (right)……. 158

Figure 89 – Reservoir configuration used for Case 4……. 158

Figure 90 – Oil production for high (top) and low (down) gas injection rate…… 159

Figure 91 – Gas production for high (top) and low (down) gas injection rate…….. 160

Figure 92 – Interpolated BHP for high (top) and low (down) gas injection rates……. 161

Figure 93 – Injector pressure for high (top) and low (down) injection gas flowrates…… 162

Figure 94 – GOR for high (top) and low (down) gas injection scenarios……. 163

Figure 95 – 2D (left) and 3D (right) reservoir configuration for Case 5, with 80 ft of thickness……. 164

Figure 96 – Oil production for 3D (top) and 2D (down) reservoirs…….. 165

Figure 97 – Gas production for 3D (top) and 2D (down) reservoirs……. 166

Figure 98 – BHP for both producers in 3D (top) and 2D (down) reservoirs……. 167

Figure 99 – Injector pressure in 3D (top) and 2D (down) reservoirs…… 168

Figure 100 – GOR in 3D (top) and 2D (down) reservoirs……169

Figure 101 – 3D (top) and 2D (down) reservoir models used for Case 6……170

Figure 102 – Arrangement of producers and injectors for both 2D and 3D reservoirs…… 171

Figure 103 – Five well classes that exist for case 6……. 171

Figure 104 – Oil production profile for Well 2 for the 2D and 3D reservoirs……172

Figure 105 – Oil production profiles for Well 3 for the 2D and 3D reservoirs…… 173

Figure 106 – Oil production profile for Well 13 for the 2D and 3D reservoirs……174

Figure 107 – Gas production profiles for Well 2 for the 2D and 3D reservoirs…….. 175

Figure 108 – Gas production profiles for Well 3 for the 2D and 3D reservoirs……... 176

Figure 109 – Gas production profiles for well 13 for the 2D and 3D reservoirs……. 177

Figure 110 – BHP profiles for Well 2 for the 3D (top) and 2D (down) reservoirs…….. 178

Figure 111 – BHP profiles for well 3 for the in 3D (top) and 2D (down) reservoirs…… 179

Figure 112 – BHP profiles for well 13 for the 3D (top) and 2D (down) reservoirs…… 180

Figure 113 – Injection pressure profiles for well 1 for the 3D (top) and 2D (down) reservoirs……. 181

Figure 114 – Injection pressure profiles for well 11 for the 3D (top) and 2D (down) reservoirs…… 182

Figure 115 – GOR profiles for well 2 for the 3D (top) and 2D (down) reservoirs……..…. 183

Figure 116 – GOR profiles for Well 3 for the 3D (top) and 2D (down) reservoirs…….. 184

Figure 117 – GOR profiles for Well 13 for the 3D (top) and 2D (down) reservoirs…… 185

Figure 118 – Average reservoir pressure for low gas injection scenario of case 4 (top) and 3D reservoir of Case 6 (down)……. 186

Figure 119 – Oil production profile using different interpolation BHP functions..... 187

Figure 120 – Gas production profile using different interpolation BHP functions..... 188

Figure 121 – BHP profile as a function of WHP and GLR (top) and GLR and WHP (down)..... 189

Figure 122 – Injector pressure for two profile function of WHP and GLR (top) and GLR and WHP (down)..... 190

Figure 123 – GOR profile for two functions of WHP and GLR (top) and GLR and WHP (down)..... 191

Figure 124 – BHP profiles for different interpolation functions implemented in the UTCOMPRS and obtained with a commercial simulator..... 192

Figure 125 – Oil rate profiles obtained with different interpolation functions implemented in the UTCOMPRS and commercial simulator..... 193

Figure 126 – Gas rate profile for different interpolation functions implemented in the UTCOMPRS and commercial simulator..... 194

Figure 127 – : Injector pressure profile obtained with different interpolation functions implemented in the UTCOMPRS and commercial simulator..... 194

Figure 128 – GOR profile obtained with different interpolation functions implemented in the UTCOMPRS and commercial simulator..... 194

Figure 129 – CPU time of different interpolation functions implemented in the UTCOMPRS..... 195

Figure 130 – Comparison of the CPU run time obtained with the logarithmic interpolation function of the UTCOMPRS with the commercial simulator. 196

Figure 131 – Reservoir configuration used in Case 9..... 197

Figure 132 – BHP profile of the UTCOMPRS and commercial simulator for Case 9..... 198

Figure 133 – Water rate plots of the UTCOMPRS and commercial simulator for Case 9. 198

Figure 134 – Oil rate profile of the UTCOMPRS and commercial simulator for Case 9 ... 199

Figure 135 – Gas rate profile of the UTCOMPRS and commercial simulator for Case 9 199

Figure 136 – Injection pressure profile of the UTCOMPRS and commercial simulator for Case 9…….. 200

Figure 137 – GOR profile of the UTCOMPRS and commercial simulator for Case 9 ….. 200

Figure 138 – WOR profile of the UTCOMPRS and commercial simulator for Case 9….. 201

Figure 139 – Water cut profile of the UTCOMPRS and commercial simulator for Case 9 201

Figure 140 – The reservoir structure for case tenth..... 202

Figure 141 – Comparison of BHP's values for 11 points (top) and 20 points (down) between UTCOMPRS and commercial simulator ……..…….. 204

Figure 142 – Comparison of water rate profile for 11 points (top) and 20 points (down) tables between UTCOMPRS and commercial simulator..... 205

Figure 143 – Comparison of the oil rate profile for 11 points (top) and 20 points (down) between UTCOMPRS and commercial simulator 206

Figure 144 – Comparison of liquid rate profile for 11 points (top) and 20 points (down) between UTCOMPRS and commercial simulator……. 207

Figure 145 – Comparison of gas rate profile for 11 points (top) and 20 points (down) between UTCOMPRS and commercial simulator……. 208

Figure 146 – Comparison of injection pressure for 11 points (top) and 20 points (down) between UTCOMPRS and commercial simulator …… 209

Figure 147 – Comparison of GOR for 11 points (top) and 20 points (down) between UTCOMPRS and commercial simulator 210

Figure 148 – Comparison of WOR for 11 points (top) and 20 points (down) between UTCOMPRS and commercial simulator …….. 211

Figure 149 – Single well connected to wellhead and separator. From (WATTS et al, 2010) …….. 212

Figure 150 – Table connection example from Watts et al. (WATTS et al., 2009) ……. 213

Figure 151 – Single well pressure profile, with the reported results of Watts et al. compared to those of UTCOMPRS …….. 213

LIST OF TABLES

Table 1 – List of commercial software packages and corresponding vendors, which can handle integrated models..... 53

Table 2 – Different method of pressure calculation and type of modeling. From (WANG, 2019)..... 71

Table 3 – Effect of different separator pressure on the rates and the manifold pressure …….. 87

Table 4 – Different correlations proposed for the choke performance relationships ……..... 91

Table 5 – Different types of selectable pressure-gradient prediction methods. From (BUILDER MANUAL, 2019)…… 98

Table 6 – Example of a simple output file of surface facility that work with SFTs 116

Table 7 – Conceptual schematic of the AFT (Top) and an example of an AFT (down) that consists of two distinguished sections, one for single-phase gas (yellow section) and one for multiphase (green section)……..…….. 117

Table 8 – Example of extended format of the output file for AFT ……..... 120

Table 9 – Example of the final output file of the UTCOMPRS simulator which works with CFTs…….……... 123

Table 10 – New keywords developed for Surface facility option of the UTCOMPRS simulator ……..... 131

Table 11 – Different conditions and explanation of connection table…….. 136

Table 12 – Reservoir information……...…….. 141

Table 13 – Reservoir and injection fluid composition (3 components) for first case study ……...…… 141

Table 14 – Reservoir and injection fluid composition (6 components) for first case study..... 142

Table 15 – Technical information of wellbore section…… 142

Table 16 – Technical information of surface facility section..... 142

Table 17 – Different independent variables for interpolation functions to calculate the BHP. ……..……... 146

Table 18 – Wellbore properties and operational conditions to generate corresponding flow table …… 147

Table 19 – The reservoir details, hydrocarbon components and injection fluid for Case 3, for assessment of wellhead pressure effects…….…….. 150

Table 20 – Modifications for the fifth case study. …….……... 164

Table 21 – Number and size of the 2D and 3D models of Case 6 …….. 169

Table 22 – The reservoir details, hydrocarbon components and injection fluid for Case 9 ……. 196

Table 23 – The 11 points table and its information ……... 203

Table 24 – The 20 points table and its information……... 203

LIST OF ABBREVIATIONS

AFT	Advanced Flow Table
CFT	Commercial Flow Tables
BHP	Bottomhole Pressure
FBHP	Flowing Bottomhole Pressure
FTHP	Flowing Tubing Head Pressure
FPSO	Floating Production Storage and Offloading
IMPEC	Implicit Pressure Explicit Composition
IPR	Inflow Performance Relationship
GOR	Gas-Oil Ratio
GLR	Gas-liquid Ratio
PPS	Petroleum Production System
PSEP	Pressure of Separator
SFT	Simplified Flow Tables
STOIIP	Stock Tank Original Oil In Place
WCUT	Water cut
WI	Well Index
WHP	Wellhead Pressure (or WHP: Pressure of Wellhead)

SYMBOLS LIST

a	Equation of state Parameter
A	Area
b	Equation of state parameter
C_f	Rock compressibility
D	Depth
f_{ij}	Fugacity
g	Gravity
k_{rj}	Phase relative permeability
$\vec{\vec{k}}$	Formation absolute permeability tensor
Mw	Molar weight
n_p	Number of fluid phases
n_c	Number of hydrocarbon components
N_i	Number of moles
P	Pressure
P_c	Capillary Pressure
q_i	Component molar flow rate
Q_j	Phase volumetric flow rate
R	Universal Gas constant
S_j	Phase Saturation
T	Temperature
$\vec{u}$	Phase velocity
V_p	Pore Volume
V_t	Total fluid volume

WI	Well index
x_{ij}	Component phase molar fraction
Z	Compressibility Factor
ρ	Phase mass density
ξ_j	Phase molar density
μ_j	Phase viscosity
λ_{rj}	Phase mobility
ϕ	Porosity
Φ_j	Phase hydraulic potential
v	Molar volume
ω	Acentric factor

SUMMERY

CHAPTER 1 ..... **29**

INTRODUCTION **29**

1.1 Problem description **29**

1.2 Research objectives **30**

1.2.1 Main objective **30**

1.2.2 Specific objectives **31**

1.3 Review of chapters **31**

CHAPTER 2 ..... **33**

BACKGROUND AND LITERATURE REVIEW **33**

2.1 Different reservoir drives **33**

2.2 The field life cycle **35**

2.3 Nodal analysis of petroleum production systems **37**

2.4 The background and literature survey of integrated models **42**

2.5 Different types of coupling **44**

2.6 Integrated models for gas reservoirs **45**

2.7 Difficulties of development of integrated models **48**

2.8 Available commercial simulators **52**

CHAPTER 3 ..... **54**

RESERVOIR ENVIRONMENT AND FLUID FLOW IN POROUS MEDIA **54**

3.1 The background and basic assumptions of the reservoir **54**

3.2 Physical model **55**

3.2.1 Mass conservation equation **55**

3.2.2 Pressure equation **57**

3.2.3 Constraint equations **58**

3.2.4 Phase behavior **59**

3.2.5 Physical properties **61**

3.2.5.1 Viscosity **61**

3.2.5.2 Density **62**

3.2.5.3 Saturation **62**

3.2.5.4 Relative permeability **63**

3.2.6 Well model **64**

CHAPTER 4 ..... **66**
SURFACE FACILITY ENVIRONMENT AND FLUID FLOW IN PROCESSING EQUIPMENT **66**
4.1 Production operations and day-to-day maintenance **66**
4.2 The criticality of surface facility equipment **67**
4.3 Separator conditions **68**
4.4 Surface facility layout **69**
4.5 Connection-based or node-based formulations **69**
4.6 Surface facility formulation **70**
4.6.1 Momentum conservation equation **70**
4.6.2 Mass conservation equation **71**
4.6.3 Primary variables and method of solving surface facility models **79**
4.7 Restrictions on flow devices through choke valves **88**
CHAPTER 5 ..... **92**
WELLBORE ENVIRONMENT AND FLUID FLOW IN TUBING **92**
5.1 Dynamic wellbore behavior **92**
5.2 Coupling configuration **93**
5.3 Gauss elimination method for a coupled linear system **95**
5.4 Wellbore boundary conditions **95**
5.5 Type of wellbore treatment **96**
5.6 The background of the flow tables **97**
5.6.1 Types of flow tables **100**
5.7 Order dependence of the flow calculation in wellbore and surface facility .. **101**
5.8 U-shape curve problem and its solution **103**
5.8.1 Dynamic well operating envelope **105**
5.8.2 Normalize values of flow table **106**
5.8.3 The safe operational zone **107**
5.9 Derivatives from flow tables **108**
CHAPTER 6 ..... **110**
NEWLY DEVELOPED FRAMEWORK FOR UTCOMPRS SIMULATOR **110**
6.1 Sequential explicit coupling of the reservoir, well and surface facility **111**
6.1.1 Reading, comparing and reporting functions **111**

6.1.2 ***Different types of flow table*** **113**
6.1.2.1 Simplified flow tables (SFTs) **113**
6.1.2.2 Advanced flow tables (AFTs) **116**
6.1.2.3 Commercial flow tables (CFTs) **120**
6.1.3 ***Advanced well control option (AWCO)*** **124**
6.1.4 ***Different interpolation functions*** **125**
6.1.5 ***Multiple wells and 3D models modifications for CFT*** **128**
6.2 Sequential implicit coupling of the reservoir, well and surface facility 132
6.2.1 ***Part One: Map of surface facility*** **132**
6.2.2 ***Table connections*** **134**
6.2.3 ***General workflow of sequential implicit formulation*** **136**
6.2.4 ***Part Two: Extension of fully implicit formulation*** **137**
CHAPTER 7 ..... **141**
DESCRIPTION, RESULTS AND ANALYSIS OF SIMULATION MODELS **141**
7.1 Explicit coupling of the reservoir, well and surface facility 141
7.1.1 ***Case 1 – AFT – Effect of reservoir fluids*** **141**
7.1.2 ***Case 2 – CFT – Interpolation functions*** **146**
7.1.3 ***Case 3 – CFT - Effect of wellhead pressure*** **149**
7.1.4 ***Case 4 – CFT - Effect of injection rate*** **158**
7.1.5 ***Case 5 – CFT - Simple multi-well study*** **163**
7.1.6 ***Case 6 – CFT- 23 wells for 2D and 3D reservoir*** **169**
7.1.7 ***Case 7 – CFT-Multivariable interpolation functions*** **186**
7.1.8 ***Case 8 – CFT-Different interpolation functions*** **191**
7.1.9 ***Case 9 – CFT-Pseudo-component case.*** **196**
7.1.10 ***Case 10 – CFT- Five-spot case with water variation*** **202**
7.2 Sequential implicit coupling of the reservoir, well and surface facility **212**
CHAPTER 8 ..... **215**
CONCLUSIONS AND RECOMMENDATIONS **215**
8.1 Conclusions **215**
8.2 Recommendations **216**
REFERENCES **217**

Appendix One – MATLAB file for IMEX tubing tables generation..... **226**

Appendix Two – Phase Envelopes..... **229**

Appendix Three - An example of flow table for Case 3..... **231**

CHAPTER 1

INTRODUCTION

By increasing global energy demand, conventional hydrocarbon resources are still the main source of energy for industry and transportation. While production from unconventional reservoirs has become a game-changing factor in the economics of oil and gas industries, this technology faces restrictions on global deployment. In December 2014, in its famous article Sheikhs vs shale, the Economist (**Economist; 2014**) reported that by decreasing the cost of a typical unconventional project from $70 per produced barrel to $57, those countries whose budgets depend on high oil prices are in particular trouble. Consequently, efficient management and continued production from conventional hydrocarbon reservoirs are determining factors; for the economy of both oil-producing and consuming countries. In reality, the continued production of hydrocarbon resources is extremely dependent on the ultimate recovery factor and technology development.

The recovery factor of oil and gas is the overall amount expected to be produced form the reservoir. In general, there are three techniques for estimating the recovery factor: (i) field analogs, (ii) analytical models (displacement calculation or material balance), and (iii) reservoir simulation. Three production stages identified as primary, secondary, and tertiary may occur during the life of a hydrocarbon reservoir. In the earlier production stage of petroleum reservoirs, the available information is limited to those acquired during exploration, drilling, seismic operations, well logging, and initial reservoir simulation models. In the next stages, reservoir simulation studies only are not sufficient and need to include the development and construction of surface facility equipment. It is essential to have simulators that enable the handling of the interactions of both subsurface and surface facility simultaneously, which is the main objective of this study. Therefore, since production fluids and required facility depend on reservoir characterization, before any simulator model is developed, it is required to be aware of the different stages and the status of production operations.

Considering the complex relationship between engineering design factors, the layout and configuration of surface equipment, such as tubing diameter, length of seafloor flowlines and risers, depend on the reservoir drives and operating conditions, e.g., deep offshore reservoir. Fluid characterization tools, such as pressure gradient evaluation, in-situ fluid sampling, downhole sampling for PVT measurements, drill stem tests and open-

hole logs are different measurement techniques for reservoir fluid evaluation (**CANAS *et al.*; 2008**). Hence, it is important to have a tool, such as an integrated simulator for modeling flow through both the porous media and the production pipeline network.

1.1. Problem description

From a numerical point of view, the development of integrated models for simulating both subsurface and surface conditions is challenging. The number of associated variables, operational conditions, different production scenarios, different time scale windows, different types of fluid flows, uncertainties of physical properties of porous media and complex phase behavior of hydrocarbon mixtures are examples of why numerical development of such integrated models is a difficult task. However, an accurate production forecast for a project highly depends on the simulation packages that enable the coupling of a subsurface reservoir, wells and production facility.

Reliable interactions between reservoir and production surface facility are often performed by individual software, without considering mutual interactions between the two different environments. As a result, the accurate understanding of deliverability, forecasting the operational conditions and field development difficulties depend on integrated modeling. Instability, oscillations and material balance errors are some examples that heavily depend on the type of coupling between the two models. The UTCOMPRS is a compositional simulator, which has been developed at The University of Texas at Austin, for different EOR applications. However, the simulator has been developed only for porous media environments. Adding the surface facility models to UTCOMPRS, the simulator can be used as a tool for understanding the behavior of petroleum production systems, while identifying the main factors that affect production operations. Hence, in this work, an integrated production system model is proposed by considering both sequential explicit and sequential implicit formulations for the UTCOMPRS simulator.

1.2. Research objectives

1.2.1 Main objective:

The main objective of this thesis is to develop a framework to model the compositional fluid flow from reservoir, wells, and surface facility using flow tables to evaluate the pressure loss through wells and pipes.

1.2.2. Specific objectives

The following are the specific objectives of this dissertation.

1- To develop a new capability for the simulator to receive the information and models of the surface facility for both sequential explicit and implicit approaches;

2- To couple the new developed framework to the UTCOMPRS from the University of Texas at Austin that is a multicomponent/multiphase compositional reservoir simulator;

3- To evaluate the head loss through the wells and pipes using pre-calculated flow tables in conjunction with well restrictions.

1.3. Review of chapters

The remaining chapters of this dissertation are structured as follows.

The second chapter will explain some essential background and topics associated with the objectives of this work and provide the literature review for the development of integrated models. The third chapter will discuss the fundamental equations for the compositional reservoir simulation. The original formulation here was implemented as a set of partial differential equations for fluid flow in porous media under isothermal, multicomponent and multiphase flow conditions. The fourth chapter will explain the fundamentals and provide the background of surface facility equipment and equations for the simulation. The original surface facility formulation is explained as three sets of partial differential equations for fluid flow in processing equipment. The main focus here is to develop a surface model which works with hydraulic relationships and treats the processing units as an extension of the reservoir grid blocks. The fifth chapter will explain the fundamentals and background of wellbore hydraulics and equations for the simulation as a linking connection between the surface and sub-surface systems. Although the approaches of a homogenous model, a drift flux model and a pre-calculated table are discussed, the main focus is on the last method. In this context, regardless of the shape of the table, we refer to the pre-calculated tables as flow tables. The sixth chapter will explain the framework for the two developments for UTCOMPRS. The first is sequential explicit coupling, while the second is sequential implicit coupling. For sequential explicit coupling, three classes of flow tables are developed which are working in conjunction with an IMPEC reservoir formulation. Also, some additional tools for controlling and reporting the integrated models are described.

For sequential implicit coupling, a new tool named connection tables is developed, holding the information, details and map for the structured surface facility. Once the connection table is fed to the simulator, it can generate the surface facility configuration without the need for any third-party simulator. The connection table can be consistent with as many unknowns as the user requires. The condition of each segment, whether it needs to be a flow equation or a flow table, is also explained. Next, the process of adding the wellbore equations into the fully implicit formulation of the UTCOMPRS simulator is detailed. Chapter seven shows the validation and different simulation results from the developed numerical packages. In chapter eight, the conclusions from the simulated results are presented and some suggestions for the improvement for future works are provided.

CHAPTER 2

BACKGROUND AND LITERATURE REVIEW

2.1. Different reservoir drives

Petroleum reservoirs are geological systems in which hydrocarbon fluids are accumulated. From the petrophysical point of view, there are three essential sub-systems: source rocks, reservoir rocks and cap rocks, which generate, transfer and accumulate the hydrocarbons fluids, respectively. To manage the profitability of a hydrocarbon reservoir, it is important to know how hydrocarbon fluids are being produced and what physics and mechanisms are involved during the harvest of these natural resources. During the production stage of a reservoir, pressure decline analysis should be carried out and monitored carefully, due to the withdrawal of hydrocarbon fluids. In porous media, reservoir drives are the main driving forces for the transport of reservoir fluids. Compactions, wellbore instability, asphaltene, wax, hydrate precipitations, stable emulsions and surface facility damage due to blockages, erosion and corrosions are examples of failures that may occur if pressure decline is not properly understood (**STANKO; 2021**). Additionally, as noted by Ahamad (**AHMAD; 2010**), reservoir drives have different behavior in terms of ultimate recovery factor, pressure decline rate, gas-oil ratio (GOR) and water production. Thus, the reservoir performance forecast, additional development plans and simulation studies are tied with the characteristics of reservoir drives. Next a quick review of the different reservoir drives is presented.

2.1.1 Water drive reservoirs

Water drive is an important reservoir mechanism. In general, hydrocarbons fluids are associated with saline waters (or aquifers). Due to the volume of the aquifer, and values of permeability, especially in the horizontal direction, water can flow and displace the oil bank The pressure decline, in this case, is satisfied by the movement of water and replacing the voidage that is the result of production from the bank of oil. The typical recovery factor of these reservoirs varies from 30% to 70% of STOIIP (stock tank original oil in place). From an operational point of view, in the oil field, obtaining the information of permeability and understanding how the compressibility of water is acting are difficult tasks to be performed, because of the location of drilled wells that are mainly in the column of the oil phase. Hence, the information on the aquifer portion is often not available. Besides, the water-oil and gas-oil contact detection and displacement are additional difficulties that exist in the production of the reservoirs driven by water influx.

From the surface facility design point of view, it is important to note that in the water drive reservoir, the values of water cut (amount of produced water over total produced liquid) can often reach 90%. As a consequence, the reservoir drive can have a significant impact on the type of required surface facility, their design, optimization and location on the ground or in a floating production unit.

2.1.2 Solution gas drive

The solution gas drive represents a significant production mechanism. For this type of drive, the compressibility factor of the oil phase and the amount of dissolved gas in the oil phase are important parameters. In other words, oil compressibility is the dominant energy drive for the production of the fluids from this type of reservoir. Once the production from the reservoir begins, the solution gas will be released from the oil due to the decline of reservoir pressure. The range of recovery factor of these reservoirs is 5-30%. During the production of these classes of reservoirs, it is common that the values of GOR increase remarkably until the reservoir pressure is unable to sustain production. Also, by increasing the GOR value, part of the released gas is produced at the surface. Accordingly, the shape of the GOR curve has a maximum value. This behavior and the maximum amount of GOR values should be considered in surface facility design. Performing accurate phase behavior studies is a prerequisite of production from this type of reservoir.

2.1.3. Gas cap drive

The third important mechanism is the gas cap drive. In this mechanism, the available initial gas in the upper section of the reservoir is essential. The magnitude of pressure decline is lower in the gas cap drive reservoir. Also, the value of GOR increases during production. The recovery factor of gas cap reservoirs is about 20% to 50%. Since the value of produced gas in these types of reservoirs is high, the surface facility equipment should be able to receive a high volume of the produced gas.

2.1.4. Rock Compaction

The fourth type of drive that may exist is the expansion of the rock due to withdrawal of the fluids. Although this mechanism might not be as powerful as water drive reservoirs, it is still capable of causing displacement of porous media, compaction, and surface subsidence, as well as wellbore instability. From reservoir engineering point

of view, during the integrated model development for such reservoirs, the geomechanics and geotechnical aspect of deformable rocks should be addressed. Also, the design of the required surface facility for this type of reservoirs is sometimes more complex and expensive. Moreover, the fluids contact movement tracking is necessary for this mechanism. And surveillance equipment should be considered in surface facility design. Ultimately, it takes magnificent computational efforts to build a simulator that can handle a deformable reservoir that is connected to surface facility equipment.

2.2 The field life cycle

The different stages of an oilfield should be determined and evaluated precisely. Various activities should be carried out for field development and they are under six categories, including gaining access, exploration, appraisal, development, production, and decommissioning. Pressure response to the production, which is mainly due to fluid displacement, should be monitored as the main operational parameter over the field life cycle. Because of the risks involved in full-field implementation, a pilot test is performed to assess the technical and economic viability of the projects. Where to apply the pilot? How long it should run? How to design? What data should be collected? These are some examples of questions that pressure response to production can clarify. Hence, pressure profile evaluation plays a dominant role in the development of surface facility simulators. Evaluation of the number of the wells is another influential parameter that impacts the field life cycle, because the dynamic interaction of the reservoir and wells, is what specify the scope of the surface facility equipment and the cost of the development. Fig 1. shows the theoretical production profile of an oilfield during its life cycle.

Figure 1- Different stages of a theoretical production profile of an oilfield. From (**Höök *et al.*; 2009**).

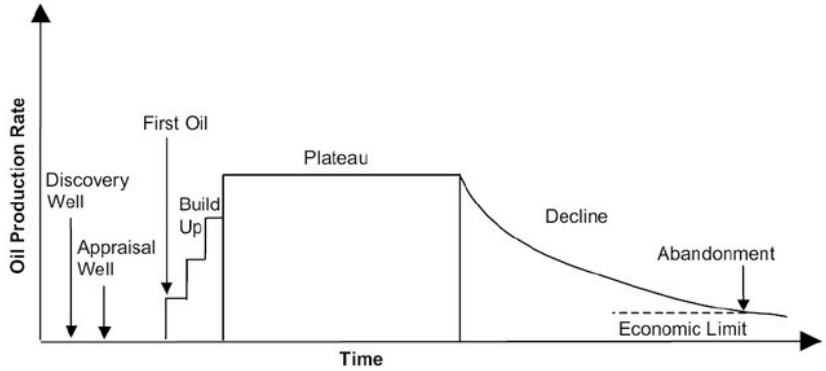

The number of the production wells can be obtained by the following equation:

$$\text{Number of the producing wells} = \frac{\text{Plateau production rate}}{\text{Stabilized production rate}} \quad (2.1)$$

where stabilized production rate is the rate achieved during the exploration and appraisal phase. Different subsurface development plans can lead to different surface development plans and the final economic evaluation of the project can be assessed. Hence, it is important to know how to integrate and test the reservoir and surface facility (**KALAYDJIAN; BOURBIAUX; 2002**). Integrated reservoir management can be considered as the continuous process of measurement, analysis, decision and action (**BRAVO** *et al.***, 2014**). Aside from evaluation of production profiles, reservoir management should assess five domains during the field life cycle:

- well design and management;
- reservoir characterization;
- reservoir modeling;
- surface facility design;
- economics

All the above domain depends on the accuracy of the coupled reservoir, well and surface facility simulators. Commercial and environmental constraints, advanced well technology, artificial intelligence and data science are some technological developments that can accelerate the performance of coupled models.

Due to the number of variables and uncertainties, oil and gas industries require surveillance and monitoring technologies. Well testing and well-model updating are two common practices in which the oil, gas and water rates, as well as inlet pressure (for surface facility) are kept monitored and updated to achieve the most accurate history match analysis. Fluid flow transfer is taking place at different time scales; therefore, optimization should be carried out with respect to short-term reservoir response, model-predictive control for constraints, and long-term reservoir performance for economic purposes (**SAPUTELLI** *et al.,* **2010**). An example of a self-learning reservoir management workflow is presented in Fig 2. For such a system, the objective function can be defined as a function of well and separator, where for separator-function, the oil rate and for well-function, the flowing tubing head pressure, oil rate, and chock pressure can be considered. More mathematical details about a self-learning reservoir management workflow can be found in (**SAPUTELLI** *et al.,* **2010**).

Figure 2. An example of a self-learning reservoir management workflow that shows the importance of monitoring individual oil, gas, water rates, and bottom hole pressures as the controlling parameters. From (**SAPUTELLI** et al.**, 2010**).

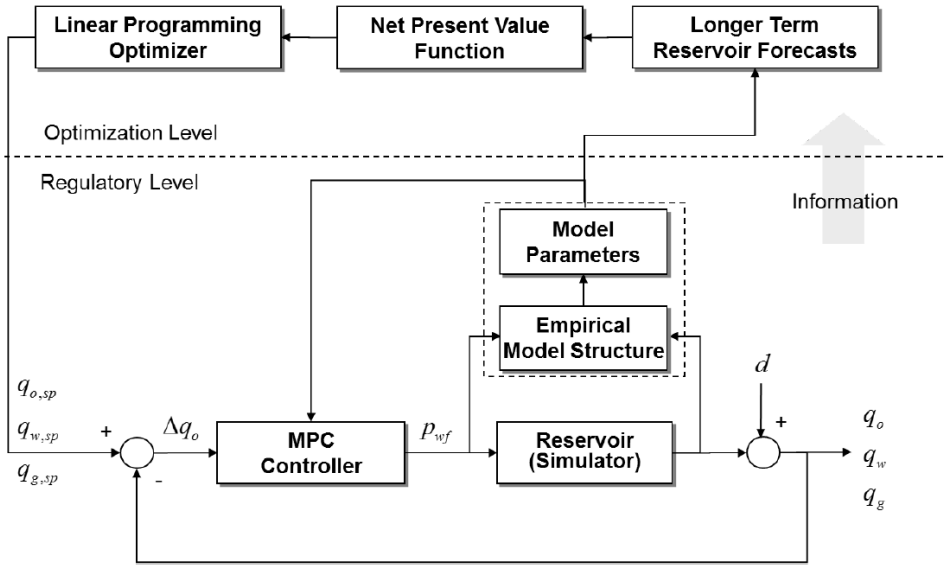

2.3. Nodal analysis of petroleum production systems

Based on what has been discussed above, it is necessary first to define a type of analysis to address the elements of the petroleum production system individually and then dependently. In this context, Petroleum Production Systems (or PPS) are referred to as the systems consisting of the reservoir, wells and surface facility equipment. Another concept which is important for integrated modeling of PPS is the coupling point. According to the nodal analysis of PPS, each section of the PPS model can be treated as a node of pressure and flow rate. Hence, the coupling point refers to the point in which the total PPS is divided into two sub-systems for analysis of the inflow and outflow performance of hydrocarbon fluids. As reported by Agbi (**AGBI**; 1981), the concept of flow analysis in the network has been applied in civil engineering literature for water distribution systems and electrical engineering literature for electrical networks.

Nodal analysis is a trademark of Schlumberger company that has been introduced in the work of Gilbert (**GILBERT;** 1954), later became popular by the work of Brown (**BROWN**;1984). There are six objectives for the nodal analysis reported by Brown:

1- To determine the flow rate at which an existing oil or gas well will produce considering wellbore geometry and completion limitations.

2- To determine under which flow conditions (which may be related to time) a well will load or die.
3- To select the most economical time for the installation of artificial lift and to assist in the selection of the optimum lift method.
4- To optimize the system to produce the objective flow rate most economically.
5- To check each component in the optimized system to determine whether it is restricting the flow rate unnecessarily.
6- To permit quick recognition by the operator's management and engineering staff of ways to increase production rates.

Nodal analysis can be done at any location of the integrated model, but generally, there are three preferred locations for coupling point (**PIPESIM Manual**; 2017): a) bottom hole, b) wellhead, and c) riser based (for offshore systems). Fig. 3 shows a general schematic of the main idea that exists behind the nodal analysis of PPS. According to this logic, the fluid flow begins from the node where has the highest potential. For PPS, the driving force is pressure. Hence, the direction of fluid flow is from the reservoir, passing through the bottom of a producing well and finally reaching the wellhead at the surface. Once the fluids pass through the wellhead, they are transferred to the separation facility.

Figure 3 - An example of analysis flow in the network for PPS.

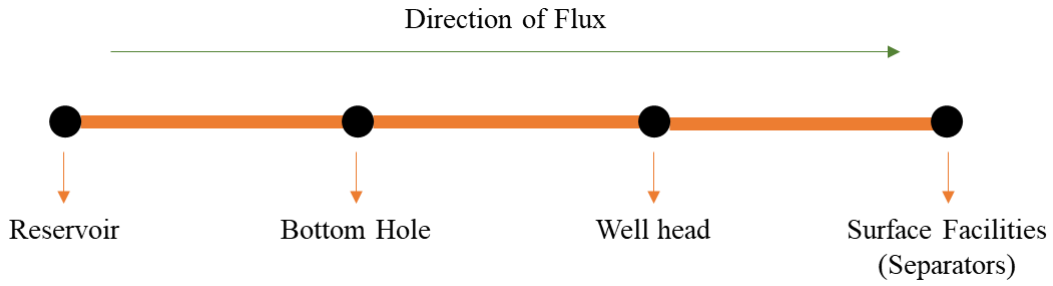

Fig. 4 illustrates an example of floating production storage and offloading (FPSO) unit, which is a common type of production unit in Brazil. After the fluids reach a subsea wellhead, they will be transferred to a seafloor flowline and then to a riser until they reach the floating production unit. This example can be converted into simplified PPS by Nodal Analysis where the inlet pressure, the pressure at FPSO unit, is known (green point) and the rest of the locations and nodal points are unknown.

Figure 4 - Application of Nodal Analysis for floating production storage and offloading (FPSO) unit.

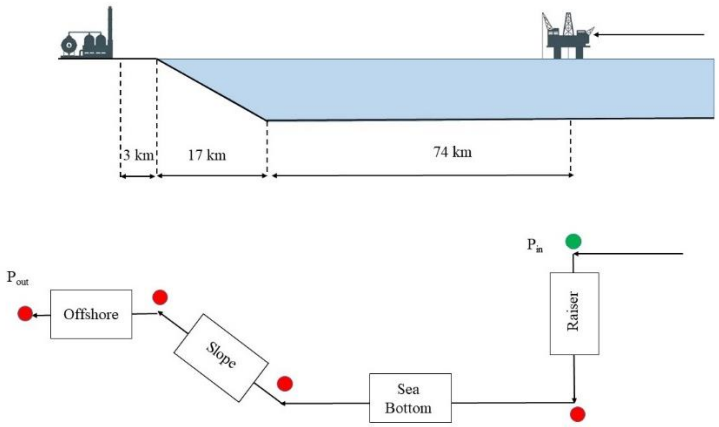

The degree of resolution of the Nodal Analysis, or how many nodes are required for a given system, varies for each project. For example, a wellbore that has lots of sub-surface equipment is a case where details of the producing well are highly required. However, from the numerical modeling point of view, designing such a complex and well-defined well requires a significant effort. One example of a simulator that can simulate the wellbore with a high degree of resolution is the VFP designer^{TM} from the Tnavigator simulator (**ROCK FLOW DYNAMICS; 2020**). VFP designer is capable of modeling thirteen types of options inside the well, such as gas lift valves, sub-critical valves, Autonomous inflow control device (AICD), spiral inflow control devices (SICD) etc. However, this level of detail is beyond the scope of this dissertation. According to Fig. 5 five nodal points are presented as follows: (1) reservoir pressure, (2) bottom hole pressure, (3) wellhead pressure, (4) (choke) downstream pressure and (5) separator pressure.

Figure 5 - PPS that works with a choke, flowline, and a separator.

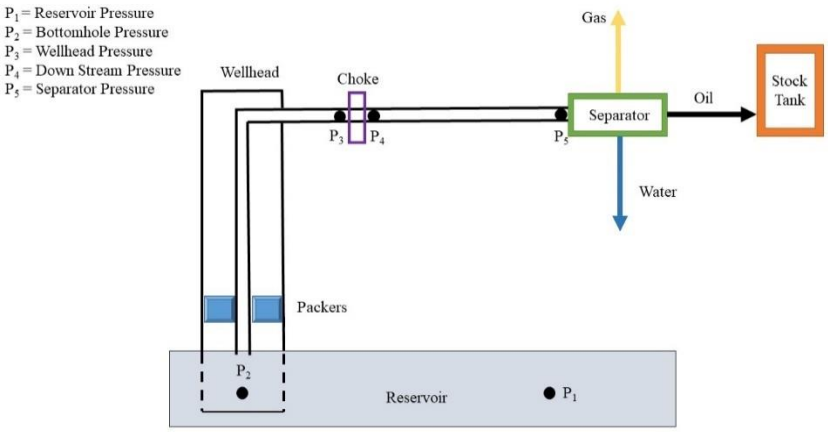

The choke valve is a mechanical device that can control the rate of production fluids on the surface. In general, the downstream can not receive the full potential of the reservoir hydrocarbon flow due to operational capacities and required day-to-day plans. Hence, the choke valves are used to restrain production. By using a choke device, the production profile inside the pipeline will be independent of the upstream points. This information is important for one who wants to developt different surface facility equipment. This issue will be discussed in more detail in Chapter 3. The existence of the choke in the integrated model can also change the production profiles remarkably. For example, Schiozer and Aziz (**SCHIOZER; AZIZ**; 1992) reported the effects of different choke sizes on the liquid rate. Fig.6 shows the effect of different choke valve sizes on the liquid rate production.

Figure 6 - Effect of choke valve size on the liquid rate production.
From Schiozer and Aziz (**SCHIOZER; AZIZ; 1992**).

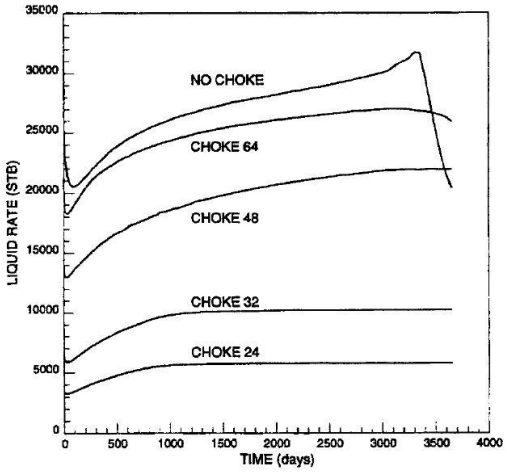

However, one can also neglect the choke device if the separator is capable of receiving all of the production fluid. This way, the wellhead is connected to the separator, interacting directly. (**BIGDELI** et al., **2019**) reported an example of such an integrated model without considering the choke valve. For the same integrated model, different types of fluids (3 and 6 components) showed different behavior for pressures at the wellhead and separator.

The last and simplest type of surface facility consideration is without the surface pipeline and choke valves. In this case, all of the produced fluids enter the separator units immediately from the wellhead. Fig. 7 shows a system that does not have the flow line and choke valves.

Figure 7 - Example of PPS that is connected to separator directly.

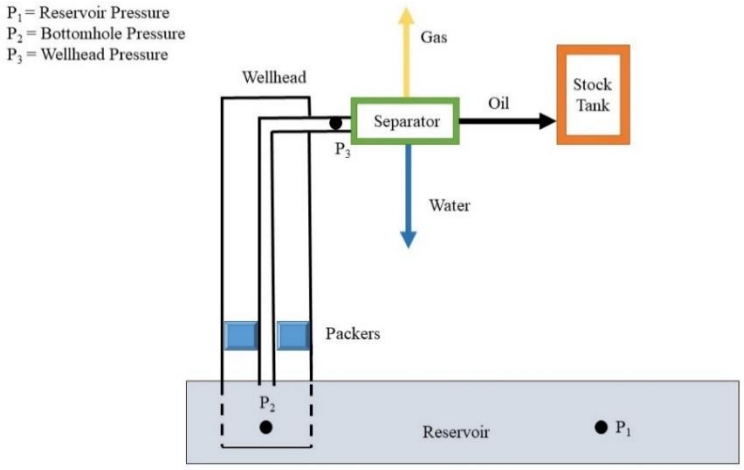

As can be seen from Fig. 7, the wellhead pressure (P_3) is equal to the inlet pressure of the separator. Regarding this notation, Brill and Mukherjee (**BRILL; MUKHERJEE; 1999**) noted two important assumptions:

1) In the absence of the flow line, the pressure of the separator can be equal to the wellhead pressure;
2) The separator or wellhead pressures are normally known and can be used as input values for determining the unknown pressures.

The above two assumptions are rather important. We will use these two assumptions throughout the course of this thesis. The nodal analysis concept present various technical difficulties. A reliable nodal analysis description is an essential step for accurate modeling of the integrated models. Associated physics and fluid flow mechanisms can be intensely

affected as nodal analysis of the integrated model changes. Hence, the experiences of using nodal analysis should be strongly considered. Additional information, more advanced and complex nodal analysis of PPS, as well as their MATLAB codes, can be found in Jansen's textbook (**JANSEN; 2017**).

Various numerical strategies tried to tackle integrated simulation of sub-surface and surface models. Next, a literature survey of previous studies is presented.

2.4. The background and literature survey of integrated models

During the 1970s, in the earlier stages of development of integrated models, single-phase flow such as network facility of water distribution and steady-state natural gas distribution systems were developed without considering reservoir or wellbore sections (**SHAMIR** *et al.*; **WYLIE** *et al.* 1971). The work presented by Dempsey *et al.* (**DEMPSEY** *et al.*1971) is one of the earlier works that addressed the element of PPS. They considered reservoir, tubing and surface pipeline for single-phase (gas) and two-phase (gas and water) systems. Following that, Emanuel and Ranney (**EMANUEL; RANNEY**; 1981) introduced a new approach for coupling surface and subsurface facility by using tubing flow tables. Flow tables are typical tables that hold information and interactions of the bottom hole and wellhead of wells. These tables can be used not only for tubing but also for surface facility (**ROSSI** *et al.*; 2017). Breaux et al. (**BREAUX** *et al.*; 1985) extended the framework of Emanuel and Ranney (1981) for multiple wells. Their framework determined total system potential, the number of drilled wells required, location of drilled wells, network constraints etc. Schiozer (**SCHIOZER**; 1994) discussed three types of coupling strategies including explicit, implicit and fully implicit. Trick (**TRICK**; 1998) presented a procedure of coupling Eclipse with FORGAS commercial simulator. Byer's dissertation (**BYER**; 2000) was focused on improving the computational efficiency of a fully coupled reservoir-surface facility. Barroux (**BARROUX** *et al.*; 2000) used two commercial simulators to study several case studies and discussed four coupling configurations. Ghorayeb and his co-workers (**GHORAYEB** *et al.*; 2003) presented a general-purpose multi-platform reservoir and network coupling controller. Zapata *et al.* (**ZAPATA** *et al.*; 2001) coupled two commercial simulators which the reservoir simulator was a fully implicit 3D reservoir with black-oil, compositional, thermal, miscible and polymer formulations, while the surface simulator was a multiphase wellbore-surface network simulator. Hence, in that work, well was

considered as a part of surface facility equipment. Coats *et al.* (**COATS** *et al.* 2004) work replaced a conventional well model with a generalized network model. Additionally, they considered different downhole equipment for wellbore configurations. Jiang's dissertation (**JING**; 2007) developed a framework that extended Stanford general-purpose research simulator capabilities by adding unstructured models and advanced wells. Details of derivatives of the global Jacobian matrix for full implicit coupling were discussed in Jing's dissertation. Killough *et al.* (**KILLOUGH** *et al.;* 2013) introduced a new capability that was based on well-head pressures (WHP) and producing water-cut for automatically switching the flow lines . Olivares (**OLIVARES**; 2015) implemented a fully coupled compositional simulation for surface facility. In his work, he also modeled asphaltene precipitations. Cao *et al.* (**CAO** *et al.*;2015) reviewed methodologies for coupling reservoir-surface facility network simulators and discussed the pros and cons of all the aforementioned work. Using surface response functions and sub-surface response functions, Boogaart (**BOOGAART**; 2016) tried to coupled surface and subsurface models. Those functions were used to balance the proper rate and pressure of the integrated model, by generating two sets of tables for IPR and wellbore models. Seth *et al.* (2015) extended Olivares's work and included pumps, seafloor manifolds and determined the optimal well-operating rates using the explicit formulation. Zhou et al. (**ZHOU** *et al.*;2017) work focused on coal bed methane reservoirs, while optimizing the coupled surface and sub-surface models considering length, diameter and layout of pipeline network as optimization factors.

More recently, Zaydullin *et al.* (**ZAYDULLIN** *et al.*;2019) introduced a new framework that enables their simulator to generate dynamic flow tables. In that framework, they introduced additional coupling steps, using pipe-flow simulator updated values for the tables during the simulation. Also, they pointed out that the generation of flow tables is based on the mean average of auxiliary parameters, such as input temperature. For the generation of flow tables, auxiliary variables are assumed to be constant and this assumption increased the inaccuracy of the tables. Furthermore, the generation of such flow tables is time-consuming. Additionally, to have accurate sets of data, the table density should be increased; however, from the numerical point of view,

the increase of table density may increase the computational efforts. Finally, readers should note that dynamic flow tables were developed for black oil models.

2.5. Different types of coupling

According to the above survey, three classes of coupling strategies can be summarized, as described below.

2.5.1. Explicit coupling

In this strategy, fluid flow equations from reservoir and wells are considered together. Then one reservoir simulator solves the equations for reservoir-well and, separately, another simulator solves the equations of surface facility network. This is mainly due to different types of fluid flow and time scale windows of surface and sub-surface facility. In this approach, a third-party software acts as a communicator between these two simulators (one for reservoir-well and another for surface facility network) at the coupling point. The advantage of this approach is the accuracy of surface facility information. Nevertheless, this approach may presnt numerical instability in some cases. Additional details can be found in Cao *et al.* (**CAO** *et al.*;2015).

2.5.2. Iterative coupling

The second approach tries to solve reservoir and facility equations iteratively. When the reservoir equations are solved, the constraints are passed to the wells. Then the surface facility equations start to be solved based on these constraints. This approach keeps iterating until convergence is reached. Further details regarding this approach can be found in the work of Emanuel and Ranney (**EMANUEL; RANNEY**; 1981).

2.5.3. Implicit coupling

The third and most difficult approach is fully implicit coupling. In this strategy, all reservoir, wellbore and surface facility equations are solved simultaneously. Since this approach solves all the equations implicitly, it is much more accurate than the other strategies. However, the implementation of such models presents difficulties and it is more time-consuming. Additional information about fluid flow equations and their derivatives for the global Jacobian matrix can be found in Olivares (**OLIARES**; 2015). Fig. 8 shows the accuracy versus computational cost for each approach.

Figure 8 - Comparison of accuracy vs computation effort for three different mathematical formulations.

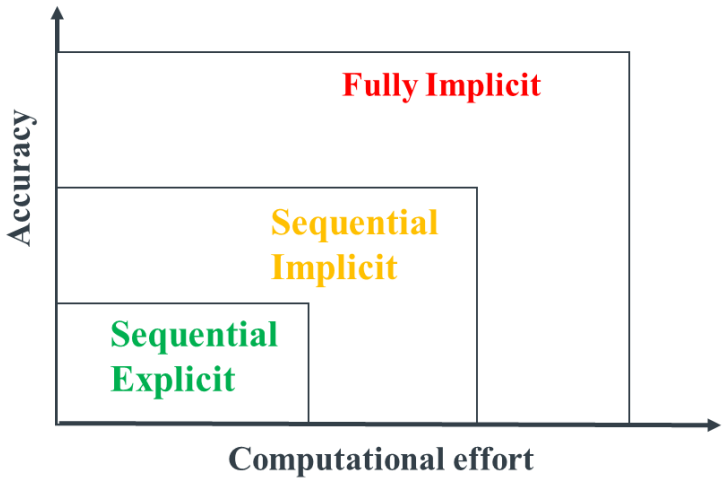

2.6. Integrated models for gas reservoirs

Compared to the oil field, the majority of the experience involving integrated models is reported for gas reservoirs. Hence, in this section, some examples of integrated models for the gas reservoirs are reviewed.

As it was mentioned in the previous section, Dempsey (1971) was the first researcher who reported the concept of integrated models. His work was originally for a gas reservoir, where for the tubing he used the Eaton correlation and for the surface pipeline network, a modified Hagedorn-Brown correlation for two-phase fluid (gas and water) was used. Later, Chevron was the first company that tried to use surface facility simulation technology for oil fields.

Puchyr (**PUCHYR**; 1991) reported the development of the sequential coupled reservoir and gas gathering system. In their work, the surface facility equations were solved. Then, the reservoir system equations were computed with boundary conditions being the well rates calculated by the gathering system solution. In other words, they considered the well equations acting as the boundary condition for each system. Also, the coupling point was reported to be bottomhole. Fig. 9 shows the example of the coupled system used by Puchyr.

Figure 9 - The surface facility model of Puchyr (**PUCHYR**; 1991).

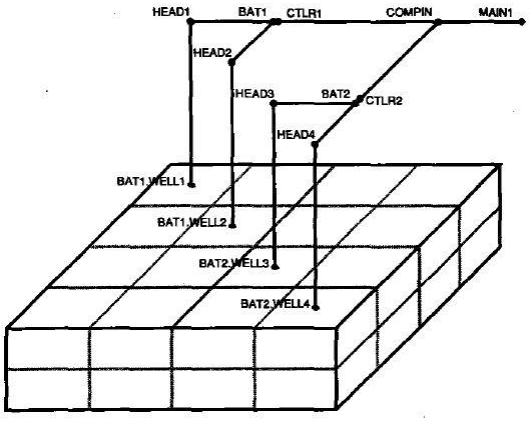

Tiangs *et al.* (**TIANGS** *et al.;* 1996) reported the coupling of GCOMP and PIPEPHASE simulators, which the wellbore was considered in two ways: one by flow tables in the reservoir simulator and another as the element for nodal analysis of surface facility simulator. In the first approach, the surface facility begin with wellhead pressure, while the operational parameters of the table were gas flow rates, condensate-gas ratio, water-gas ratio and tubing head pressures. While in the second approach, the surface facility begin with bottom hole pressure. This work was used to assess the production analysis of the gas reservoirs in the North Sea.

De Swan *et al.* (**DE SWAN** *et al.* 2002) reported the coupled reservoir and surface facility simulator for a tight gas reservoir in Mexico. The information of both simulators was not reported. The flow tables were generated in the surface facility simulator. However, any further information about the coupling process was not provided in their report.

Biswas (**BISWAS**; 2006) reported the coupling of a control finite volume-based reservoir simulator with a network simulator for single phase gas. The main focus of that work was history matching. Vertical and horizontal permeabilities and porosity were reported as the history matching parameters. Also, the mathematical formulations of both reservoir and network simulators were presented. Fig. 10 shows the surface facility reported by Biswas et al. (2006).

Figure 10 - The surface facility model used by Biswas (2006) to investigate the sensitivity analysis.

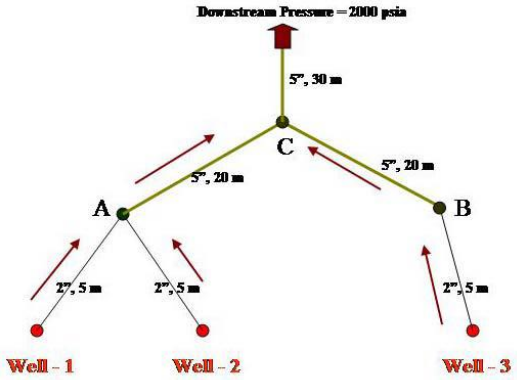

Alexis (**ALEXIS**; 2009) provided a vast literature survey of single-phase gas reservoirs and surface network models. Considering pipeline, compressor, wellbore and taking into account looped surface condition, Alexis (2009) developed an in-house simulator. Through a series of case studies, he demonstrated different capabilities of the developed simulator for gas gathering and production systems located near the town of Snow Shoe, Pennsylvania. He also performed a sensitivity analysis on the variation of the suction pressure of the compressor on the total production. Fig. 11 shows the network for a demonstration model presented in the Alexis's work.

Figure 11 - The surface facility configuration of the Alexis' report.

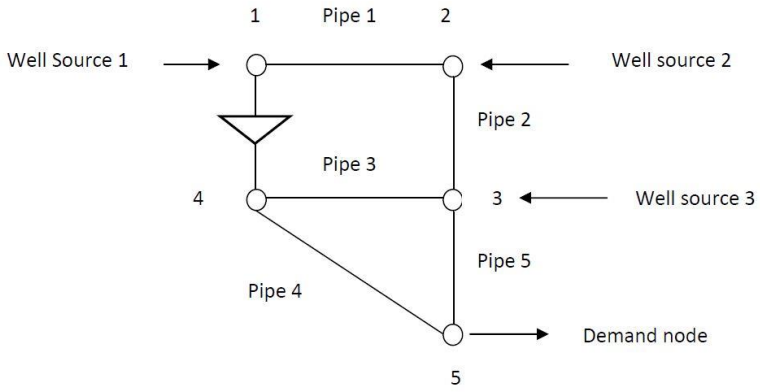

Bartolomeu and Abdrakhmanov (**BARTOLOMEU; ABDRAKHMANOV;** 2014) reported the coupling of the Sensor[1] and the HYSYS simulators, for reservoir and surface facility through the Petrostreams Pipe-It software. In that study, three different strategies were investigated for a gas condensate field: (1) for natural depletion, (2) for different

[1] System for Efficient Numerical Simulation of Oil Recovery

numbers of injectors (3) a combination of them. It should be noted that in this methodology, the reservoir is solved first, then the surface facility model is calculated.

These above examples show that there is a significant effort for the development of integrated models, especially for gas reservoirs. It should be considered that the development of coupled models is more industrial act, rather than a purely academic research activity. Various industrial patents tackled the challenges that exist in the development of these models [**WATTS et al; 2010, FLEMING; MA; 2007, LU; FLEMING; 2012, FLEMING; WANG; 2013,**]. Readers can refer to them for more advanced topics. However, reviewing those patents is beyond the scope of this literature survey.

2.7. Difficulties of development of integrated models

Aside from the type of coupling, the degree of complexity of the integrated model is beyond the scope of fluid flow formulations. Below is a list of some of the additional difficulties.

2.7.1. Number of associated variables

The first issue that exists for the numerical development of integrated models is the number of associated variables. PPS are systems that consist of three elements, reservoir, wells and surface facility. Each element can have different types of variables due to the type of studies that are under investigation. Generally, compositional simulation has greater numerical effort due to equilibrium conditions and required thermodynamic calculations. Hence, the development of a simulator that works at the most optimized condition for all of the variables is an ambitious task.

2.7.2. Advantage of compositional formulation for the development of integrated models

The second issue is the failure of black oil formulation to capture thermodynamic interaction of the fluids. In addition, when hydrocarbon fluids reach the surface, temperature change may cause the formation of some undesirable products such as wax, hydrate, or asphaltenes. In the black oil formulation, oil is treated as a single component with no interaction with the gas or water phases. This shows why compositional simulation has advantages over black oil formulation. Although compositional models

are able to capture interaction between various hydrocarbon phases, from a computational perspective, they require more robust implementations. The scope of each one of the aforementioned formulations is different due to the physical phenomena that they are trying to model. The level of accuracy, scale of operations, simulation run time, readability, programming language, computational power and CPU capacity are examples of the topics that differ for each class of the simulators.

2.7.3. Different temperature windows and time scales

The third issue that has to be dealt with when it comes to the development of simulators is the different types of physical environments. In general, fluid flow at the reservoir takes place in tiny interconnected porous spaces. As a result, capillary pressure and interfacial phenomena, such as relative permeability and wettability of the reservoir rocks cause hydrocarbon fluids to have relatively low velocity. Also, reservoir pressure and temperature may be under-saturated, when single-phase flow occurs in the presence of cognate water. As pressure drop occurs inside the reservoir, the saturation pressure may be reached causing the appearance of a second hydrocarbon phase in the porous media. Either way, as fluids enter the tubing, changes in pressure and temperature often leads to two-phase flow. Thus, the type of fluid flow equation changes, and the velocity of the fluid flow increases at the surface condition. This change of velocity and corresponding properties variations of this unsteady flow can cause difficulties in selecting the time step. It is common to consider that the surface facility are in a steady-state condition. Moreover, the temperature of the fluids is decreasing when they are passing from the reservoir into surface facility equipment. The change of the temperature results in different equilibrium conditions. And aside from momentum and mass conservation equations, the energy conservation equation should also be solved. This is why compositional simulation has advantages over black oil simulation for integrated models. Figure 2.12 shows different stages of hydrocarbon fluids with changes in time.

Figure 12 - Different time scales and elements of PPS. From (**SANKARAN** et al.; 2017).

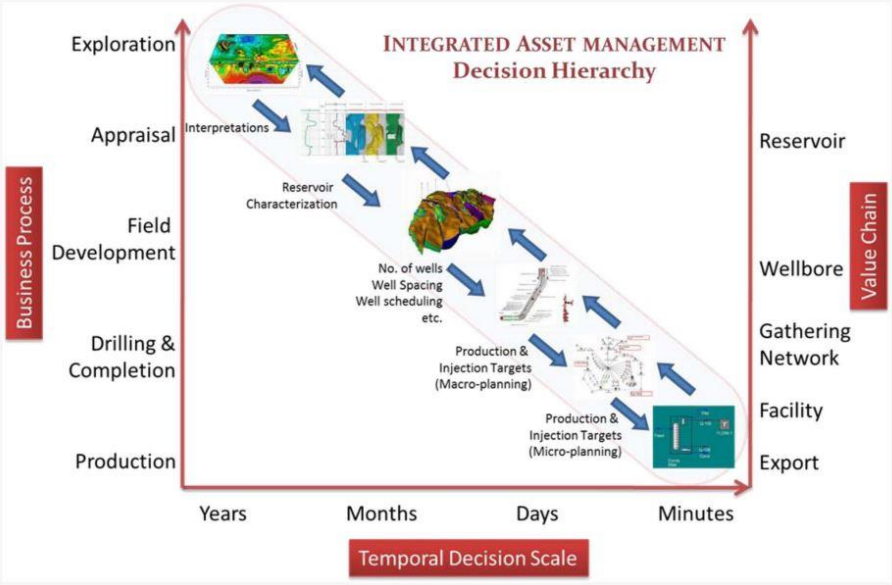

2.7.4. Lumping

Lumping and delumping are common activities for the compositional modeling of hydrocarbons. These approaches allow simulators to identify important physical properties of components and preserve them for precise modeling of fluid flow through porous media and pipelines. Lumping and delumping can be used for multi-reservoirs systems which are using a common surface gathering unit (**GHORAYEB** *et al.*; 2003). As the fluids are passing from each reservoir and being combined in a shared surface facility, such as manifolds, gathering centers, or pressurizing units, the in-situ fluid composition may vary due to the mixing of the different hydrocarbon fluids or operational conditions. Thus, lumping and delumping increase the numerical efforts of fluid modeling. Torrens et al. (**TORRENS** et al.; 2015) work is an example of compositional modeling of implicit coupled simulators that used lumping and delumping in their work. Fleming and Wong (**FLEMING; WANG;** 2013) also provided a good literature survey about lumping techniques. Thermodynamics association studies have a huge impact on the degree of reliability of the results of integrated model solutions.

2.7.5. Uncertainties of physical properties of porous media and wellbore

The reliability of gathered data is another determining factor for the development of integrated models. Typically, surface facility data is more reliable than reservoir and

wellbore information. This is mainly due to the scope of operations and the type of tools that are measuring information. Compared to surface facility environments, well and reservoir environments are measured indirectly by industrial tools, such as logging, or downhole equipment. High salinity, high temperature, high pressure, large well spacing are examples of uncertainties of the physical properties of porous media and wellbore. For example, if the relative permeability of the reservoir was not determined precisely, it may result in increasing uncertainties of the relative flow of oil and gas in the porous media. Therefore, GOR and WOR may not be calculated in the wellbore correctly, and WHP and pressure of the separator are calculated mistakenly. Because of this, uncertainty analysis should be taken into account when developing integrated models. Machine learning and artificial intelligence are tools that can diminish the risk of uncertainties, while increasing the computational cost of integrated models.

2.7.6. Automatic surface facility switching

During the production of hydrocarbon fluids, it is common that plans of surface facility operations change. It is mainly due to the capacity of the downstream section for receiving produced fluids or the criticality of surface facility. This will be discussed in Chapter Three. Also, sometimes reservoir management of hydrocarbon resources requires shutting in some wells and open others. Well-testing, workovers, well start-up, artificial lift and erosion of surface equipment due to the sand production are examples of operations that may result in modifying plans for surface facility operation. Avoiding water coning or increase of GOR and WOR at high rated wells are other examples that may result in activation or inactivation of some sections of surface facility (**STANKO**; 2021). Installation of new units or extension of old ones are other examples that may impact the plans of surface facility operations. These types of operations should be done even carefully in offshore facility. Hence, integrated modeling simulators need to have switching options, which enables them to operate based on the current plans of the surface facility. Numerical algorithms that can perform automatic facility switching is another type of difficulty and it is mainly for industrial applications. Killough et al. (2013) is an example of work that used automatic facility switching for flow lines with more than 500 wells among six different separator units at a gathering center (**KILLOUGH** *et al.;* 2013).

2.7.7. Asphaltene precipitation and looped gathering systems

Two additional issues that may appear during the development of integrated models are asphaltene precipitation and looped gathering surface facility. During the production of heavy and extra heavy crude oils, asphaltene precipitation may take place due to changes in temperature and pressure. Thus, by the blockage of surface facility and tubing, the pressure of surface facility is increasing. To model the asphaltene precipitation for surface facility, complex EOSs, such as PC-SAFT has to be included in fluid modeling. Those EOS will increase the complexity of the surface calculations.

On the other hand, looped gathering systems are used when the separators are not able to receive all the produced gas. For the simulation of looped gathering units, two additional criteria will be added to the convergence examination of the total system; pressure balance and mass balance at each node of the looped section have to be reevaluated. The surface facility section will converge when all of the criteria are satisfied.

2.8. Available commercial simulators

As it was mentioned in the literature survey section, some reports mentioned the name of the simulator that has been coupled with surface facility. However, some of those simulators are out of date or the information about them does not exist nowadays. To the best of the author's knowledge, Table 1. shows the available simulators that are working with surface facility equipment (**WIKIPEDIA**).

Table 1. List of commercial software packages and corresponding vendors, which can handle integrated models

Name	**Vendor**
CoFlow	CMG Ltd
Nexus	Halliburton
enersight	3esi-Enersight
Pipe-It	Petrostreamz
Avocet	Schlumberger
GasAssure	Stochastic Simulation
IPM	Petroleum Experts (PETEX)
ReO	Weatherford
RAVE	Ingen
PetroVR	Caesar Systems
FUTURE	Serafim Ltd
Maximus	KBC Advanced Technologies

CHAPTER 3

RESERVOIR ENVIRONMENT AND FLUID FLOW IN POROUS MEDIA

3.1. The background and basic assumptions of the reservoir

Before developing a mathematical description for a reservoir environment, it's crucial to understand the reservoir's characteristics. In general, four major elements can be used to describe a reservoir:

- Type of fluids (compressible, slightly compressible, and incompressible fluids)
- Flow regime (steady-state flow, unsteady-state flow, pseudo-steady-state flows)
- Reservoir geometry (linear, radial, spherical flows)
- Number of Phases (single-phase, two-phase, three-phase flow)

Although the focus here is on flow regime, Ahamad goes into great mathematical detail the characterization of each part of the reservoir (**AHMAD; 2010**).

The term steady-state flow refers to a flow regime in which the pressure and other variables in each reservoir location is constant and do not change over time. This type of regime exists under two conditions: substantial aquifer support or pressure maintenance operations at surface facility.

Unsteady-state flow is a type of flow in which the rate of change of pressure in respect to time is not constant at any point in the reservoir. The pressure of the system is also determined by the reservoir's position in this situation. This is the most typical form of flow regime during the reservoir's existence.

Finally, the regime in which the rate of change of pressure with respect to time at any region of the reservoir remains constant but different from zero is known as pseudo steady-state flow.

Based on what has been above discussed the following is the mathematical description of the UTCOMPRS simulator.

The original formulation of the UTCOMPRS simulator was implemented as a set of partial differential equations for fluid flow in porous media under the isothermal,

multicomponent and multiphase miscible gas flooding condition by Chang (**CHANG**;**1990**). During the development of the UTCOMPRS simulator, the following assumptions have been considered:

1. The reservoir is isothermal.
2. The reservoir is surrounded by impermeable zones. Hence, no flow exists along the reservoir boundaries.
3. Permeability tensor is orthogonal and aligned with the coordinate system.
4. There is no precipitation or chemical reaction.
5. Adsorption effects are neglected.
6. Fluid flow in porous media is characterized by Darcy's flow for the multiphase system and the physical dispersion follows Fick's law.
7. Slightly compressible formation.
8. The production/injection through the wells are treated as the source or sink terms.

Additional notations regarding the UTCOMPRS simulation are as follows (**FARIAS, 2020**):

9. A maximum of four phases is considered for the simulation: one aqueous and three hydrocarbons, including oil, gas, and a nonaqueous liquid.
10. Instantaneous local equilibrium is considered for phase behavior.
11. Capillary pressure does not affect the phase behavior.
12. Water is also considered slightly compressible with constant viscosity.
13. No mass transfer is considered between the water and the hydrocarbon phases.

3.2. Physical model

The equations and physical model of the reservoir environment and fluid flow in porous media are described below.

3.2.1. Mass conservation equation

The material balance equation for multiphase and multicomponent fluid flow in an isothermal porous medium can be written as

$$\frac{\partial N_i}{\partial t} + \nabla . \left(\sum_{j=1}^{n_p} \xi_j x_{ij} \vec{u}_j \right) - \frac{q_i}{V_b} = 0 \quad ; \qquad i = 1, n_c \tag{3.1}$$

where the term N_i denotes the number of moles of component *i* per buck volume and it is given by

$$N_i = \phi \sum_{j=1}^{n_p} \xi_j S_j x_{ij} \tag{3.2}$$

In the mass conservation equation, V_b, ξ_j , x_{ij} , $\vec{u}_j$, n_c and S_j are the bulk volume (or volume of the control volume), the molar density of the phase j, the molar fraction of component i in phase j, the velocity of phase j, number of hydrocarbon components, and the saturation of the phase j, respectively.

The term $\frac{q_i}{V_b}$ in Eq. 3.1 is the source or sink term, where q_i is the injection or production flow rate in a given control volume and equals to zero when there is no well in that grid block. For the water phase, the material balance equation is modified as follows:

$$\frac{\partial N_w}{\partial t} + \nabla . \left(\sum_{j=1}^{n_p} \xi_w \vec{u}_w \right) - \frac{q_w}{V_b} = 0 \tag{3.3}$$

where the term N_w is given by

$$N_w = \left(\phi \xi_w S_w \right) \tag{3.4}$$

The phase velocity is calculated from Darcy's law, which for its multiphase version, is given by the following equation:

$$\vec{u}_j = -\vec{\vec{k}} \lambda_{rj} \left(\nabla P_j - \gamma_j \nabla D \right) \tag{3.5}$$

where $\vec{\vec{k}}$, λ_{rj} , P_j , γ_j are the absolute permeability tensor, the relative mobility of phase j, the pressure of the phase j, the specific weight of phase j, and D is the value of the depth, which is positive in a downward direction.

The relativity mobility can be determined from

$$\lambda_{rj} = \frac{k_{rj}}{\mu_j} \tag{3.6}$$

where k_{rj} and μ_j are, the relative permeability and the viscosity of phase j, respectively.

The permeability tensor of the rock is given by

$$\vec{\vec{k}} = \begin{vmatrix} k_{xx} & k_{xy} & k_{xz} \\ k_{yx} & k_{yy} & k_{yz} \\ k_{zx} & k_{zy} & k_{zz} \end{vmatrix} \tag{3.7}$$

In Chang's (1990) dissertation, the pressure of phase j is calculated from the following modification:

$$P_j = P_r + P_{crj} \tag{3.6}$$

where P_r is the reference pressure, and P_{crj} is the capillary pressure between the phase j and the reference phase. It should be noted that in the current version of the UTCOMPRS simulator, P_r denotes the oil phase.

3.2.2. Pressure equation

In order to obtain the pressure equation, the main assumption is that the pore volume should be completely filled by the total fluid volume. Mathematically speaking, this assumption can be written as follows:

$$\vec{u}_j = -\vec{\vec{k}}\,\lambda_{rj}\left(\nabla P_j - \gamma_j \nabla D\right) \tag{3.9}$$

where the total volume of fluid is a function of pressure (P) and a total number of moles (N) of each component. On the other hand, the pore volume is a function of pressure only.

Using the chain rule and deriving Eq. (3.9) with respect to time, Eq. (3.10) can be obtained as:

$$\left(\frac{\partial V_t}{\partial P}\right)_N \left(\frac{\partial P}{\partial t}\right) + \sum_{i=1}^{n_c+1}\left[\left(\frac{\partial V_t}{\partial N_i}\right)_{P,N_{k(k\neq 1)}} \frac{\partial N_i}{\partial t}\right] = \frac{\partial V_P}{\partial P}\frac{\partial P}{\partial t} \tag{3.10}$$

Recalling assumption number seven of Change (1990) notation, for a slightly compressible formation, the definition of the porosity can be written as

$$\phi = \phi^o\left[1 + c_f\left(P - P^o\right)\right] \tag{3.11}$$

where ϕ^o is the porosity at the reference pressure (P^o) and c_f is the compressibility factor of the reservoir rock. The pore volume variation with respect to pressure is written in terms of Eq. (3.12).

$$\frac{dV_P}{dP} = \phi^o V_b c_f = V_p^o c_f \tag{3.12}$$

The partial molar volume is the last term that is necessary to define to get the final form of the pressure equation. Equation (3.13) describes the mathematical expression of partial molar volume

$$\vec{V}_{ti} = \left(\frac{\partial V_t}{\partial P}\right)_{P, N_{k\,(k\neq 1)}} \tag{3.13}$$

Combing the aforementioned equations and correlations will give us the final shape of the pressure equation for the UTCOMPRS simulator.

$$\begin{aligned}&\left[\phi^o c_f - \left(\frac{\partial V_t}{\partial P}\right)_{N_i}\right]\frac{\partial P}{\partial t} = \vec{V}_{tw}\vec{\nabla}.\left(x_{kw}\xi_w \frac{k_{rw}}{\mu_w}\vec{\vec{k}}\left(\nabla P - \gamma_w \nabla D\right)\right) + \\ &\sum_{i=1}^{n_c+1}\left\{\vec{V}_{ti}\vec{\nabla}.\left[\sum_{j=1}^{n_p}\xi_j x_{ij}\vec{\vec{k}}\frac{k_{rj}}{\mu_j}\left(\nabla P - \gamma_j \nabla D\right)\right]\right\} - \sum_{i=1}^{n_c+1}\vec{V}_{ti}\frac{q_i}{V_b}\end{aligned} \tag{3.14}$$

Based on the numerical formulation, Eq. (3.14), can be either solved by IMPEC, adaptive implicit or fully implicit formulations.

3.2.3. Constraint equations

With the aim of accurately solve the numerical model, a set of physical constraints is required to verify properties calculations. Saturation of phases sum to unity according to the following equation

$$\sum_{j=1}^{n_p} S_j = 1 \tag{3.15}$$

For the non-aqueous phases, compositions are calculated as

$$x_{ij} = \frac{n_{ij}}{n_j} \tag{3.16}$$

$$\sum_{i=1}^{n_c} x_{ij} = 1 \tag{3.17}$$

where n_{ij} and n_j are the number of moles of a certain component in phase j and the total number of moles of phase j, respectively.

3.2.4. Phase behavior

The UTCOMPRS simulator is a compositional simulator. Thus, the phase behavior should be addressed precisely. One of the constraints related to adequate modeling of the phase is that the fugacity of a component needs to be the same for all phases. This criterion of phase equilibrium states that fugacity is a function of pressure and phase composition at a given temperature. To obtain fugacities, a thermodynamic correlation or equation of state (EoS) must be used. Herein, the presented work uses the original work of Peng Robinson equation of state, however, a literature review of more than 220 modifications to the Peng Robinson equation can be found in (**LOPEZ** *et. al;* 2017). The Peng-Robinson EOS (**ROBINSON** *et. al;* 1985) can be written as

$$P = \frac{RT}{v-b} - \frac{a}{v(v+b)+b(v-b)} \tag{3.18}$$

where

$$a = 0.45724\frac{\alpha\left(RT_c\right)^2}{P_c} \tag{3.19}$$

$$b = 0.0778\frac{RT_c}{P_c} \tag{3.20}$$

where R, P_c, and T_c are the universal constant of gases, the critical pressure, and critical temperature, respectively. The parameter α is calculated using the following equations:

$$\alpha = \left\{1+m\left[1-\left(\frac{T}{T_c}\right)^{0.5}\right]\right\}^2 \tag{3.21}$$

$$m = \begin{cases} 0.34746+1.54226\omega-0.26992\omega^2, & \text{if } \omega \le 0.49 \\ 0.379642+1.48503\omega-0.164423\omega^2+0.016666\omega^3, & \text{if } \omega \ge 0.49 \end{cases} \tag{3.22}$$

where ω is the acentric factor.

The previous equations presented in this section are used for a single component in a two-phase situation. However, in reservoir simulation, it is common to have several components and the presence of more than two phases. To apply the equation of state, a mixing rule is used to work with a mixture of several components. Hence, Eq. (3.18) is rewritten as:

$$P = \frac{RT}{v_j - b_j} - \frac{a_j}{v_j\left(v_j + b_j\right) + b_j\left(v_j - b_j\right)} \tag{3.23}$$

where the subscript j is the index of the phases. The parameters a_j and b_j of the mixing rule are given by

$$a_j = \sum_{i=1}^{n_c}\sum_{k=1}^{n_c} x_{ij} x_{kj} a_{ik} \tag{3.24}$$

$$b_j = \sum_{i=1}^{n_c} x_{ij} b_i \tag{3.25}$$

$$a_{ik} = \left(1 - k_{ik}\right)\left(a_i a_k\right)^{0.5} \tag{3.26}$$

where the term k_{ik} is the binary interaction parameter between the components of the mixture. The equation of state can be rewritten in terms of the compressibility factor Z. Using this approach results in a cubic expression with three possible roots. The equation is given by

$$Z_j^3\left(1 - B_j\right) Z_j^2 + \left(A_j - 3B_j^2 - 2B_j\right) Z_j - \left(A_j B_j - B_j^2 - B_j^3\right) = 0 \tag{3.27}$$

$$A_j = \frac{a_j P}{\left(RT\right)^2} \tag{3.28}$$

$$B_j = \frac{b_j P}{RT} \tag{3.29}$$

As previously mentioned, Eq. (3.27) will result in three roots for Z, where three of these values may be real roots for the solution. In this case, the root that gives the minimum value of Gibbs free energy is chosen. With the value of Z is possible to calculate the fugacity of each phase and calculate the compositions through a flash procedure.

3.2.5. Physical properties

This section presents the main correlations used in the simulator to calculate the physical properties of components. Although the UTCOMPRS has several correlations, only the equations used to perform the simulations are presented here. The models used to calculate viscosity, density, saturation, and relative permeability are discussed below.

3.2.5.1. Viscosity

UTCOMPRS has several methods to calculate the viscosity of the hydrocarbon phases. The present work uses the correlations proposed by Lohrenz et al. (**LOHRNZ** *et al.*; **1964**) to calculate only oil viscosity since water viscosity is kept constant during the simulation. Initially, the viscosity of the pure component at low pressures is calculated using the correlation proposed by Yoonm and Thodos (**YOONM, THODOS; 1970**).

$$\tilde{\mu} = \left(4.610 T_{r,i}^{\ 0.618} - 2.040 e^{-0.449 T_{r,i}}\right) + \frac{1.94\times10^{-4}\times e^{\left(-0.449 T_{r,i}+0.1\right)}}{\xi_i} \tag{3.30}$$

where $T_{r,i}$ is the reduced temperature of component i and the parameter ξ is calculated as

$$\xi_i = \frac{5.44 T_{c,i}^{\ 1/6}}{MW_i^{\ 1/2} P_c^{\ 2/3}} \tag{3.31}$$

The parameter MW in Eq. (3.31) is the molar weight of the component. Using Eqs. (3.30) and (3.31), the viscosity of the mixture at low pressures is calculated as

$$\mu_j^* = \frac{\sum_{i=1}^{n_c} x_{ij}\,\tilde{\mu}_i \sqrt{MW_i}}{\sum_{i=1}^{n_c} \tilde{\mu}_i \sqrt{MW_i}} \tag{3.32}$$

The viscosity at a given temperature is evaluated as

$$\mu_j = \begin{cases} \mu_j^* + 2.5\times10^{-4}\,\dfrac{\xi_{jr}}{\eta_j}, & \text{if} \quad \xi_{jr} \le 0.18 \\ \dfrac{\mu_j^* + \left(\chi_j^4 - 1\right)}{10^4 \eta_j}, & \text{if} \quad \xi_{jr} > 0.18 \end{cases} \tag{3.33}$$

where ξ_{jr} is the reduced phase molar density and η and χ are parameters of the model, which are calculated as

$$\xi_{jr} = \xi_j \sum_{i=1}^{n_c} x_{ij} v_{c,i} \tag{3.34}$$

$$\eta_j = 5.44 \frac{\left(\sum_{i=1}^{n_c} x_{ij} T_{c,i} \right)^{1/6}}{\left[\left(\sum_{i=1}^{n_c} x_{ij} MW_i \right)^{1/2} \left(x_{ij} P_{c,i} \right)^{2/3} \right]} \tag{3.35}$$

(3.35)

$$\chi_j = 1.023 + 0.23364 \xi_{jr} + 0.58533 \xi_{jr}^3 + 0.093324 \xi_{jr}^4, \qquad \text{j=1,...,n}_\text{p} \tag{3.36}$$

3.2.5.2. Density

The molar density of each hydrocarbon phase is calculated from the below correlation:

$$\xi_j = \frac{P}{Z_j RT} \tag{3.37}$$

As stated at the beginning of the present chapter, water is considered to be slightly compressible. Therefore, the water molar density is given by

$$\xi_w = \xi_w^o \left[1 + C_w (P - P^o) \right] \tag{3.38}$$

where ξ_w^o is the water molar density at a reference pressure P^o. From the molar density, it is possible to calculate the mass density as

$$\rho_j = \xi_j \sum_{i=1}^{n_c} MW_i x_{ij} \tag{3.39}$$

3.2.5.3 Saturation

In order to calculate the saturation of each phase for all grid blocks, the following expressions are used respectively for water and oil and gas saturations:

$$S_w = \frac{N_w}{V_p \xi_w} \tag{3.40}$$

$$S_J = (1 - S_w) \frac{\frac{L_j}{\xi_j}}{\sum_{m=2}^{n_p} \frac{L_m}{\xi_m}} \tag{3.41}$$

where v_w is the water phase molar volume and L_j is the mole fraction of each phase.

3.2.5.4. Relative permeability

The present work uses the Stone II model (**STONE, 1973**) to calculate relative permeabilities. In this model water and gas permeabilities are a function of their saturations, while oil permeability is a function of the saturation of three phases. For a two-phase system composed of oil and water, the permeabilities are calculated from the following equations:

$$k_{rw} = k_{rw}^{o}\left(\frac{S_w - S_{or}}{1 - S_{wr} - S_{or}}\right)^{e_w} \tag{3.42}$$

$$k_{ro} = k_{ro}^{o}\left(\frac{S_w - S_{or}}{1 - S_{wr} - S_{or}}\right)^{e_o} \tag{3.43}$$

where k_r is the relative permeability, k_r^o is the end-point relative permeability, S is the saturation of each phase, S_r the residual saturation, and e is a variable model parameter. The subscripts w and o represent water and oil phases, respectively.

For a three-phase system composed of oil, gas, and water the relative permeabilities are calculated as follows:

$$k_{rw} = k_{rw}^{o}\left(\frac{S_w - S_{or}}{1 - S_{wr} - S_{or}}\right)^{e_w} \tag{3.44}$$

$$k_{rg} = k_{rg}^{o}\left(\frac{S_g - S_{gr}}{1 - S_{gr} - S_{wr} - S_{or}}\right)^{e_g} \tag{3.45}$$

$$k_{ro} = k_{row}^{o}\left[\left(\frac{k_{row}}{k_{row}^{o}} + k_{rw}\right)\left(\frac{k_{rog}}{k_{row}^{o}} + k_{rg}\right) - \left(k_{rw} + k_{rg}\right)\right] \tag{3.46}$$

where S_{org} and S_{orw} are the residual oil saturation of gas and water and is the end-point relative permeability for oil in water. The relative permeability of oil in gas and water are calculated by

$$k_{row} = k_{row}^{o}\left(\frac{1-S_w-S_{orw}}{1-S_{wr}-S_{orw}}\right)^{e_{ow}} \tag{3.47}$$

$$k_{rog} = k_{rog}^{o}\left(\frac{1-S_g-S_{wr}-S_{org}}{1-S_{gr}-S_{wr}-S_{org}}\right)^{e_{og}} \tag{3.48}$$

3.2.6. Well model

The last variable to be defined is the source and sink terms, which are presented in the mass conservation and pressure equations. Due to the complexity of representing the physics of the flow from the porous medium to the well, a Well Index (WI) approach is used. The present work uses the model proposed by Peaceman (**PEACEMAN**; **1978**) and Peaceman (**PEACEMAN;**1983) for structured grids [62,63]. In the UTCOMPRS simulator, two well conditions are implemented:

- Constant flow rate
- Constant bottom hole pressure.

The volumetric flow rate for a given phase in a well is calculated from the following correlation:

$$Q_j = WI_{j,s}\left(P_{wf,s}-P_{j,s}\right) \tag{3.49}$$

where the WI is the productivity index, P_{wf} is the pressure of the well, and the subscript *s* denotes the segment of the well. For a three-dimensional simulation, *WI* of phase *j* is given by

$$WI_j = \frac{\sqrt{k_x k_y}\,\Delta z\,\lambda_{rj}}{25.14872\ln\left(\frac{r_o}{r_w}\right)} \tag{3.50}$$

The parameter Δz is the height of the grid block and r_w and r_o are the well radius and equivalent well radius, respectively. The equivalent well radius is calculated by

$$r_o = 0.28 \frac{\left[\left(\frac{k_x}{k_y} \right)^{\frac{1}{2}} \Delta x^2 + \left(\frac{k_y}{k_x} \right)^{\frac{1}{2}} \Delta y^2 \right]^{\frac{1}{2}}}{\left(\frac{k_y}{k_x} \right)^{\frac{1}{4}} + \left(\frac{k_x}{k_y} \right)^{\frac{1}{4}}} \tag{3.51}$$

Regardless of the operation of injection and production wells, in this work, they are respectively treated as constant flow rate and constant bottom hole pressure. For the injection well, the molar flow rate is given by

$$\dot{q}_{k,s} = \frac{WI_s \sum_{j=1}^{n_p} \lambda_{j,s}}{\sum_{l=1}^{n_s} WI_l \sum_{j=1}^{n_p} \lambda_{j,l}} \dot{q}_{k,T} \tag{3.52}$$

where $\dot{q}_{k,s}$ is the total molar flow rate of the well and n_s is the number of segments. For the production well, the molar flow rate is calculated from the following equations for water and oil phases, respectively.

$$\dot{q}_{w,s} = \xi_{w,s} \dot{Q}_{w,s} \tag{3.53}$$

$$\dot{q}_{k,s} = \sum_{j=2}^{n_p} x_{kj,s} \xi_{j,s} \dot{Q}_{j,s}, \quad \text{k=2,....,n}_\text{p} \tag{3.54}$$

Also, this work only deals with IMPEC and the Full implicit formulation of the UTCOMPRS simulator. Details and algorithms of each one of them are reported in Fernandes' thesis (**FERNANDES**, 2014).

CHAPTER 4

SURFACE FACILITY ENVIRONMENT AND FLUID FLOW IN PROCESSING EQUIPMENT

4.1. Production operations and day-to-day maintenance

During the field life cycle, it is important to know, in terms of original oil and gas in place, how much is the field capacity, how the hydrocarbon fluids will be produced, what are the operational restrictions, what type of processing units are required and how often does the facility equipment should be maintained. The design of the facility crucially depends on the accurate knowledge of the aforenoted questions. Generally, the typical development, planning and execution period of an oil field may be 5 or 6 years, while producing a lifetime of the field can often be 25 or 30 years. Therefore, rather than experimental investigation, a robust simulation model is the main required tool for the integration of surface and sub-surface models. Figs. 13 and 14 show an example of surface facility and their targeted reservoirs.

Figure 13 - Different onshore and offshore reservoirs and the corresponding surface facility equipment. From **(YOUTUBE)**.

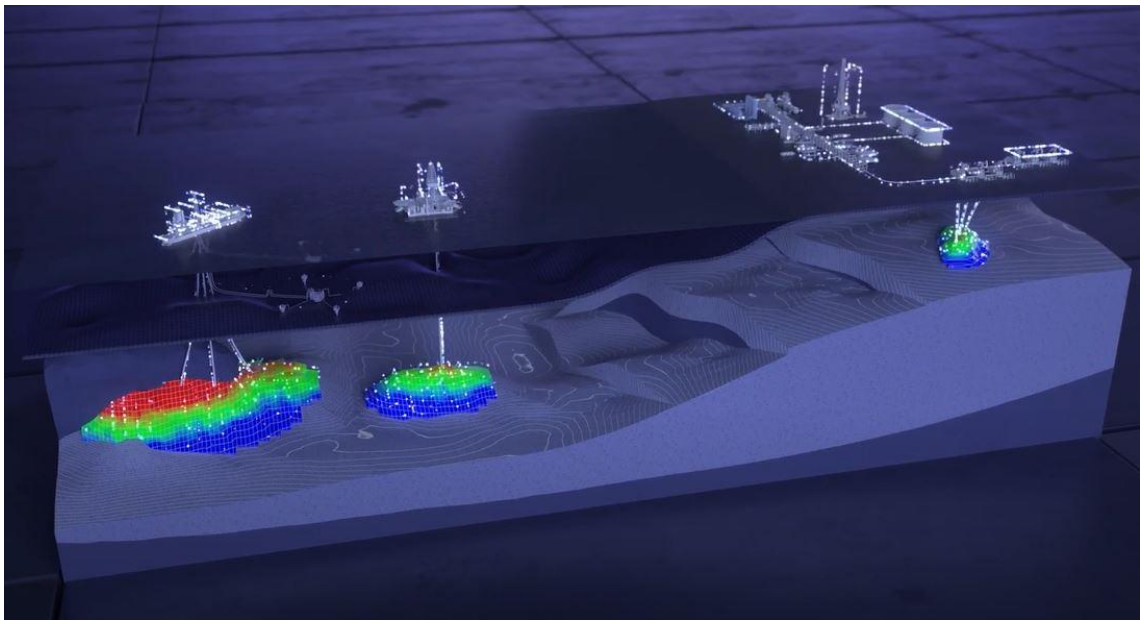

Figure 14 - An example of integrated surface and subsurface for the onshore reservoir. From (**YOUTUBE**).

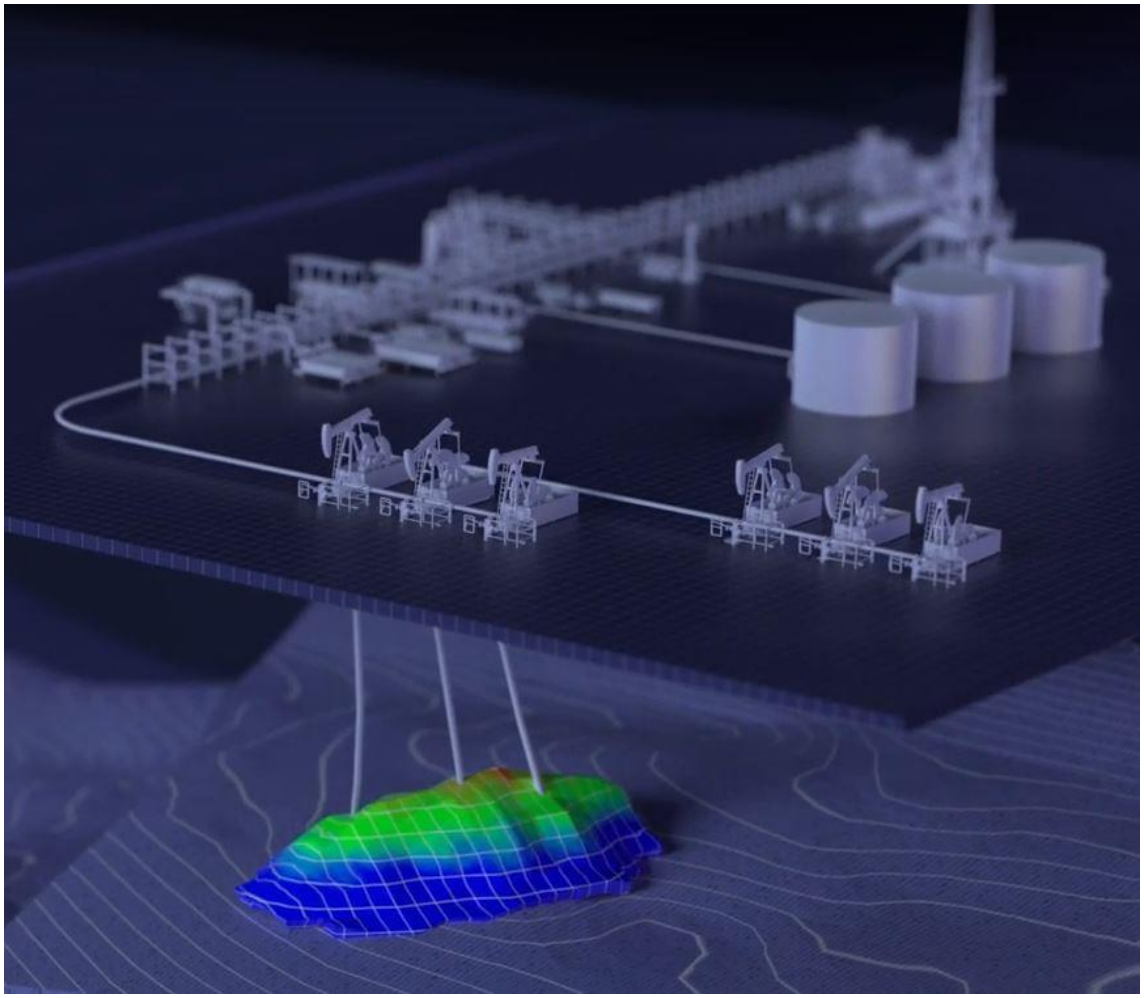

4.2. The criticality of surface facility equipment

To obtain the best maintenance strategy and operational program, an engineer/manager is required to know the criticality of each surface facility equipment. Critically refers to how important an equipment item is to the process (**JAHN et al.; 1998**). Let us consider a processing unit such as the one in Fig. 15. As it can be seen, the critically of this system depends on the capacity of each unit.

Figure 15 - Surface facility equipment with different process capacity. From (**JAHN et al.; 1998**).

In general, the surface facility equipment is designed with a capacity larger than the reservoir. In other words, criticality is an indicator that guarantees the production level will not fall below a certain value. Understanding the criticality and capacity of surface facility equipment can change the mathematical formulation of coupled surface and subsurface models. For example, Fig. 16 shows the effect of different water cuts of the surface model on the production rate of the sub-surface model.

Figure 16 - Different water cut values can change the operational point of surface facility model coupled with the subsurface model. From (**ARSALAN** et al.; 2003).

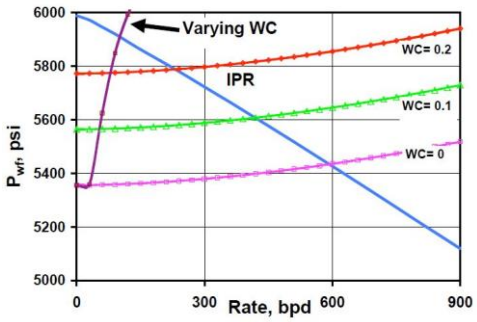

4.3. Separator conditions

One of the criticalities of surface facility equipment is the separator pressure. There are two types of separators in the downstream industries, two-phase and three-phase separators. Regardless of the type of the separator, the separator pressure is a critical parameter for coupling reservoir model with surface facility. The reason behind that is the fact that separator pressure can be treated as a fixed value and consequently can act as the boundary condition of the integrated model. Accordingly, there should be a realistic estimation regarding the separator pressure. Rodrigzie et al. [**RODRIGZIE** et al.; 2007] reported three criteria, low pressure (60 psi), medium pressure (550 psi), and high pressure (1300 psi) for separator conditions.

4.4. Surface facility layout

Apart from separator pressure, the layout of surface facility, including the length and diameter of the pipeline, depends on the mathematical formulation of the integrated models. Zhou et al. (**ZHOU et al.; 2017**) coupled a pipeline network and a wellbore/reservoir simulator for a coal bed methane reservoir. The results of their study showed that for the different layout of the surface facility, including concatenated, star and tree structures, the cumulative gas productions were different, as illustrated in Fig. 17.

Figure 17- Results of the cumulative coal bed methane production for different surface facility layout. From (**ZHOU et al.; 2017**).

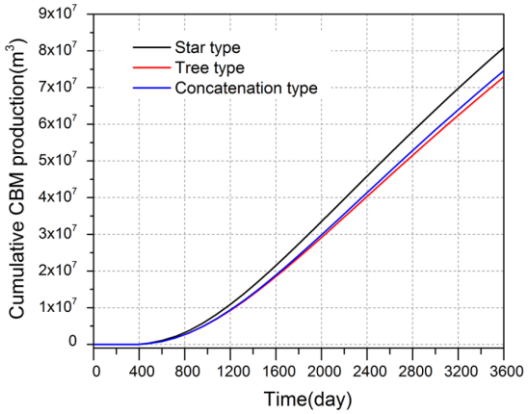

4.5. Connection-based or node-based formulations

One of the most important concerns of the mathematical formulation of the surface facility or tubing is whether to consider it as node or connection. Similar to reservoir modeling, the surface network structure can be represented with the graph edges corresponding to pipes and the graph nodes corresponding to pipe joints. Fig. 18 illustrates a manifold (the node), where three production lines (connections) are inflows and outflows.

Figure 18 - The conceptual diagram of connections and nodes that can be used for surface facility modeling. From (**CAO et al.; 2015)**.

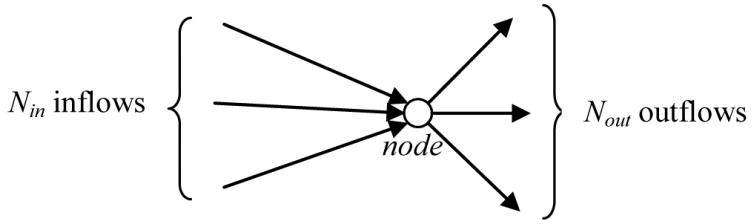

For such a system, one can either define pressure and temperature unknowns at the nodes and flow rate in the flow paths or flow rate at each node and pressure and temperature in the middle of each flow path (Olga software is using this approach for example (**OLGA MANUAL**).

However, the first approach is more common in the literature. Fig. 19 shows these two types of formulations.

Figure 19 - Mathematical discretization of a horizontal pipeline which considers 1) pressure and temperature unknowns at the nodes (upper figure), and 2) flow rates at each node (lower figure).

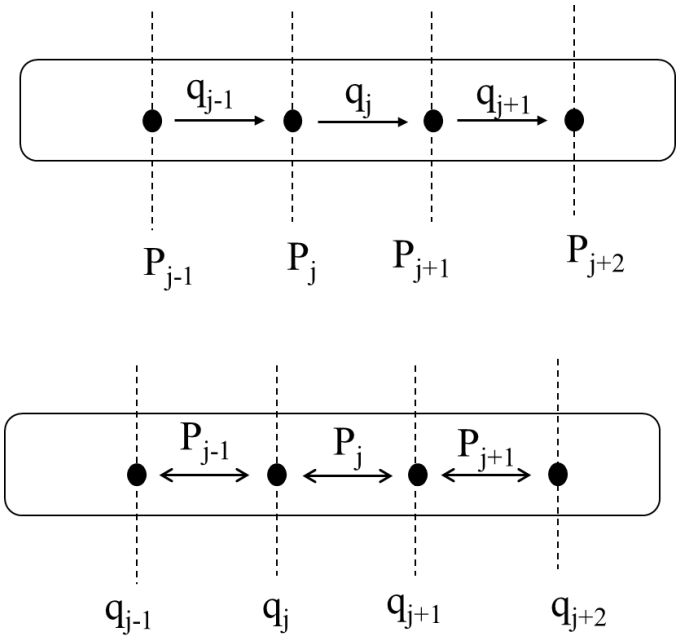

4.6. Surface facility formulation

In the following, different conservation laws are explained, except the energy conservation equation. In this work, for the surface facility, the isothermal condition is

assumed. For more details about the coupling of the energy conservation equation, with other equations, the reader can refer to Wang's (2019) dissertation (**WANG, 2019**).

4.6.1. Momentum conservation equation

One gap that existed in the literature is the mathematical formulation of the surface facility. In terms of the pressure equation (momentum balance), most of the previous aforementioned works applied the steady-state, one-dimensional, multi-phase flow equation as follow:

$$\frac{dP}{dL} = -\rho_m g \sin\theta - \rho_m u_m \frac{du_m}{dL} - \frac{d\tau_m}{dL} \tag{4.1}$$

,

where the total pressure loss can be considered in terms of gravity, acceleration, and friction, regardless of the direction of the pipe, which can be vertical, horizontal, or inclined. Table 2 shows different pressure drop calculation methods.

Table 2 - Different method of pressure calculation and type of modeling. From (**WANG,** 2019).

Author	Year	Type	Flow Pattern
Duns Ros	1963	empirical	Vertical
Hagedorn-Brown	1964	empirical	Vertical
Eaton	1964	empirical	Horizontal
Orkiszewski	1967	empirical	Vertical
Aziz	1972	drift flux	Vertical
Beggs-Brill	1973	empirical	All angles
Hasan Kabir	1988	mechanistic	Vertical
Ansari	1990	mechanistic	Vertical
Gomez	1999	mechanistic	All angles

Since the Begs and Brill method considered all of the angles and used 2,429 data points of experimental pressure drop, measured from eleven different sources, this method is the best reported in the literature (**WANG, 2019**). It also has to be noted that six methods, including Beggs-Brill's, are available in the Builder simulator, from CMG, to predict the pressure loss in the wellbore. They are presented in the next chapter.

4.6.2. Mass conservation equation

The mass conservation of surface facility can be classified into three sub-categories as follows.

4.6.2.1.Black oil formulation

Similar to reservoir grid blocks, the pipeline and tubing of the network system can be divided into several segments and for each segment, the material balance can be applied. As reported by Gao (**GAO, 2014**), let us consider a pipeline similar to Fig. 20,

Figure 20 - Example of a pipeline, where rates are calculated at nodes for a black oil formulation. From (**GAO, 2014**).

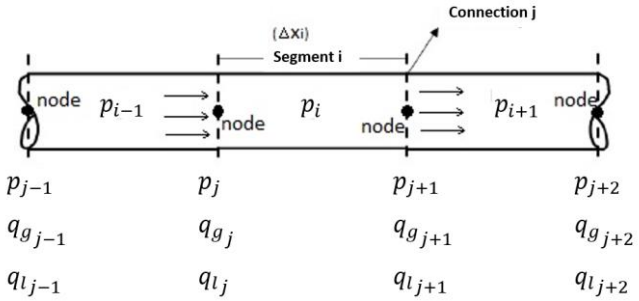

For the system above, in each segment, we can write

$$\text{Mass}_{in} - \text{Mass}_{out} = \text{Mass}_{Accumulation} \tag{4.2}$$

where, the accumulation term on the right-hand side can be represented by the holdup. Hence, for the liquid and gas flow, it is going to be

$$\tilde{q}_{lin} - \tilde{q}_{lout} = V_{segment} \frac{\partial}{\partial t}\left(y_l \rho_l\right) \tag{4.3}$$

$$\tilde{q}_{gin} - \tilde{q}_{gout} = V_{segment} \frac{\partial}{\partial t}\left(y_g \rho_g\right) \tag{4.4}$$

where, $V_{segment}$ is the volume of each segment of pipeline and the parameter, $y_p (p = l; g)$ indicates the holdup for each phase. According to Fig. 20, subscript i indicates the properties of fluid within the segment, while subscript j indicates the properties of the fluid at the interface between two segments. Assuming the length and area of each segment as Δx and A, Eqs. 4.3 and 4.4 can be rewritten for each phase in the following form:

$$\tilde{q}_{wj} - \tilde{q}_{wj+1} = \Delta x_i A_i \frac{\partial}{\partial t}\left(y_w \rho_w b_w\right)_i \tag{4.5}$$

$$\tilde{q}_{oj} - \tilde{q}_{oj+1} = \Delta x_i A_i \frac{\partial}{\partial t}\left(y_o \rho_o b_o\right)_i \tag{4.6}$$

$$\tilde{q}_{gj} - \tilde{q}_{gj+1} = \Delta x_i A_i \frac{\partial}{\partial t}\left(y_g \rho_g b_g + R_s y_o \rho_o b_o\right)_i \tag{4.7}$$

where b is the volume factor of each phase and R_s is the solution gas in the oil phase. It should be noted that according to Gao's notation, the holdup and volume factor of each phase has to be determined based on the average pressure at interfaces of the segment or mathematically speaking

$$p_i = \frac{p_j + p_{j+1}}{2} \tag{4.8}$$

By applying time-scale discretization on Eqs. 4.5, 4.6, and 4.7, flow rate change with time within each timestep can be calculated. For example, for the oil phase, a discretized equation with respect to time and after dividing by density is given by

$$q^*_{oj} - q^*_{oj+1} = \frac{\Delta x_i A_i}{\Delta t} \frac{\partial}{\partial t}\left(\left[y_o b_o\right]^{n+1} - \left[y_o b_o\right]^n\right)_i \tag{4.9}$$

However, since the velocity of flow in the surface facility network is faster than in the porous media, it is common to assume the system is at steady-state condition. As a result, the right-hand side of the above equations will be equal to zero. For further discussion, readers can refer to Gao's dissertation (**GAO, 2014**) which explains the mathematical aspects of coupled surface and subsurface models for black-oil models with more details.

4.6.2.2. Compositional formulation

Similar to the previous formulation, Olivares (**OLIVARES, 2015**) presented a continuity equation for component i and water in a pipe segment, including the accumulation term. The advantage of using this method is that it can be applied for any component and if the corresponding phase behavior of the system is determined adequately, other chemicals, such as inhibitors, can also be modeled with this formulation. Hence, this method is more precise than the previous one. For example, Fig .

21 shows the effect of inhibitors injection on the bottom hole pressure as an advantage of compositional modeling over other formulations.

Figure 21 - Different calculated values of BHP value as a function of inhibitors injections based on compositional modeling. From (**OLIVARES, 2015**)

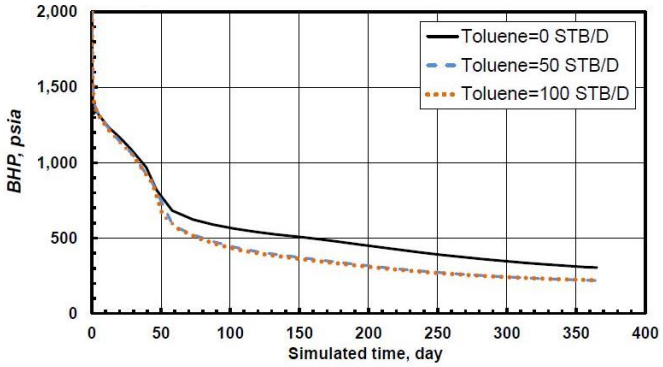

The mathematical expression for continuity equation, with accumulation term of component i and water in a surface network, are as follows:

$$\nabla.\left[A\left(\bar{y}_o x_i \tilde{\rho}_o u_o + \bar{y}_g y_i \tilde{\rho}_g u_g\right)\right] = V_{segment}\frac{\partial}{\partial t}\left(F_i\right) - \dot{n}_{i_{s/s}}, \quad \text{i=1 to } n_c \tag{4.10}$$

$$\nabla.\left[A\bar{y}_w \rho_w u_w\right] = V_{segment}\frac{\partial}{\partial t}\left(W\right) - \dot{m}_{w_{s/s}} \tag{4.11}$$

where A is the segment connection area; $\bar{y}_o$, $\bar{y}_g$ and $\bar{y}_w$ are oil, gas, and water volumetric holdups; x_i and y_i are liquid and vapor molar compositions of component i respectively; $\tilde{\rho}o$, and $\tilde{\rho}g$ are oil and gas molar densities; ρw is water density; uo, ug, and u_w are oil, gas and water superficial velocities; $Vseg$ is segment volume; F_i is number of moles of component i per unit volume; W is mass of water per unit volume; $\dot{n}_{is/s}$ is the net molar rate of component i from sources and sinks; $\dot{m}_{ws/s}$ is the net water mass rate from sinks and sources; nc is the number of hydrocarbon components. Fig. 22 shows an example of the surface pipeline and tubing with 23 segments and 24 connections spanning from bottom hole reference depth to separator, applying the above equation. Note that for such a network, the diameter and length of each section have to be user specified. Hence, the area and length of each segment for equation 4.10 can be determined.

Figure 22 - Surface facility pipeline and tubing with 23 segments and 24 connections spanning. From (**OILVARES**, 2015)

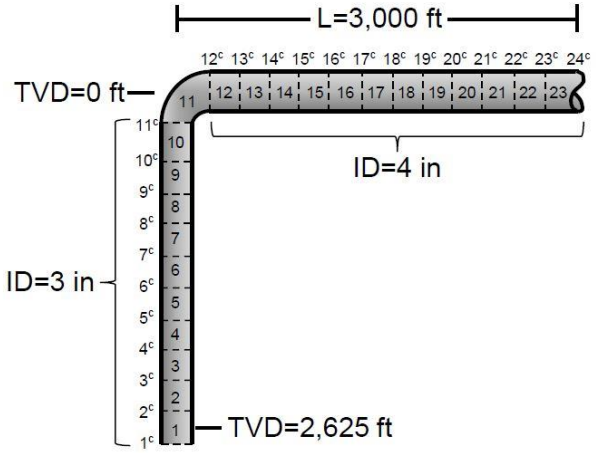

Also, it worth mentioning that the UTWELL simulator is using the same configuration, but the simulator can only evaluate fluid properties up to the wellhead (**SHRDEL, 2013**). Since this method of solving surface facility is not the objective of this dissertation, the additional information regarding phase behavior and how to assemble equations are not discussed in detail here.

4.6.2.3. Surface facility as an extension of the reservoir model

The hydraulic relationship is the last form of the continuity equation regarding the fluid flow in the network. This method of expressing continuity equation is easier than the previous methods and seeks to treat the surface facility network similar to reservoir grid blocks. Figs 23 and 24 show a conceptual and a commercial application, respectively, where the network structure is treated as an extension of the reservoir grid blocks.

Figure 23 - The conceptual schematic of the surface facility network as an extension of the reservoir grid blocks. From (**WATTS et al., 2010**).

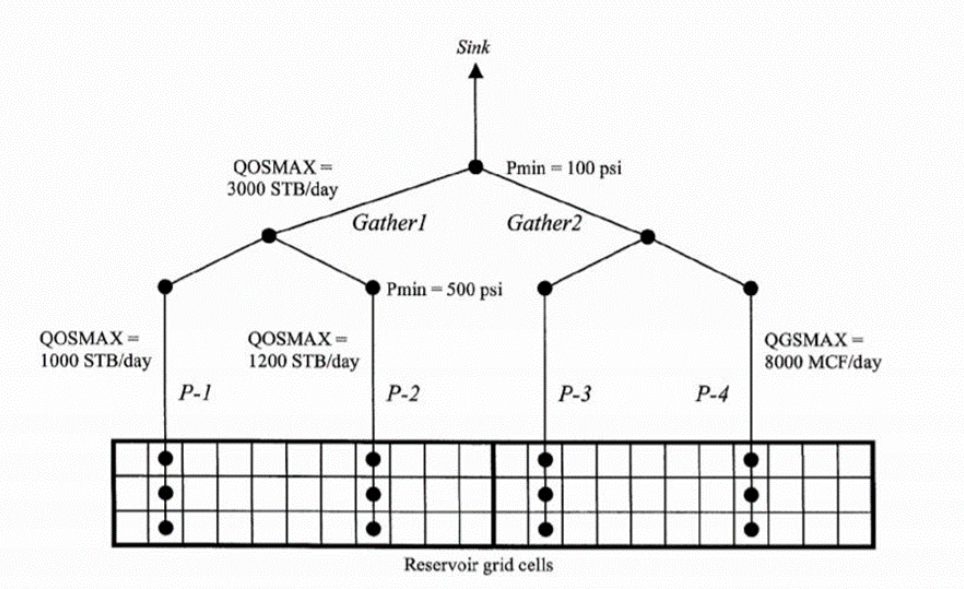

Figure 24 - Example of SurfNet^{TM} Software, from Nexus simulator package that the surface facility nodes are solved as an extension of the reservoir model (**NEXUS® MANUAL**).

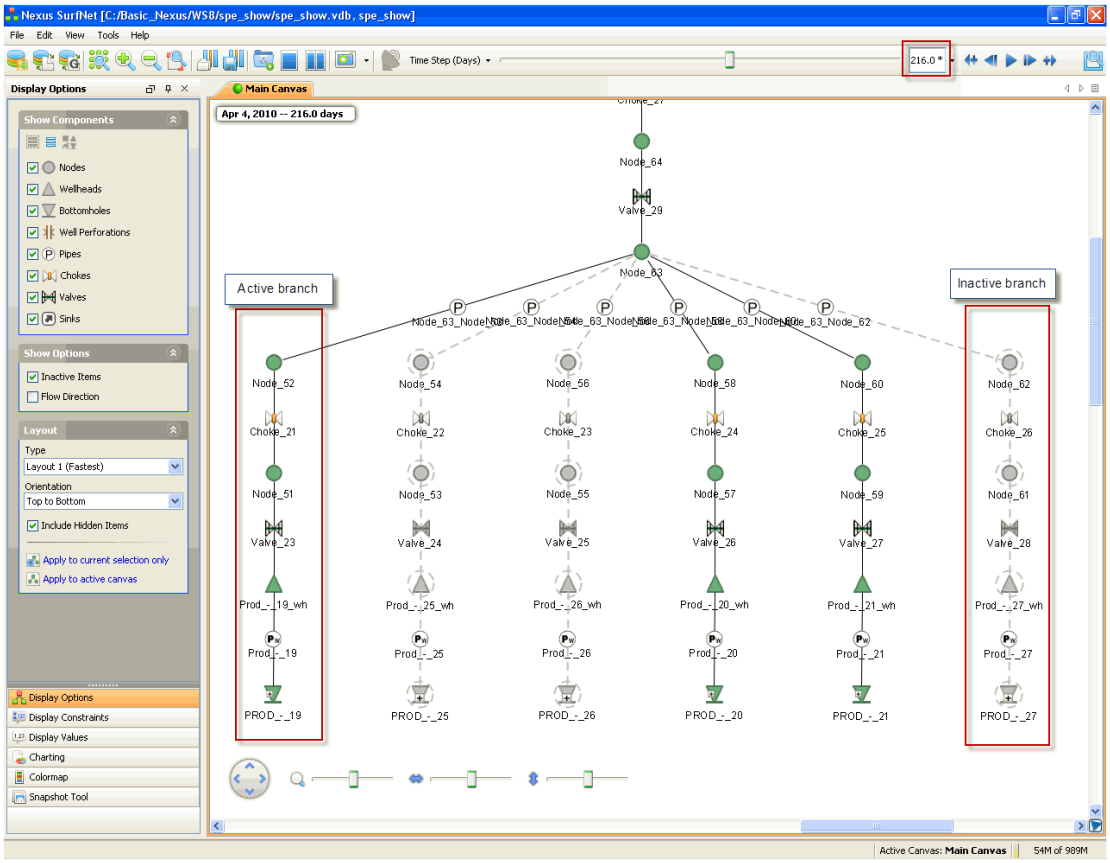

In this method, the perforation is treated as a connection and, as discussed in section 4.3, the separator pressure is constant and fixed. By using this method, the amount of rate is directly related to the pressure difference of each piece of equipment and the pressure profile is not solved for each segment, alongside the pipeline or tubing. The nodes and connections are treated as having no accumulation volume, so the network flow computations are at a steady-state. Streams merge and split at nodes and the nodes are governed by their mass balance equations. Pressures are defined at nodes and flow rates at connections. Thus, pressure drops occur in the connections. Herein, what matters are only the upstream pressure, downstream pressure and flow rate between them. Suppose a simpler network system reported by Shiralkar et al (**SHIRALKAR et al.; 2005**), represented by Fig. 25, with two wellhead pressures (p_1,p_2), a manifold (p_3) and one separator (p_4). For component i, the flow rate between node 1 and 3 is passing through connection 1, the flow rate between node 2 and 3 is passing through connection 3 and the flow rate between nodes 3 and 4, from the manifold to the separator, is passing through connection 3.

Figure 25 - A simple surface facility network consisted of two wellheads that are connected at the manifold and separator. From (**SHIRALKAR et al.; 2005)**

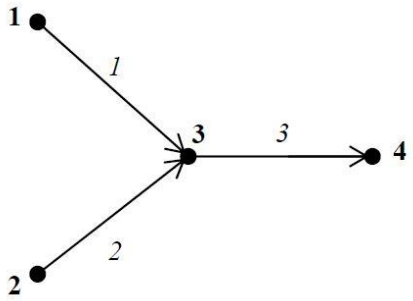

For this system, hydraulic relationships are used to calculate the mass flow rates between nodes in the following format:

$$F\left(\vec{q}, P_{in}, P_{out}\right) = 0 \tag{4.12}$$

The hydraulic relationship can be classified into two categories, flow tables, and flow equations. There is a difference between their shape, but the calculation logic is similar. The format of flow equation is given by

$$\vec{q} = F\left(P_{in}, P_{out}\right) \tag{4.13}$$

And the format of flow table is given by

$$P_{in} = F(\vec{q}, P_{out}) \tag{4.13}$$

We will discuss the flow tables in more detail in the next chapter. The following is some extra information about the flow equations. First of all, the amount of flux in flow equation is assumed to be linear, with respect to the number of components. For example, Watts *et al*. (**WATTS et al.; 2010**) have suggested, for two component fluids, the shape of the equation that works with a linearized flow equation is as follows:

$$-cP_{in} - P_{out} + \alpha q_1 + \beta q_2 = d \tag{4.15}$$

where α and β are rate coefficients, d is the right-hand side coefficient and c is unity or close unity. One of the disadvantages of this method is that flow equations or the method of their generation are not explained well in the literature. For example, for the network of Fig. 25, Shiralkar et al (**SHIRALKAR et al.; 2005)** reported the following flow equations for two components flow. The flow rate of component 1 in connections 1 and 2

$$q_{1,1} = 5(p_i - p_3) \tag{4.16}$$

The flow rate of component 2 is

$$q_{2,1} = 15(p_i - p_3)\text{, (for i=1 and 2)} \tag{4.17}$$

The pressure drops across connection 3 is

$$p_3 - p_4 = 0.02\, q_{1,3} + 0.03\, q_{2,3} \tag{4.18}$$

However, it is not clear how these coefficients are obtained[2]. The final information about the flow equation is that the unit of these equations should be selected carefully. Recalling Eq. 4.15, Litvak and Darlow (**LITVAK, DARLOW; 1995**) reported, the rate in terms of molar rates of hydrocarbon component, while Watts *et al*. (**WATTS et al.; 2010)** report them in terms of black oil model with unit of STB/D. Hence, before using the hydraulic relationship, the standard amount of the rate has to be defined, transparently.

[2] In this work, the hydraulic relationship is selected as the surface facility option of the UTCOMPRS simulator per Petrobras request.

4.6.3. Primary variables and method of solving surface facility models

Similar to reservoir models, once the method of solving the surface facility and its required equations are determined, it has to be clarified that these equations and models have to be solved with respect to specified variables. For example, in the case of black oil, the primary variables are pressure and rates of oil, water and gas. But for compositional modeling, Olivares (**OLIVARES, 2015)** reported six primary variables and implemented the first five of them:

1- Natural logarithm of equilibrium ratio;
2- Network pipe segment pressure;
3- Moles of component i per segment volume;
4- Mass of water per segment volume;
5- Vapor molar fraction;
6- Fluid velocity at connection.

In terms of hydraulic relationships, Wang *et al*. (**WANG et al.; 2015**) reported, pressure and component composition, while Shiralkar and his coworkers (**SHIRALKAR et al.; 2005)** reported pressure and rate as the primary variables. Hence, in general, three primary variables can be considered for a hydraulic relationship, pressure, rates and compositions which can be related to rate by Eq. 4.19.

$$Z = \frac{\sum_{i=1}^{Nin} q_{c,i}}{\sum_{i=1}^{Nin} q_{T,i}} \tag{4.19}$$

where $q_{c,i}$, $q_{T,i}$, and Z are component molar rate, total molar rate and molar fraction (composition), respectively. Readers can refer to the reports of Cao *et al*. (**CAO et al.; 2015**) for the mathematical details of the above equation, which holds two important and practical information. First, the component molar rate of each connection is the product between the total molar rate of that connection and the component inflow fraction at the upstream node of the connection. Second, the hydraulic relationships seem to treat the fluid formulation neither compositional nor black-oil, but rather something between them, *i.e*., semi-compositional. Also, it is important to mention that in all of the work that

reported hydraulic relationships, the temperature effect was not discussed. After selecting the primary variables, a method of solving the equation and their derivatives with respect to those variables has to be determined. The following section describes two methods of solving the surface facility models.

4.6.3.1. Newton-Raphson iterative procedure

In terms of the numerical solution, the most common method for solving nonlinear equations is the Newton-Raphson's iterative procedure. Below is a short description of two independent variables, x, and y.

Consider a set of equations given by

$$F(x, y) = 0 \tag{4.20}$$

$$G(x, y) = 0 \tag{4.21}$$

Based on the number of independent variables, the same number of equations (F, G, H, L, etc) are required. Assuming (x_0,y_0) as an approximate solution, the solution that satisfies both equations is searched by applying the Taylor series truncated at the first order terms, as indicated below.

$$F\left(x_0 + \Delta x_0, y_0 + \Delta y_0\right) = F\left(x_0, y_0\right) + \Delta x \frac{\partial F}{\partial x}\left(x_0, y_0\right) + \Delta y \frac{\partial F}{\partial y}\left(x_0, y_0\right) + \ldots\ldots \tag{4.22}$$

$$G\left(x_0 + \Delta x_0, y_0 + \Delta y_0\right) = G\left(x_0, y_0\right) + \Delta x \frac{\partial G}{\partial x}\left(x_0, y_0\right) + \Delta y \frac{\partial G}{\partial y}\left(x_0, y_0\right) + \ldots\ldots \tag{4.23}$$

Assuming that x+ Δx, y+Δy are the search roots, we can write

$$F\left(x_0 + \Delta x_0, y_0 + \Delta y_0\right) \cong F\left(x_0, y_0\right) + \Delta x \frac{\partial F}{\partial x}\left(x_0, y_0\right) + \Delta y \frac{\partial F}{\partial y}\left(x_0, y_0\right) \cong 0 \tag{4.24}$$

$$G\left(x_0 + \Delta x_0, y_0 + \Delta y_0\right) \cong G\left(x_0, y_0\right) + \Delta x \frac{\partial G}{\partial x}\left(x_0, y_0\right) + \Delta y \frac{\partial G}{\partial y}\left(x_0, y_0\right) \cong 0 \tag{4.24}$$

Therefore,

$$\Delta x \frac{\partial F}{\partial x}\left(x_0, y_0\right) + \Delta y \frac{\partial F}{\partial y}\left(x_0, y_0\right) \cong -F\left(x_0, y_0\right) \tag{4.26}$$

$$\Delta x \frac{\partial G}{\partial x}\left(x_0, y_0\right) + \Delta y \frac{\partial G}{\partial y}\left(x_0, y_0\right) \cong -G\left(x_0, y_0\right) \tag{4.27}$$

Now there are two equations and two unknowns solving for Δx and Δy that can be written in a matrix form as

$$\begin{pmatrix} \dfrac{\partial F}{\partial x} & \dfrac{\partial F}{\partial y} \\ \dfrac{\partial G}{\partial x} & \dfrac{\partial G}{\partial y} \end{pmatrix}^{k} \begin{pmatrix} \Delta x \\ \Delta y \end{pmatrix}^{k+1} = -\begin{pmatrix} F(x,y) \\ G(x,y) \end{pmatrix}^{k} \tag{4.28}$$

Regarding this notation, for a coupled surface and sub-surface model, Jing (**JING, 2017**) presented the schematic of the global Jacobian matrix and its four sub-categories as shown in Fig. 26.

Figure 26 - Global Jacobian matrix and its four sub-categories. From (**JING, 2017**).

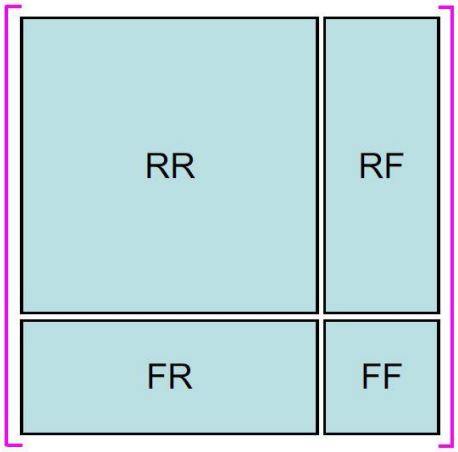

where the terms that appear in Fig. 26 are respectively denoted by:

- RR as the derivatives of reservoir equations with respect to reservoir variables;
- RF as derivatives of reservoir equations with respect to facility variables;
- FR as derivatives of facility equations with respect to reservoir variables;
- FF as derivatives of facility equations with respect to facility variables.

One of the failures of the above classification is that it is not clear whether to consider the wellbore as a part of the reservoir or the facility. Because of that, to achieve a more precise set of equations, one can redefine the above system into a more detailed Jacobian matrix as shown in Fig. 27.

Figure 27 - Global Jacobian matrix and its nine sub-categories

$$\begin{pmatrix} RR & RW & RF \\ WR & WW & WF \\ FR & FW & FF \end{pmatrix}$$

where the terms that appear in Figure 4.15 are respectively denoted by:

- RR is derivatives of reservoir equations with respect to reservoir variables;
- RW is derivatives of reservoir equations with respect to wellbore variables;
- RF is derivatives of facility equations with respect to reservoir variables;
- WR is derivatives of wellbore equations with respect to reservoir variables;
- WW is derivatives of wellbore equations with respect to wellbore variables;
- WF is derivatives of wellbore equations with respect to facility variables;
- FR is derivatives of Facility equations with respect to reservoir variables;
- FW is derivatives of facility equations with respect to wellbore variables;
- FF is derivatives of facility equations with respect to facility variables.

Since the facility and reservoir do not have direct connection, FR and RF are equal to zero. Accordingly, the final shape of a fully coupled model is presented in Fig. 28.

Figure 28 - Modifications for the global Jacobian matrix and its seven sub-categories. From (**OLIVARES, 2015)**.

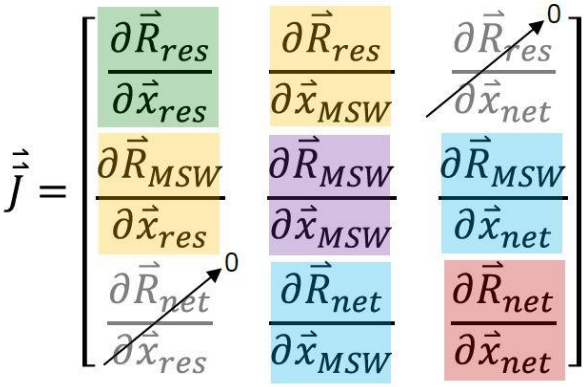

In the next chapter, we will explain one additional treatment for computation of the Jacobin matrix with the Gauss elimination method, but what has been said here is the common method of assembling and solving the coupled reservoir, well, and surface facility.

4.6.3.2. Assembling algebraic equations

One of the difficulties of using hydraulic relationships is that the process of assembling equations and models of the surface network has not been described in the literature. There is only one patent that describes a very simple system. Hence, the following will show the example illustrated by the patent of Watts *et al*. (**WATTS et al.; 2010**).

Suppose a single well is connected to a surface facility network that includes a separator and wellhead, as illustrated in Fig. 29.

Figure 29 - A single well connected to a separator and wellhead.
From (**WATTS et al.; 2010**)

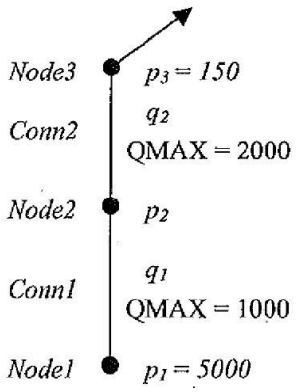

As it can be seen, the total system consists of three nodes and two connections. In this system, reservoir pressure (pressure at node 1), and pressure at the separator (node 3) are fixed and their values are 5000 psi and 150 psi, respectively. The fluid of the network has just one hydrocarbon component and since the unit of the system is not mentioned in the original work, herein we assume it is mole per day. Regardless of the maximum productivity of the reservoir, two restrictions are imposed: (1) on the tubing (conn1) by downhole choke and (2) on the surface flow line (conn2) by surface choke, which are 1000, 2000 mole per day, respectively. For this system, the unknown parameters are rate inside tubing (or conn1) q_1, rate inside flow line (or conn2) q_2, and pressure at the wellhead, p_2.

For such a condition, the following equations can be written:

$$q_1=1000 \tag{4.29}$$

$$q_2=2000 \tag{4.30}$$

And based on the continuity equation, there is no accumulation in the surface facility. Hence, the third equation is

$$q_1-q_2=0 \tag{4.31}$$

Herein is important to stress two important aspects of the above equations:

1- The three above equations are contradictory and cannot all be satisfied;

2- The wellhead pressure does not appear in any of the above equations.

Now let's order the unknown as q_1, q_2, and p_2. Now, we can write a series of algebraic equations and put them in a matrix form as

$$\begin{pmatrix} 1 & 0 & 0 \\ 0 & 1 & 0 \\ 1 & -1 & 0 \end{pmatrix} \begin{pmatrix} q_1 \\ q_2 \\ p_2 \end{pmatrix} = \begin{pmatrix} 1000 \\ 2000 \\ 0 \end{pmatrix} \tag{4.32}$$

Before we demonstrate how to solve this matrix, there is a very important issue that has to be clarified. We can rewrite the above matrix, in the following format:

$$(J)\times(U)=(R) \tag{4.33}$$

where J, U, and R stand for Jacobian, unknowns, and residuals. Although the shape of these matrices is quite similar to Equation 4.28, the method of solving and assembling them is completely different from Newton Raphson's iterative procedure.

Observing the coefficients in the matrix of Eq. 4.36, we can clearly see that the matrix is singular and therefore cannot be inverted. The main clue to solve this problem is the QMAX constraint at Conn2. This constraint can be replaced since its value is greater than the QMAX constraint at Conn1. In other words, the rate must be equal to or less than the smaller of the two QMAX constraints, which in this example is QMAX=1000 at Conn1. To do so, we will replace the second equation (q_2=2000) with hydraulic equations. For conn2, let us consider a hydraulic equation as follows:

$$-P_2 + P_3 + b_2 q_2 + c_2 = 0 \tag{4.34}$$

where b and c are constants determined by the hydraulics correlation properties, such as length, diameter and roughness of the pipeline. By replacing the rate equation, the linear system of Eq. 4.32 is be transformed to

$$\begin{pmatrix} 1 & 0 & 0 \\ 0 & 1 & 0 \\ 0 & b_2 & -1 \end{pmatrix} \times \begin{pmatrix} q_1 \\ q_2 \\ p_2 \end{pmatrix} = \begin{pmatrix} 1000 \\ 2000 \\ -c_2 - 150 \end{pmatrix} \tag{4.35}$$

and based on the values of b_2 and c_2, the above linear system can be solved.

Here, with another example, we will show the above method for a system that does not contain any restrictions, but it is a little more complex. Let us consider the shape of Fig. 25. Here, for sake of simplicity, we assume the system is working with one component fluid and its units are mole per day. For this system, the wellhead pressure and pressure of the separator are fixed (green color), and the corresponding flow equation for each connection are given by

$$\text{PWH1}=2000 \text{ psi} \tag{4.36}$$

$$\text{PWH2}=1500 \text{ psi} \tag{4.37}$$

$$\text{PSEP}=50 \text{ psi} \tag{4.38}$$

$$q_{c1}=5(\text{PWH1-PMF}) \tag{4.39}$$

$$q_{c2}=3.5(\text{PWH2-PMF}) \tag{4.40}$$

$$q_{c3}=8.21(\text{PMF-PSEP}) \tag{4.41}$$

Here, the unknowns are the pressure of manifold and rate in the three connections. For each connection also the corresponding hydraulic equations are specified, but one can choose any sort of coefficients. Here, the coefficients have been selected in the way that the pressure of the manifold would be the same value that was obtained in Shiralkar et al. (**SHIRALKAR et al.; 2005)** for two hydrocarbon components (920 psi). Equation 4.42 shows the Jacobian of the network presented in Fig 25.

$$\begin{pmatrix} 1 & 0 & 0 & 0 & 0 & 0 & 0 \\ 0 & 1 & 0 & 0 & 0 & 0 & 0 \\ 0 & 0 & -8.21 & 8.21 & 0 & 0 & 1 \\ 0 & 0 & 0 & 1 & 0 & 0 & 0 \\ -5 & 0 & 5 & 0 & 1 & 0 & 0 \\ 0 & -3.5 & 3.5 & 0 & 0 & 1 & 0 \\ 0 & 0 & 0 & 0 & 1 & 1 & -1 \end{pmatrix} \times \begin{pmatrix} PWH1 \\ PWH2 \\ PMF \\ PSEP \\ q_{c1} \\ q_{c2} \\ q_{c3} \end{pmatrix} = \begin{pmatrix} 2000 \\ 1500 \\ 0 \\ 50 \\ 0 \\ 0 \\ 0 \end{pmatrix} \tag{4.42}$$

For the above matrix, two explanations are required. First, for the pressure of the manifold, we used the hydraulic equation of connection three. Second, for the rate at connection number three, we assume it is equal to the summation of rates from

connections 1 and 2. Solving the above equation will give us the result presented in Eq. 4.43.

$$\begin{pmatrix} PWH1 \\ PWH2 \\ PMF \\ PSEP \\ q_{c1} \\ q_{c2} \\ q_{c3} \end{pmatrix} = \begin{pmatrix} 2000 \\ 1500 \\ 937.19 \\ 50 \\ 5314 \\ 1969.9 \\ 7283.9 \end{pmatrix} \tag{4.43}$$

As it can be seen, the calculated pressure of the manifold is equal to 937.19, which is a reasonable value, since it is between the separator and wellhead pressures. Table 3 shows five different studies to demonstrate the effect of the separator pressure as the boundary condition.

Table 3 - Effect of different separator pressure on the rates and the manifold pressure

	Case # 1	Case # 2	Case # 3	Case # 4	Case # 5
PSEP	0	50	900	1500	2500
PMF	912.627	937.193	1354.82	1649.61	2140.93
q_{c1}	5436.86	5314.03	3225.91	1751.94	-704.67
q_{c2}	2055.8	1969.82	508.139	-523.64	-2243.3
q_{c3}	7492.67	7283.86	3734.05	1228.31	-2947.9

As presented in Table 3, the first case study considered the pressure of the separator equal to zero to investigate the maximum potential of this network which is 7492.67 mole per day. Case number 2 and 3 show the higher acceptable separator pressure. By increasing the separator pressure, it acts as a barrier to the flow. In case number 4, the separator pressure is set equal to wellhead pressure number two (PSEP=WHP2). As it can be seen, the manifold pressure for this case is equal to 1649.61 psi, where connection number one is acceptable but for connection number two it is not, and, as can be expected, the flux becomes negative -523.64 towards wellhead number two. The last case study shows the situation, in which the pressure is set at a higher level than both wellhead pressures and as can be seen for both connections, the flux is from the manifold to the

wellhead. This example shows how important it is to select the proper operational condition. Therefore, to have control over the production of the surface facility, there is a need for some restriction devices. The next section will address this issue.

4.7 Restrictions on flow devices through choke valves[3]

As explained earlier, sometimes it is required to put restriction on flow based on the operational condition. Below are some examples of the condition, where the restriction devices are required.

- The flow of the reservoir is higher than the capacity of the processing units;.
- The surface facility is damaged by erosion, corrosion or scale (wax or asphaltene), thus requiring well shut-in and/or workover;
- When there is some fluid contaminated, such as H_2S, requiring the installation of monitoring equipment.

Adjustable equipment refers to equipment, such as chokes, electrical submersible pumps (ESPs), jet pumps, gas lift, and inflow control valves (ICV) that let a production engineer impose multiple operational settings on PPS to control the hydraulic performance of the wells as required (**STANKO, 2021**). For example, Figs. 30 and 31 show the impact of the choke valve when it is fully open or 75% open and the use of ESP to achieve a required specific flow rate.

Figure 30 - Impact of the choke valve on PPS, when it is fully open or 75% open. From (**STANKO,2021**).

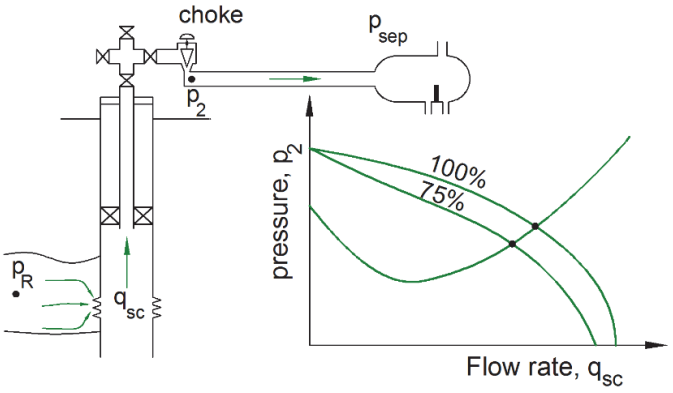

[3] In this work, a new function named **valve_choke.f90** has been developed for UTCOMPRS simulator which works with different choke valve's correlations that is explained in this section.

Figure 31 - The use of ESP to achieve a required specific flow rate.
From (**STANKO,2021**).

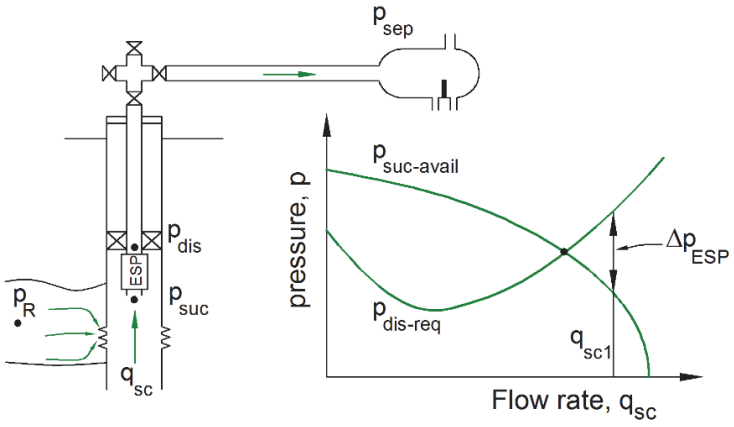

From a mathematical standpoint, the cross point between IPR and tubing intake pressure, similar to Fig. 31 could have a variety of values. This intersection can be used to calculate the steady (natural) flow condition. The bottomhole pressure acquired by IPR should be equivalent to the required pressure estimated by tubing intake pressure at the bottomhole, taking into account the wellbore's physical condition. Hence, the natural flow condition is defined as the pressure and rate at which these criteria are satisfied. The mathematical solution of natural flow is examined in further depth in section 5.8 of this thesis. However, readers might refer to Golan and Whitson Textbook (**GOLAN, WHITSON, 1991**) for a more detailed treatment, which includes the effects of variations in wellhead pressure and gas/liquid ratio on natural point behavior.

To explain the restriction devices, here, let us consider a schematic presented in Fig. 32, where gas or gas-liquid mixtures can flow through a choke.

Figure 32 - Conceptual schematic of the choke value and its relation with up and downstream pressures. From (**ECONOMIDES et al. 2013**).

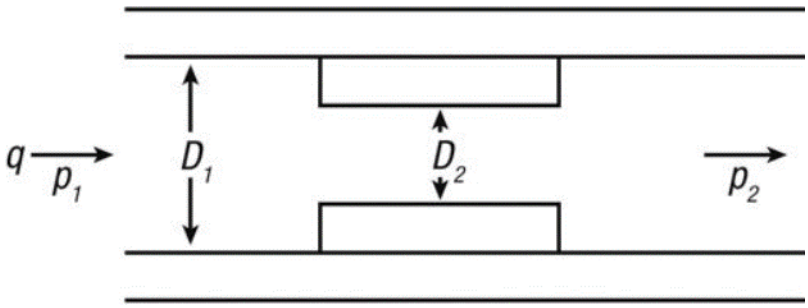

As fluids pass through cross-sectional areas with reduced diameter (D_2), fluid velocity increases. As soon as the velocity reaches sonic velocity in the throat of a choke, the condition is known as "critical," and changes in the pressure downstream of the choke do not affect the flow rate, since the pressure disturbances cannot travel upstream faster than the sonic velocity. In other words, for such a condition, the downstream pressure is independent of the upstream condition, which is dynamic owing to the change of reservoir pressure as the main source of the driving force. Determining whether or not the flow is at the critical condition is the main task for the proper design of choke valves. Fig. 33 shows the relationship between the flowrate through a choke and the ratio of the upstream to the downstream pressure.

Figure 33 - Flow rate through a choke versus the ratio of the upstream to the downstream pressure**.** From **(JANSEN; 2017)**

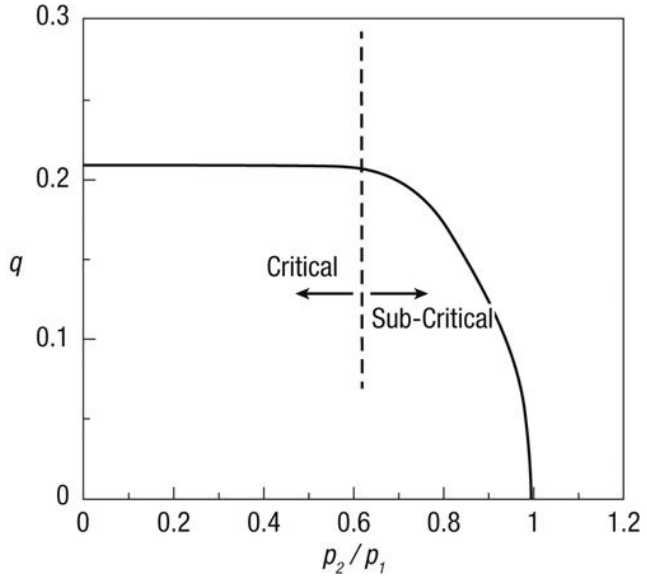

There are several correlations to study gas-liquid flow behavior through choke valves. These correlations have been developed theoretically or empirically by using experimental or field production data and they are referred to as CPR or choke performance relationships, similar to Eq. 4.44.

$$q_l = \frac{A.P_{wh}.d^C}{GOR^B} \tag{4.44}$$

where q_l is the liquid rate; WHP is the wellhead pressure; d is the choke diameter; A, B, and C are coefficients. Table 4 shows different empirical coefficients for two-phase flow (**MIRZAEI, SALAVATI, 2013**).

Table 4 Different correlations proposed for the choke performance relationships

Correlation	*A*	*B*	*C*
Gilbert	0.100000	0.546	1.89
Baxendell	0.104600	0.546	1.93
Ros	0.057470	0.500	2.00
Achong	0.261780	0.650	1.88
Pilehvari	0.021427	0.313	2.11

According to Eq. 4.44, for a given flow rate, **valve_choke.f90** function will calculate the wellhead pressure required for surface facility. Then, based on this wellhead pressure, and its downstream pressure, the corresponding flow table can be used.

CHAPTER 5

WELLBORE ENVIRONMENT AND FLUID FLOW IN TUBING

5.1. Dynamic wellbore behavior

The dynamic wellbore behavior heavily depends on the production mechanism of the reservoir, how the wellbore is completed in the subsurface reservoir and the limitations of the surface facility equipment. For a vertical producing well, a linear relationship is the prevailing mathematical expression between flow rate (toward the well) and pressure drawdown, if the fluid is undersaturated. This relationship is illustrated by the Darcy equation, mathematically expressed by Eq. (5.1):

$$q = J\Delta P \tag{5.1}$$

where q is flow rate, J is productivity index (or PI) and ΔP is pressure drop between bottom hole and average reservoir pressure.

Well testing associated with production are important means of assessing flow potential. Production testing and bottom hole pressure evaluation should be performed by engineers to see if the production from the wellbore is at the best possible conditions or if some remediation procedure or workover is required. Workover refers to the series of processes of pulling and replacing completion or production hardware to extend the life of a well.

As the daily duties of an oil and gas maintenance managers and field operator's responsibilities, each producing well should be evaluated by measuring operational parameters, such as liquid flow rate, gas-liquid rate, water cut and gas lift operation. The operational parameters and the flowing tubing head pressure (FTHP) are recorded through separators on the surface. During the production tests of each well, individual production (or injection) volumes are also required to understand the fluid dynamics and frontal displacement inside the reservoir, because it can be used to check whether the developed physical models are satisfying the historical field data. Redefining pressure boundaries, the depth of water-oil contact or gas-oil contact, grid refinement and infill drilling are some examples of reservoir simulation activities that are depended on the accuracy of FTHP and production profiles (liquid flow rate, gas-liquid rate, water cut, and gas lift). It is important to mention that all this information is representing the surface

conditions, but it would be desirable that bottom hole pressure is also collected. The BHP can be used to calculate permeability and formation damage near the wellbore. The BHP can also be determined in two different modes, static or flowing conditions (SBHP, FBHP). The SBHP is mainly used to determine the reservoir pressure near the wellbore, while the FBHP is useful for PI calculation or detecting anomalies, such as faults or fractured regions. Takacs (2018) (**TKACS, 2018**) demonstrated the mathematical relation between SBHP and FBHP as follow

$$FBHP = SBHP - \frac{q}{PI} \tag{5.2}$$

Note that this equation should not be confused with Equation 5.1, because in that equation the ΔP is the pressure difference between reservoir pressure and FBHP. Also, the fundamental design of electrical submersible pumps is based on the FBHP, as reported in Takacs work (**TKACS, 2018**). Fig. 34 shows the details of a producing well, the location of FTHP, choke valve, manifold and separator.

Figure 34 - Details of a producing well, the location of FTHP, chock valve, manifold and separator. From (**JAHN et al., 1998**)

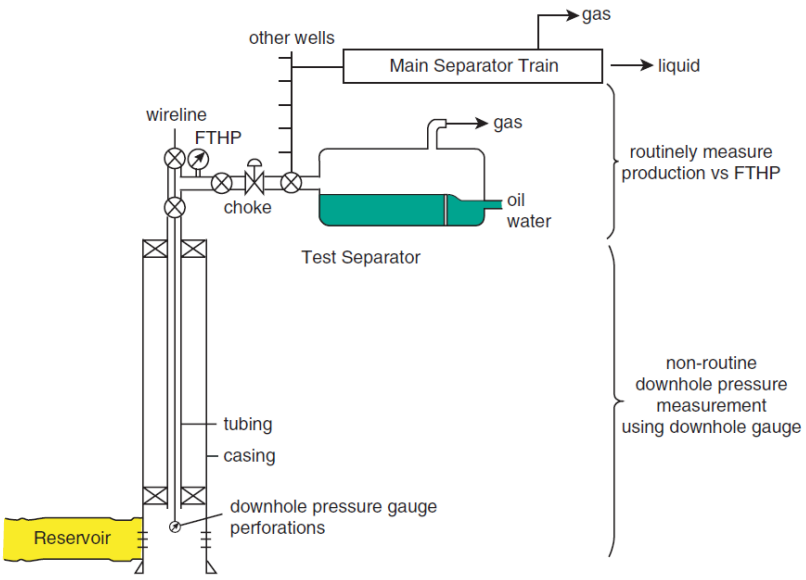

5.2. Coupling configuration

Whether to consider the wellbore as a part of the surface, or as an element of sub-surface facility, is a practical issue that has been discussed vastly in the literature. This is because the bottom hole pressure and wellhead pressure are obtained at a fixed location. Hence, from this perspective, they can be considered as boundary conditions for each system.

Integration procedure, the coupling location, the nature of the algorithm (explicit or implicit) and the type of fixed boundary conditions for exchanging information between the programs are some issues that are related to the type of coupling or coupling configuration (**BARROUX et al., 2000**). It is noticeable to mention that according to Tingas et al. (**TINGAS et al.; 1998**), coupling at the wellhead reduces accuracy in wellbore hydraulics calculations. Fig. 35 shows a coupling configuration at the wellhead. The first section of the network is starting from the node at the wellhead (J2). For such a system, convergence of the integrated model is checked in terms of wellhead pressure**.**

Figure 35 - Coupling configuration where the coupling point is at the wellhead level. From (**BARROUX et al., 2000).**

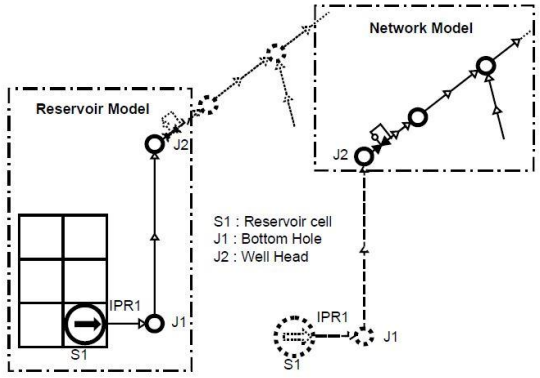

The second type of coupling configuration is at bottomhole (S1). Fig. 36 illustrates the second type of coupling configuration.

Figure 36 - Coupling configuration where the coupling point is at the bottom hole level. From (**BARROUX et al., 2000**)

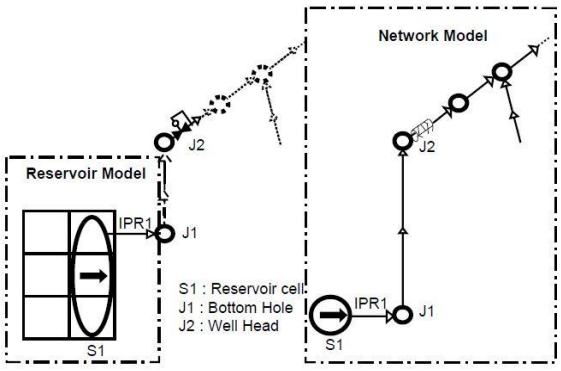

As shown in Fig. 36, the reservoir model is only considered up to the bottom hole pressure node and the network model is also considered as a reservoir cell. These details are very important for the mathematical formulation of the integrated model. More coupling configurations can be found in Barroux et al. (**BARROUX et al., 2000**).

5.3. Gauss elimination method for a coupled linear system

Additional information about coupling between two systems, surface and subsurface models, is reported by Cao *et al.*(**CAO et al.; 2015**) As noted by Cao, the general fully implicit formulation of the integrated system can be represented in the following format.

$$\begin{pmatrix} RR & RW & RF \\ WR & WW & WF \\ FR & FW & FF \end{pmatrix} \tag{5.3}$$

However, instead of solving a fully coupled approach one can apply the Gauss elimination method and have two sub-systems as follows:

$$\begin{pmatrix} RR & RW \\ WR & WW \end{pmatrix} \tag{5.4}$$

$$\begin{pmatrix} WW & WF \\ FW & FF \end{pmatrix} \tag{5.5}$$

This highlights the importance of the wellbore and its treatment. Here it is important to emphasize that the reservoir and facility are interacting through the well. Therefore, it is important to consider the wellbore as a part of the surface or subsurface facility. Compared to the fully implicit formulation, this Gauss elimination method is known as weak coupling.

5.4. Wellbore boundary conditions

The wellbore boundary condition should be defined precisely. Fig. 37 shows two boundary conditions for tubing **(SHIRDEL, 2013)**. In both situations, the wellhead is considered as a pressure node at the tubing top. The difference is at the bottom hole condition. On the first case, the boundary condition of the bottomhole is treated as a pressure node. On the second case, the bottom hole is considered as a mass source node.

This means that the mass that is coming from the reservoir has to enter the bottom hole, due to the continuity equation.

Figure 37 - different wellbore boundary conditions. From **(SHIRDEL, 2013).**

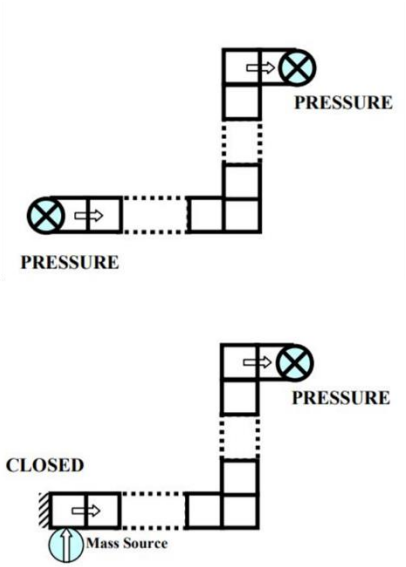

For the horizontal well, the same methodology can be used with some extension of external nodes as shown in Fig. 38 **(TRINA, JOHANSEN, 2012)**. However, this type of well is not considered in this work.

Figure 38 - Boundary condition of a horizontal well as an extended model of vertical wells. From (**TRINA, JOHANSEN, 2012)**

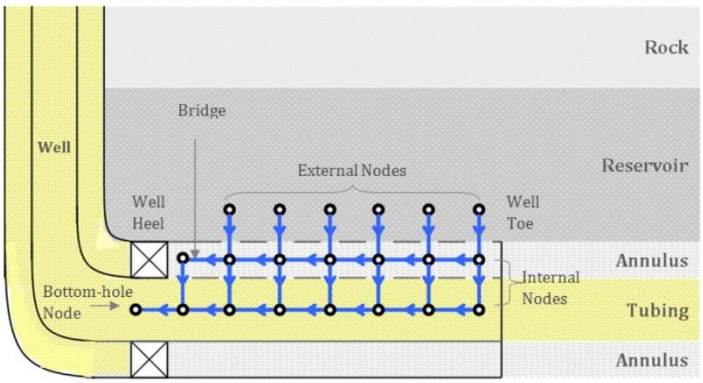

5.5. Type of wellbore treatment

During modeling of integrated PPS, the well section and pressure drop across the tubing are treated differently by simulators. In general, there are three approaches as reported by Holmes et al. **(HOLMES et al., 1998)**: (1) a homogenous flow model that assumes the

same velocities for oil, gas and water phases; (2) the drift flux model, which allows different phases (oil, gas, water) to have different velocities; and (3) a pre-calculated pressure drop table. From a mathematical point of view, each type of tubing treatment can significantly change the set of equations and residuals for a system.

Eq. (5.6) shows the pressure drop across the tubing for a homogeneous model, where the terms of acceleration, elevation, and friction are described by Eq. (4.1).

$$P_{up} - P_{down} - \Delta P_{ac} - \Delta P_{ele} - \Delta P_{fri} = 0 \tag{5.6}$$

The drift flux model expresses gas-liquid slippage as the combination of two mechanisms. The first is due to the non-uniform profiles of gas holdup and flow velocity across the area of the pipe, represented by a profile parameter, C_0. The other mechanism results from the tendency of a gas to rise through the liquid due to buoyancy and it is represented by a drift velocity, v_d. A formulation that combines the two mechanisms is as follows:

$$Vg=C_0V_m+V_d \tag{5.7}$$

The mathematical details of the profile parameter will not be discussed here.

For a pre-calculated pressure drop table

$$BHP(WHP, q_o, q_w, q_g) + H_{w,tab} = 0 \tag{5.8}$$

where $H_{w,tab}$ is the hydrostatic pressure difference between the table bottom hole reference depth and the depth of the top segment node, which is calculated from the mixture density in the top segment. It is important to mention that the basics of a pre-calculated pressure drop table can be generated based on both the homogenous model or drift flux models.

5.6. The background of the flow tables

The concept of using a pre-calculated pressure drop table to determine the pressure profile along the tubing is referred with different terminologies in the literature, such as lift tables (CoFlow simulator), vertical lift performance (Pipesim simulator), Vertical Flow Performance (Tnavigator simulator), Tubing Tables (GEM simulator), Tubing Performance Curves, hydraulic tables and flow tables. We only considered the “flow table” terminology here, because these tables may encompass flow beyond the tubing.

They can be used for any sort of pipeline, including the surface facility networks (**ROSSI et al.; 2017**). And with this perspective in mind, flow tables terminology seems a more general and adequate way of referring to these tools. McAfee (**MCAFEE,1961**) reported a comprehensive analysis of different parameters of flow tables, including gas-injection pressure, formation gas, bottom-hole pressure and valve spacing. Fossmark (**FOSSMARK, 2011**) also provided details of the mathematical equations for pressure gradient calculations of flow tables and he has categorized them into empirical correlations and mechanistic models. Table 5 shows the six types of selectable pressure-gradient prediction methods that exist for Builder (**BULIDER MANUAL, 2019**).

Table 5 - Different types of selectable pressure-gradient prediction methods. From (**BUILDER MANUAL, 2019**)

Method	**Notes**
Beggs-Brill	for all inclinations include upward and downward flow
Mukherjee-Brill	the liquid-holdup correlation is expressed by separate equations for upward and downward flow
Petalas-Aziz	tuned against 5,951 data points from the Stanford Multiphase Flow Database.
Aziz-Govier	for vertical producer
Drift-flux	mechanistic approach for bubble or slug flow, valid for upward flow only
Simplified mixed density	all flow is assumed to occur in the bubble regime.

Fig. 39 shows tubing pressure methodology of the GEM simulator.

Figure 39 - Builder tubing pressure calculator software for the GEM Simulator.

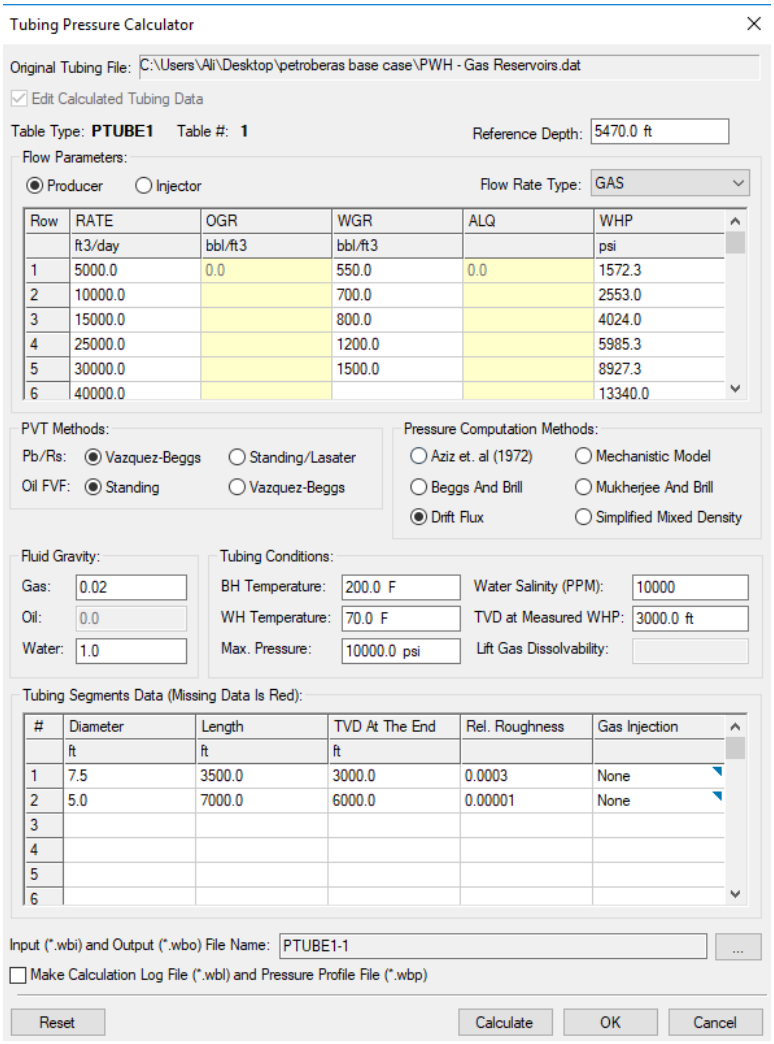

Regardless of which computational method is used, the outcome of this function will be a series of BHPs values as indicated in Fig. 40.

Figure 40 - Example of a pre-calculated table generated by Builder.

```
 *PTUBE1    1                  **tabular tubing data for the producer.
  *DEPTH                       **used with pwellbore option.
   8400.0
  *GOR
   100.0 125.0
  *WCUT
   0.0 0.5
  *OIL
   0.0 10.0 20.0 30.0
  *ALQ
   1.0
  *WHP
   500.2 4964.2 15825.3
  *BHP
** iflo igfr iwfr iadd bhp(1)   bhp(2)   bhp(3)
    1    1    1    1   12002.4  15846.9  19707.9
    2    1    1    1   11776.3  15863.5  19727.8
    3    1    1    1   11765.2  15908.7  19769.8
    4    1    1    1   11914.1  16062.0  19923.1
    1    1    2    1   14594.8  18444.9  22306.9
    2    1    2    1   14440.4  18483.5  22344.5
    3    1    2    1   14506.6  18577.3  22440.5
    4    1    2    1   14872.8  18935.8  22796.8
    1    2    1    1   11018.9  14727.2  18588.3
    2    2    1    1    9277.6  14749.3  18610.3
    3    2    1    1    8069.6  14804.4  18668.3
    4    2    1    1    7860.0  15008.5  18869.6
    1    2    2    1   13501.0  17231.4  21092.4
    2    2    2    1   12074.1  17275.5  21136.6
    3    2    2    1   11152.9  17385.8  19757.6
    4    2    2    1   11472.9  17821.6  21682.6
```

Although the method of BHPs calculation behind the simulator is not described in the manuals, Jackson (**JACKSON, 2017**) explained them with details and provided a MATLAB file to generate the same table and it can be found in Appendix One.

5.6.1. Types of flow tables

As we discussed in Section 4.6.3.2, the general shape of the hydraulic tables is as follows:

$$P_{in} = F\left(\vec{q}, P_{out}\right) \tag{5.9}$$

According to this mathematical expression, three elements, including upstream pressure, downstream pressure and the rate should necessarily be reported in the tables. In general, to the best of the author's knowledge, we can classify four types of flow tables as follows:

Simplified Flow Tables (SFTs): where the information of single-phase flow, upstream pressure, downstream pressures are included.

Advanced Flow Tables (AFTs): where the information of multiphase, gas-oil ratio, water-cut upstream pressure, downstream pressure or any additional pressure nodes are available.

Commercial Flow Tables (CFTs): where upstream pressure, downstream pressures, gas-liquid ratio, liquid rate, water cut and gas lift rate are included. Also, in this class, the flow rate is translated into a series of indices.

Dynamic Flow Tables (DFTs): This is an improved version of CFTs in which, if the table's information isn't sufficient for the running scenario, the table's information is changed using a pipeline simulator. The algorithm and flowchart of how to use them can be found in Zaydullin *et al.* (**ZAYDULLIN et al.; 2019**). We will provide more technical information about how to use the first three types of flow tables during the reservoir simulation discussion in the next chapter.

5.7. Order dependence of the flow calculation in wellbore and surface facility

One of the challenges of using a flow table for the wellbore and surface facility is the order dependence of the flow calculation. To address this issue, suppose the network system that is shown in Fig. 41 As can be seen, nodes number 1 to 4 are bottom hole pressure nodes, nodes numbers 5 and 6 are wellhead pressure nodes, and node numbers 7 and 8 are manifold and separator pressure nodes, respectively.

Figure 41 - Different levels of the flow calculation in wellbore and surface facility. From (**BYER, 2000**)

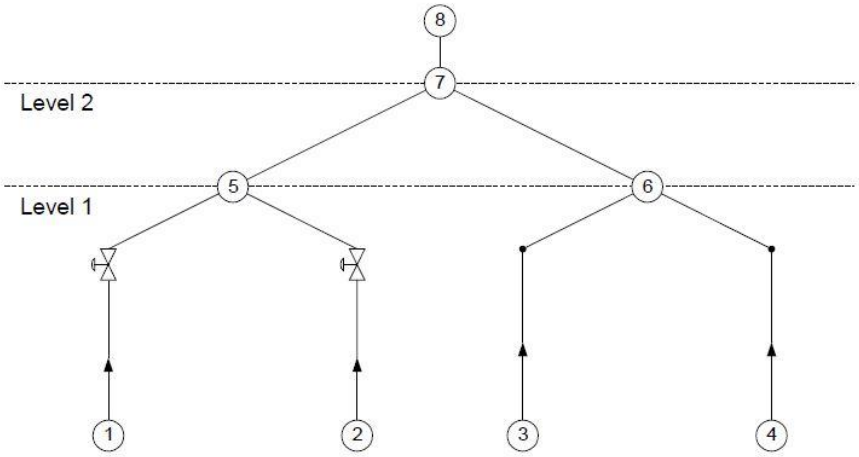

Regarding this configuration and method of solving the system, two considerations should be taken into account. First of all, by changing the numbering order, the arrangement of the mathematical description of the system will change. For example, one may want to solve the pressure drop between nodes 5 and 7 with flow tables and the pressure drop between nodes 7 and 6 with an empirical correlation. CoFlow is an example of a simulator that uses this option (**PATHAK et al, 2019, Hamedi et al, 2020, KUMAR et al, 2020**). Hence, the mapping of the surface facility and which nodes are assigned to

the wells and which nodes are assigned to surface facility have to be clear for a simulator. Shiralkar *et al.* (2005) presented an example of the method of assigning different numbers to the nodes. Fig. 42 illustrates the surface network and its connection data reported in the work of Shiralkar *et al.* (**SHIRALKAR et al., 2005**).

Figure 42 - The network facility configuration and its corresponding connection data. From (**SHIRALKAR et al., 2005**).

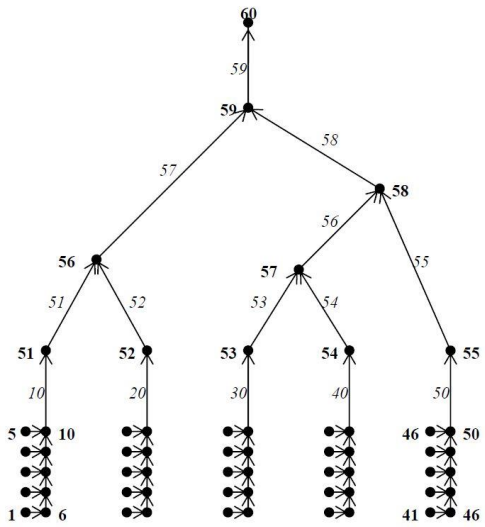

Connection	Inlet Node	Outlet Node	Source or Normal	Table Entry	Rate 1	Rate 2	Rate 3
1	1	6	S	1	4.24	12.73	0.85
2	2	7	S	1	4.27	12.81	0.85
3	3	8	S	1	29.48	88.44	5.90
4	4	9	S	1	228.61	685.84	45.72
5	5	10	S	1	1776.55	5329.66	355.31
6	6	7	N	1	4.24	12.73	0.85
7	7	8	N	1	8.51	25.53	1.70
8	8	9	N	1	37.99	113.97	7.60
9	9	10	N	1	266.60	799.80	53.32
10	10	51	N	6	2043.15	6129.46	408.63
11	11	16	S	2	8.72	1.05	0.70
12	12	17	S	2	3.12	0.37	0.25
13	13	18	S	2	40.27	4.83	3.22
14	14	19	S	2	629.08	75.49	50.33
15	15	20	S	2	9836.35	1180.36	786.91
16	16	17	N	2	8.72	1.05	0.70
17	17	18	N	2	11.84	1.42	0.95
18	18	19	N	2	52.10	6.25	4.17
19	19	20	N	2	681.19	81.74	54.49
20	20	52	N	7	10517.53	1262.10	841.40

As noted by Wang (**WANG, 2003**), the multiphase flow in a gathering system is described by mass conservation and Kirchoff's law. According to Kirchoff's law, the pressure for a node should be the same no matter from which path it is computed. In other words, due to the tree-like structure of the system, for a flowing system, the pressure at a given location must be the same if calculated countercurrent or concurrent from a location with a fixed pressure. Regardless of the direction of the calculation, the final result will be the same. The second consideration regarding Fig. 43 is the level of production. In general, the production rate from the first level (in tubing) is lower than the second level (manifold). Hence, instead of using seven flow tables, for each connection, three flow tables can be used for each level of production. An example of production level classification is reported by Moncorgé (**MONCORGÉ, 2011**).

Figure 43 - Surface network consisted of seven connections that uses only three sets of flow tables. From (**MONCORGE, 2011**)

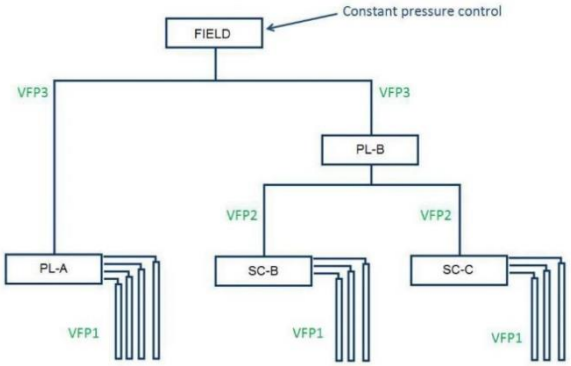

It is important to note that the range of each table should be in the range of the production level.

5.8. U-shape curve problem and its solution

As noted by Cao et al. (**CAO et al., 2015**), one of the disadvantages of using Flow Tables for hydrocarbon reservoirs is the U-Shape curve problem. During the production stage, the final bottom hole pressure in the tubing is adjusted as the result of final interactions between pressure drops due to the combination of friction and gravity terms. At a low flow rate, friction diminishes quickly and gravity becomes dominant, while at the high flow rate the opposite occurs. Fig. 44 shows an example of a tubing intake curve for varying production rates (**JANSEN, 2017**). The effect of gravity and friction terms are shown in the black and gray curves, respectively.

Figure 44 - Tubing intake curve for varying production rates. From (**JANSEN, 2017**)

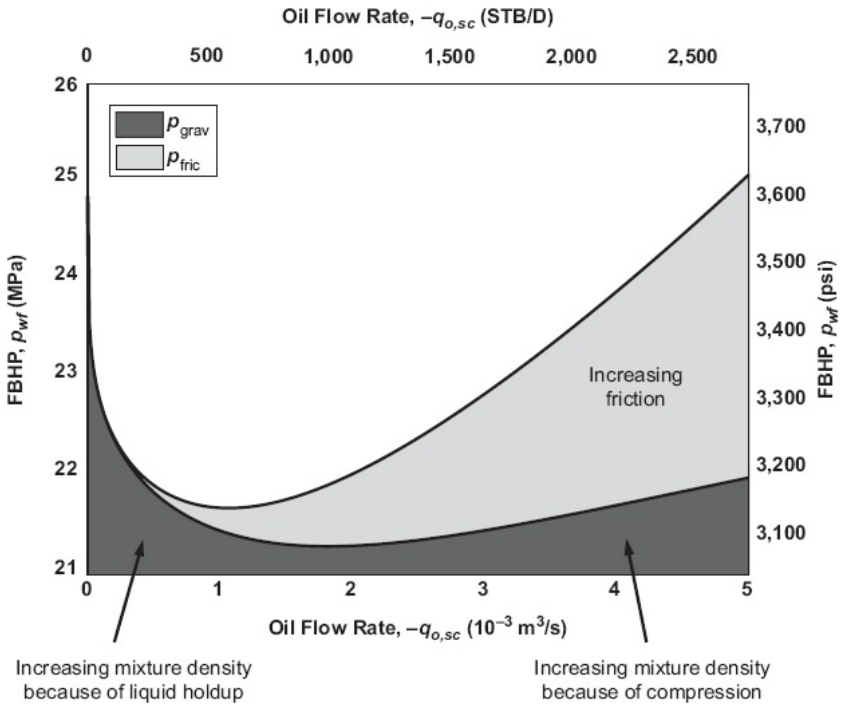

This U-shape behavior may cause a problem for the nonlinear solution. Considering the IPR solution for the reservoir, the usage of Flow Table can result in the following situations, schematically shown in Fig. 45:

1- During the simulation earlier time, where the average reservoir pressure is high, the combination of IPR and tubing curves will have two solutions.
2- During the simulation middle time, where the reservoir fluid is withdrawn from the reservoir, the combination of IPR and tubing curves will have one solution.
3- During the simulation late time, where the reservoir pressure is not sufficient enough to be produced at the required level to deliver the fluids at the surface, the combination of IPR and tubing curves will have no solution.

Figure 45 - The different situations of IPR and Flow Table solutions.
From (**CAO et al., 2015**)

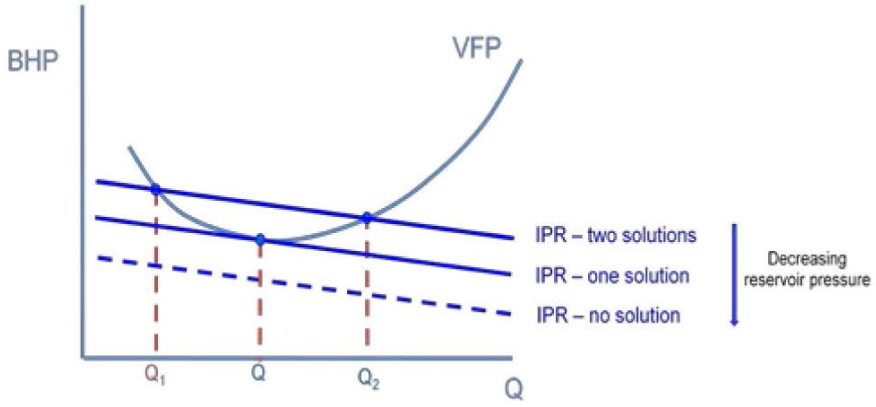

From an industrial point of the view, the third stage is known as a condition in which the wellbore fluids collapse and the corresponding well becomes dead. Well start up or nitro lift refers to an operation where a stream of the gas is injected in the wellbore to lighter the weight of the column of the wellbore. In flow tables, this is known as the LFG parameter in Builder pre-processor. To avoid the described problem, three solutions are possible, as described next.

5.8.1. Dynamic well operating envelope

The first approach is relatively new and proposed by engineers at Petronas (**ISLAMOV et al., 2020**). In this method, the original IPR and tubing curves are selected first. Then, based on the required parameters, such as tubing length, diameter and roughness, different scenarios will be re-run as demonstrated by Fig. 46.

Figure 46 - Original IPR and tubing curves with different scenarios.
(**ISLAMOV et al., 2020).**

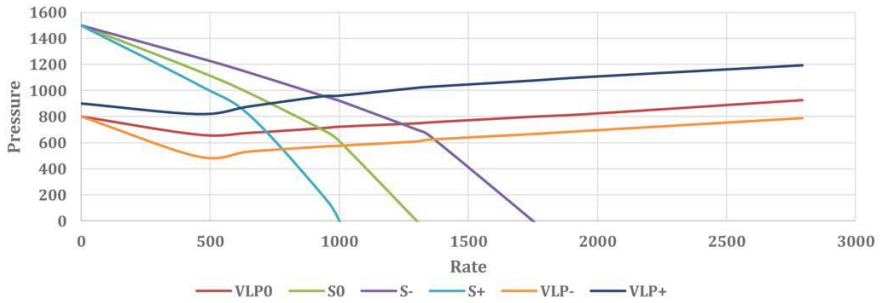

Presented by Fig. 46, S_0 and VLP_0 are original IPR and tubing curves. Next, the tolerable situations are defined in terms of pressure and rate. Later, these operational limits are translated into an envelope and the impact of each limit is considered. Fig. 47 shows an

example of the dynamic well operating envelope. As long as the operational condition is inside this envelop, the U-shape problem will not cause any problem during the simulation.

Figure 47 - Example of detected dynamic well operating envelope.
From **(ISLAMOV et al., 2020).**

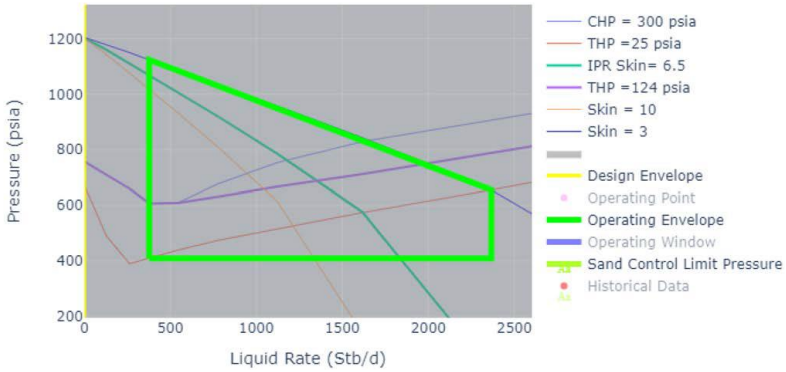

In addition to tubing and reservoir, the same logic can be used for the wellbore and surface facility to indicate the surface facility operating envelope. Readers can refer to Islamove *et al.* **(ISLAMOV et al., 2020)** for the details, algorithm and additional examples of dynamic well operating envelope.

5.8.2 Normalize values of flow table

The second approach for avoiding the U-Shape problem of the flow tables is the table normalizing method. This method is only available in the Tnavigitor simulator (**TNAVIGATOR MANUAL, 2020**). In this method, all points belonging to the region where BHP locally decreases, are assigned to the same value of BHP. Thus, the tubing curves becomes constant in this region. The details of the normalizing process are explained in the Jansen textbook (**JANSEN, 2017**). Fig. 48 shows this method.

Figure 48 - Example of the normalizing method of the flow table by Tnavigator simulator (**TNAVIGATOR MANUAL, 2020)**

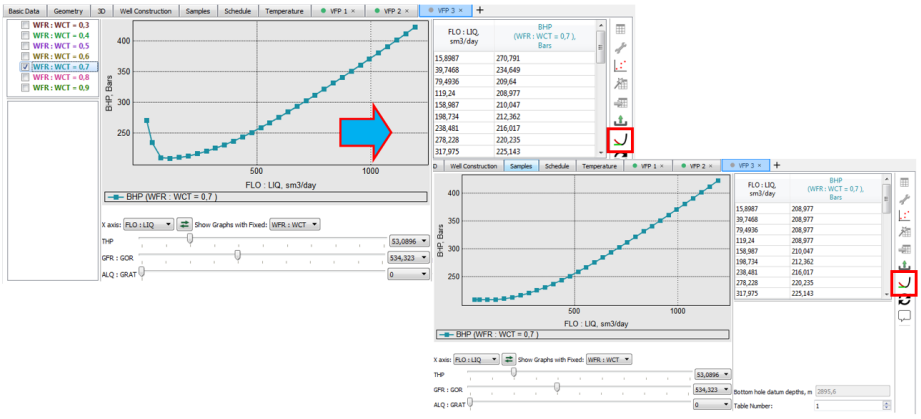

5.8.3. The safe operational zone

The last available approach is similar to the first one. UTCOMPRS simulator is designed based on this approach. In this method, a safe operational zone has to be detected by the user, before running the simulator with flow tables. To do so, first, a reservoir simulator must be run with a constant bottom hole pressure value. Based on that, a series of rates for the multi-phase conditions are obtained. These rates later will be used to check if, with the targeted WHP, the corresponding BHP values obtained from the Flow tables are similar to the initial constant bottom hole pressure or not. As long as values of BHPs from the table, and constant BHP, are in the same range, the simulator will not face any problem. Otherwise, the WHP must be changed. There are some disadvantages of using this method. First of all, it relies on the experience of the user to select the most adequate values. Second of all, if the values of the BHPs do not match during the simulation run time, the user has to stop the simulation and provide another operating condition. Therefore, it is more time-consuming than previous methods. Due to the previous problem, for some specific required WHP, if the simulation and obtained rates do not work, the user has to operate in a different condition, which may not be desired by the user.

Let us clarify this approach with an example. Suppose an average reservoir pressure of 3000 psi and a constant BHP value of 2500 psi. For the sake of simplicity, the productivity index of the well is assumed to be unity. As a result, the user may obtain 500 bbl of the oil from the simulator with this pressure difference. Now, with a 500 bbls/day oil rate, if the WHP is selected at 2250 psi, and due to the fixed length of the tubing, the

BHP from the flow table is obtained at a 3250 psi value. This BHP value is not acceptable because it is higher than the average reservoir pressure (3000 psi), and the user has to change the WHP of the table, as in the input file, until the obtained BHP from the table becomes less than the average reservoir pressure. Although there are some solutions and optimization methods for this problem in commercial simulators, they are beyond the scope of this thesis.

5.9. Derivatives from flow tables

As we discussed in the previous chapter, there is an inherent usage difference between the flow table and the flow equation. The general shape of flow tables are as follows:

$$P_{in} = F\left(\vec{q}, P_{out}\right) \tag{5.9}$$

Young *et al.* (**YANG et al. 2009**) reported a mathematical procedure for derivatives of the above equation, considering multiphase flow and the black oil formulation rate at the bottom hole node, the derivative of the rate with respect to pressure will be

$$\frac{dq_i}{dp} = \begin{cases} -PI \times GOR, & \text{if i = gas} \\ -PI, & \text{if i = oil} \\ -PI \times \dfrac{WCUT}{1-WCUT}, & \text{if i = water} \end{cases} \tag{5.10}$$

$$\begin{aligned} \frac{\partial p_{downstream}}{\partial p_{upstream}} &= \frac{\partial p_{downstream}}{\partial p_{upstream}}\bigg|_{q_o, GOR, WCUT} + \frac{\partial p_{downstream}}{\partial q_o}\bigg|_{p_{upstream}, GOR, WCUT} \times \frac{dq_o}{dp_{upstream}} \\ &+ \frac{\partial p_{downstream}}{\partial GOR}\bigg|_{p_{upstream}, q_o, WCUT} \times \frac{dGOR}{dp_{upstream}} + \frac{\partial p_{downstream}}{\partial WCUT}\bigg|_{p_{upstream}, GOR, q_o} \times \frac{dWCUT}{dp_{upstream}} \end{aligned} \tag{5.11}$$

where

$$\frac{dGOR}{dp_{upstream}} = \frac{1}{q_o}\left[\frac{dq_g}{dp_{upstream}} - GOR \times \frac{dq_o}{dp_{upstream}}\right] \tag{5.12}$$

$$\frac{dWCUT}{dp_{upstream}} = \frac{1}{(q_o + q_w)}\left[\frac{dq_w}{dp_{upstream}} - WCUT \times \left(\frac{dq_o}{dp_{upstream}} + \frac{dq_w}{dp_{upstream}}\right)\right] \qquad (5.13)$$

As it was discussed in the previous chapter, these formulations can be used to determine the Jacobian of Newton-Raphson iterative procedure of the system that works with flow tables. Also, to the best of the author's knowledge, there is not any information in the literature that shows the derivative of flow tables for the compositional model.

CHAPTER 6

NEWLY DEVELOPED FRAMEWORK FOR UTCOMPRS SIMULATOR

6.1.The concept of intergraded models

The concept of intergraded models and determining its elements play an important role in the accurate development of the software. Fig. 49 provides useful information about the concept of intergraded models reported by Peña (**PENA, 2018**).

Figure 49 Elements and different parts of integrated models.

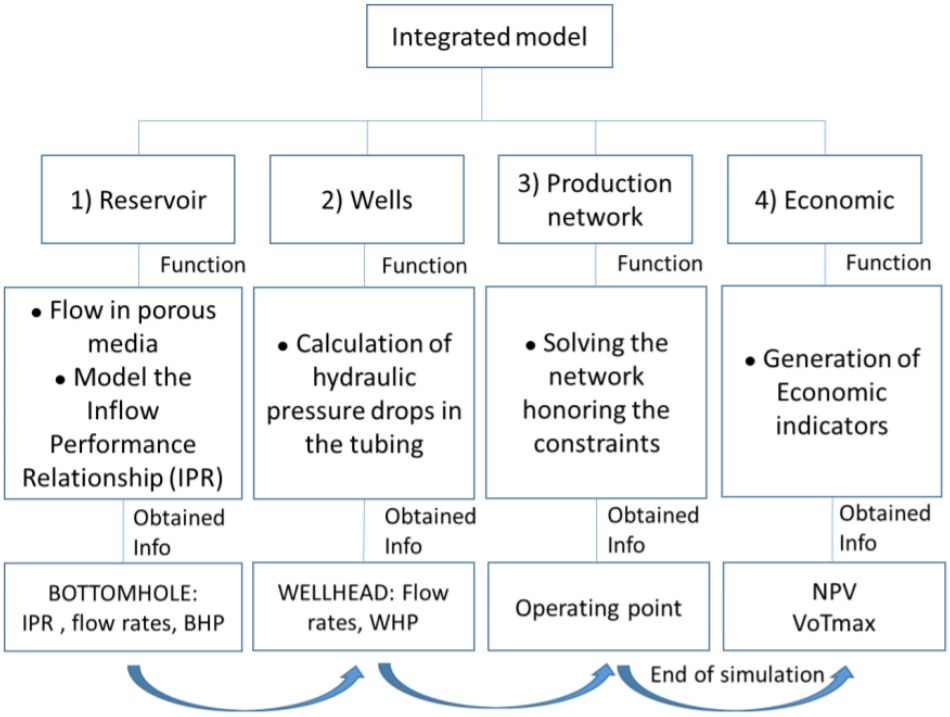

An integrated model should be able to assess four sections, *i.e.*, reservoir, wells, surface facility and the economics of the PPS. However, in this work, the economic aspects of integrated models are neglected and the main focus is on the engineering applications. It should be noted that each integrated model can be used for three different engineering applications (**PUCHYR, 1991**): history matching, deliverability and forecasting. But most of the focus here is on deliverability rather than the two other applications. By deliverability, we are trying to solve the entire system with and without restriction with a fixed terminal pressure, whether at the wellhead or the separator.

6.1. Sequential explicit coupling of the reservoir, well and surface facility

6.1.1. Reading, comparing and reporting functions

The first task to develop the capability of handling the surface facility model for the UTCOMPRS simulator was to provide a method that enables the simulator to recognize this request. As a result, in the input file of UTCOMPRS, at the well section, a new option, option number -5, was designed for a new type of producer. Originally, the simulator had two options for the type of producers, including constant bottomhole pressure and constant flowrate. With this new type of producer, the simulator realizes that the corresponding well is in association with the surface facility and some additional information has to be provided for the simulator. Fig. 50 shows the conceptual illustration of the new option.

Figure 50 - New feature in the well section of the input file of the UTCOMPRS simulator.

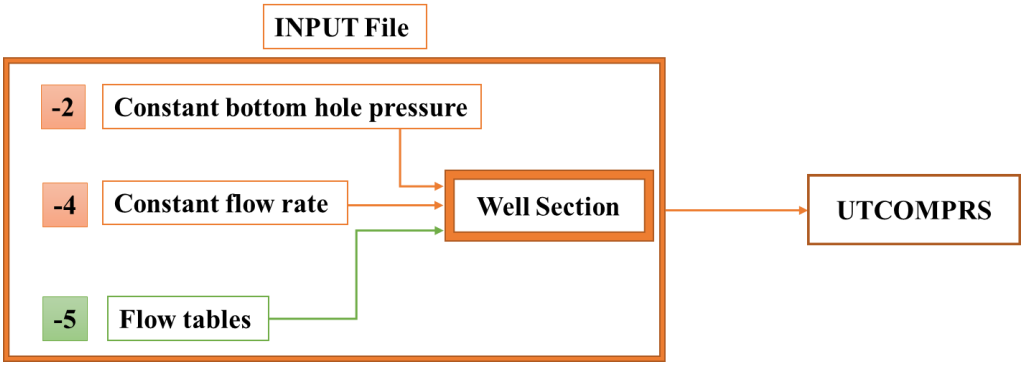

The second task of the development of the surface facility option was to develop three functions to read the flow tables, to compare their information, locate the required information and, finally, report the output of the table. These three functions were designed in a way that they are independent of the reservoir mathematical formulations as demonstrated in Fig. 51.

Figure 51- Three functions to read, compare and print the information that is in association with option number -5.

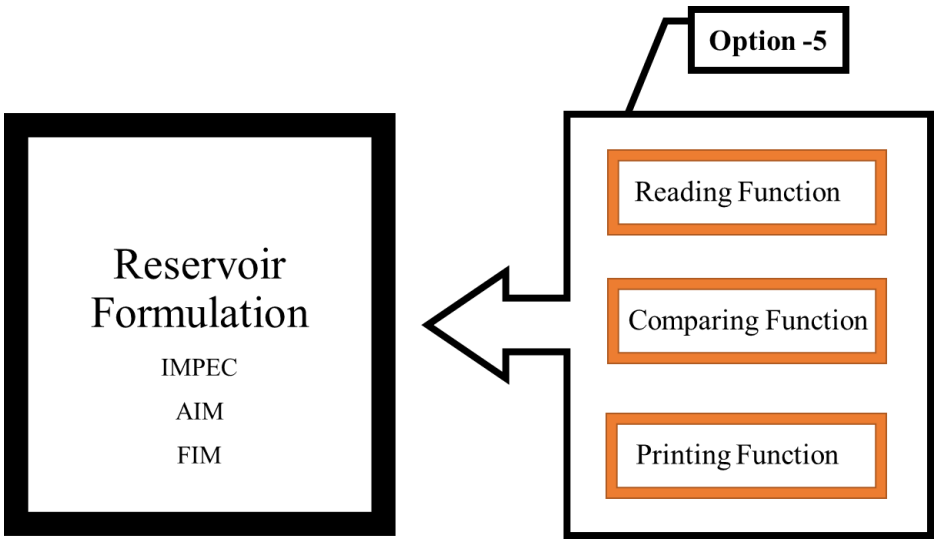

Option number -5 is designed in a way that as soon as it is called, it requests the user to provide a flow table in addition to the input file of the simulator. Since the size of the flow table can be long, this way of input requesting was designed to let the user only provided the necessary information of surface facility at the well section of the input files. Also, based on the same logic, a new output file, with .txt format, will be generated by the simulator if the option number -5 is chosen. Fig. 52 shows which type of information is requested and provided during the usage of option number -5 of the UTCOMPRS simulator.

Figure 52 - Additional input and output files that are requested and provided with option number -5.

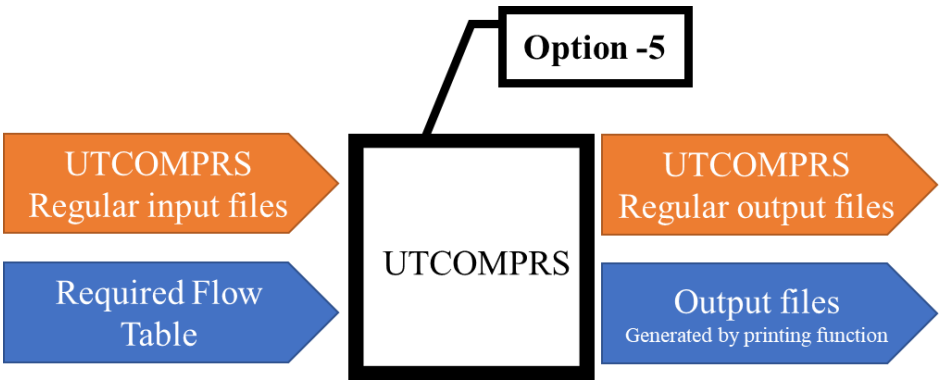

Depending on the type of the flow table, the information of the flow table and output files of the UTCOMPRS can change. Another important piece of information about option

number -5 is that the coupling point can change the type of interactions between, reading, comparing and printings functions. Therefore, a new keyword named COUPP was developed to distinguish the location of coupling, with number one for the bottom hole and number two for the wellhead. Fig. 53 shows the schematic of the impact of the coupling point on option number -5.

Figure 53 - Different locations of coupling points and their impact on reading, comparing and printing functions of option number -5.

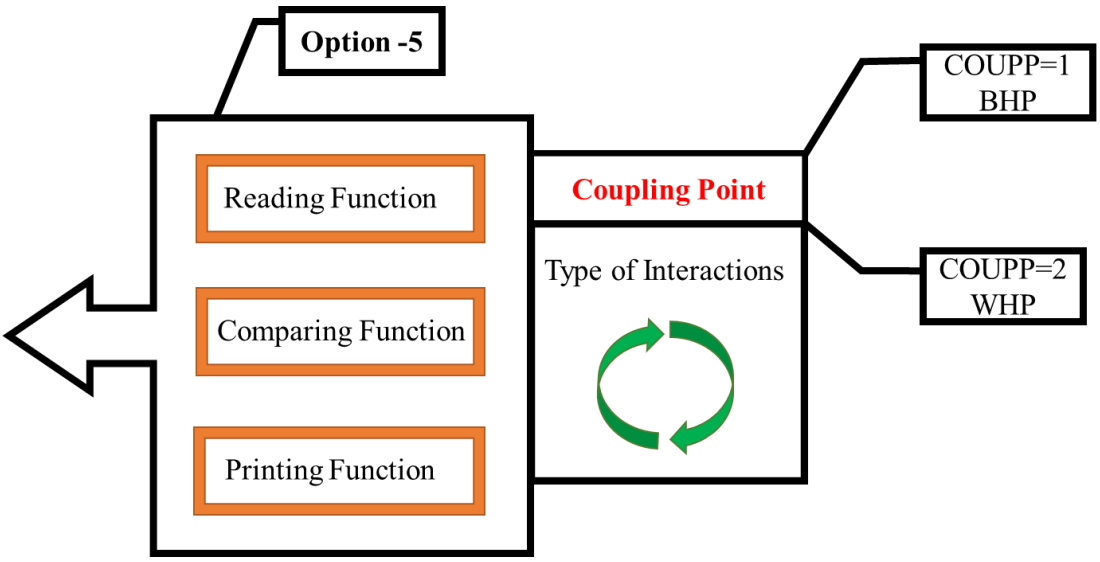

In this work, three types of flow tables have been developed for the UTCOMPRS simulator and, based on them, the corresponding algorithm and output files have changed. Hence, in the following section, different flow tables, their algorithms and the shape of the output files are discussed.

6.1.2. Different types of flow table

6.1.2.1. Simplified flow tables (SFTs)

SFTs are the first generation and simplest flow tables of the UTCOMPRS simulator. They were originally developed to investigate the application of flow tables for the simulator. As shown in Fig. 54, these tables consist of three groups of information: flow rate, WHP, and BHP.

Figure 54: Conceptual and example of SFTs.

Oil or Gas rate	PBH	PWH

Gas Rate (m^3/day)	WHP (KPa)	PBH (KPa)
3000	101.35297	141.54942
15000	1475.4786	2075.3228
30000	3530.1171	4812.5425
60000	6577.601	8639.1343
150000	9356.1893	11603.881
120000	12155.462	13126.934
150000	15540.789	18540.01

The value in each row is increasing from top to bottom; hence, there was no need for any sorting algorithm in the simulator. Once the tables were generated, they were passed as input data to the simulator and the original input with reservoir description. When using the flow table option, the user must also provide the initial well pressure, bottom hole, or wellhead, depending on the chosen coupling point. This initial pressure will be used as an initial guess for the calculation of the reservoir section. After that, the calculated single-phase flowrates are used as input parameters for the flow table section. For comparing function, an algorithm was developed to make the interpolation and find the corresponding pressure inside the table based on these flowrates. If the pressure found in the table is close enough to the initial pressure, the calculation is finished within a certain tolerance factor and the simulator goes to the next step. If not, the well pressure is updated and a new iteration is performed. This process goes on until convergence is achieved. Fig. 55 shows the algorithm.

Figure 55 - Algorithm that was designed for implementation of SFT inside the UTCOMPRS.

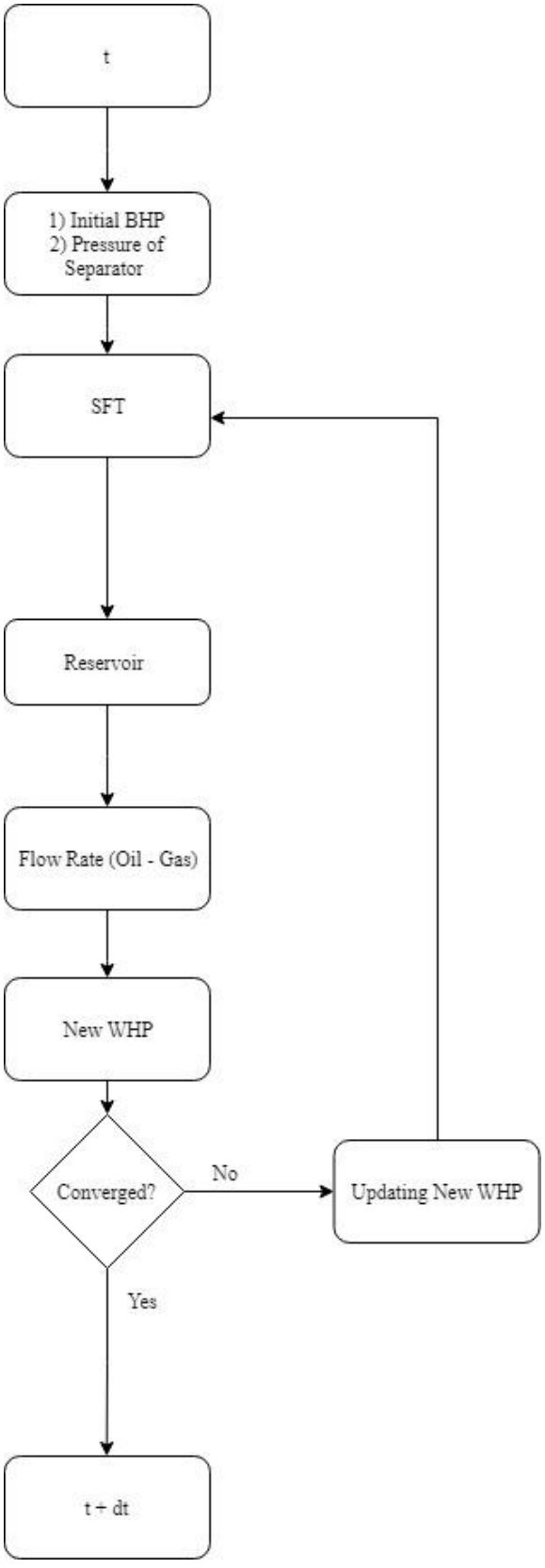

Here, we described the algorithm for the wellhead. Nevertheless, the process for the bottomhole as coupling point is the same. This approach keeps iterating until both reservoir and well sections converge. If desired, the simulator can also print an output file showing the number of iterations and the wellhead and bottom hole pressure achieved in each time step. It is important to mention here that in this approach, the separator pressure is constant. The only varying parameters are the wellhead and bottom hole pressure, both calculated based on the flow rate provided by the reservoir section. Also, Table 6 shows the output file of these classes of tables.

Table 6 - Example of a simple output file of surface facility that work with SFTs.

Time	PBH	PWH	Iteration
0.46714	1261.92	496.15	1
1.89696	1068.78	308.29	1
393316	927.53	167.06	1
6.23238	866.73	108.21	1

SFTs were tested and run to check the concept of the flow table for the UTCOMPRS simulator as in the initial draft. This flow table type, it is very simplified and it was included to just to check the behavior of flow tables in conjunction with the UTCOMPRS simulator. Due to that, this option is not available for the UTCOMPRS simulator anymore.

6.1.2.2. Advanced flow tables (AFTs)

Although it was possible to include a new framework for surface facility information by using SFT, those tables had some limitations. Firstly, they did not consider many of the operational parameters, *e.g.*, WOR (water-oil ratio) or GOR (gas-oil ratio). Secondly, those tables were generated for black oil models using a commercial simulator. Finally, when the wellhead was specified, it was necessary to insert a pipeline equation. Because of that, the pipe equations had to be used to calculate the pressure drop of the surface pipeline with a fixed separator value in each iteration. Hence, the separator values could not change as a function of the dynamic behavior of WHP. The AFT was a new set of tables that were designed to overcome all of the aforementioned limitations. A sample of such tables is shown in Table 7.

Table 7 - Conceptual schematic of the AFT (Top) and an example of an AFT (down) that consists of two distinguished sections, one for single-phase gas (yellow section) and one for multiphase (green section).

Gas rate	PBH	PWH

Oil Rate	GOR	WOR	PBH	PWH	PSEP

7

Gas Rate (m/day)	PBH(Pa)	PWH(Pa)	PSEP(Pa)
3000	141549.4228	106110.36	101352.97
15000	2075322.76	1547666.8	1475478.6
30000	4812542.48	3709656.7	3530117.1
60000	8639134.28	6932198.5	6577601
90000	11603881.08	9884672.7	9356189.3
120000	13126933.56	12865277	12155462
150000	18540009.64	16462136	15540789

30

Flux of Oil (m3/day)	Flux of Gas(m3/day)	GOR	WOR	PBH(Pa)	WHP(Pa)	PSEP(Pa)
1.6	0	0	0	24062712	22137695	17488779
1.6	30	18.75	0	24062712	22137695	17488779
1.6	300	187.5	0	24062712	22137695	17488779
1.6	750	468.75	0	24062712	22137695	17488779
1.6	1500	937.5	0	24062712	22137695	17488779
80	0	0	0	24062712	22137695	17488779
80	30	0.375	0	20711859	19054910	15053379
80	300	3.75	0	13058675	12013981	9491045.3
80	750	9.375	0	12107199	11138623	8799511.9
80	1500	18.75	0	8515028.6	7833826.3	6188722.8
400	0	0	0	11203985	10307666	8143056.3
400	30	0.075	0	11707302	10770718	8508867.4
400	300	0.75	0	10500719	9660661.9	7631922.9
400	750	1.875	0	9294136.5	8550605.6	6754978.4
400	1500	3.75	0	8652923.8	7960689.9	6288945
1.6	0	0	100	8515028.6	7833826.3	6188722.8
1.6	30	18.75	100	10721352	9863643.7	7792278.5
1.6	300	187.5	100	11645250	10713630	8463767.4
1.6	750	468.75	100	12334726	11347948	8964878.6
1.6	1500	937.5	100	10266298	9444993.8	7461545.1
80	0	0	100	8521923.4	7840169.5	6193733.9
80	30	0.375	100	8473660	7795767.2	6158656.1
80	300	3.75	100	8542607.6	7859199	6208767.2
80	750	9.375	100	9487189.8	8728214.6	6895289.5
80	1500	18.75	100	13044886	12001295	9481023.1
400	0	0	100	13396519	12324797	9736589.8
400	30	0.075	100	8811503.3	8106583	6404200.6
400	300	0.75	100	8521923.4	7840169.5	6193733.9
400	750	1.875	100	9494084.5	8734557.8	6900300.6
400	1500	3.75	100	11197090	10301323	8138045.2

These tables contain both single-phase gas and multiphase conditions. The information in each section is passed to the simulator by two numbers (7 and 30) located above each section of AFT. In the AFT, the GOR, WOR and pressure of the separator for different flow rates are included. Additionally, this table is generated for compositional

fluid, with fixed pipeline diameter and length. Compared to SFT, AFT is much more accurate. The algorithm of AFTs is shown in Fig. 56.

Figure 56 - AFT algorithm, used for both WHP and BHP as coupling points.

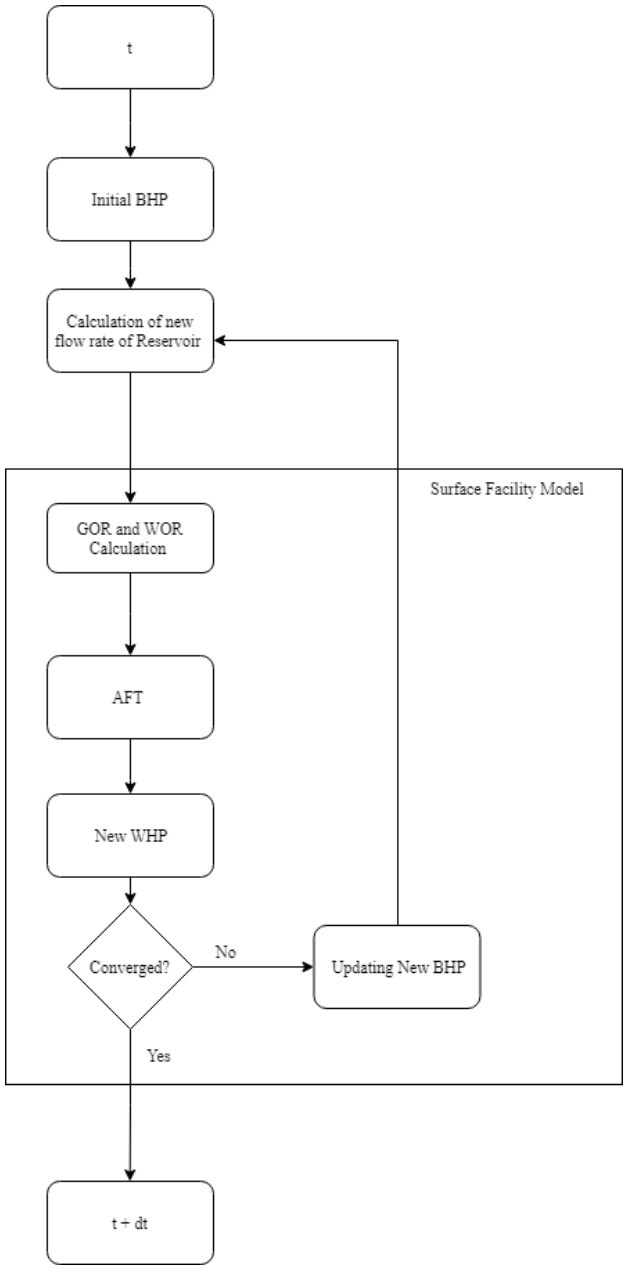

As in the initial algorithm of SFTs, here the user must also provide the initial BHP. This BHP is passed to the simulator and it calculates the rates of oil, gas, and water. Thus, GOR and WOR are calculated next. Based on that information, the algorithm will search and calculate the appropriate pressures. First, it will search in the WOR section, then in the oil rate section and finally in the GOR section. Almost always, the calculated values

from the reservoir section do not match any exact value inside the table; so, it is necessary to perform a linear interpolation with the appropriate values from the table. Subsequently, it is possible to find the new wellhead, bottom hole and separator pressures.

Here, as in the SFT algorithm, a comparison is made between the pressure from the previous time step with the new pressure from the flow table. If the difference is within the tolerance, the simulator proceeds to the next time step. If not, the BHP is updated and a new iteration is performed. Based on the work of Emanuel and Ranney (**EMANUEL, RANNEY, 1981**), the tolerance is set to 103.4 kPa, (or 15 psi). Also, it is important to mention that the algorithm switches from multiphase to single phase in two conditions: (1) when the oil rate becomes zero, (2) when the value of calculated GOR goes higher than the highest GOR of a multi-phase section of AFT. In both conditions, the comparing function switches to the single-phase section of AFT, when the values of BHP, WHP and PSEP are adjusted, based only on gas rate (instead of oil rate, GOR and WOR). In the single-phase section, if the gas rate value becomes greater than the highest value in the table, the simulation stops, when the user should provide a new AFT.

This algorithm is more complex than the first one in two ways. First, it needs to perform the comparison in three different sections: WOR, oil rate and GOR. Second, it switches from multiphase to single phase. Of course, the computational effort is higher when compared to the first algorithm, but it results in greater accuracy, since the simulator will be able to handle more realistic cases and support more operational parameters, such as GOR and WOR.

The number of iterations and pressure values are monitored and reported, if desired, they are printed in an output file, as presented in Table 8.

Table 8 - Example of extended format of the output file for AFT.

Time (Day)	PBH (KPa)	PWH(KPa)	PSEP(KPa)	WOR	GOR	P Inj (KPa)	Oil Rate (m3/day)	Niter
0.04274	23435.26	7960.69	628.8945	0	111	39178.73	485.8512	1
0.13611	23435.26	7833.826	618.8723	0	111	39178.73	365.9168	1
0.23611	23435.26	9863.644	779.2278	0	111	39178.73	323.0208	1
0.33611	23435.26	10713.63	846.3767	0	111	39178.73	300.8944	1
0.43611	23435.26	11347.95	896.4879	0	111	39178.73	286.568	1
0.53611	23435.26	9444.994	746.1545	0	111	39178.73	276.1936	1
0.63611	23435.26	7840.169	619.3734	0	111	39178.73	268.1968	1
0.73611	23435.26	779.5767	615.8656	0	111	39178.73	261.7984	1
0.83611	23435.26	785.9199	620.8767	0	111	39178.73	256.5632	1
0.93611	23435.26	872.8215	689.529	0	111	39178.73	252.232	1
1.03611	23435.26	1200.13	948.1023	0	111	39178.73	248.6352	1
1.13611	23435.26	1232.48	973.659	0	111	39178.73	245.6544	1
1.23611	23435.26	810.6583	640.4201	0	111	39178.73	243.1984	1
1.33611	23435.26	784.0169	619.3734	0	111	39178.73	241.2	1
1.43611	23435.26	950.3755	690.0301	0	111	39178.73	239.6	1

This output table has information for dynamic separator pressure, WOR, GOR, injector pressure and oil flowrate. The user can use this data to monitor the behavior of wells and surface facility along the simulation.

6.1.2.3. Commercial flow tables (CFTs)

Two functions were developed for reading and comparing the values of the flow table and reporting the corresponding results. However, since those tables were in-house designed tables, they cannot be validated by any other commercial simulator. Hence, to solve this problem a third class of flow tables here is presented. Since they are designed in a way that enables the UTCOMPRS simulator to be compared with commercial simulators, the third generation of tables is named commercial flow tables (CFT). Fig. 57 shows a conceptual schematic of CFT.

Figure 57 - Conceptual shape of the CFTs generated by a commercial simulator.

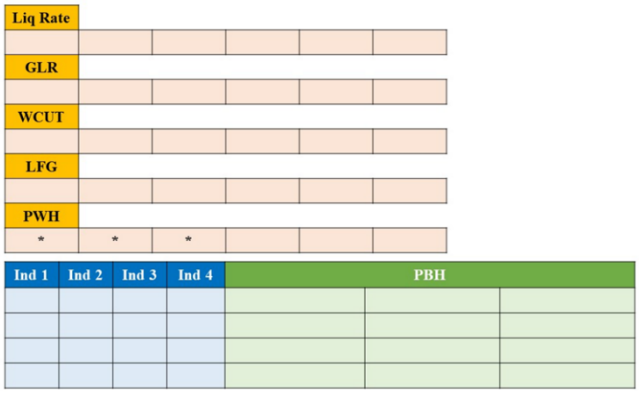

The CFTs consist of two sections. In the upper section, there are a series of ranges of flow conditions, such as liquid rate, gas-liquid ratio, water cut, lift gas injection rate (LFG) and WHP (the yellow section). Then, based on the value of the flow inside the tubing, these four values (Liq, GLR, WCUT, LFG) are converted into a set of four indices (the blue section) and, based on the fixed values of WHP, a series of BHP values are set in the bottom right side of the table (the green section).

Fig 58 shows the general workflow that we developed for this new set of flow tables. As mentioned earlier, the type of information that exists in each type of table will change the corresponding algorithm of the simulation. Initially, the CFT and three types of information are passed as input files to the simulator: (1) initial bottom hole pressure, (2) fixed value of WHP and (3) initial value LFG, which is usually assumed to be zero, but it is required anyway in the commercial simulator. Once these values are received by the simulator, a reading function is called to obtain the information from the CFT. Then, the initial bottomhole value is passed to the simulator, followed by oil, water and gas flowrates calculation. Next, based on these flowrates, the values of liquid rate, GLR, WCUT and LFG are evaluated. This information is used by a comparing function. This function will convert this information, based on the upper side of the table, into four indices (yellow part of Fig. 57) and locate the corresponding row inside the CFT (blue part of Fig. 57).

Based on the WHP values and their range in the table, the corresponding bottomhole columns are located (green part of Fig. 57). A series of bottom hole values (two sets for lower indices and two sets for high indices) are located. At last, these values are interpolated, resulting in the final BHP output value for this function. This bottomhole pressure will be checked against the initial guessed bottom hole pressure. If their difference is less than 103.421 kPa (or 15 psi), again according to Emanuel and Ranney (**EMANUEL; RANNEY**; 1981), the simulation goes to the next time step. If the tolerance is not achieved, the last BHP is used for the next iteration and all parameters are calculated again. This process continues until the end of the simulation. Fig. 58 illustrates the flowchart of the algorithm.

Figure 58 - General algorithm of commercial flow tables for the UTCOMPRS Simulator.

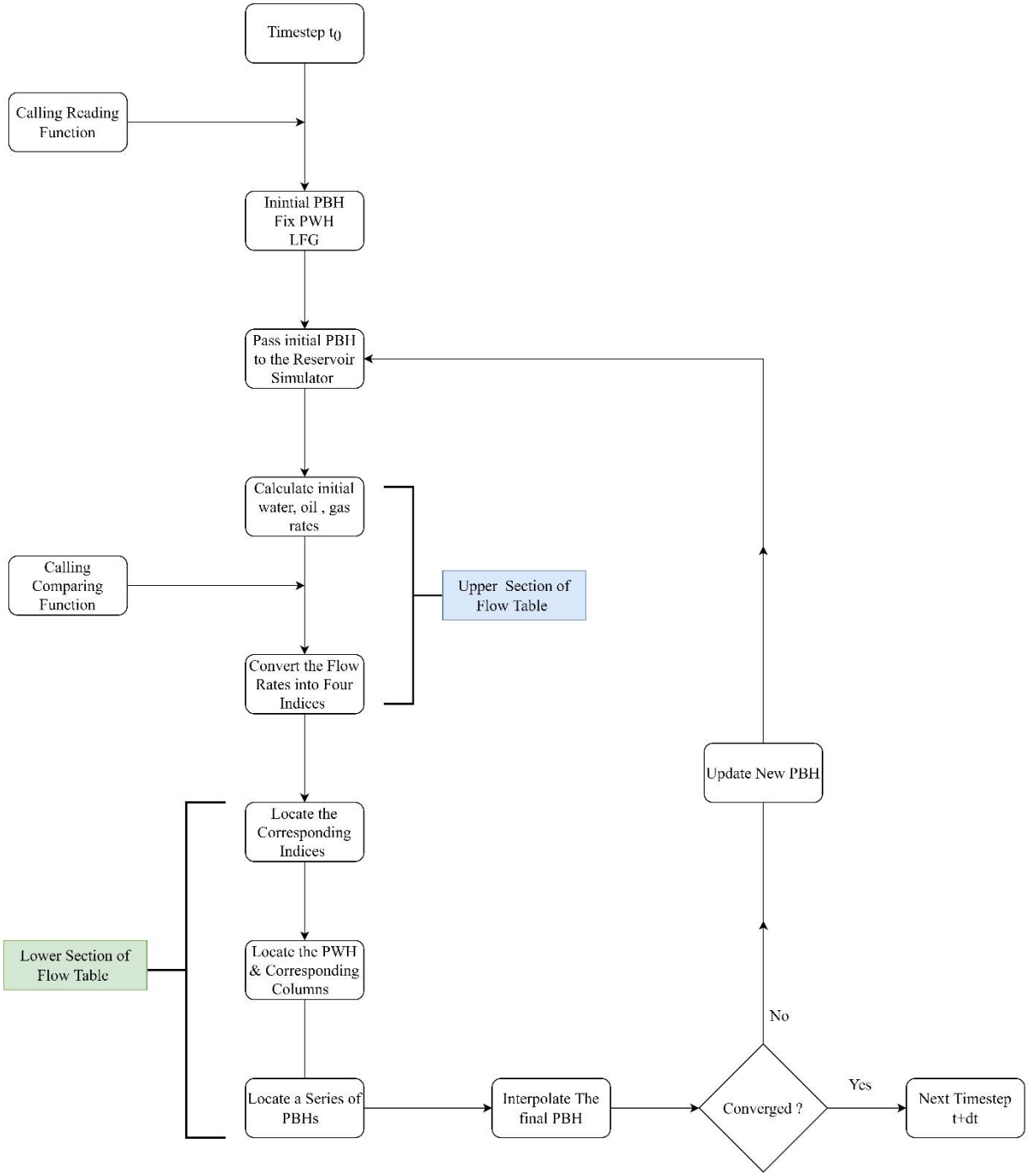

Fig. 59 shows an example of CFT to clarify how the bottomhole pressure values are selected.

Figure 59 - Example of a commercial flow table to clarify how the bottomhole pressure values are selected.

```
LIQ
 500.0 2500.0 7500.0
GLR
 500.0 890.0
WCUT
 0.12 0.39 0.47
LFG
 0.0 500.0
WHP
 500.0 4500.0 7320.0
BHP
**iflo  igfr  iwfr  iadd     bhp(1st whp).....bhp(nth whp)
  1     1     1     1        620.1425      4614.5997     7445.50651
  1     1     1     2        620.143789    4614.55643    7445.46524
  1     1     2     1        632.716541    4619.91253    7451.99695
  .     .     .     .
  .     .     .     .
  .     .     .     .
  2     2     2     2        652.970116    4532.33072    7363.72065
  2     2     3     1        652.973856    4532.46361    7366.84968
```

Suppose the values of Liq, GLR, WCUT, LFG and WHP are 1000 m^3/day, 600 m^3/m^3, 0.2, 450 m^3/day and 550 kPa, respectively. By comparing the upper section of the table, the current values will stand between indices 1 and 2 for each set of parameters. As a result, the corresponding code for fluid flow inside the tubing will be 1111 and 2222. Now, based on the values of WHP, which is 550 kPa, columns number 1 and 2 are located. For the lower indices (1111) we have two bottom hole pressure values: 620.14 and 4614.59 kPa. And for the higher indices (2222) we got 652.97 and 4532.33 kPa. Now the question is how to interpolate these four values and report the final bottom hole pressure from the above table, which will be answered in Section 4.1.6. Table 9 shows the final output file that has been developed for the UTCOMPRS simulator based on CFTs.

Table 9 - Example of the final output file of the UTCOMPRS simulator which works with CFTs.

Time(Days)	PBH	PWH	PSEP	LIQ	Qw	Qo	Qg	Pinj	GOR	#iterAA	AB	AC	AD	BA	BB	BC	BD
0.32701	1267.90	1200.00	600.00	408.44	0.00	408.44	1030893.71	1672.43	2523.95	1	2	2	2	1	1	1	1
1.32701	1267.90	1200.00	600.00	349.73	0.00	349.73	909865.85	1694.13	2601.64	1	2	2	2	1	1	1	1
2.32701	1267.90	1200.00	600.00	310.07	0.00	310.07	823175.72	1710.11	2654.84	1	2	2	2	1	1	1	1
3.32701	1267.90	1200.00	600.00	282.24	0.00	282.24	759877.72	1722.01	2692.27	1	2	2	2	1	1	1	1
4.32701	1267.90	1200.00	600.00	262.05	0.00	262.05	712636.36	1731.10	2719.46	1	2	2	2	1	1	1	1
5.32701	1267.90	1200.00	600.00	246.93	0.00	246.93	676565.82	1738.17	2739.88	1	2	2	2	1	1	1	1
6.32701	1267.90	1200.00	600.00	235.29	0.00	235.29	648399.30	1743.79	2755.78	1	2	2	2	1	1	1	1
7.32701	1267.90	1200.00	600.00	226.08	0.00	226.08	625931.97	1748.31	2768.62	1	2	2	2	1	1	1	1
8.32701	1267.90	1200.00	600.00	218.63	0.00	218.63	607656.91	1752.00	2779.38	1	2	2	2	1	1	1	1
9.32701	1267.90	1200.00	600.00	212.48	0.00	212.48	592529.05	1755.03	2788.69	1	2	2	2	1	1	1	1
10.32701	1267.90	1200.00	600.00	207.30	0.00	207.30	579811.99	1757.54	2797.02	1	2	2	2	1	1	1	1
11.32701	1267.90	1200.00	600.00	202.87	0.00	202.87	568978.00	1759.63	2804.67	1	2	2	2	1	1	1	1
12.32701	1267.90	1200.00	600.00	199.03	0.00	199.03	559642.33	1761.37	2811.85	1	2	2	2	1	1	1	1
13.32701	1267.90	1200.00	600.00	195.66	0.00	195.66	551519.55	1762.82	2818.72	1	2	2	2	1	1	1	1
14.32701	1267.90	1200.00	600.00	192.68	0.00	192.68	544394.21	1764.03	2825.40	1	2	2	2	1	1	1	1
15.32701	1267.90	1200.00	600.00	190.01	0.00	190.01	538100.97	1765.04	2831.96	1	2	2	2	1	1	1	1
16.32701	1267.90	1200.00	600.00	187.61	0.00	187.61	532510.82	1765.87	2838.46	1	2	2	2	1	1	1	1

Since the CFTs do not work with separators, their information can be either equal to the wellhead or some lower values, since they do not have physical meaning. In the above

example, they are set to be half of the WHPs, so the simulator will not face any difficulties during the generation of output files. Also, in this version of output files, the liquid, oil, water and gas flowrates are reported individually. The higher (AA, AB, AC, AD) and lower (BA, BB, BC, BD) indices were included inside the output files. So, the user can understand the interpolated values are based on which set of BHPs values. Before we explain how the interpolation functions are working, it is important to have a feature that can control the injection rate for the injection wells. This feature will allow us to control the use of CFT more efficiently and increase the accuracy of our tables in comparison with other commercial simulators. Hence, the next section will discuss the well control injector option and, after that, the interpolation functions are presented.

6.1.3 Advanced well control option (AWCO)

One of the advantages of using CFTs is that the fluid rates are reported in terms of the volumetric rates. Thus, from the surface facility engineering point of view, this technique can be used for any required surface facility capacity. However, during the simulation run time, sometimes it is necessary to control the injection rate into the reservoir with its producing well using the CFTs. Hence, a new feature was designed for our simulator that enables the user to control production. The new feature is designed in a way that puts a restriction on the injection rate, while collaborating with the producing well which is operating with the flow table option. Later, we will show the injector pressure limit, in which once the pressure of the injector reaches the specific limit, the injector constraint will switch from constant rate injection to constant bottom hole pressure.

Fig. 60 illustrates the surface facility option, how the CFT is included in UTCOMPRS and its corresponding relation to the injector well control option. Besides, FT_TYPE is a new keyword that is designed to distinguish the type of flow table for the simulator. This is because each table type has different information and constraint operating conditions. FT_TYPE keyword enables the simulator to distinguish which type of information is required. Also, the injector well control option is designed in a way that can collaborate with both FT_TYPE and COUPP keywords. However, for the CFT case, since the wellhead pressure is fixed, the coupling point is always set at the bottom hole condition (COUPP = 1).

Figure 60 - General structure of the surface facility option for UTCOMPRS, with dashed lined arrows indicating the newly added features.

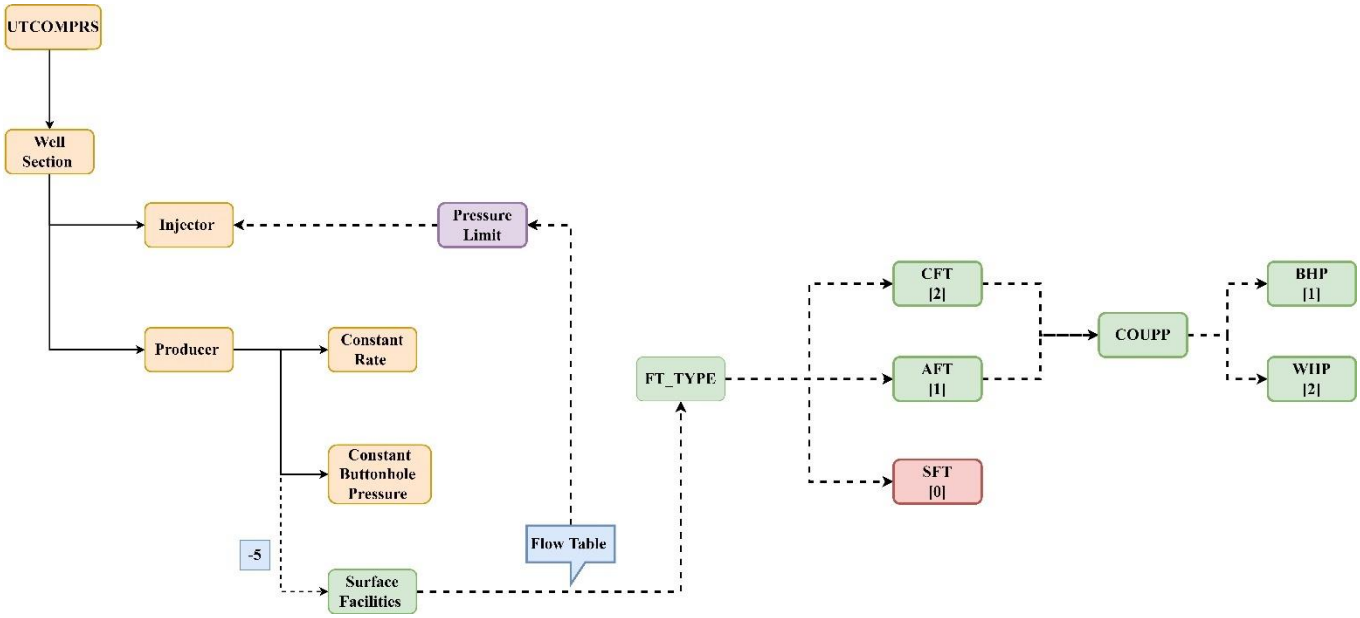

6.1.4. Different interpolation functions

As discussed in Section 6.1.2.3, different values of bottom hole pressure are obtained from the table. One can select different formulations such as linear, bilinear or quadratic interpolation functions. However, based on the notations of Stackel and Brown (**STACKEL, BROWN, 1981**), and Emmanual and Rammny (**EMANUEL; RANNEY**; 1981), after checking the results of the quadratic interpolation function, which was not promising, we decided to use a linear interpolation function. Fig. 61 and Eq. (6.1) demonstrate the relationship between the independent and dependent variables.

Figure 61 - General geometric visualization of dependent (Y) and independent (X) variables for two given values (up and down) and a linear interpolated point between them.

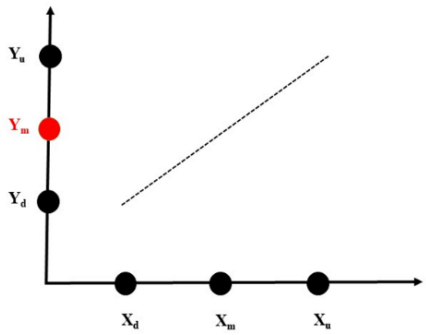

$$\frac{Y_m - Y_d}{X_m - X_d} = \frac{Y_u - Y_d}{X_u - X_d} \tag{6.1}$$

The objective here is to find the middle value, Y_m, that exists between up and down values. Inserting Eq. (6.1) into Eq. (6.2) leads to the general form of the equation used to interpolate different parameters.

$$Y_m = Y_d + \left[\left(\frac{Y_u - Y_d}{X_u - X_d} \right) \times (X_m - X_d) \right] \tag{6.2}$$

For our purpose, which is to evaluate the bottom hole pressure, we consider the dependent variable Y as the bottom hole pressure and set different parameters for independent values X. This is done because the CFT is a multidimensional table, which means that one can choose any parameter as the reference for interpolation. Eq. (6.2) may be expressed in the form of logarithmic and quadratic interpolations using the same logic. The logarithm and quadratic interpolations are respectively given by

$$Y_m = Y_d + \left[\left(\frac{\mathrm{Log}_{10}(X_m) - \mathrm{Log}_{10}(X_d)}{\mathrm{Log}_{10}(X_u) - \mathrm{Log}_{10}(X_d)} \right) \times (Y_u - Y_d) \right] \tag{6.3}$$

$$Y = Y_0 \frac{(X - X_1)(X - X_2)}{(X_0 - X_1)(X_0 - X_2)} + Y_1 \frac{(X - X_0)(X - X_2)}{(X_1 - X_0)(X_1 - X_2)} + Y_2 \frac{(X - X_0)(X - X_1)}{(X_2 - X_0)(X_2 - X_1)} \tag{6.4}$$

Because three values are required for quadratic interpolation, this formulation has been implemented in such a way that if the values of the wellhead (independent (X) variables) were set at the table's borders (first and last WHP values), the code is switched to a linear interpolation formulation.

We also verify the interpolation factor method briefly here. The notations of Stackel and Brown **(STACKEL, BROWN, 1981)** include the logic behind this method of treating table data. According to this method, an interpolation factor I_q can be derived at standard conditions, which are defined as null water cut and bubble point (GOR, WCUT = 0) conditions, in order to employ flow tables data more effectively. Eq. (6.5) shows the mathematical expression of the interpolation factor.

$$I_q = \left(\frac{BHP_{line} - BHP_1}{BHP_2 - BHP_1} \right) \tag{6.5}$$

where BHP_{line}, BHP_1, and BHP_2 denote, respectively the average BHP from solid line, the lower BHP and the higher BHP. After calculating the interpolation factor under standard conditions, a sequence of bottomhole values as a function of different liquid rates is found under non-standard conditions (based on the current and none-zero water cut and GOR values). The interpolation factor and sequence of bottomhole data acquired are then utilized to calculate a new bottomhole pressure. We demonstrate the interpolation factor method used by Stackel and Brown (**STACKEL, BROWN, 1981**) with an example. Consider the hypothetical scenario in Fig. 62, where the solid line (For A1=68, B1 = -117800) depicts the linear approximation at the intersection of two sets of bottomhole values. (Indicated by dashed lines).

Figure 62 - Hypothetical case at standard condition demonstrated by Stackel and Brown (**STACKEL, BROWN, 1981**). The solid line shows the linear approximation at between two sets of bottomhole values.

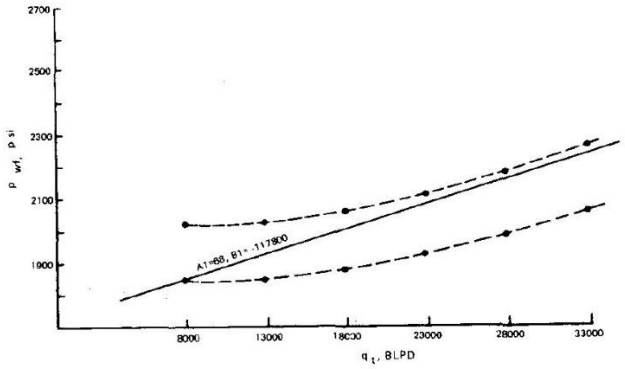

Fig. 63 presents the predicted bottomhole at higher water cut condition using the interpolation factor obtained from Fig 62.

Figure 63 - The calculated bottomhole at nonstandard condition (higher water cut condition). (**STACKEL, BROWN, 1981**).

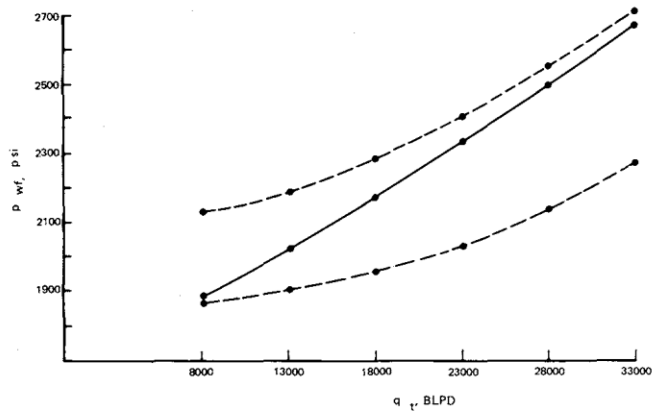

After determining the computed BHP under non-standard conditions (solid line of Fig. 63), the final value of BHP can be interpolated as a function of the current liquid rate, and this will be the final interpolated value from the table.

6.1.5Multiple wells and 3D models modifications for CFT

One of the deficiencies of the developed framework for the surface facility was multiple well capability. The option of multiple wells is based on the same methodology, however, for each well that is working with option -5, a separate text file will be generated. To do so, a new algorithm was designed and performed successfully inside UTCOMPRS. Figure 6.20 shows the flow chart of the multiple well algorithm. To detect which well is working with a flow table, we designed a new keyword named **NWFT**. Once this keyword detects the type of wells, another new keyword was designed and named **FTCount**, which is a counter condition for each well. Both **NWFT** and **FTCount** are used inside the simulator. Users are not required to inform the simulator of their values. They are explained here to clarify the development of the multiple-well algorithm**.** Since an initial guess is required for the bottom-hole of each well, a new vector was assigned to receive the initial values. For this option, a general CFT is passed to the simulator for all of the wells. Fig. 64 shows the algorithm of the multiple-well working with the flow table.

Figure 64 - Algorithm of the multiple-well working with the flow table.

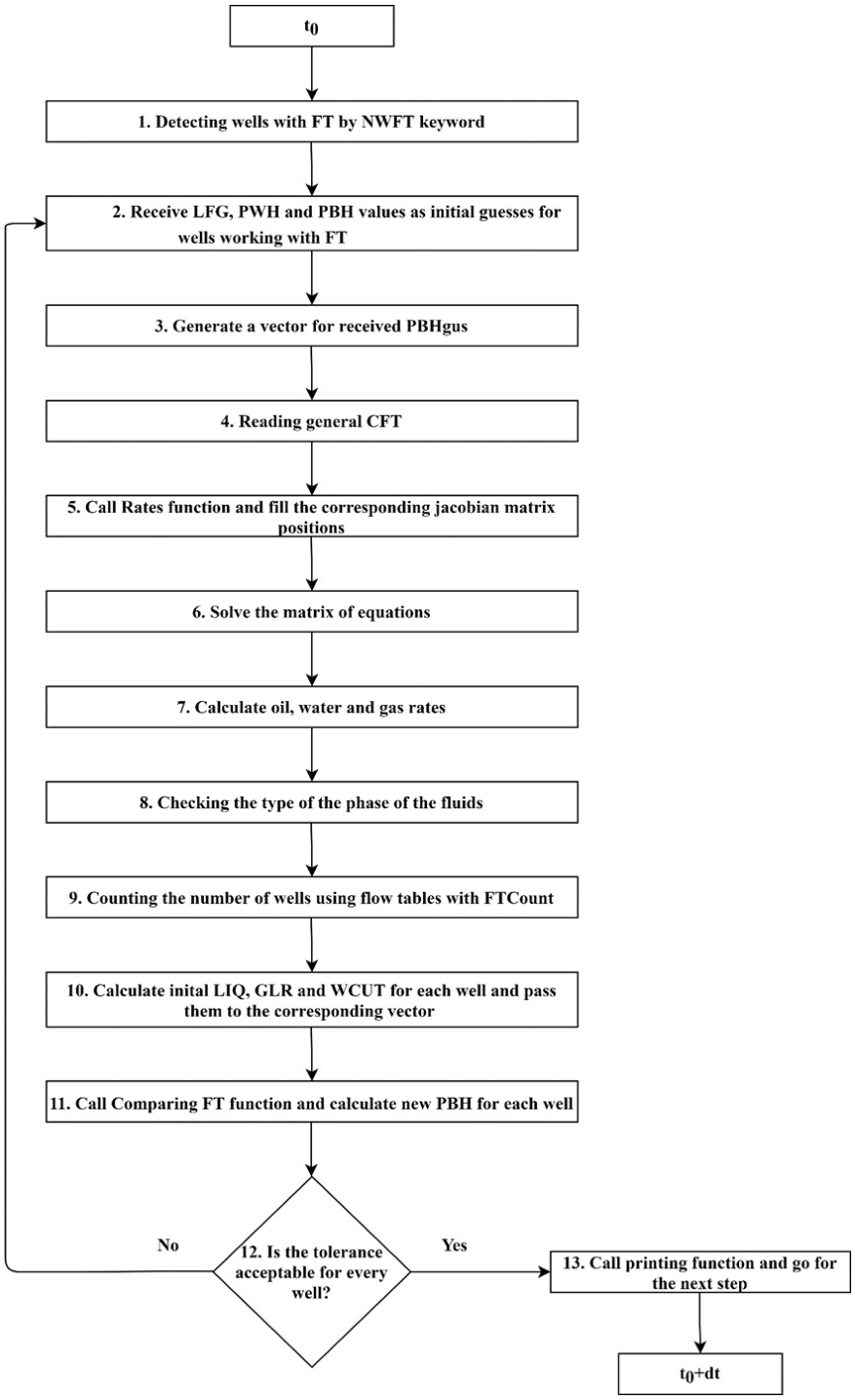

Additional development regarding how to treat the flow tables for 3D reservoirs is the last topic of the sequential explicit coupling method. Fig. 65 shows 2D and 3D reservoirs that are assigned with the flow table option. As can be seen, for the 2D reservoir the BHP is the one that is obtained from the flow table, directly. But, for 3D reservoirs, an additional consideration is required. For a given reservoir, with four layers, the first layer is assigned with the value that has been received from the flow table, but for the

other layers, the hydrostatic pressure should be added to the BHP of the first layer. Consequently, the value of BHP for the fourth layer is a function of WHP through the value of bottom hole pressure; mathematically Fig. 64 shows this with red and blue notations.

Figure 65 - Example of 2D and 3D reservoirs and how the 2D calculation can be extended for 3D models.

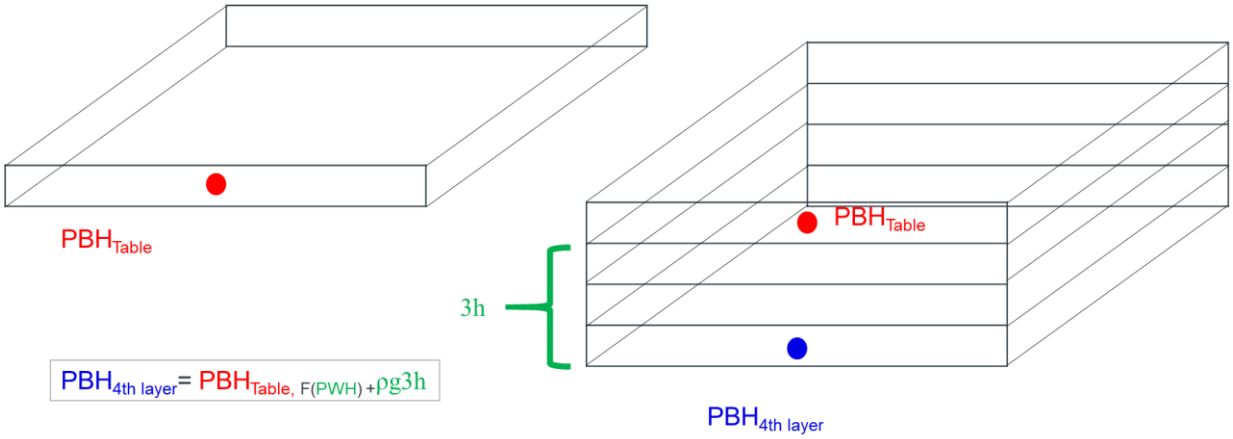

The above discussion relates to the developed tools and algorithms for sequential explicit coupling of the reservoir, multiple-wells and surface facility. Table 10 and Fig. 66 show the example of the newly implemented keywords for UTCOMPRS to work with the flow table.

Table 10 - New keywords developed for Surface facility option of the UTCOMPRS simulator

Keyword	Mean	Value	Explanation
FT_TYPE	Type of table	0, 1 or 2	SFT, AFT or CFT respectively.
COUPP	Coupling point	1 or 2	Point of coupling at the bottom hole or wellhead respectively.
AWCO	Advanced well control option	0 or 1	if the well has a maximum injection or production pressure
PMAX	Maximum injection pressure	Any postive value	if AWCO = 1, PMAX must be provided if AWCO = 0, no PMAX
BHP	Bottom hole pressure	Any value greater or equal to 0	The initial pressure of the bottom hole

Figure 66 - Examples of new keywords developed for the Flow Table option.

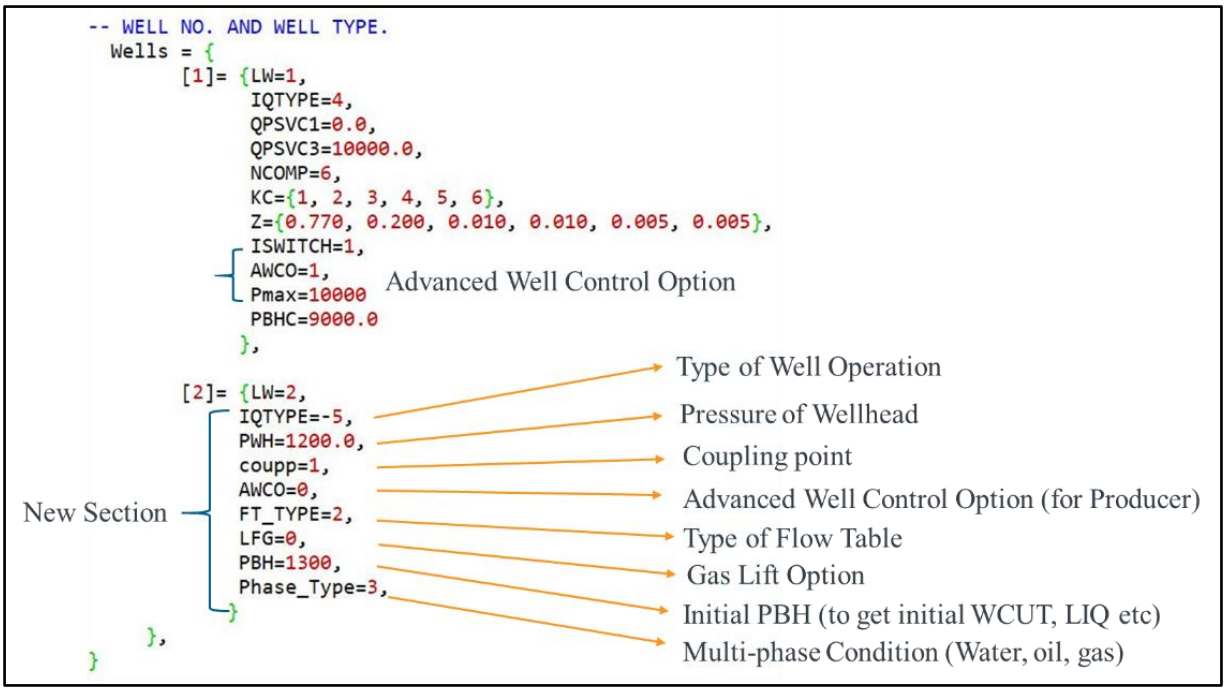

The next section presents the development of the sequential implicit coupling of the reservoir, well and surface facility

6.2. Sequential implicit coupling of the reservoir, well and surface facility

The sequential implicit coupling is based on the Gauss elimination approach as discussed in the previous chapter. Hence, two series of development are reported. In the first part, a new tool is developed to enable the simulator to receive the different types of surface facility equipment and assemble Eq. (5.5). The second part is to add the wellbore equation to the fully implicit formulation of the UTCOMPRS simulator and assemble Eq. (5.4).

6.2.1. Part One: Map of surface facility

Suppose a system of a single well that is operating under Fig. 66 configuration.

Figure 67 - Example of a well that works with wellhead and a separator

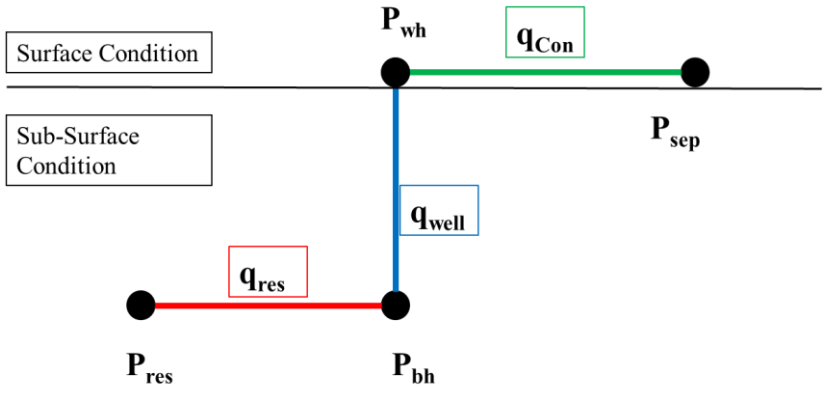

For simplicity, we assume the system is only producing single-phase oil. P_{res}, BHP, WHP, P_{sep}, q_{res}, q_{well}, q_{Con} indicate reservoir pressure, bottom hole pressure, wellhead pressure, separator pressure, flowrate in a single perforation, flowrate in the tubing and flowrate in connection line, respectively. Also, each section of this system is distinguished by a different color, so the three sub-systems existed. Here, we are assuming that the conservative law is valid for the mass of oil moving from the reservoir to the well and from well to the surface pipeline. The reservoir and separator pressures are also considered constant. Considering rate and pressure as the primary variable, the system presented in Fig. 67 has 7 unknowns; 4 nodes of pressures and 3 connections. However, since the two nodes are boundary conditions (reservoir pressure and separator), five equations are required for the aforementioned system.

For flow at the perforation, we can write the well equation as follows:

$$q = WI\ \lambda\ \rho\ x\ (p_{res} - p_{bh}) \tag{6.6}$$

where WI is the well index, x is the hydrocarbon component mole fraction, λ is the mobility and ρ is the molar density.

Based on continuity law, for flowrate in tubing and connection, we can write:

$$q_{res} - q_{well} = 0 \tag{6.7}$$

$$q_{well} - q_{con} = 0 \tag{6.8}$$

Now two additional equations are required for BHP and WHP. Since the system is working with the flow table, an additional explanation is required. For a simple connection like the one presented in Fig. 68, the flowrate (q) occurs based on the pressure difference between the upstream node (P1) and downstream node (P2).

Figure 68 - Flow rate between two nodes through a connection.

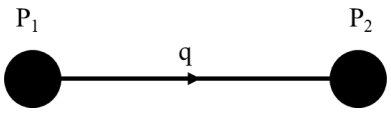

For such a system, we can write the flow equation as:

$$P_1 - P_2 - cq - d = 0 \tag{6.9}$$

where c and d are constants that vary for each system based on the operational condition, roughness and mechanical characteristic of the pipe. Here it is important to recall the difference between the flow equation and flow table. From a mathematical point of view, in order to solve a system that is working with the flow table, the downstream pressure is a function of upstream and rate, as indicated below:

$$P_2 = F\ (P_1 \text{ and } q) \tag{6.10}$$

But for the flow equation, the flowrate is a function of upstream and downstream pressures as shown in the following expression:

$$q = F\ (P_1 \text{ and } P_2) \tag{6.11}$$

Combining Eqs (6.9), (6.10) and (6.11) results in two additional equations, which are the flowrate in tubing and connection with flow table, in the format of flow equation, as follows:

$$P_{\text{bhp}}\text{-}P_{\text{whp}}\text{-}c_b q_{\text{well}}=0 \tag{6.12}$$

$$P_{\text{whp}}\text{-}P_{\text{sep}}\text{-}c_h q_{\text{con}}=0 \tag{6.13}$$

where c_b and c_h are constants that can be calculated from known values of upstream pressure, downstream pressure and flowrate of previous timesteps obtained from flow tables. Eqs. (6.12) and (6.13) are the final equations required for the BHP, and WHP unknowns, respectively. The system of equations can be written in the following format, similar to Eq. (4.33).

$$\begin{pmatrix} 1 & 0 & 0 & 0 & 0 & 0 & 0 \\ C_{res} & 1 & -C_{res} & 0 & 0 & 0 & 0 \\ 0 & 0 & 1 & -C_b & -1 & 0 & 0 \\ 0 & -1 & 0 & 1 & 0 & 0 & 0 \\ 0 & 0 & 0 & 0 & 1 & -C_h & -1 \\ 0 & 0 & 0 & -1 & 0 & 1 & 0 \\ 0 & 0 & 0 & 0 & 0 & 0 & 1 \end{pmatrix} * \begin{pmatrix} P_{res} \\ q_{res} \\ P_{bhp} \\ q_{well} \\ P_{whp} \\ q_{con} \\ P_{sep} \end{pmatrix} = \begin{pmatrix} R_{res} \\ R_{qr} \\ R_{Pb} \\ R_{qw} \\ R_{qw} \\ R_{qc} \\ R_{Pse} \end{pmatrix} \tag{6.14}$$

where C_{res} is the constant of Equation 6.6.

6.2.2. Table connections

Other issues that can change the method of solving the system are the layout and the map of the surface facility. The location and boundary value conditions should be passed to the simulator, adequately. Here, with an example, we show how mapping works for the sequential implicit coupling. Let us consider two ways of mapping: (i) based on the location of surface facility and how the fluid flow travels from higher pressure nodes toward lower pressure conditions as shown in red numbers in Fig. 69; (ii) considering pressure nodes first and connections next, as indicated by green numbers in the same figure.

Figure 69 - Two ways of mapping surface facility: on the left, the mapping increasing along the flow trajectory; and, on the right, pressure nodes are numbered first, and then connections

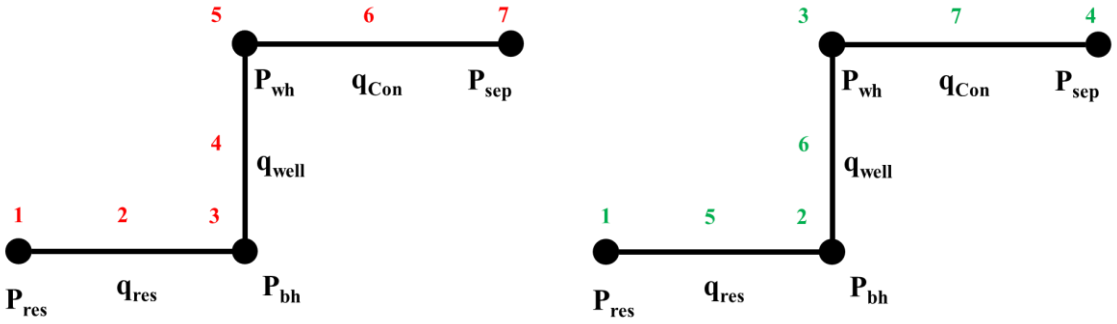

.

In the first approach, the separator boundary condition is set at node 7, while in the second approach it is located at node 4. Hence, in the second mapping, an additional computational effort is required to sort the system based on the numbering. This is illustrated mathematically by

$$\begin{pmatrix} P_{res} \\ q_{res} \\ P_{bhp} \\ q_{well} \\ P_{whp} \\ q_{con} \\ P_{sep} \end{pmatrix} = \begin{pmatrix} 1 \\ 2 \\ 3 \\ 4 \\ 5 \\ 6 \\ 7 \end{pmatrix} \qquad \begin{pmatrix} P_{res} \\ q_{res} \\ P_{bhp} \\ q_{well} \\ P_{whp} \\ q_{con} \\ P_{sep} \end{pmatrix} = \begin{pmatrix} 1 \\ 5 \\ 2 \\ 6 \\ 3 \\ 7 \\ 4 \end{pmatrix} \tag{6.15}$$

Additionally, based on how the connection is treated by the user, with a flow table or flow equation, the behavior of surface facility is different. Therefore, the shape of the matrix will be different. For example, in Fig. 68, let us consider the red mapping. For such a condition, if connection 6 is working with the flow table, node number 5 is a function of nodes number 6 and 7, while if the connection is working with flow equation, then node number 6 is a function of nodes number 5 and 7. The simulator should be able to distinguish these types of information. To do so, we have introduced a new tool named **connection tables**, which holds the information, details and map of surface facility structure, similar to the work of Alexis (**ALEXIS, 2009**). Once the connection table is fed to the simulator, the simulator can generate the surface facility configuration without the need for any third-party simulator. The connection table can be consistent with as many unknowns as the user requires. The condition of each segment, whether it needs to

be a flow equation, or a flow table, is also included. Fig. 70 shows an example of a table connection.

Figure 70 - Example of table connection.

```
#_Connection_Nodes
                3
#_Pressure_Nodes
                4
#_Boundry_Conditions
                2
!Vec_Unknown
 1 2 3 4 5 6 7
#_ROW_FOR_SURFACE_TABLE
                7
                        nodes       upstream     downstream  Condition
                            1              0              0          1
                            2              1              3          2
                            3              4              5          3
                            4              2              0          4
                            5              6              7          3
                            6              4              0          4
                            7              0              0          5
```

Table 11 shows the definition of each condition that we considered for a table of connection.

Table 11 - Different conditions and explanation of connection table.

Condition	Definition	Explanation
1	Reservoir Condition	The reservoir pressure is passed to the system
2	Perforation Condition	The required information is coming from the reservoir simulator
3	Flow Table Option	The connection is working with a flow table
4	Constant Rate	The rate is constant according to the conservative law
5	Separator Pressure	The separator pressure is read from the input

6.2.3. General workflow of sequential implicit formulation

The final remarks regarding sequential implicit formulation are how this formulation can be coupled with a reservoir simulator. Fig. 71 shows the general workflow of the sequential implicit formulation. First, the reservoir simulator is solved based on the initial WHP and BHP, calculating the flowrate of oil and gas. Based on those values, the C_b and

C_h coefficients are calculated, then the surface facility and their corresponding equations are assembled, with help of table connection. After the surface facility equipment is solved, new values of BHP, WHP and flowrate are calculated. The values of BHP and WHP and flowrate are checked with ones that have been obtained from the reservoir. If convergency occurs, the simulation goes to the next timestep. Otherwise, the rate from the surface facility is assigned to the reservoir simulator and the pressure boundaries are recalculated.

Figure 71 - General workflow of sequential implicit coupling of the reservoir, well and surface facility.

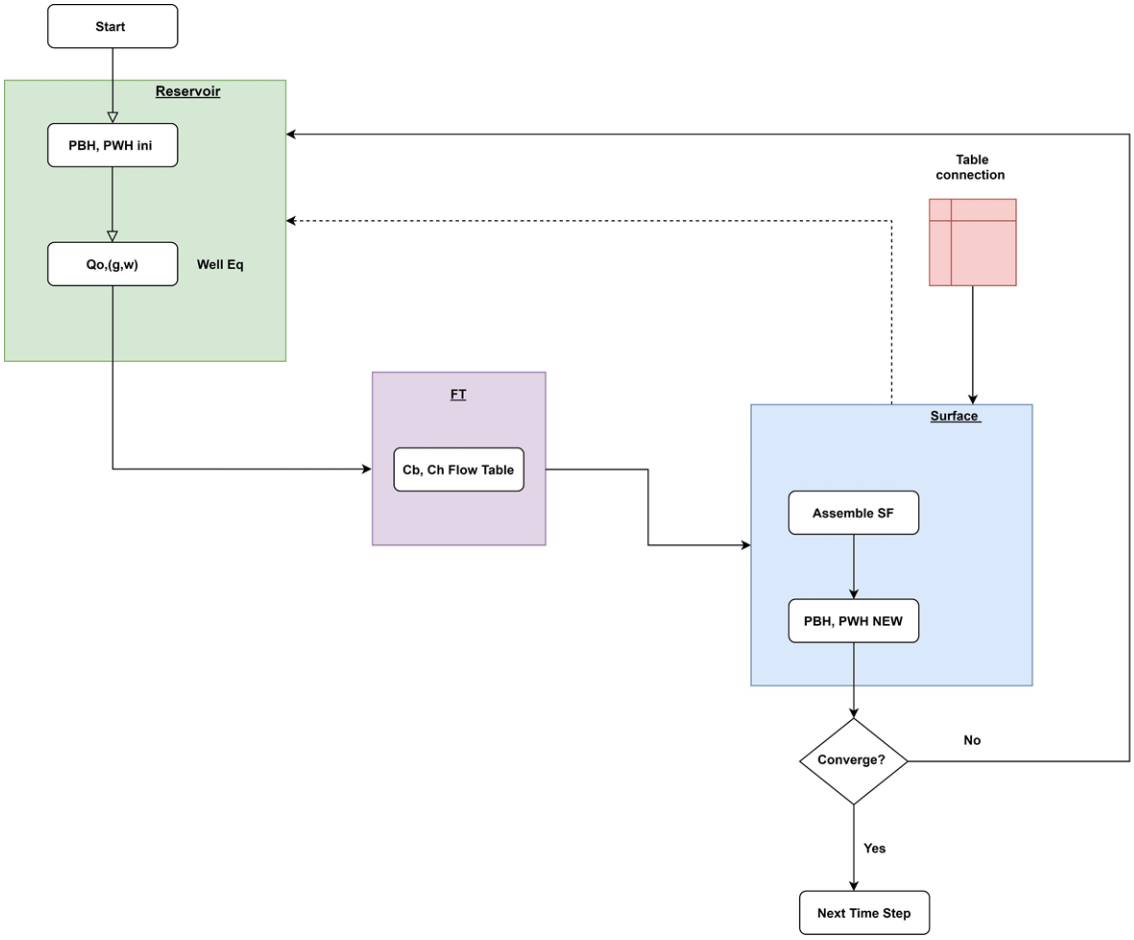

6.2.4. Part Two: Extension of fully implicit formulation

In order to extend the fully implicit formulation of the UTCOMPRS simulator, we have to add the well equation to the original formulation. Therefore, we write the well equation in the residual format as

$$R_{well} = Q_c^w - WI^w \sum_p \lambda_p \rho_p x_{cp} (p_p - p^w) \tag{6.16}$$

Also, we consider BHP as the primary variable for the wellbore, hence we can expand the original system of equations of the fully implicit formulation as follow:

$$\begin{pmatrix} RR & RW \\ WR & WW \end{pmatrix} \times \begin{pmatrix} \begin{pmatrix} \partial P \\ \partial N_1 \\ . \\ . \\ \partial N_{nc} \\ \partial Nw \end{pmatrix} \\ \left(\partial P_{BHP}\right) \end{pmatrix} = \begin{pmatrix} -RP_i \\ -RN_1 \\ . \\ . \\ -RN_{nc} \\ -RN_w \\ -R_{well} \end{pmatrix} \tag{6.17}$$

Rewriting the above equation, we have the following system which RP_i, $RN_{1,}$, RN_{nc} and RN_W are residual equations, in accordance with Fernandes dissertation (**FERNANDES, 2014**).

$$\begin{pmatrix} \begin{pmatrix} \frac{\partial RPi}{\partial Pj} & \frac{\partial RPi}{\partial N_1} & \frac{\partial RPi}{\partial N_{nc}} & \frac{\partial RPi}{\partial N_W} \\ \frac{\partial RN_1}{\partial Pj} & \frac{\partial RN_1}{\partial N_1} & \frac{\partial RN_1}{\partial N_{nc}} & \frac{\partial RN_1}{\partial N_W} \\ . & . & & . \\ . & . & & . \\ \frac{\partial RN_{nc}}{\partial Pj} & \frac{\partial RN_{nc}}{\partial N_1} & \frac{\partial RN_{nc}}{\partial N_{nc}} & \frac{\partial RN_{nc}}{\partial N_W} \\ \frac{\partial RN_W}{\partial Pj} & \frac{\partial RN_W}{\partial N_1} & \frac{\partial RN_W}{\partial N_{nc}} & \frac{\partial RN_W}{\partial N_W} \end{pmatrix} & \begin{pmatrix} \frac{\partial RPi}{\partial P_{BHP}} \\ \frac{\partial RN_1}{\partial P_{BHP}} \\ . \\ . \\ \frac{\partial RN_{nc}}{\partial P_{BHP}} \\ \frac{\partial RN_W}{\partial P_{BHP}} \end{pmatrix} \\ \begin{pmatrix} \frac{\partial R_{well}}{\partial Pj} & \frac{\partial R_{well}}{\partial N_1} & .. & \frac{\partial R_{well}}{\partial N_{nc}} & \frac{\partial R_{well}}{\partial N_W} \end{pmatrix} & \begin{pmatrix} \frac{\partial R_{well}}{\partial P_{BHP}} \end{pmatrix} \end{pmatrix} \times \begin{pmatrix} \partial P_i \\ \partial N_1 \\ . \\ . \\ \partial RN_{nc} \\ \partial N_w \\ \partial P_{BHP} \end{pmatrix} = \begin{pmatrix} -RP_i \\ -RN_1 \\ . \\ . \\ -RN_{nc} \\ -RN_w \\ -R_{well} \end{pmatrix} \tag{6.18}$$

For the derivative of reservoir with respect to the well, since the well primary variable is BHP, we can use the same derivative of the reservoir system, with a different reference pressure. Thus, the upper right-hand side of Eq. (6.18) (RW) becomes as follows:

$$\frac{\partial RPi}{\partial P_{BHP}} = \frac{\partial RPi}{\partial Pj} \tag{6.19}$$

$$\frac{\partial RN_1}{\partial P_{BHP}} = \frac{\partial RN_1}{\partial Pj} \tag{6.20}$$

$$\frac{\partial RN_W}{\partial P_{BHP}} = \frac{\partial RN_W}{\partial Pj} \tag{6.21}$$

$$\frac{\partial RN_{nc}}{\partial P_{BHP}} = \frac{\partial RN_{nc}}{\partial Pj} \tag{6.22}$$

The lower right-hand side equation (WR) is also a simple derivative of Equation 6.17 with respect to BHP, resulting in Eq. (6.23).

$$\frac{\partial R_{well}}{\partial P_{BHP}} = WI^w \lambda_p \rho_p x_{cp} \tag{6.19}$$

The first deviate of well with respect to the reservoir is similar to Eq. (6.23), but with a negative sign as follows:

$$\frac{\partial R_{well}}{\partial P_j} = -WI^w \lambda_p \rho_p x_{cp} \tag{6.24}$$

The only three derivates that still remains are $\frac{\partial R_{well}}{\partial N_1}$, $\frac{\partial R_{well}}{\partial N_{nc}}$ and $\frac{\partial R_{well}}{\partial N_W}$, but since we assume the BHP as the primary variable, the rate is constant, we can write:

$$\frac{\partial R_{well}}{\partial N_1} = 0 \tag{6.25}$$

$$\frac{\partial R_{well}}{\partial N_{nc}} = 0 \tag{6.26}$$

$$\frac{\partial R_{well}}{\partial N_W} = 0 \tag{6.27}$$

The final shape of Equation 6.18 is illustrated by Eq. (6.28).

$$\begin{pmatrix} \begin{pmatrix} \frac{\partial RPi}{\partial Pj} & \frac{\partial RPi}{\partial N_1} & \frac{\partial RPi}{\partial N_{nc}} & \frac{\partial RPi}{\partial N_W} \\ \frac{\partial RN_1}{\partial Pj} & \frac{\partial RN_1}{\partial N_1} & \frac{\partial RN_1}{\partial N_{nc}} & \frac{\partial RN_1}{\partial N_W} \\ \frac{\partial RN_{nc}}{\partial Pj} & \frac{\partial RN_{nc}}{\partial N_1} & \frac{\partial RN_{nc}}{\partial N_{nc}} & \frac{\partial RN_{nc}}{\partial N_W} \\ \frac{\partial RN_W}{\partial Pj} & \frac{\partial RN_W}{\partial N_1} & \frac{\partial RN_W}{\partial N_1} & \frac{\partial RN_W}{\partial N_W} \end{pmatrix} & \begin{pmatrix} \frac{\partial RPi}{\partial P_{BHP}} \\ \frac{\partial RN_1}{\partial P_{BHP}} \\ \frac{\partial RN_1}{\partial P_{BHP}} \\ \frac{\partial RN_W}{\partial P_{BHP}} \end{pmatrix} \\ \begin{pmatrix} -WI^w \lambda_p \rho_p x_{cp} & 0 & 0 & 0 \end{pmatrix} & \begin{pmatrix} WI^w \lambda_p \rho_p x_{cp} \end{pmatrix} \end{pmatrix} \times \begin{pmatrix} \partial P_i \\ \partial N_1 \\ \partial N_{nc} \\ \partial N_w \\ \partial P_{BHP} \end{pmatrix} = \begin{pmatrix} -RP_i \\ -RN_1 \\ -RN_{nc} \\ -RN_w \\ -R_{well} \end{pmatrix} \qquad (6.28)$$

This part of the implementation is still under development for the UTCOMPRS simulator, and therefore we are not presenting the results of this approach in this dissertation.

CHAPTER 7

DESCRIPTION, RESULTS AND ANALYSIS OF SIMULATION MODELS

The developed new tools of this work enable UTCOMPRS to simulate more realistic cases. Different production scenarios that are simulated with new tools presented in the previous chapters are shown next. Readers can refer to Appendix Two for phase behavior of the three types of fluids used in this dissertation.

7.1. Explicit coupling of the reservoir, well and surface facility

7.1.1. Case 1 – AFT – Effect of reservoir fluids

A two-dimensional reservoir was constructed for the first case study of AFT. To decrease the uncertainties, we assumed a homogeneous and isotropic reservoir. Detailed information on the reservoir and fluid properties can be found in Tables 12, 13 and 14. Table 15 shows the information of the well section. The information for surface facility is also presented in Table 16. Also, the surface facility are indicated in Fig. 7.

Table 12 - Reservoir information.

Reservoir Parameters	Value
Grid Blocks	8 x 8 x1
Grid Blocks Size in X direction	69.9 m
Grid Blocks Size in Y direction	69.9 m
Grid Blocks Size in Z direction	7.4 m
Porosity	0.10
Permeability in X Direction	10 md
Permeability in Y Direction	10 md
Permeability in Z Direction	5 md
Formation Compressibility kPa^{-1}	$4.0x10^{-6}$
Initial Reservoir Pressure	$3.1026x10^{4}$ kPa
Reservoir Temperature	76.66 °C
Simulation Run Time	100 days

Table 13 - Reservoir and injection fluid composition (3 components) for first case study.

Hydrocarbon components (Case1)	Initial concentration	Injection concentration
CO2	0.01	0.95
C1	0.19	0.05
NC16	0.80	–

Table 14 - Reservoir and injection fluid composition (6 components) for first case study

Hydrocarbon components (Case2)	Initial Concentration	Injection concentration
C1	0.50	0.7
C3	0.03	0.2
C6	0.07	0.01
C10	0.20	0.01
C15	0.15	0.005
C20	0.05	0.005

Table 15 - Technical information of wellbore section.

Wellbore Parameters	Value
Tubing Diameter	2.61 m
Casing Diameter	12.77 m
Tubing Length	661.4 m
Casing Length	762.3 m
Perforation location	680.6 m
Packers Location	637.3 m

Table 16 - Technical information of surface facility section.

Surface facility information	Value
Pipeline Diameter	0.15 m
Pipeline Length	2235. 7 m
Surface Temperature	21.1 °C
Coupling Point	Bottomhole

In this study, it was assumed that the separator can receive all of the produced fluid, *i.e.*, no controlling device was considered. Tables 11, 13, 14, and 15 indicate 25 variables associated with this integrated model. Based on the composition of reservoir fluids and all of the associated variables, the corresponding AFT was generated and inserted into the UTCOMPRS simulator. Fig. 71 shows the oil and gas rate profiles for the three hydrocarbon components. From Fig. 71 the trend of oil and gas are the same and this is why the GOR value was constant in Fig. 72. During the early production stage, oil and gas production curves declined on the third production day. Then, gas injection increased the flowrate of oil and gas and maintained the production flowrate.

Figure 72 - Production curve of oil and gas of the first case with 3 components

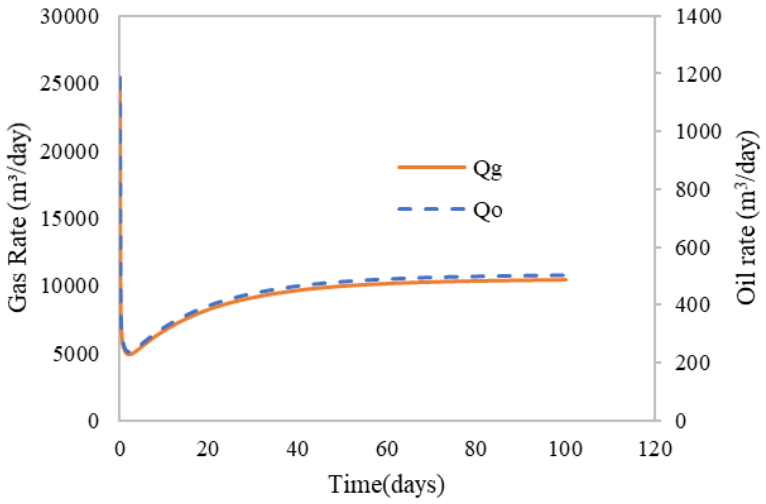

.

Fig. 73 shows the BHP and GOR constant for the first case study with 3 components.

Figure 73 - BHP and GOR overtime for the first case study with 3 components.

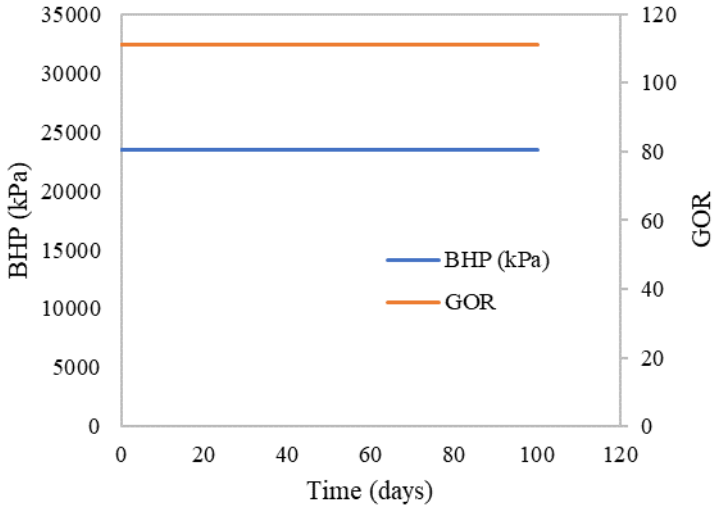

Fig. 74 shows the profiles of injector pressure, WHP, and PSEP and the average pressure of the reservoir. As indicated in this figure, wellhead and separator pressure follow the same trend. The dynamic changes of separator pressure, as an advantage of using AFT, is also shown. Additionally, since the injector pressure is high and the size of the reservoir is small (2-D reservoir model) the average pressure of the reservoir increases (orange curve). Furthermore, there were no constraints for operating wells (injector and producer), also justifying the increase in average pressure.

Figure 74 - Different pressure profiles for 3 component fluids.

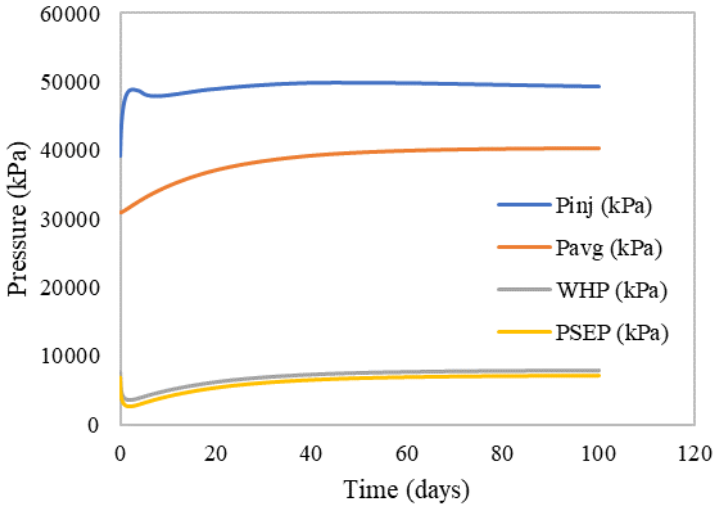

In Fig. 74, the order of magnitude of pressure is as follows: injector pressure, average pressure, WHP and PSEP for each time step. Readers should also pay attention that the AFT are generated using the commercial simulator, while the UTCOMPRS simulator only reads, interpolates and compares the calculated values with the current GOR, WOR and oil flowrates. The UTCOMPRS simulator is unable to generate individual values of AFT by itself.

AFT for 2D reservoir model with 6 components fluids

The second part of the first case study was designed to investigate the same 2D reservoir model, but now with 6 components. Therefore, the operating conditions, such as temperature, initial BHP guess and the other properties for the reservoir, well and surface facility were kept the same. Figs. 75, 76, and 77 show the profiles obtained for the 6 hydrocarbon components. The oil and gas rate profiles presented the same trend of of the 3 hydrocarbon components. However, the oil rate declines less for the 6 hydrocarbon components. Fig. 75 illustrates this behavior.

Figure 75 - Production curve of oil and gas of case two for 100 days.

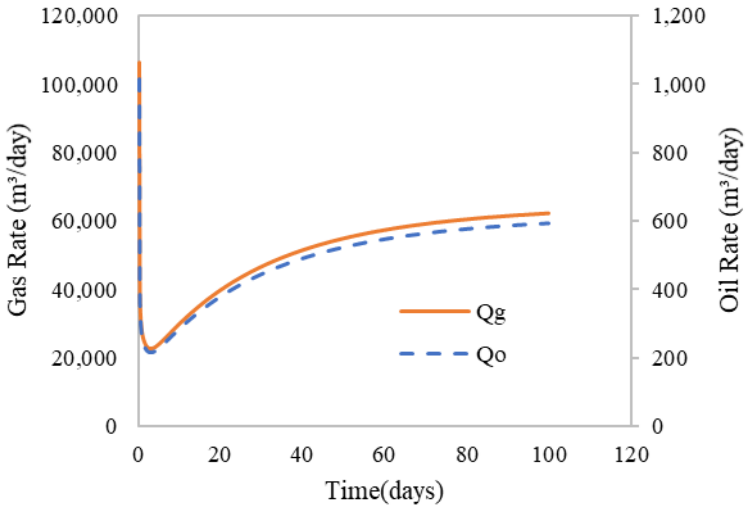

The changes of BHP and GOR for the 6 hydrocarbon components are presented in Fig 76. Also, compared to case one, case two has greater GOR values. They are 111.1 and 558.56 for cases one and two, respectively.

Figure 76 - BHP and GOR behavior of case two with a slight BHP increase of 55.6 kPa.

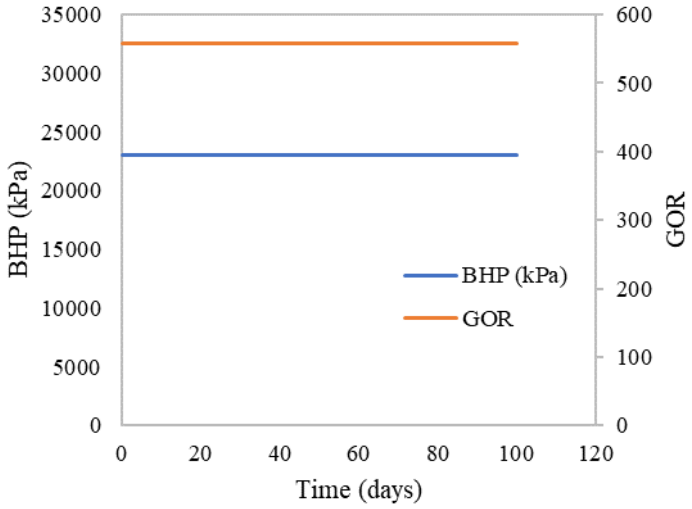

Finally, Fig. 77 shows the same trends for pressure variations for the second case. Similar to case one, the average reservoir pressure and injector pressure increased and both of them have a sharper increase in the final days of production. The variations of WHP and PSEP are not the same as in case one. They were constant for almost the first ten days of production. This information reveals that the change of surface condition is a function of the fluid type that exists in the reservoir.

Figure 77 - Different pressure changes of 6 components fluid.

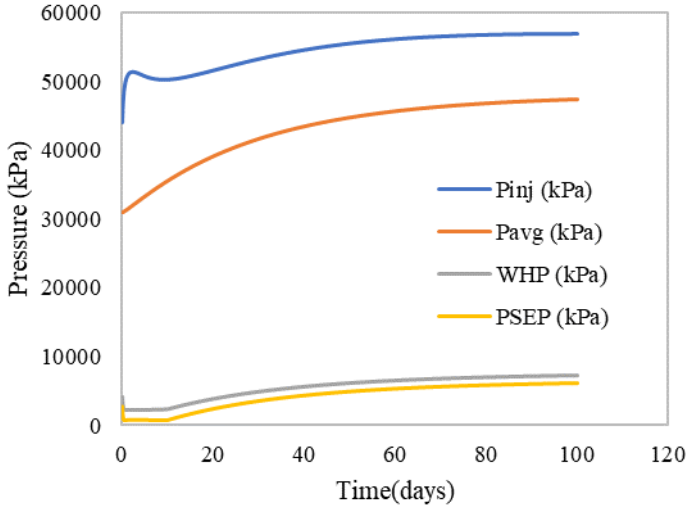

The two case studies presented above show that the new sequential coupling strategy was implemented successfully. UTCOMPRS simulator was able to read, compare, and update surface facility information that was generated by a commercial simulator. The simulator reported WHP and Dynamic PSEP properly. And based on the type of reservoir fluids, different profile pressure was observed at the surface.

7.1.2. Case 2 – CFT – Interpolation functions

In this section, firstly we show the investigation of the parameters used in the interpolation function. Also, the reservoir models used here were previously compared with a commercial simulator for the producer operating under a constant bottom hole pressure. Herein, the interpolation function results when using different parameters based on Eq. (6.2) was investigated. Table 17 shows details of the interpolation parameters that were used.

Table 17 - Different independent variables for interpolation functions to calculate the BHP.

Test	Y	X
Test 1	BHP	WCut
Test 2	BHP	GLR
Test 3	BHP	Liq
Test 4	BHP	WHP (an average of higher and lower indices values)
Test 5	BHP	WHP (Only higher index values)
Test 6	BHP	WHP (Only lower index values)

In this case, a two-dimensional reservoir was used. To decrease the uncertainties, it was assumed to be a homogeneous and isotropic reservoir. Detailed information on the reservoir, well and fluid properties can be found in Tables 12 and 13. Table 18 shows the information about the well section and surface facility. Also, here the coupling point is assumed to be bottomhole, with water injection.

Table 18 - Wellbore properties and operational conditions to generate corresponding flow table.

Wellbore Parameters	Value
Tubing Diameter	0.134112 m
Bottom Hole Temperature	76.66 °C
Wellhead temperature	26.6 °C
Tubing length	762 m
Fix wellhead Pressure	8273.709 kPa
Injector Rate (water)	1589.87 m^3/d
Injector limit (activated)	68947.57 kPa

Figs. 78(a-g) show the results of bottom hole values for UTCOMPRS and a commercial simulator using a linear interpolation. In this regard, the only parameter that matter for the simulator is the bottomhole value. Different interpolation parameters showed different BHP behavior. However, among the four parameters (WCUT, LGR, Liquid flowrate and WHP), evaluated in Tests 1 through 4, the WHP was the one with best results (Figs. 78 a-d). Now, referring only to the WHP, evaluated in Tests 4 through 6, the bottom hole pressure values obtained from lower indices (Test 6) showed the best match with the commercial simulator (Figs. 78 f).

Figure 78 - BHP as a function of different interpolation parameters: (a) water cut; (b) gas-liquid ratio; (c) liquid rate; (d) WHP average from lower and higher indices; (e) WHP from the higher index; (f) WHP from the lower index: (g) pressure of the injector

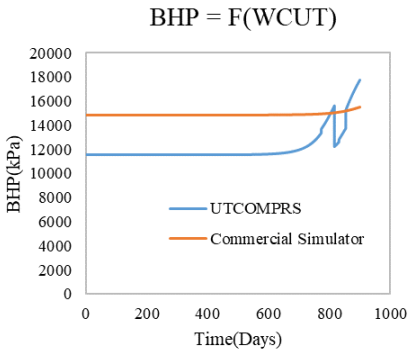

(a)

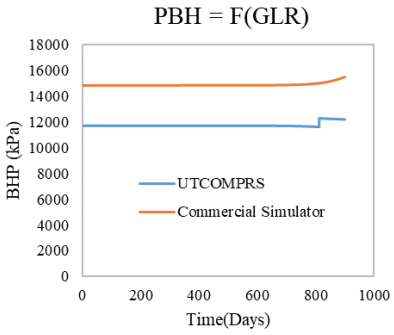

(b)

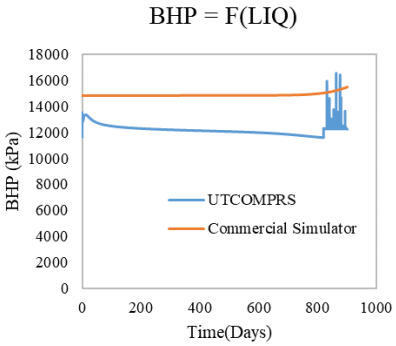

(c)

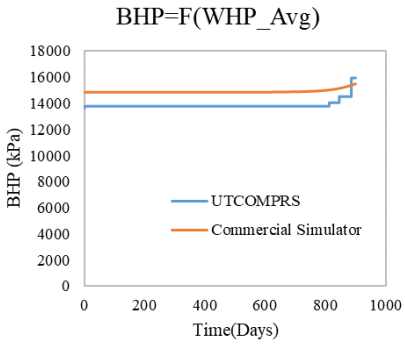

(d)

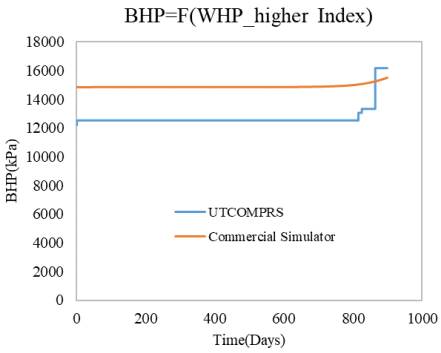

(e)

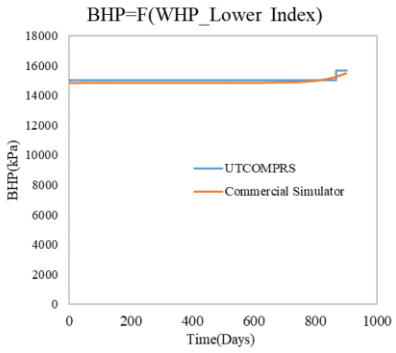

(f)

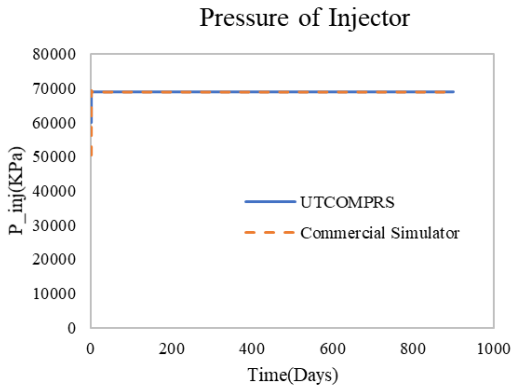

(g)

The results from Test 1 are presented in Fig. 78 a. The BHP varies unpredictably. This occurs due to the range of water cut values. Since the WCUT varies in a range from 0 to 1, a small WCUT change will result in a completely different interpolated BHP value.

Although the best result is the one from Test 6, at the ultimate days, the behavior of the bottom hole pressure curve for UTCOMPRS changes sharply, resulting in a step-like curve, while the values of the commercial simulator are changing gradually (Fig. 78f). Nevertheless, the obtained values at the end of the simulation were at accepted tolerance. This different behavior can be a result of three reasons: method of searching in the tables, method of converting flow conditions into indexes and convergence criteria for the simulators. However, for our studies, the WHP at lower indices (Fig. 78f) is the accepted interpolation parameter. Finally, for all of the six tests, the new limit for injection pressure is activated in less than a day (0.33 days). This is shown in Fig. 78g. Based on the results of this study, the interpolation function was selected as the WHP with lower values for the UTCOMPRS simulator, when the producing well is working with CFTs. In the next section, we will show, the result of different case studies for the developed framework.

7.1.3. Case 3 – CFT - Effect of wellhead pressure

To check the results of the developed framework, the third case shows the results of a 2D reservoir, with bigger gridlocks. For different production scenarios, the wellhead pressures are selected at different levels (600 and 1200 psi) based on Rodrigzie et al. [**RODRIGZIE** et al.; 2007]. Reservoir properties, hydrocarbon fluids and injection fluids are reported in Table 19.

Table 19 - The reservoir details, hydrocarbon components and injection fluid for Case 3, for assessment of wellhead pressure effects.

Properties	**Value**
Number of grid blocks in x,y,z directions	16x16x1
Size of grid blocks in x,y,z directions	30.48x30.48x24.38 m (100x100x80 ft)
Porosity	0,35
Permeability in x, y, z directions	10x10x10 md
initial reservoir pressure	10342.13 kPa (1500 psi)
Components	"C1","C3","C6","C10","NC15","C20
Initial concentration	0.50, 0.03, 0.07, 0.2, 0.15, 0.05
Injection fluid concentration	0.77, 0.20, 0.01, 0.01, 0.005, 0.005
Type of producing well	CFT
Injection rate	Constant rate, gas injection
AWCO for injector and limited pressure	activated, 11721.09 kPa (1700 psi)
Operating wellhead pressure	4136.85 and 8273.70 kPa (600 and 1200 psi)
Coupling point	bottom hole
LFG	0.0 (no gas lift condition)
Phase type (for comparing function)	Multiphase Table
Simulation run time	10000 days

Figs. 79 and 80 show the comparison of oil and gas production rates under 4136.85 kPa and 8273.70 kPa (600 and 1200 psi) wellhead pressure constraints. The shape of production is different because, by changing the WHP, the operational parameters are different, hence, a different table was used for the well that operates with 4136.85 kPa(600 psi) at the wellhead, to cover the wider range of production. Appendix three shows an example of flow table that was used. For this case study, also there was no water production. Consequently, here, we are not reporting the produced water and WOR curves.

Figure 79 - Oil production for high (top) and low (down) wellhead pressure constraints.

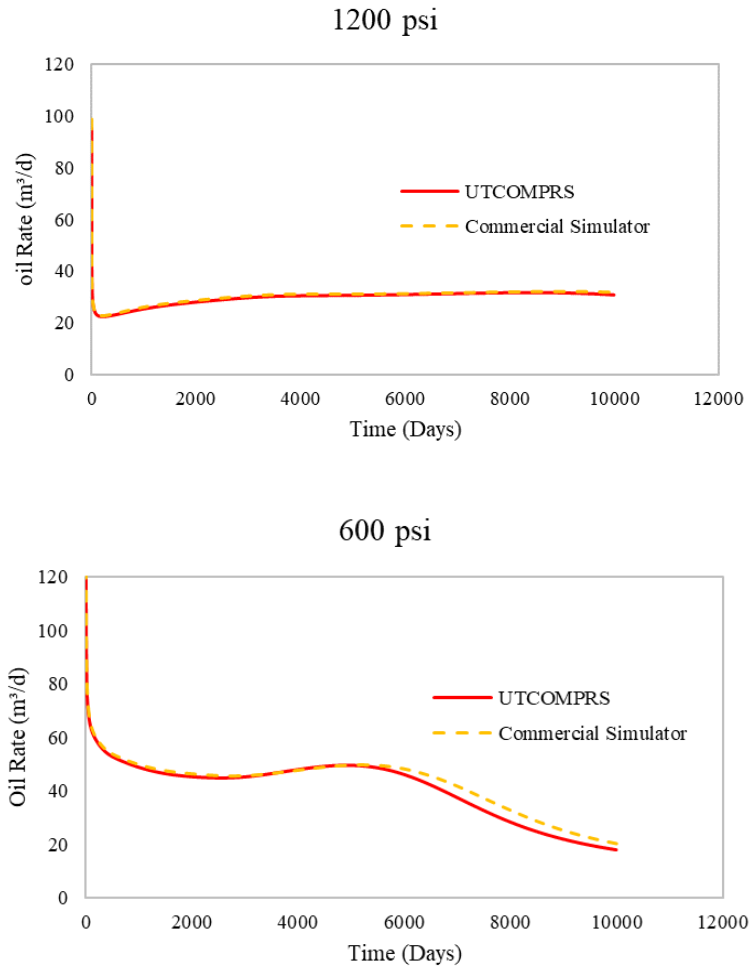

Figure 80 - Gas production for high (top) and low (down) wellhead pressure constraints.

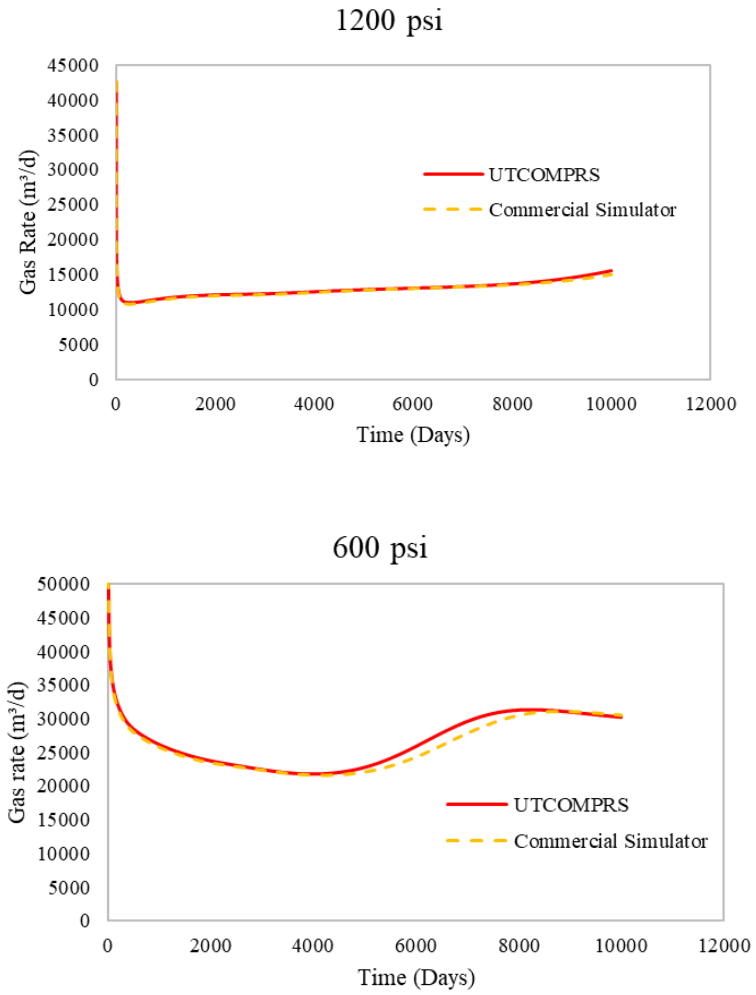

Fig. 81 shows the wellhead pressures for different scenarios of production.

Figure 81 - Comparison of wellhead pressures for different scenarios of production.

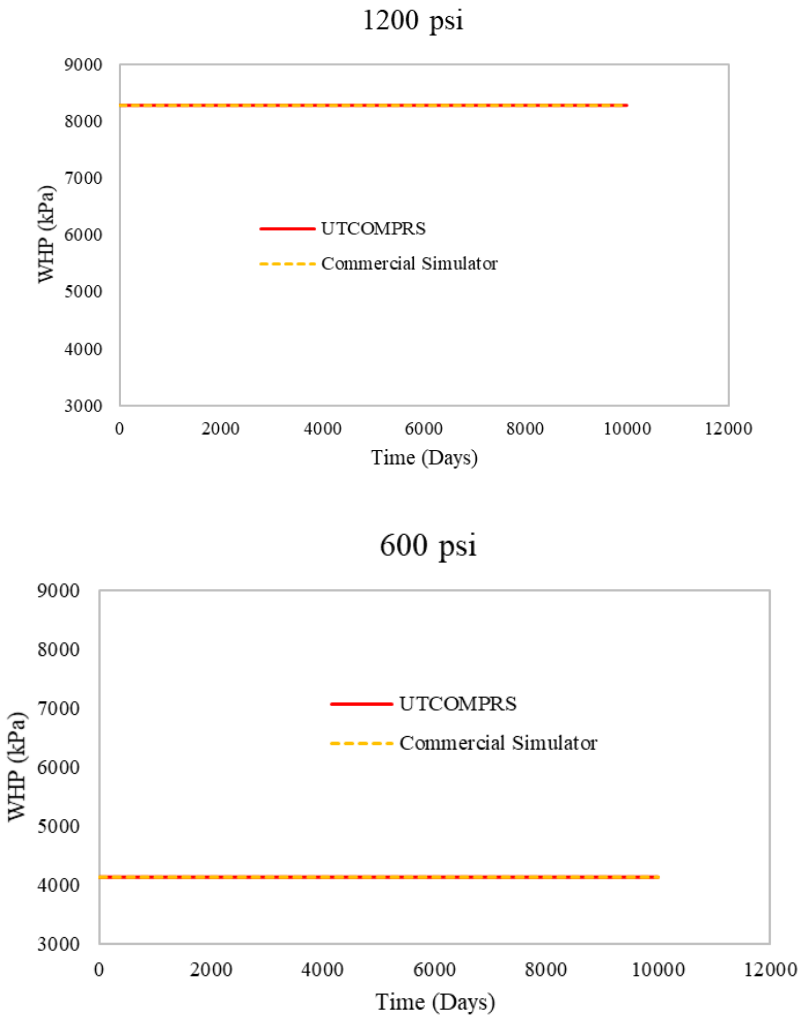

Figs. 82 shows BHP for a different production scenario.

Figure 82 - Interpolated BHP for high (top) and low (down) wellhead pressure constraints.

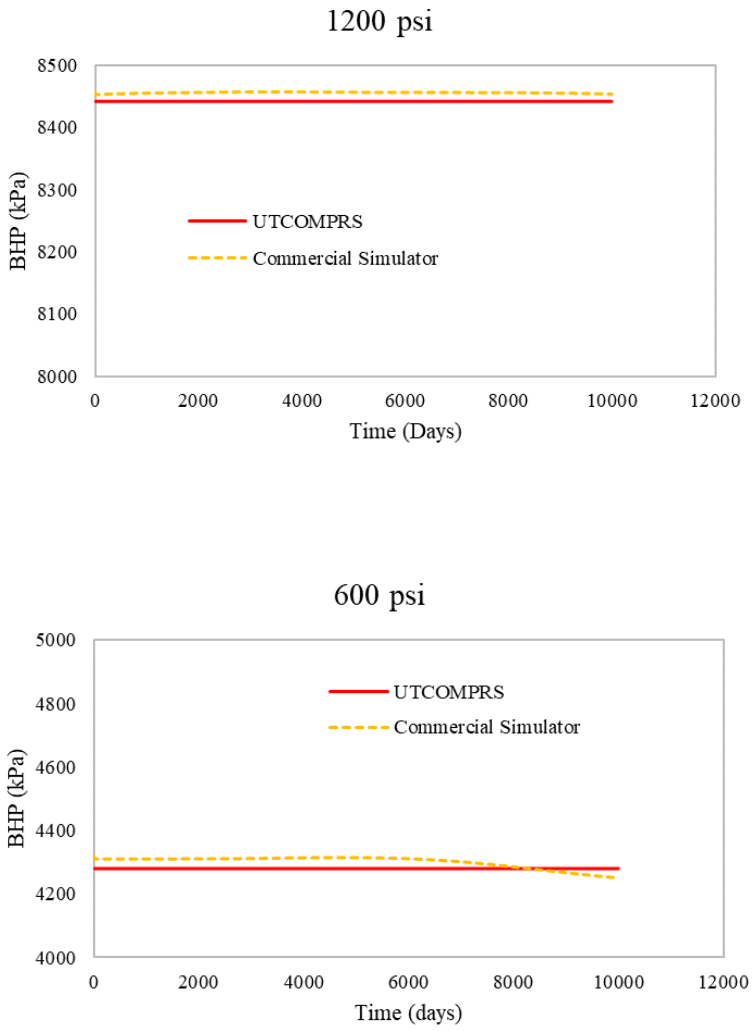

As can be seen from Fig. 82, for high wellhead pressure the results are similar, but for the low wellhead pressure scenario, there is a very small variation, 68.25 kPa (9.9 psi) in the commercial simulator.

Figs. 83 demonstrates the effect of injection pressure restriction in the production profile.

Figure 83 - Injection pressure for high (top) and low (down) wellhead pressure constraints.

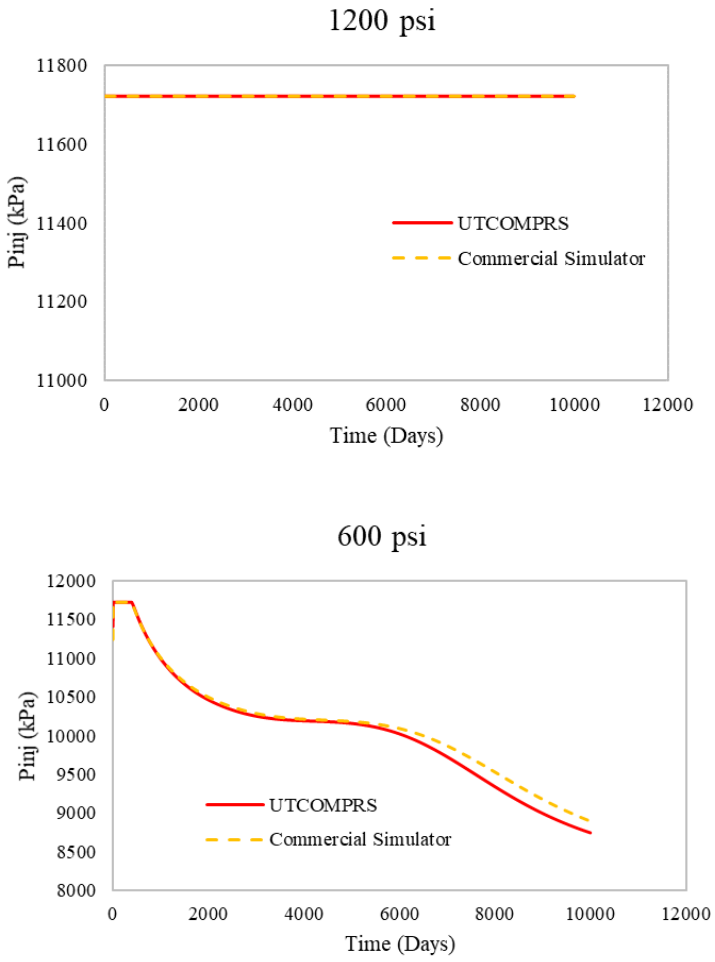

As can be seen from Fig. 83, for the higher wellhead pressure constraint, the activation of constraint for injector will take place and injection pressure remains constant until the end of the simulation. However, for the lower wellhead pressure constraint, the activation occurred only up to 67 days. Then, since the average reservoir pressure becomes less than the injector constraint, the injector constraint will be deactivated. Also, a small deviation can be noted for the UTCOMPRS simulator at the end of the simulation, 144.79kPa, (21psi).

Fig. 84 show the GOR for different production scenarios of Case 1.

Figure 84 - GOR results for high (top) and low (down) wellhead pressure constraints.

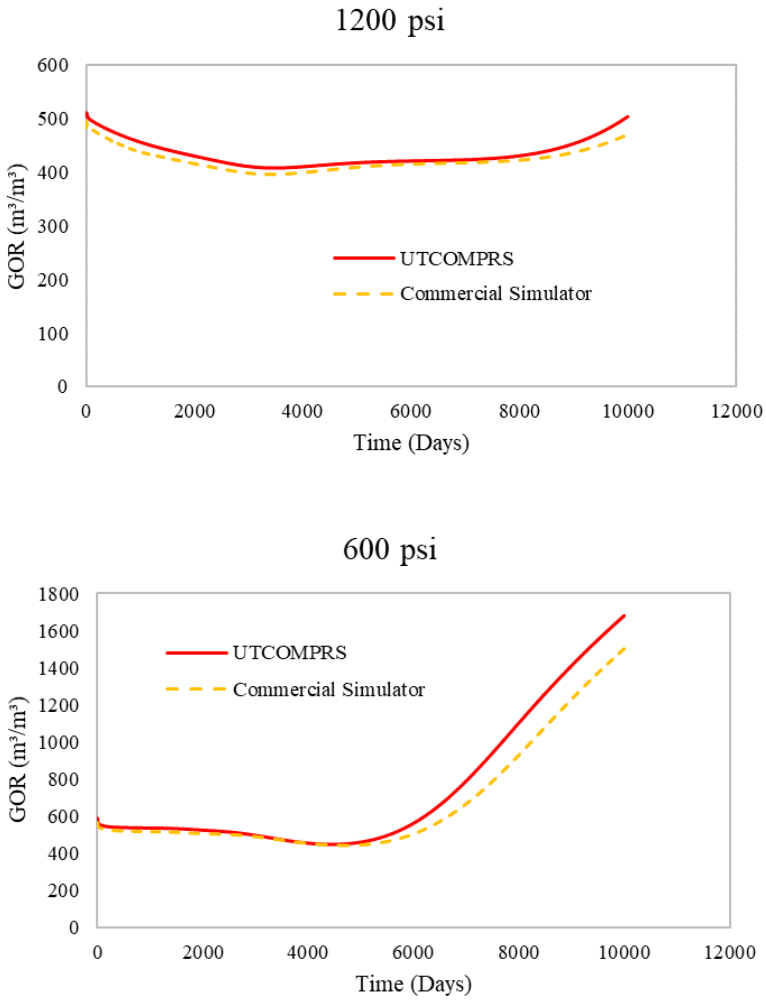

As can be seen from Fig. 84, GOR is the best indicator for showing the difference between the simulators. In this study, based on the activation of the injector, the GOR curves show a deviation between two simulators after 5000 days for low wellhead pressure constraint.

Figs. 85-88 show the comparison of the UTCOMPRS and the commercial simulator in terms of reservoir pressure at 359, 8.999 days, as well as oil production at 2.499 and 8.999 days, respectively.

Figure 85 - Pressure profile at 359 days; UTCOMPRS (left) and commercial simulator (right).

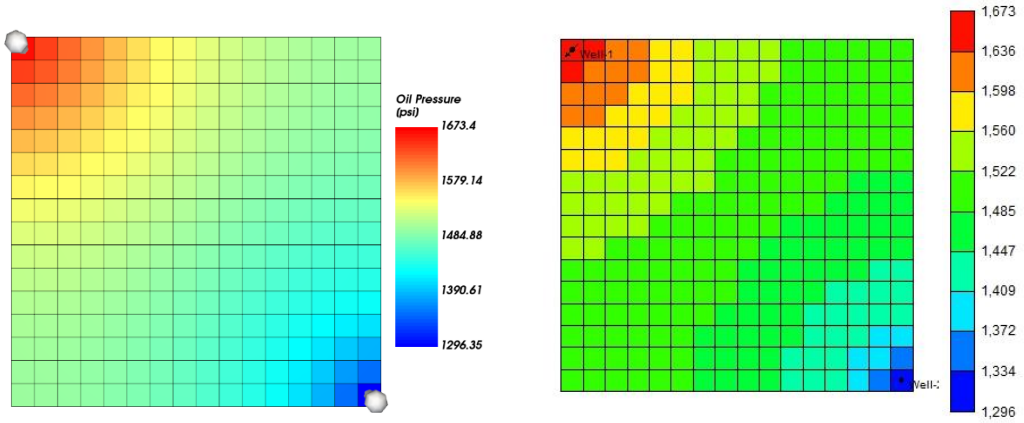

Figure 86 - Pressure profile at 8.999 days; UTCOMPRS (left) and commercial simulator (right).

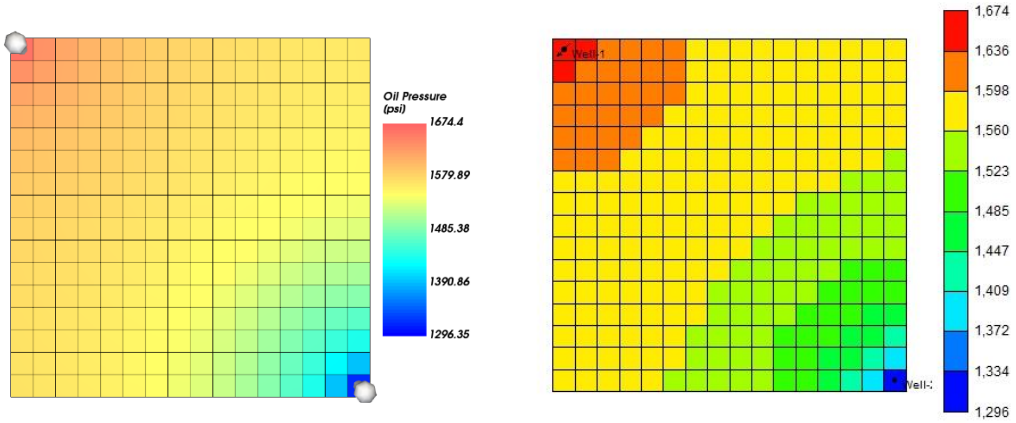

Figure 87 - Oil saturation field at 2.499 days; UTCOMPRS (left) and commercial simulator (right).

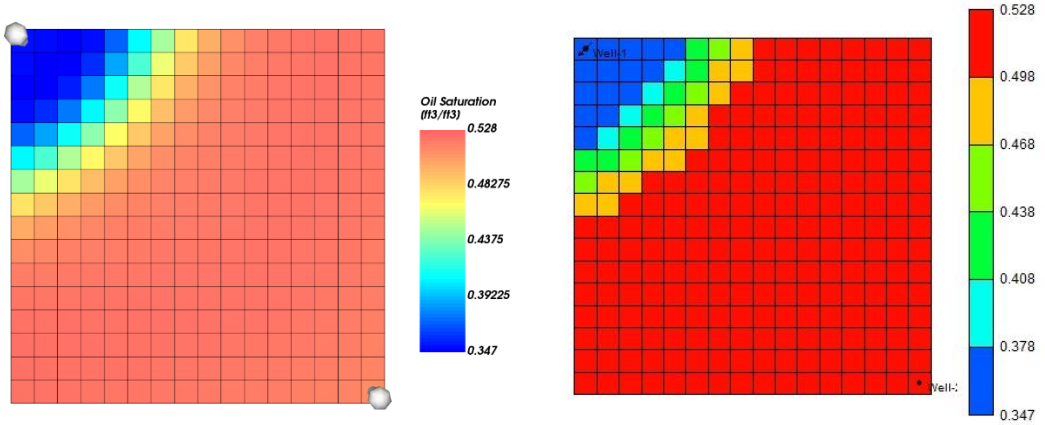

Figure 88 - Oil saturation field at 8.499 days; UTCOMPRS (left)
and commercial simulator (right).

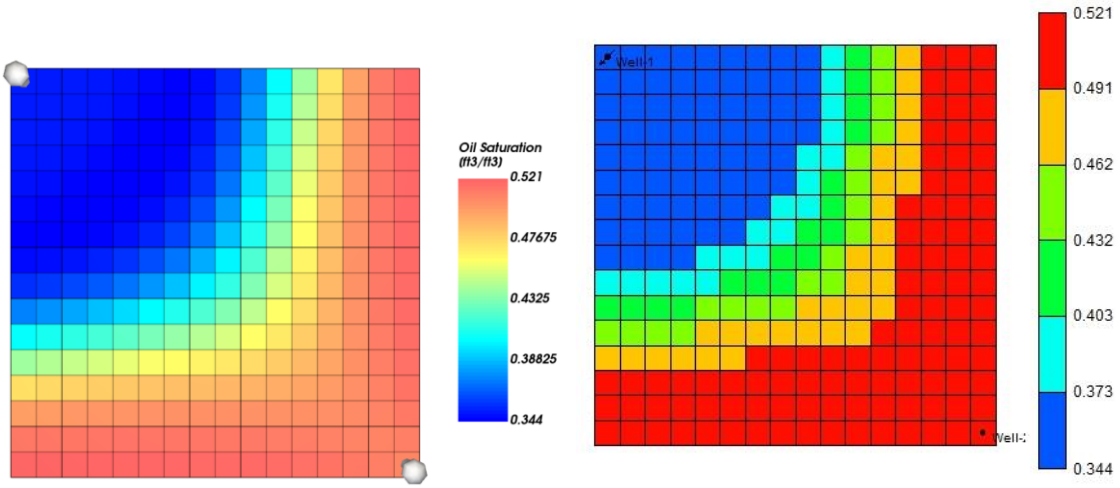

7.1.4. Case 4 – CFT - Effect of injection rate

The fourth case study is about an investigation of the same reservoir and fluid properties presented in case three, with three different modifications: first, the simulation run time decrease up to 2.000 days; second, instead of 2D, we consider a 3D reservoir model and due to that we increased the z-direction thickness from (24.38 to 30.48 m) (80 to 100 ft) for each block; and third, for the comparison parameter 1.000 and 5.000 scf/day gas injection flowrate was selected.

Fig. 89 shows the shape of the reservoir used for case 4.

Figure 89: Reservoir configuration used for Case 4.

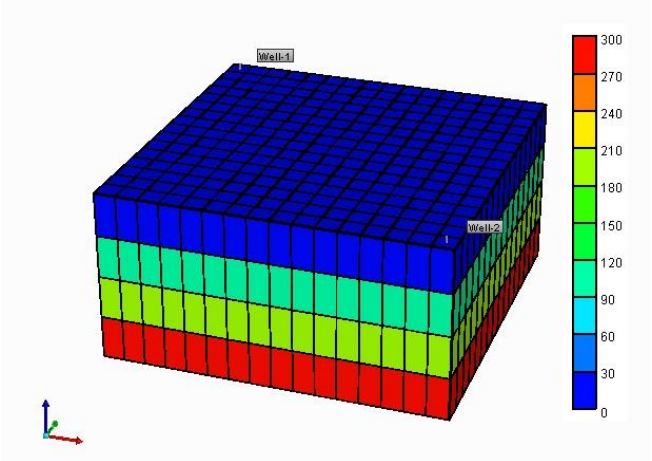

Figs. 90 and 91 show the oil and gas production rate for high (5.000 SCF/day) and low (1.000 SCF/day) gas injection rates. As can be seen, during the low injection rate scenario, for both oil and gas production profiles, there was an oscillation at 763 days for UTCOMPRS. This oscillation is due to the change of the location of the interpolated BHP in the flow table.

Figure 90 - Oil production for high (top) and low (down) gas injection rate.

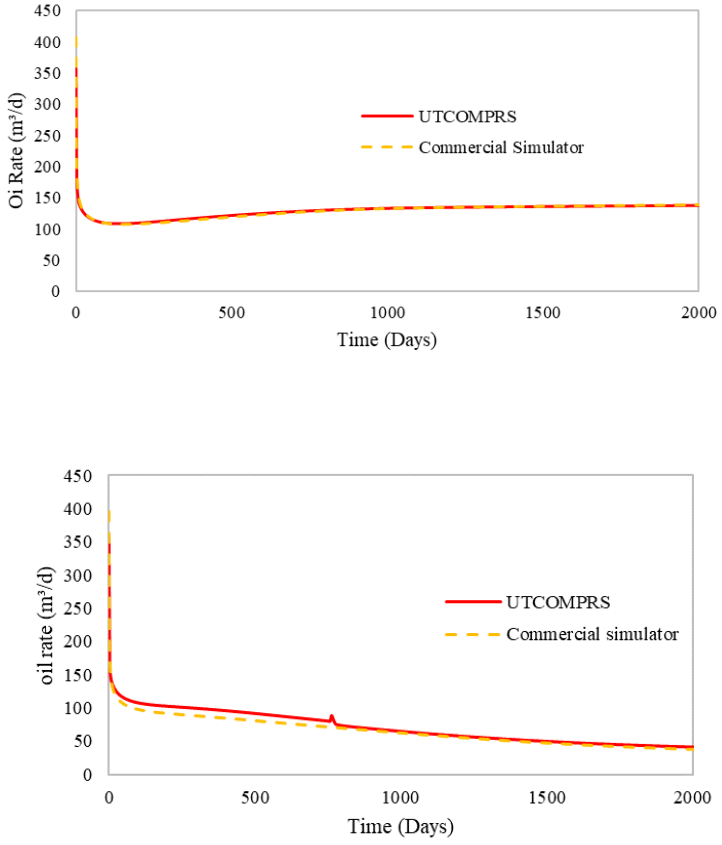

Figure 91 - Gas production for high (top) and low (down) gas injection rate.

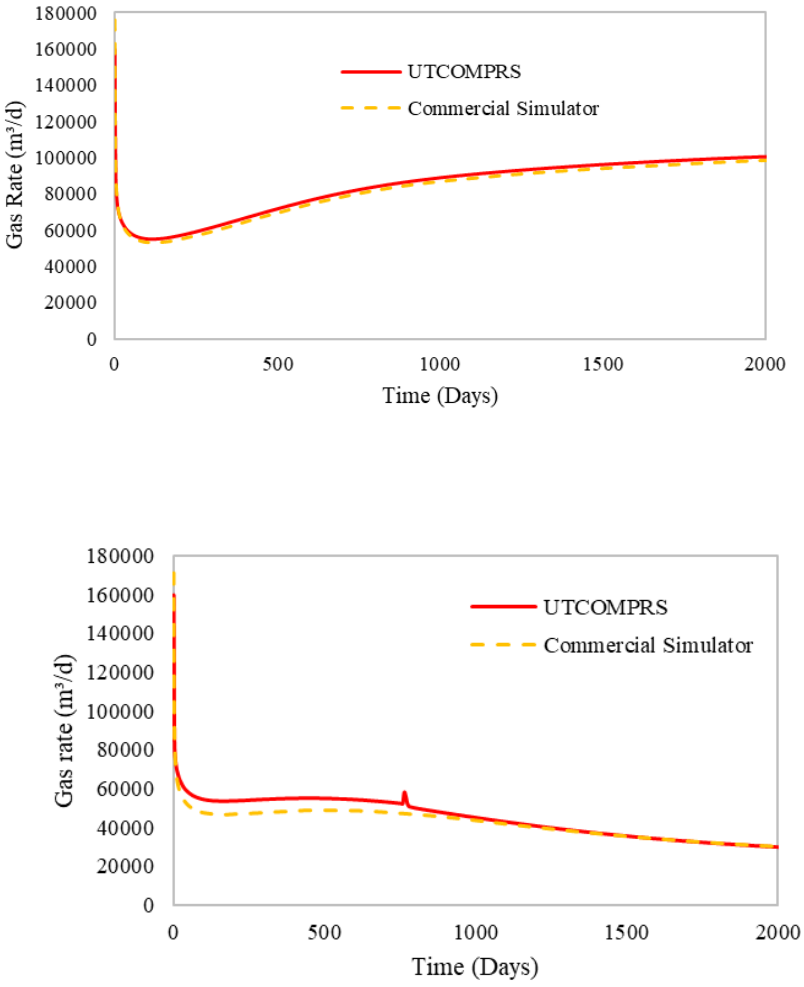

Fig. 92 shows the BHP for both low and high gas injection rates.

Figure 92: Interpolated BHP for high (top) and low (down) gas injection rates.

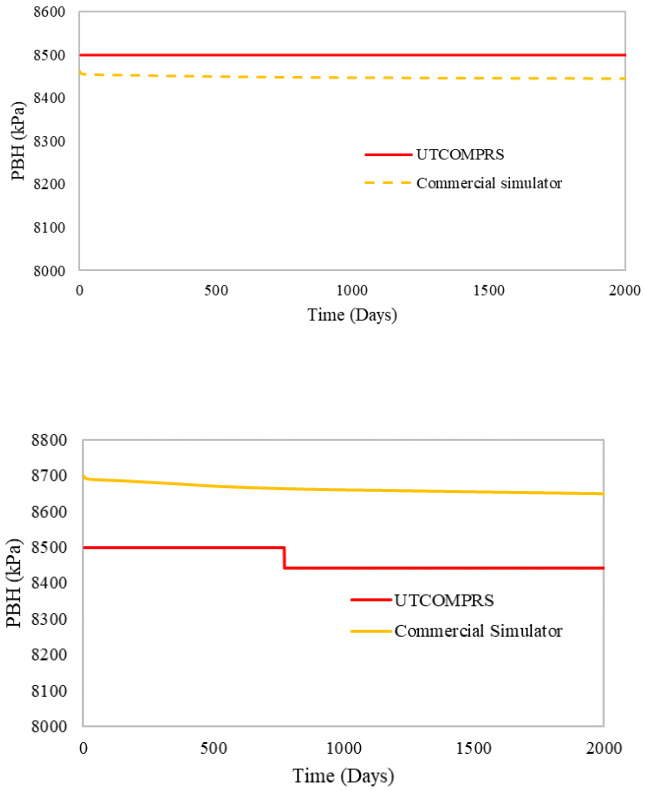

From Fig. 92, the obtained BHP profiles of the UTCOMPRS simulator, for a higher injection rate scenario, are closed enough to the commercial simulator with the maximum difference between the profiles of only 42.74 kPa (6 psi). However, for the low gas injection rate, the maximum difference between the profile of both simulators increased, 206.84 KPa (30psi). We believe this increase is due to the different injector pressures, 337.84 KPa (49psi). The notable outcome of this study is the activation of the injector limit, which is shown in Fig. 93. As can be seen due to the lower injection rate, the injector constraint is not activated. For the low gas injection rate, the BHP will change at 763 days. This is the reason for the oscillation in the oil and gas production curves. Also, for the injector pressure, in the lower injection rate, once the value of BHP shifted to the lower section of the table, the injector responded to this change. This information shows that for the successful implementation of CFTs inside UTCOMPRS, the injector plays a significant impact.

Figure 93 - Injector pressure for high (top) and low (down) injection gas flowrates.

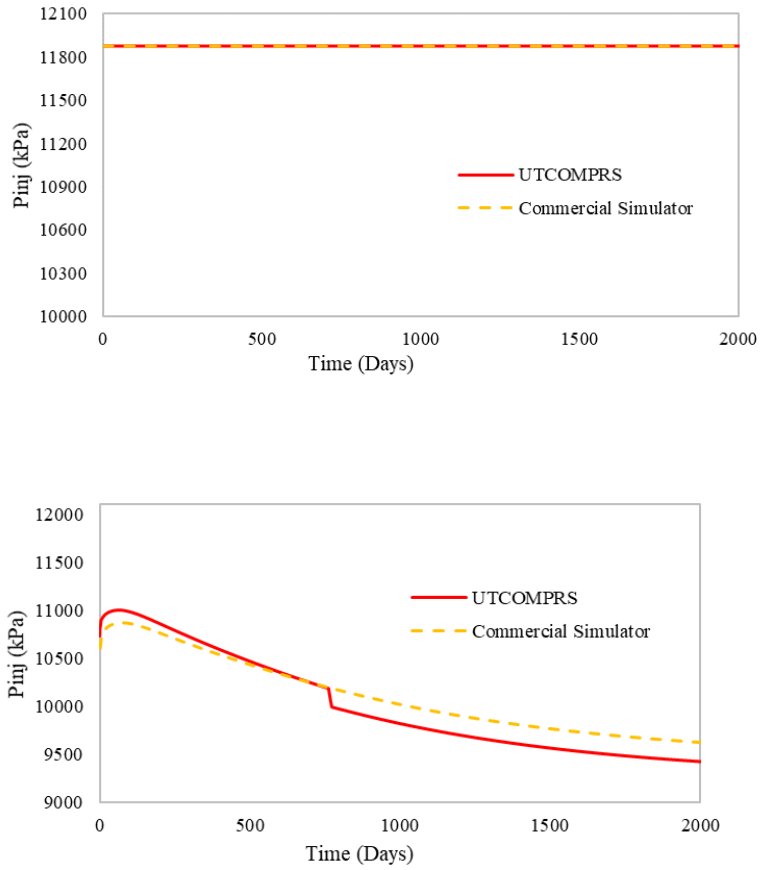

Fig. 94 shows the GOR for Case 4.

Figure 94 - GOR for high (top) and low (down) gas injection scenarios.

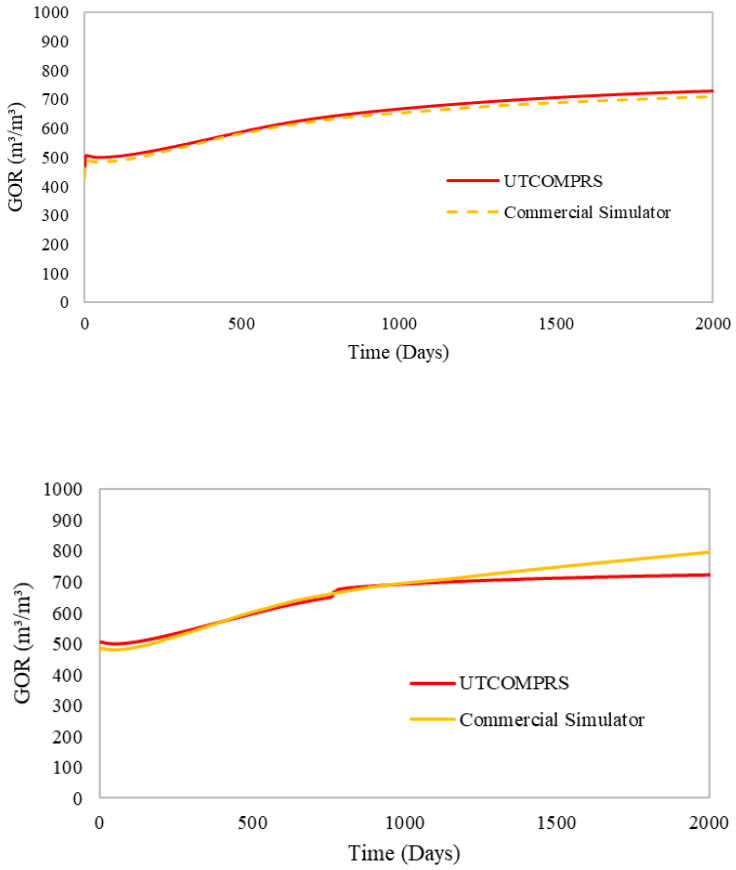

Similar to case three GOR profile between both simulators increase when shows the final difference between the commercial and UTCOMPRS simulator. Additionally, the change in the bottomhole pressure in the table is affecting the GOR at 763 days.

7.1.5. Case 5 – CFT - Simple multi-well study

In the third case two symmetric wells, working with a flow table, and an injector is used to investigate the effect of multiple-wells for CFT. Accordingly, a series of modifications were made for the shape of the reservoir. Table 20 shows these modifications.

Table 20 - Modifications for the fifth case study.

Modifications	**2D**	**3D**
Numbers of Grid Blocks	9x9x1	9x9x5
Size of the Reservoir	60.96x60.96x24.38 m (200x200x80 (ft))	60.96x60.96x4.87m (200x200x16 (ft))
Location of Injector	5,5,1	5,5,3
Location of First Producer	9,1,1	9,1,3
Location of Second Producer	9,9,1	9,9,3

In addition, since the reservoir is homogenous and the well arrangement is symmetric, the same flow table is used for both wells. Also, the multiple wells algorithm is coupled with 2D and 3D configurations to test the capability of developed codes for UTCOMPRS. Fig. 95 shows the 2D and 3D reservoir configurations.

Figure 95 - 2D (left) and 3D (right) reservoir configuration for Case 5, with 80 ft of thickness

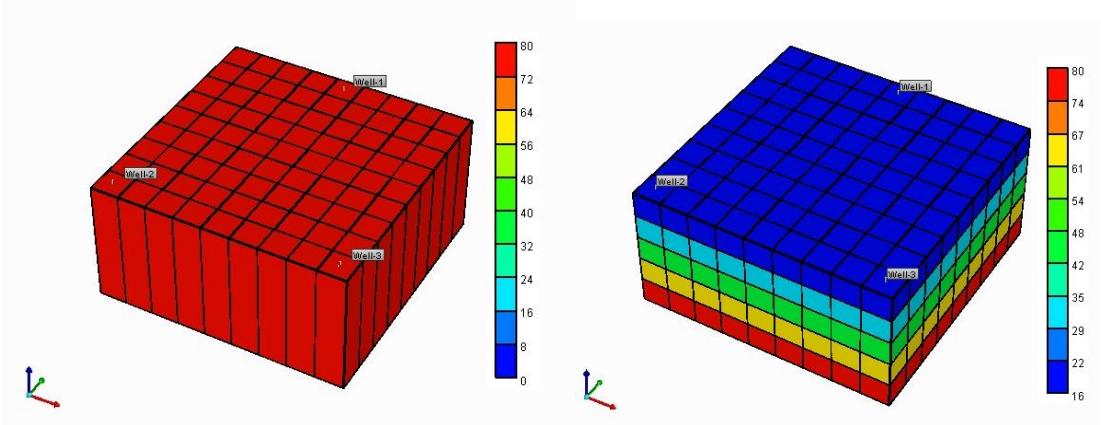

Figs. 96 and 97 show the oil and gas production rates for both wells in the 2D and 3D reservoirs. In both cases, there is a small deviation between the profiles of the UTCOMPRS and commercial simulators, before 500 days.

Figure 96 - Oil production for 3D (top) and 2D (down) reservoirs.

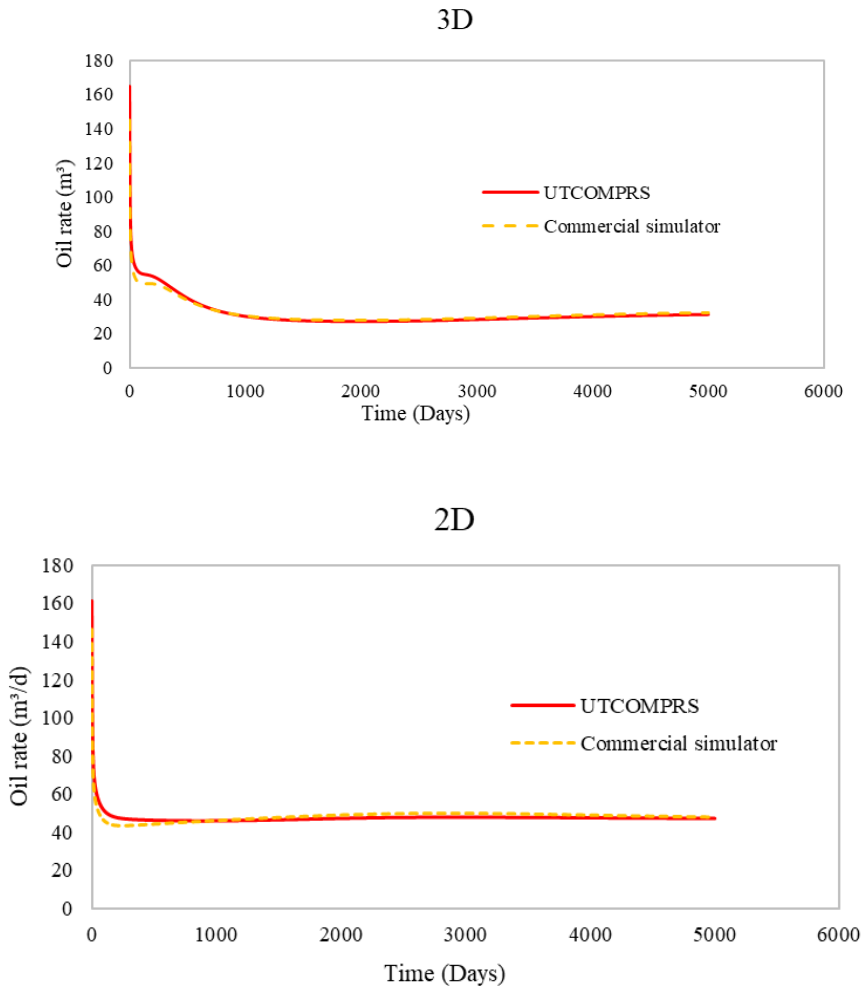

Figure 97: Gas production for 3D (top) and 2D (down) reservoirs.

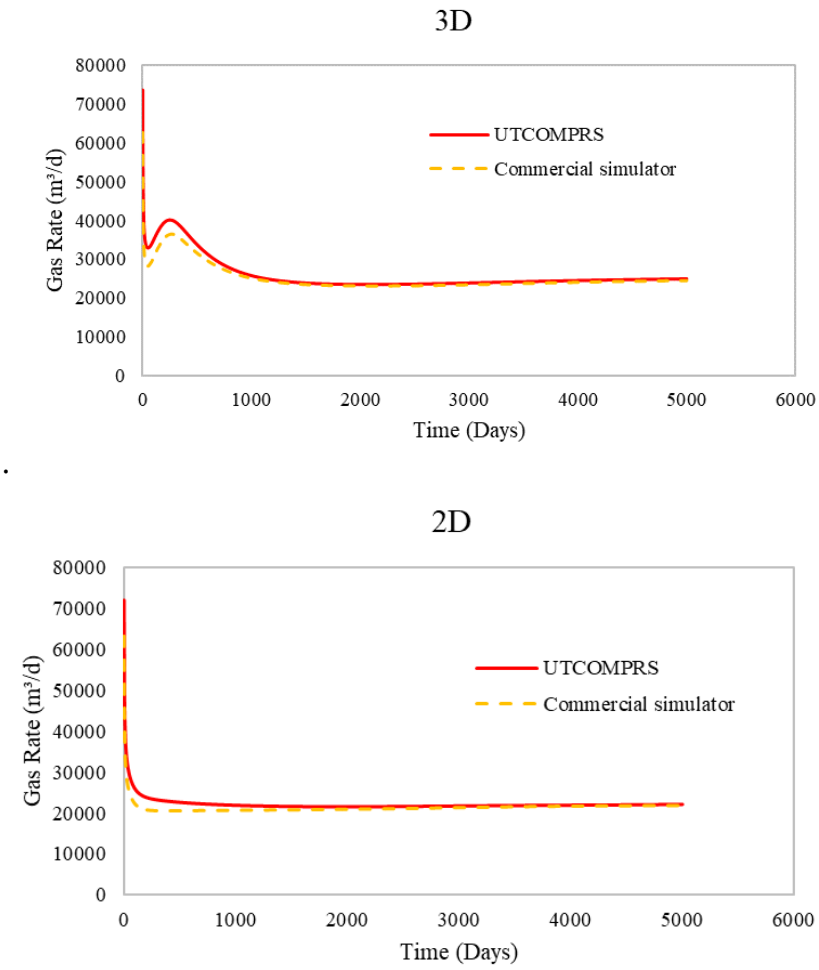

Fig. 98 shows the BHP for case 5. The BHPs deviation, for this case, is higher than the previous cases. In a 2D reservoir, the deviation is 234.422 kPa (34 psi), while for a 3D reservoir the difference between two simulators is 27 psi.

Figure 98 - BHP for both producers in 3D (top) and 2D (down) reservoirs.

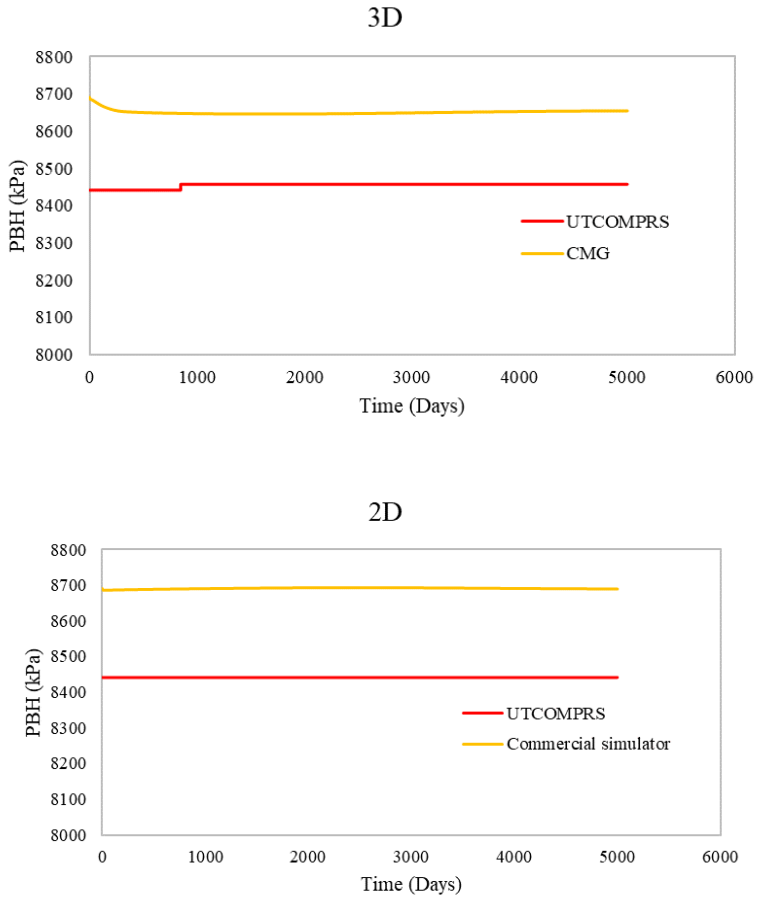

Fig. 9**9** shows the injection pressure for 2D and 3D simulations, respectively. The 2D reservoir requires a higher injection rate to produce the same level of oil and gas production.

Figure 99: Injector pressure in 3D (top) and 2D (down) reservoirs.

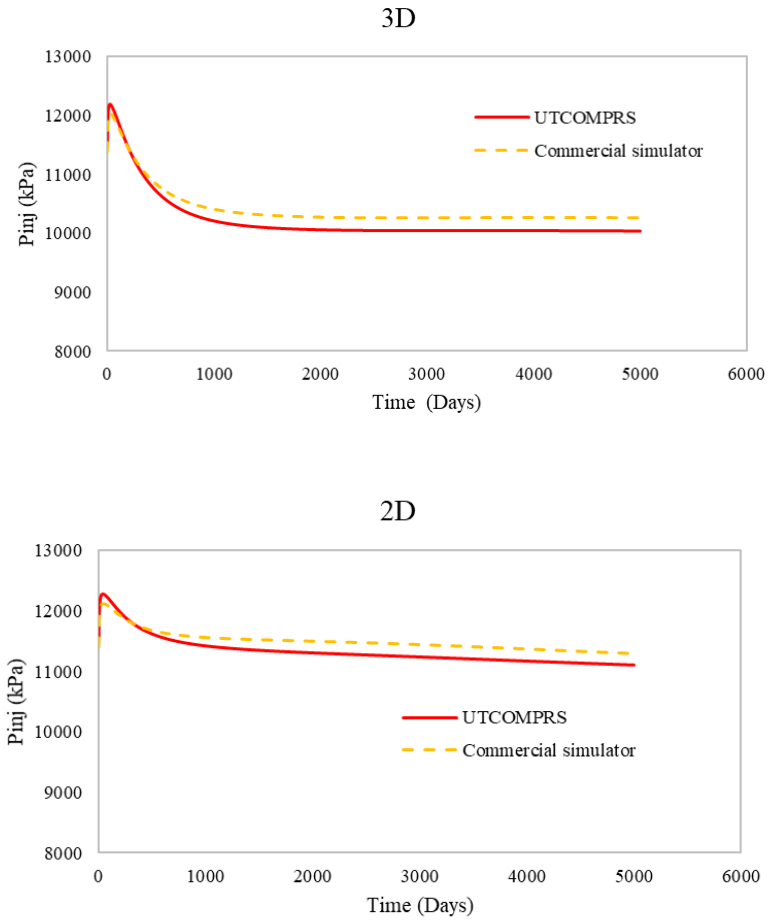

Fig. 100 shows the GOR profile for the 2D and 3D reservoirs.

Figure 100 - GOR in 3D (top) and 2D (down) reservoirs.

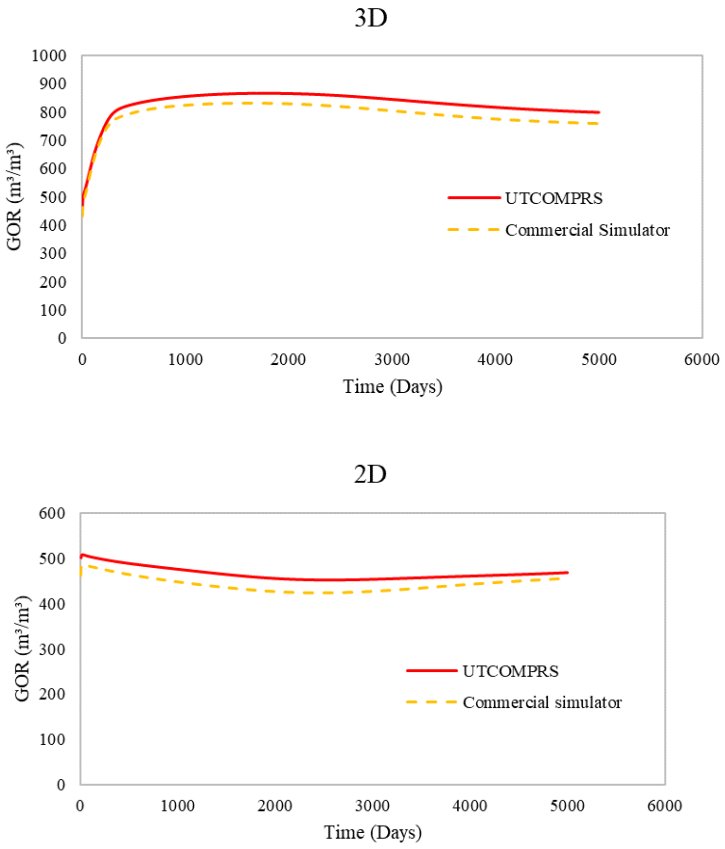

The shape of the GOR profile is alike for both simulators, but the difference observed can justify the pressure difference verified above in the bottom hole pressure profiles.

7.1.6. Case 6 – CFT- 23 wells for 2D and 3D reservoir

The sixth case is the comparison of 2D and 3D reservoirs with 23 wells, 8 injectors, and 15 producers using flow table options to demonstrate the flexibility of multiple wells algorithm, and larger number of grid blocks. The properties of the reservoir and fluid are the same. The only difference is the number and size of grid blocks. Table 21 and Fig. 101 show the size and number gridlocks used for the 2D and 3D models.

Table 21 - Number and size of the 2D and 3D models of Case 6.

Modifications	**2D**	**3D**
Numbers of Grid Blocks	153x77x1	153x77x5
Size of the Reservoir	12.19x12.19x60.96 m (40x40x200 ft)	12.19x12.19x12.192 m (40x40x40 ft)

Figure 101 - 3D (top) and 2D (down) reservoir models used for Case 6.

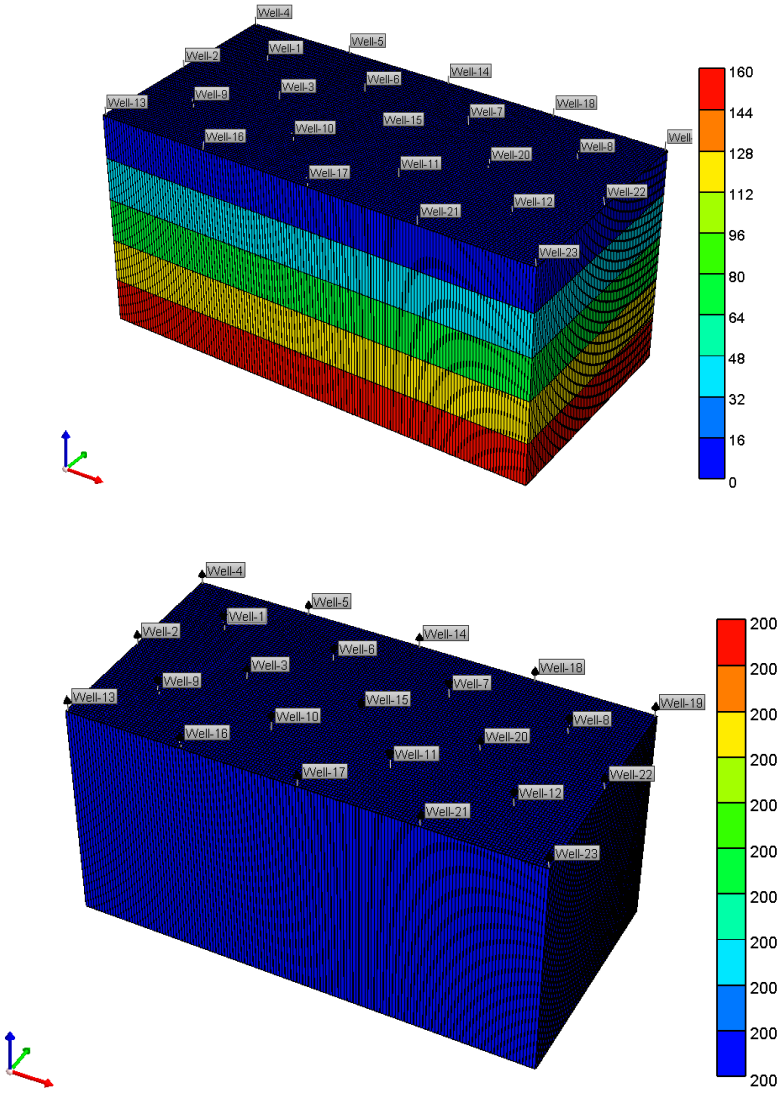

Fig. 102 shows the arrangement of producers and injectors used.

Figure 102 - Arrangement of producers and injectors for both 2D and 3D reservoirs.

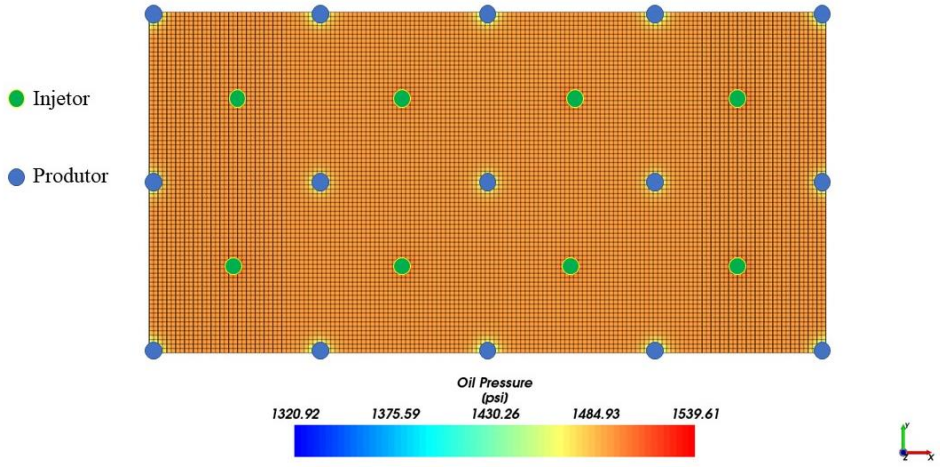

In Fig. 102, based on the well arrangement, there are three types of producing wells, including wells that are surrounded by one, two and four injectors. There are also two types of injectors; with a single or two border neighbors. These types of wells are indicated in Fig. 103. Hence, instead of 23 wells, we show the results of five classes of wells in this study. Wells number 2, 3 and 13 are selected as representative of producers and wells 1 and 11 are selected as representative of injectors.

Figure 103 - Five well classes that exist for Case 6.

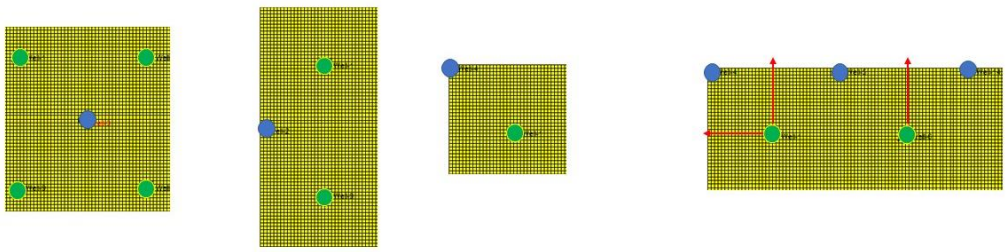

Figs 104-106 show oil production profiles for wells 2, 3 and 13 for the 2D and 3D reservoirs.

Figure 104 - Oil production profile for Well 2 for the 2D and 3D reservoirs.

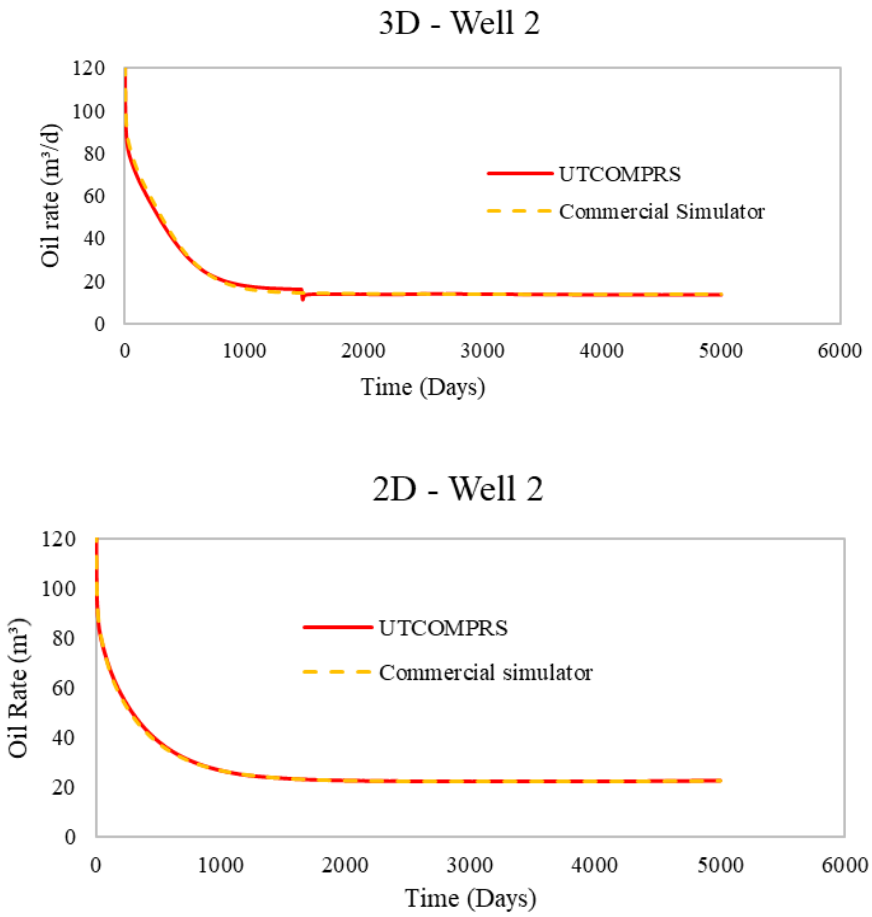

Figure 105: Oil production profiles for Well 3 for the 2D and 3D reservoirs.

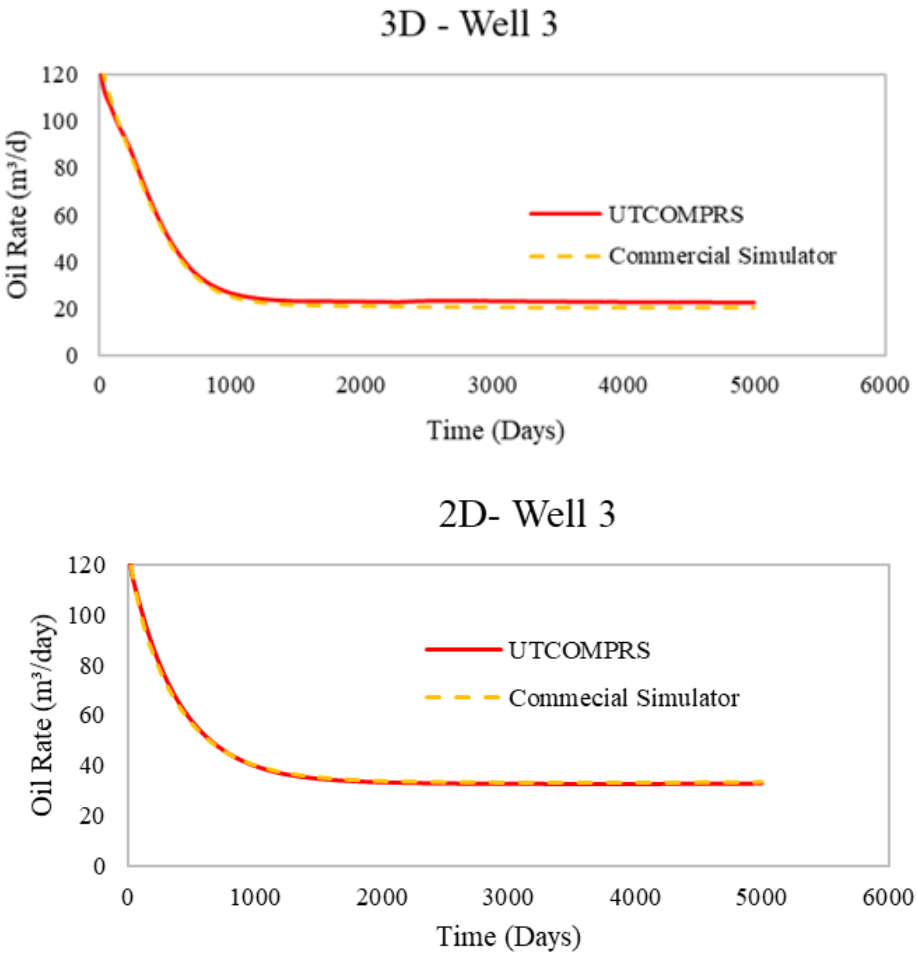

Figure 106 - Oil production profile for Well 13 for the 2D and 3D reservoirs.

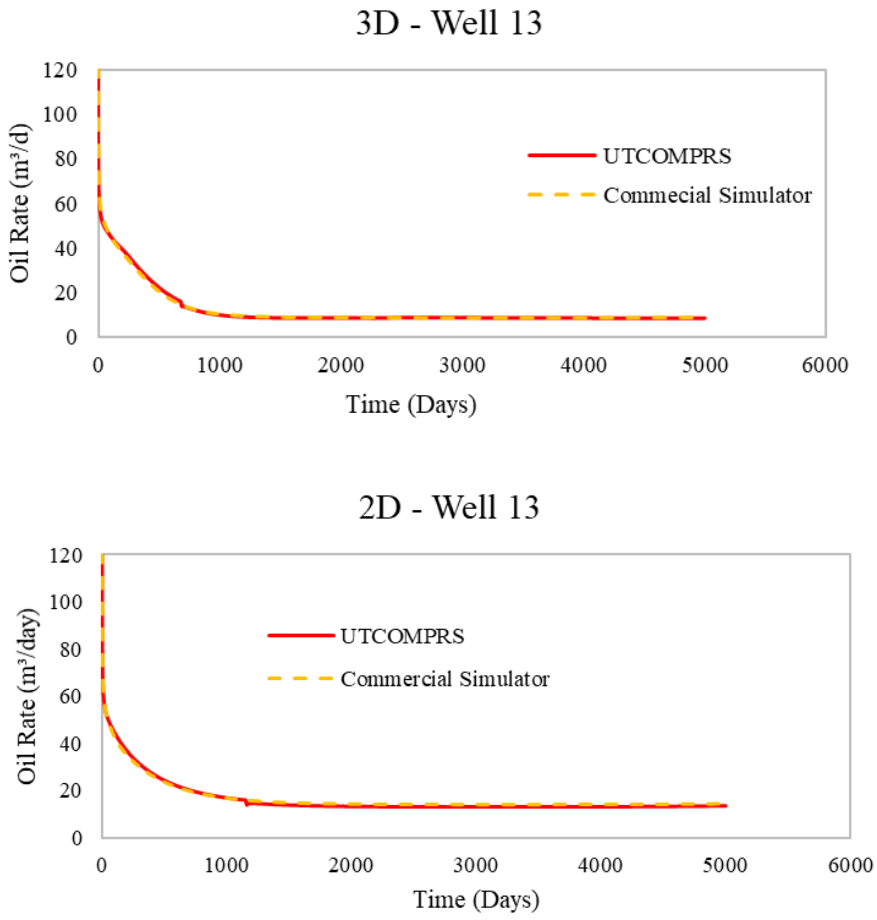

In Fig. 104, there is an oscillation for oil production of Well 2 for the 3D reservoir. This oscillation is due to the change of BHP in the flow table of the UTCOMPRS simulator.

Figs. 107-109 present the gas production for Wells 2, 3 and 13 for 2D and 3D reservoirs. Similar to the oil production curves, there is an oscillation for gas production.

Figure 107 - Gas production profiles for Well 2 for the 2D and 3D reservoirs.

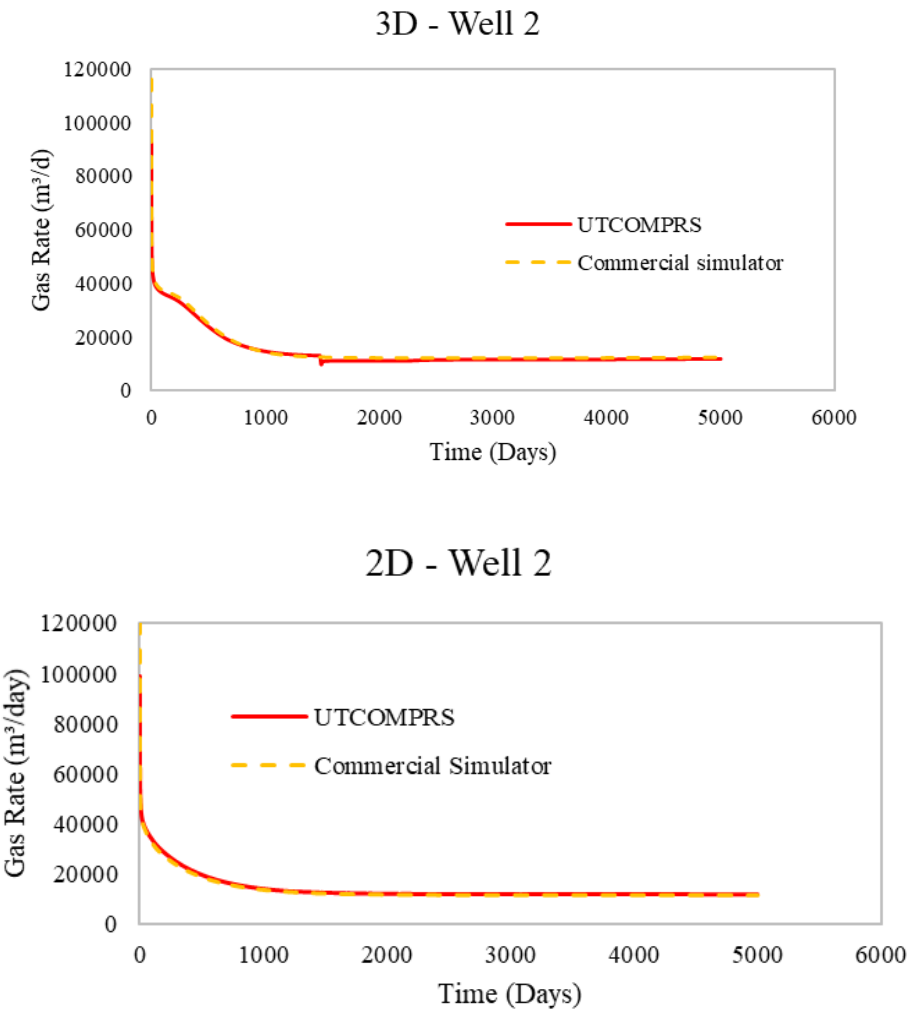

Figure 108 - Gas production profiles for Well 3 for the 2D and 3D reservoirs.

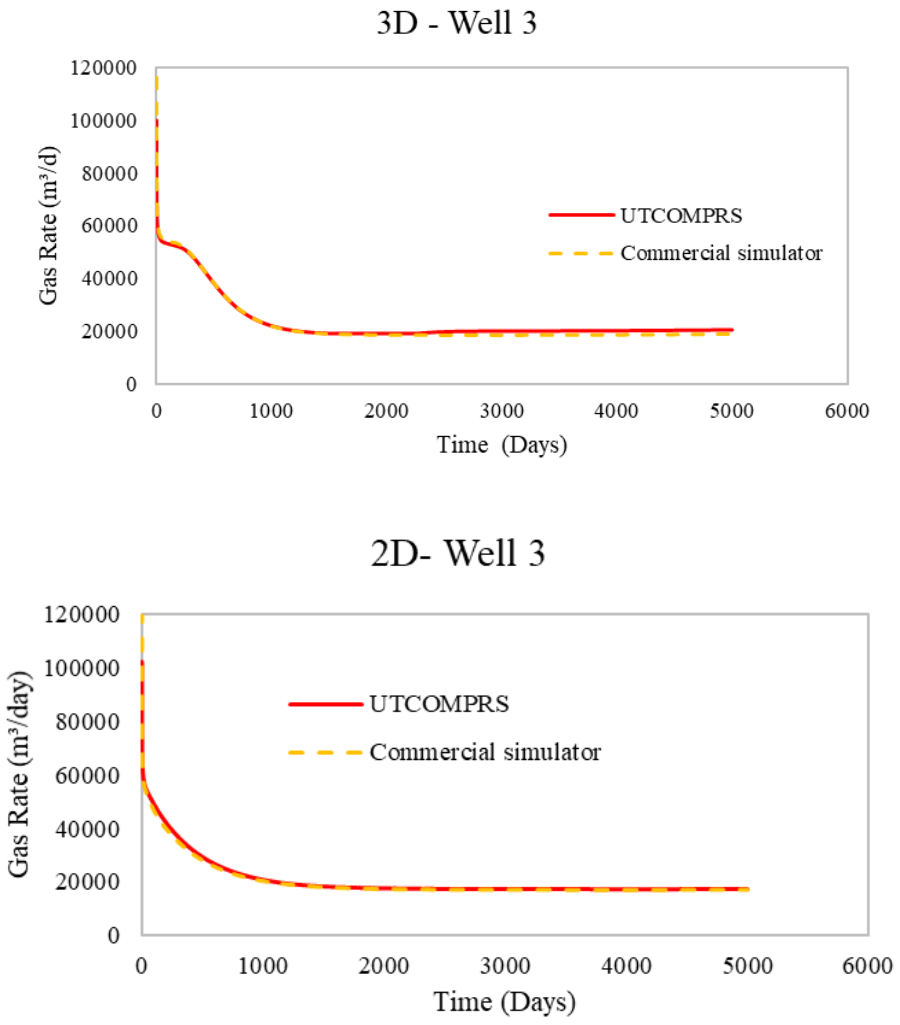

Figure 109 - Gas production profiles for well 13 for the 2D and 3D reservoirs.

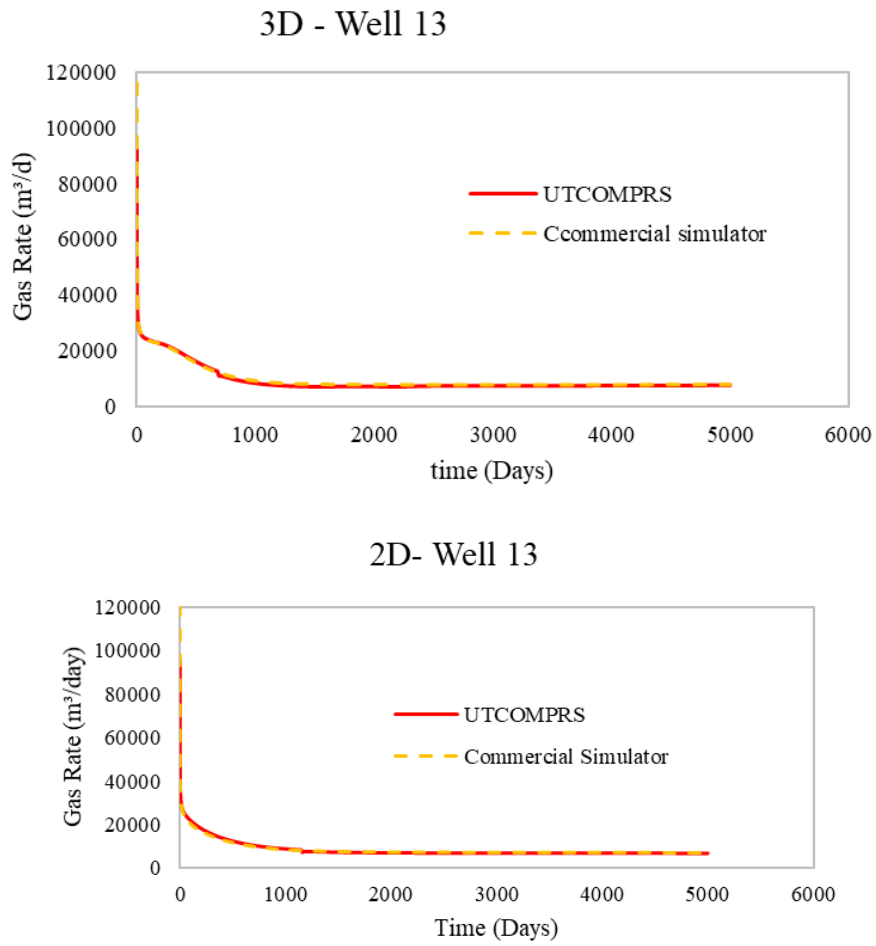

Figs. 110-112 show the BHP profiles for wells 2, 3, and 13 for the 2D and 3D reservoirs.

Figure 110 - BHP profiles for Well 2 for the 3D (top) and 2D (down) reservoirs.

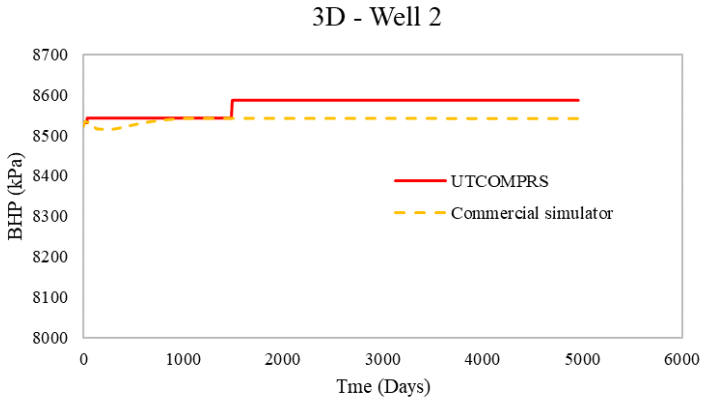

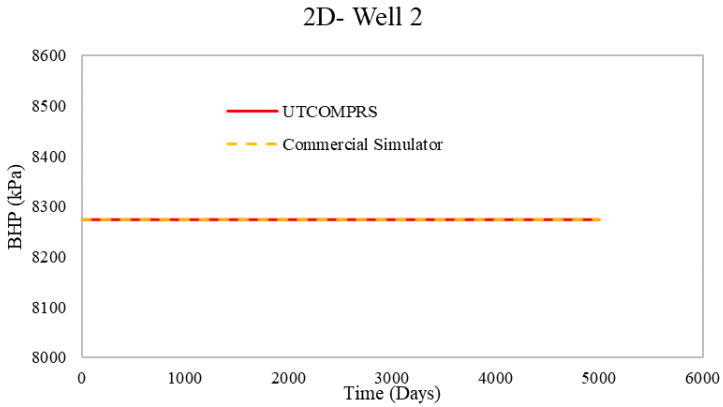

Figure 111: BHP profiles for well 3 for the in 3D (top) and 2D (down) reservoirs.

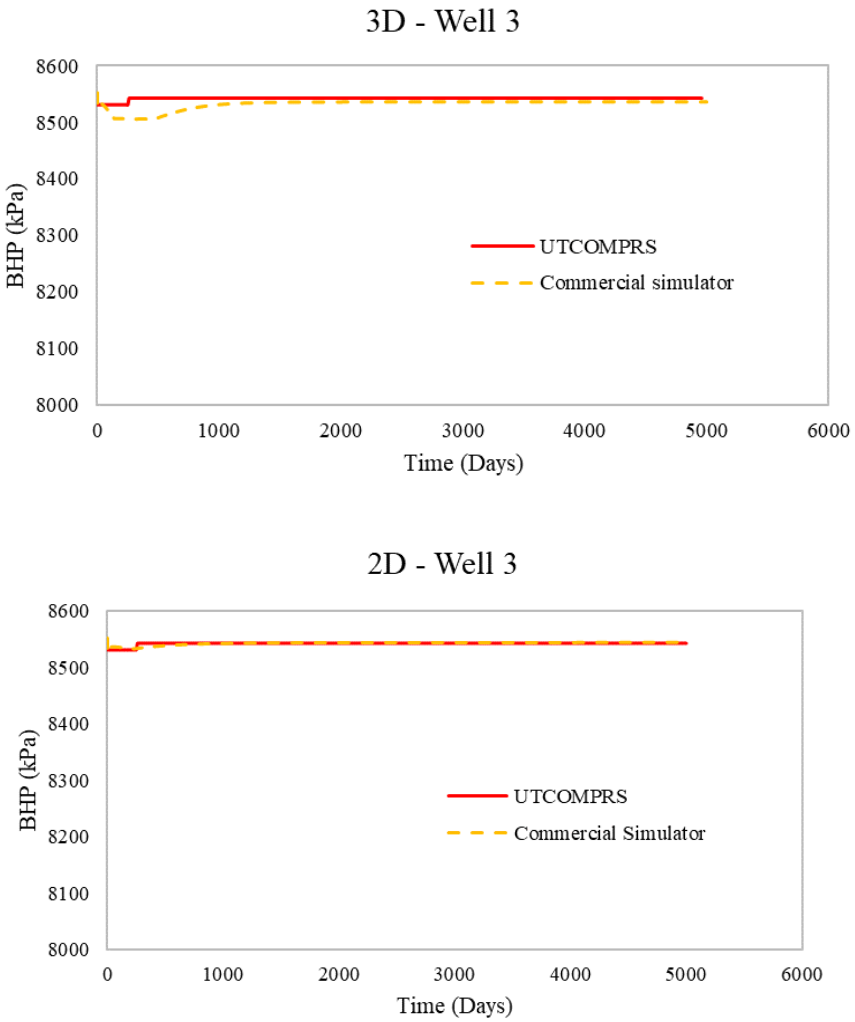

Figure 112: BHP profiles for well 13 for the 3D (top) and 2D (down) reservoirs.

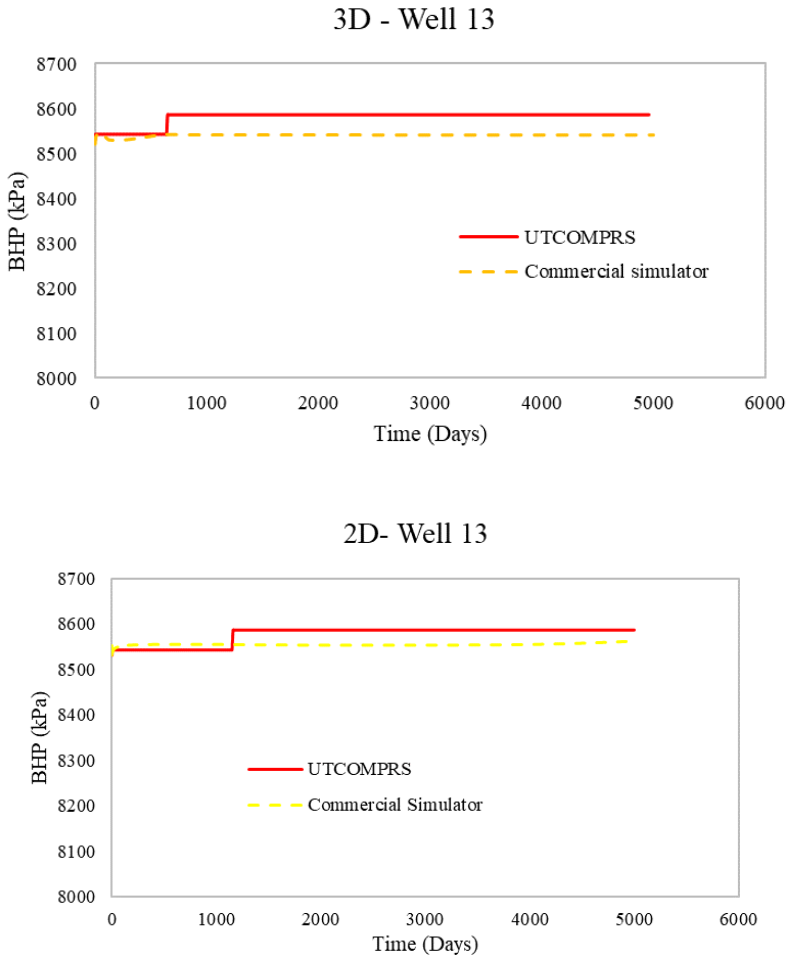

Fig. 113 shows the pressure of injector profiles for wells 1, and 11 for the 2D and 3D reservoirs.

Figure 113- Injection pressure profiles for well 1 for the 3D (top) and 2D (down) reservoirs.

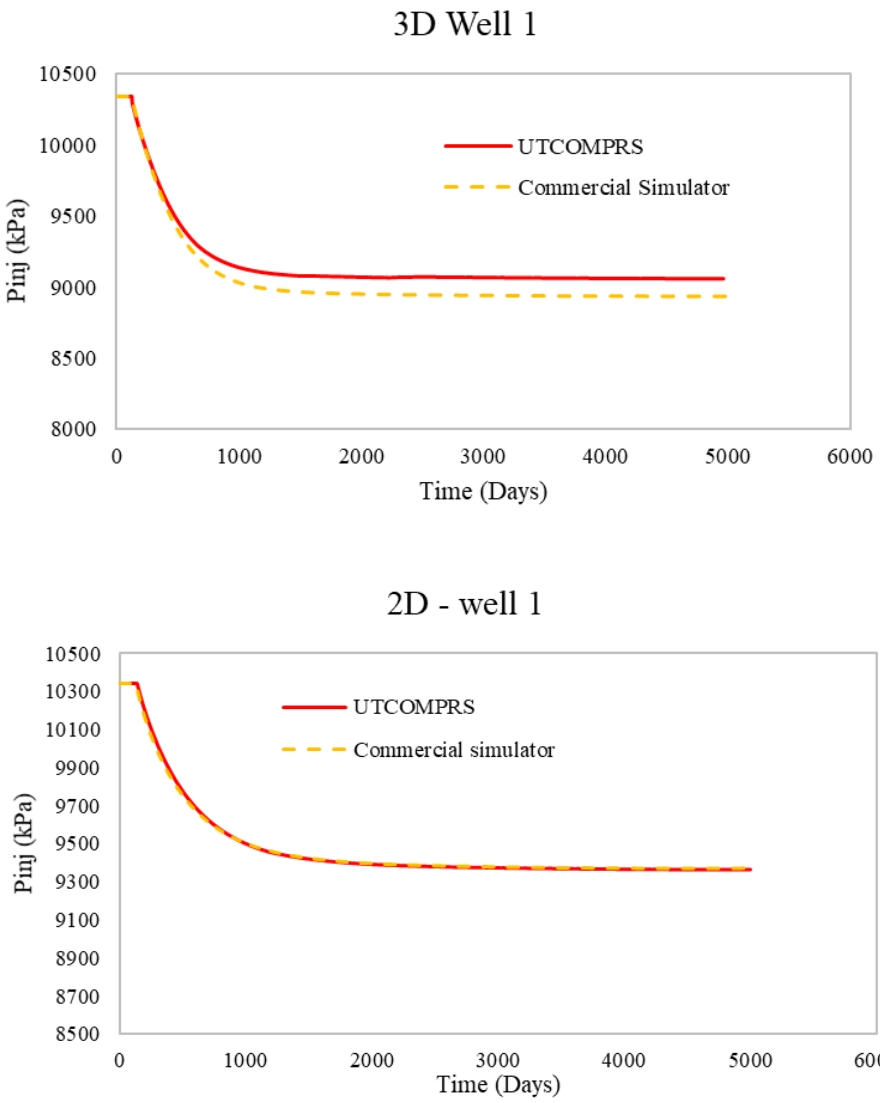

Figure 114 - Injection pressure profiles for well 11
for the 3D (top) and 2D (down) reservoirs.

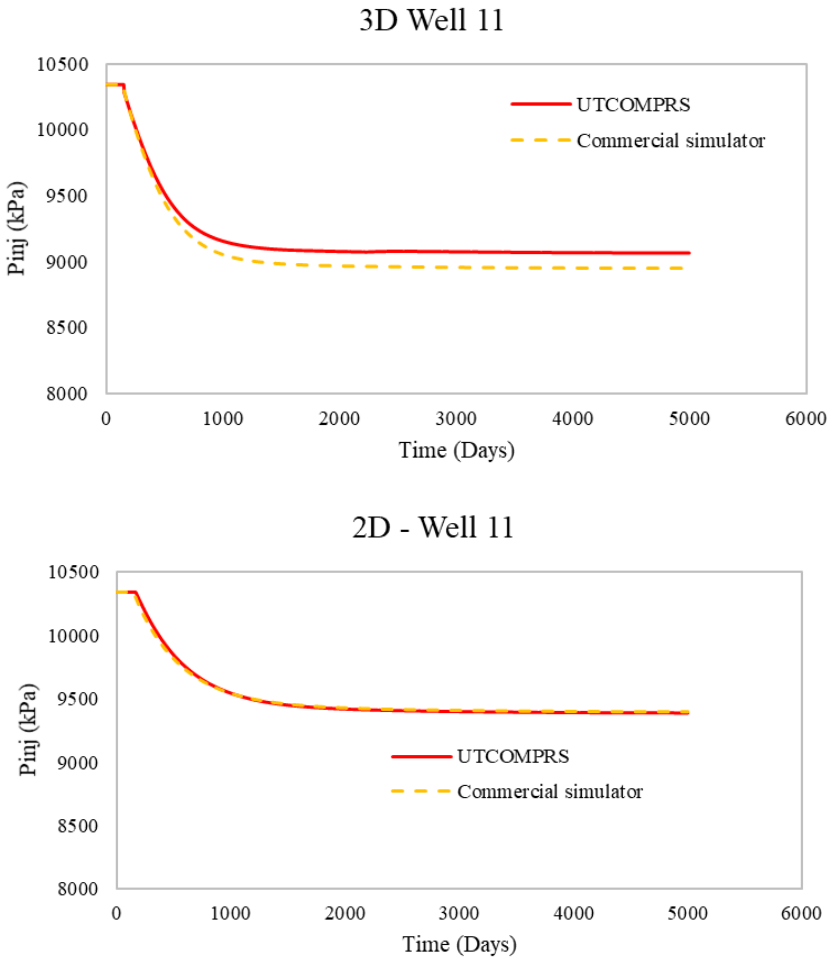

Figs 115-117 show GOR profiles for wells 2, 3, and 13 for the 2D and 3D reservoirs.

Figure 115 - GOR profiles for well 2 for the 3D (top) and 2D (down) reservoirs.

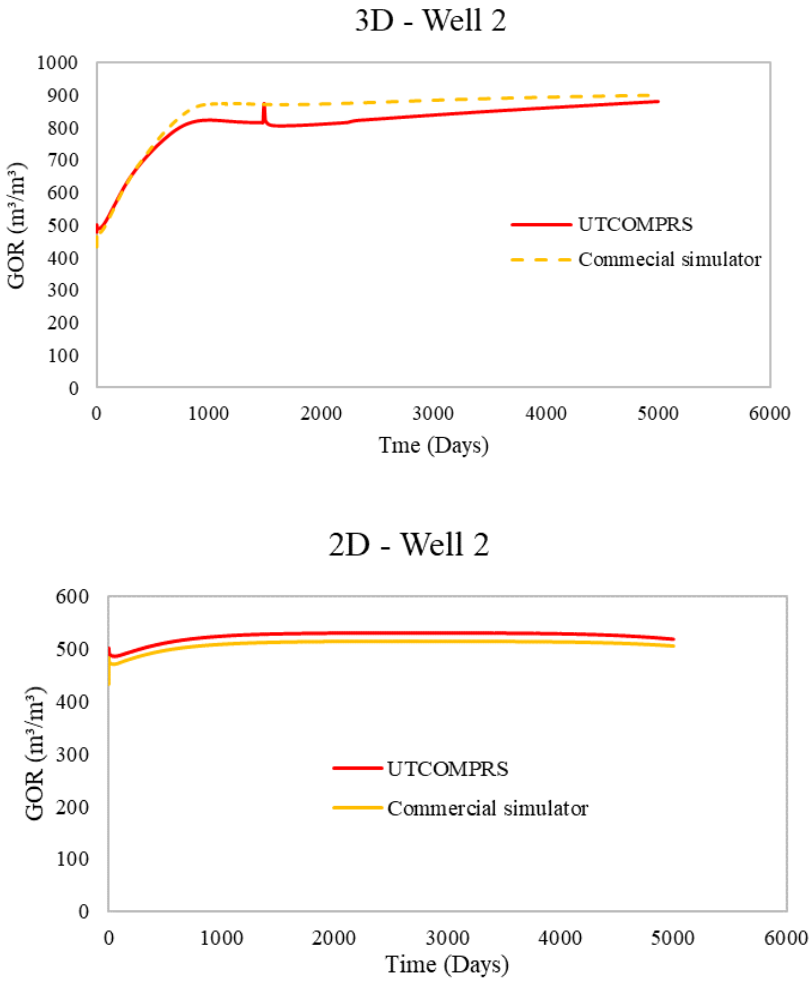

Figure 116 - GOR profiles for Well 3 for the 3D (top) and 2D (down) reservoirs.

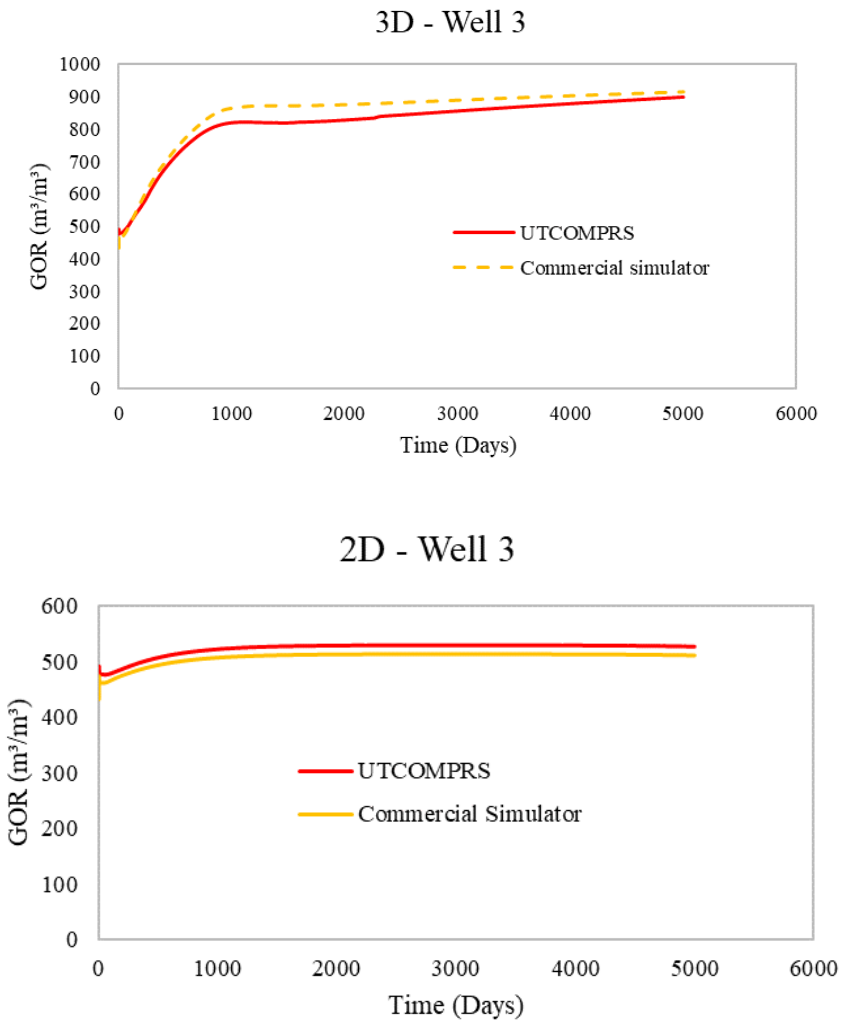

Figure 117 - GOR profiles for Well 13 for the 3D (top) and 2D (down) reservoirs.

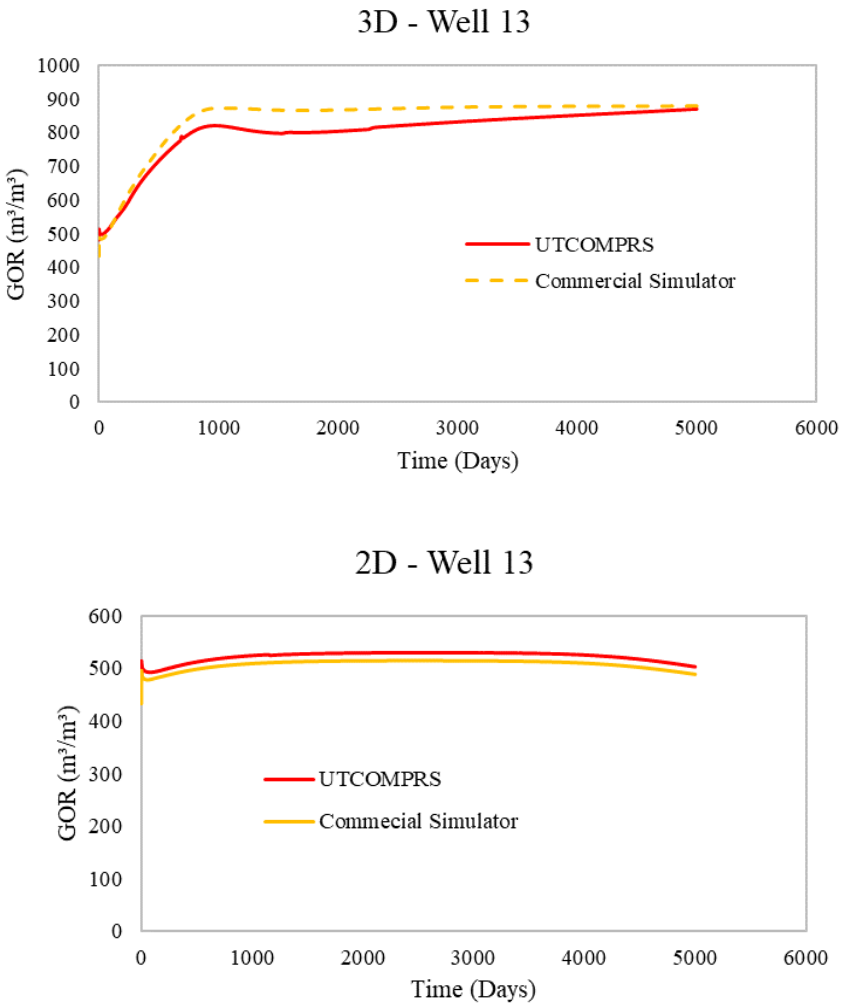

The BHP change also shows an oscillation in GOR profile for the 3D reservoirs. That difference in GOR plots of 3D reservoirs also can be the result of different injector pressure of Well 1. These results show that the code can run a higher number of grid blocks, 1.1781 for 2D, and 5.8905 for 3D reservoirs.

Also, it should be noted that the average reservoir pressure is a result of the driving force inside the reservoir, which is the difference between injector pressure and BHP. However, since these two values are not completely matched, we did not show the average reservoir pressure for the previous case studies. Herein we only presented two cases to demonstrate the behavior of average reservoir pressure as the function of injector pressure and BHP. Fig. 118 shows the average reservoir pressure for the low gas injection scenario of Case 4 and the 3D reservoir of Case 6.

Figure 118 - Average reservoir pressure for low gas injection scenario of case 4 (top) and 3D reservoir of Case 6 (down).

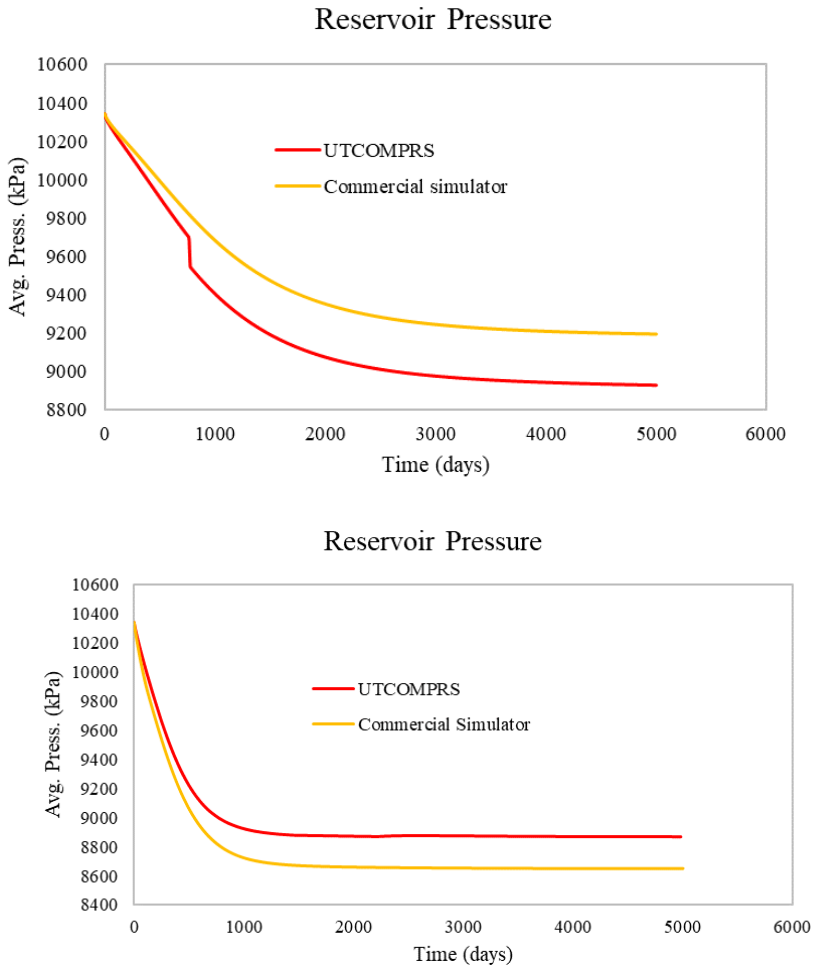

7.1.7. Case 7 – CFT-Multivariable interpolation functions

The seventh case study shows the effect of multiple parameters on interpolation function. In the previous studies, all of the interpolated BHP were stepwise, since the BHP was only the function of WHP. Hence, to check the effect of another parameter, we re-run case one with lower wellhead pressure constrain and we interpolated BHP as a function of WHP, and GLR in two ways. In the first approach, we interpolated BHP values with WHP first, and then with GLR, while in the second test, we first interpolated BHP with GLR, then with WHP.

Figs 119 and 120 show the oil and gas daily production for interpolated BHP function considering the two aforementioned parameters.

Figure 119 - Oil production profile using different interpolation BHP functions.

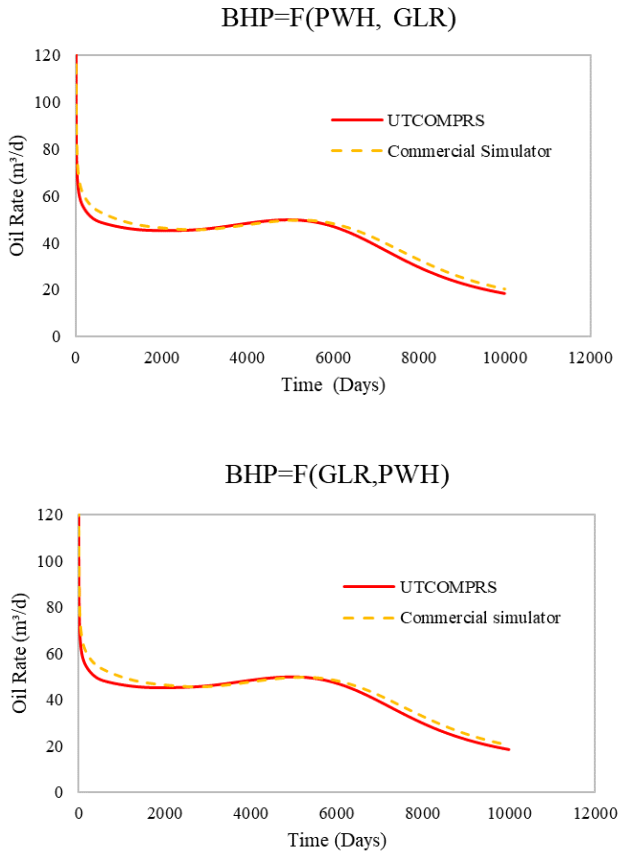

Figure 120: Gas production profile using different interpolation BHP functions.

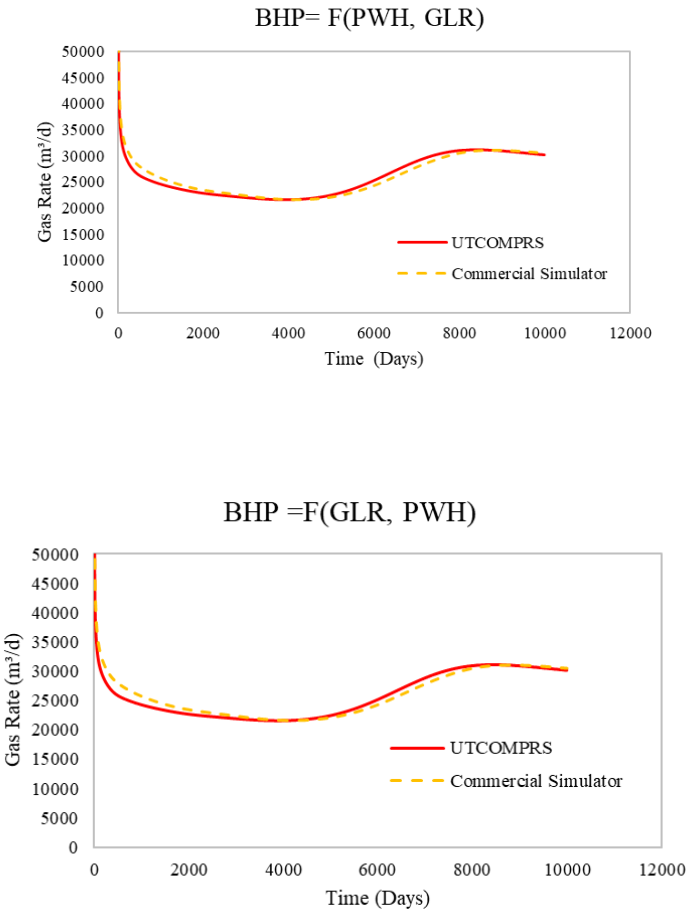

Fig. 121 shows the interpolated BHP profile. On the last day, the difference between UTCOMPRS and commercial simulator was 1703 kPa (247 psi) and 1565 kPa (227 psi) for the interpolation functions. This is due to the multi variable interpolation function (which responds to GLR values).

Figure 121 - BHP profile as a function of WHP and GLR (top) and GLR and WHP (down).

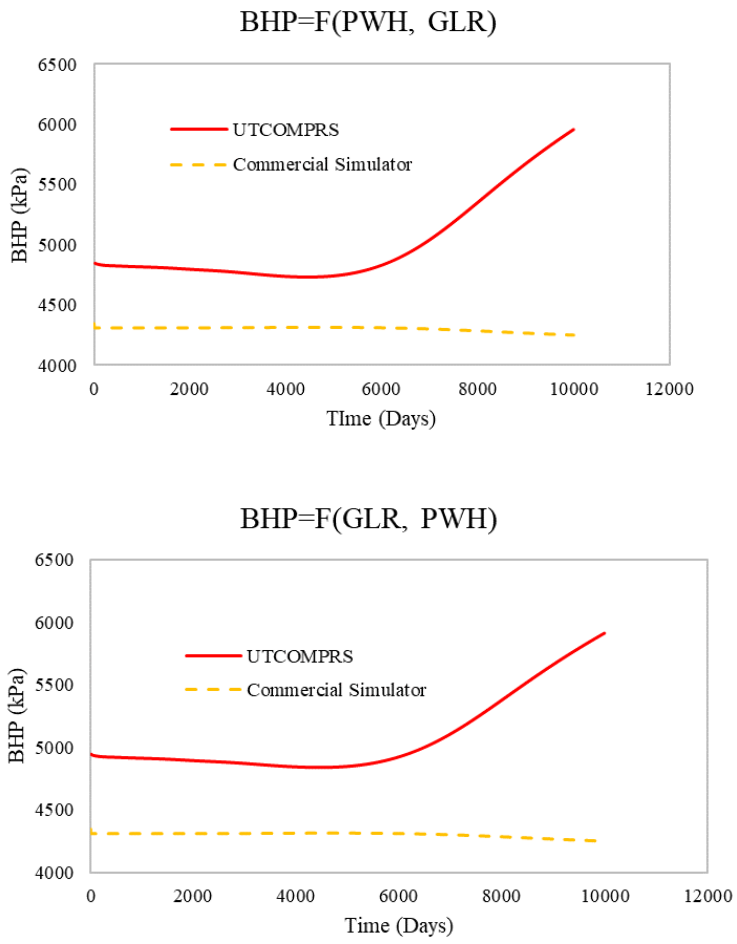

Figure 122 presents the injector pressure profile.

Figure 122 - Injector pressure for two profile function of WHP and GLR (top) and GLR and WHP (down).

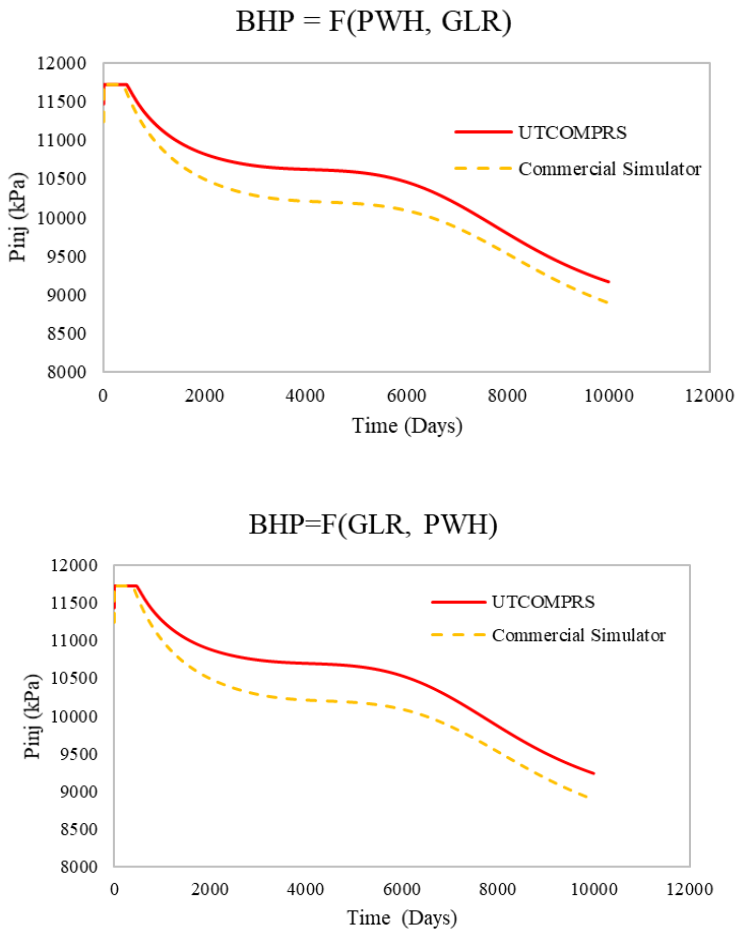

From Fig. 122, the injector pressure change for the first function (WHP and GLR) is 275 kPa (39.8 psi), while the difference for the second function is around 347 kPa (50.3 psi). This shows that the proper selection of each interpolation function can affect all of the operating parameters. Finally, Fig. 123 shows the GOR profile for the seventh case study.

Figure 123: GOR profile for two functions of
WHP and GLR (top) and GLR and WHP (down).

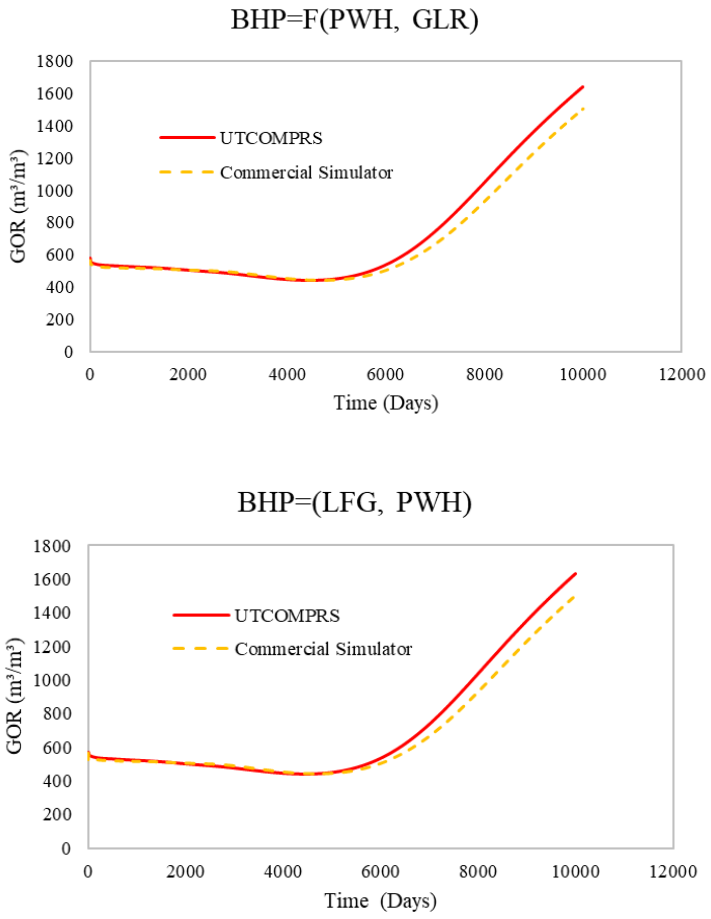

An important observation about the last case is that the values of BHPs are not step-wise anymore, although they are quite different from when the interpolation is only a function of the wellhead pressure.

7.1.8. Case 8 – CFT-Different interpolation functions

The low gas injection scenario of Case 4 was rerun with three additional interpolation function, logarithmic, quadratic, and interpolation factor (Eqs 6.3, 6.4, and 6.5) with the same low gas injection scenario to investigate more interpolation functions.

Figure 124 shows the BHP profile obtained for low gas injection rate, with different interpolation functions.

Figure 124 - BHP profiles for different interpolation functions implemented in the UTCOMPRS and obtained with a commercial simulator.

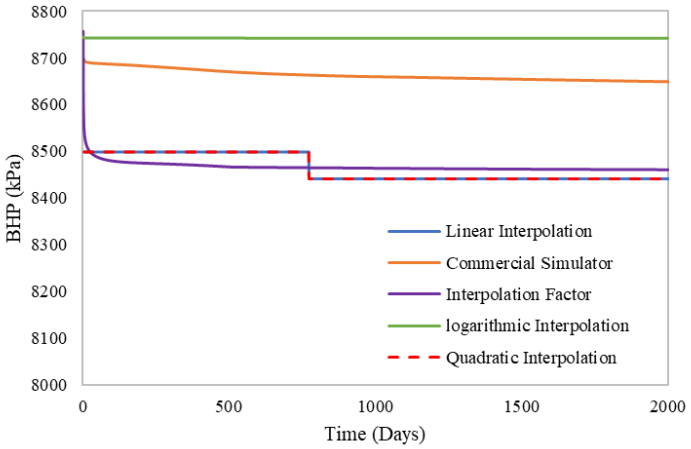

Figure 124 contains three interesting information. First of all, the logarithmic interpolation function, has a better agreement with the commercial simulator (eventually the maximum deviation between the simulators was 100 kPa). Second, despite the fact that the quadratic interpolation function was chosen, the simulator switched to the linear interpolation factor since the operation WHP was set at the table's borders (last values of the table). Finally, because the interpolation factor function's final values are interpolated as liquid rates, the behavior of the BHP obtained by using this method is similar to the liquid rates (see Figs 125). Fig. 125 shows the oil rate profile obtained for case study eight.

Figure 125 - Oil rate profiles obtained with different interpolation functions implemented in the UTCOMPRS and commercial simulator.

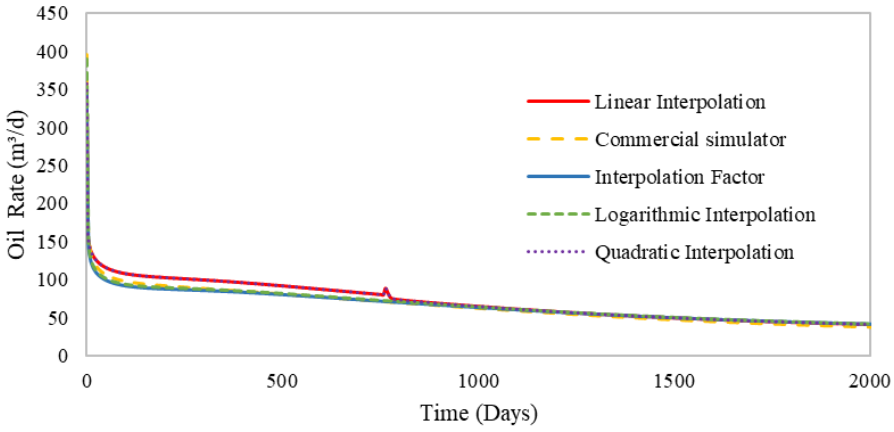

From Fig. 125, it can be observed that except for the linear and quadratic interpolations, which have already been discussed, the remaining interpolation functions were able to effectively represent the oil rate trend. It is important to remember that there is no produced water in this example, thus the liquid rate is equal to the oil rate. This is significant because the interpolation factor's final BHP values are interpolated with regard to the liquid rate. As a result, the trends of the obtained BHP (see Fig. 124) are similar to the trend of the oil rate (see Fig. 125) for the interpolation factor approach.

Fig 126, shows the gas rate profile obtained for case study eight.

Figure 126 - Gas rate profile for different interpolation functions implemented in the UTCOMPRS and commercial simulator.

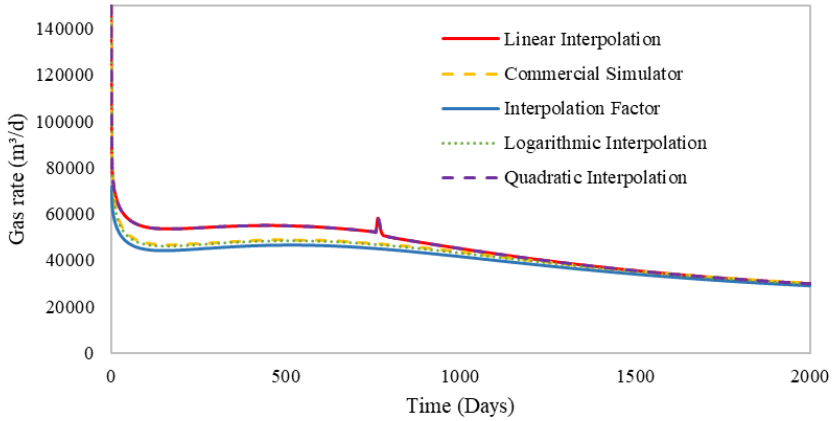

The gas rate obtained with the other interpolations were similar to the oil rate trend. Also, the logarithmic interpolation was clearly able to better capture the trends in the gas rate once more.

Fig. 127 presents the results of injection pressure for this case study.

Figure 127 - Injector pressure profile obtained with different interpolation functions implemented in the UTCOMPRS and commercial simulator.

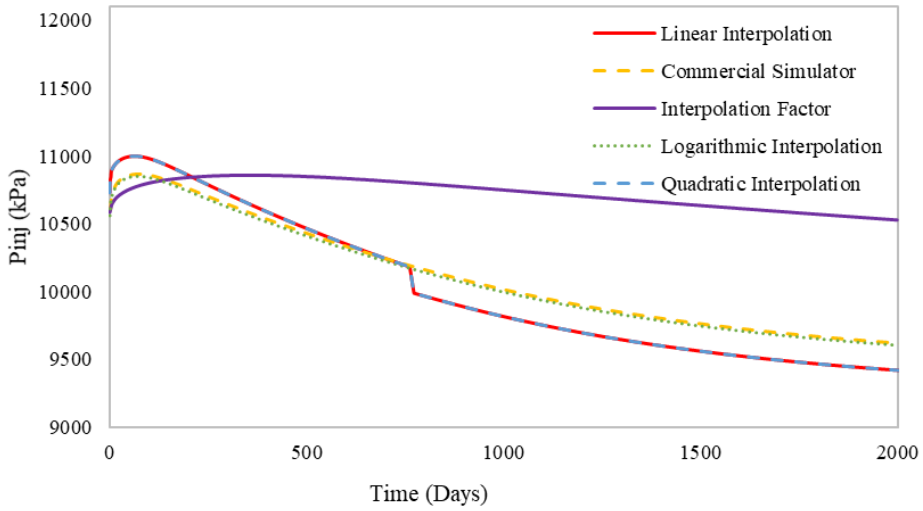

Two more intriguing facts can be found in the injection pressure profile. First is that the logarithmic interpolation function was the only one capable of capturing the same trend as the commercial simulator. Second, despite the fact that the injection gas rate needed for the interpolation factor was higher (see Fig. 127), the injection pressure obtained by this method was higher but did not exceed the activation limiting pressure (11721.09 kPa). The accuracy of the presented framework for the UTCOMPRS simulator is strongly dependent on the interpolation function used for the BHP values, as shown in this plot.

The last figure, Fig. 128, shows the GOR profile for case study 8.

Figure 128 - GOR profile obtained with different interpolation functions implemented in the UTCOMPRS and commercial simulator.

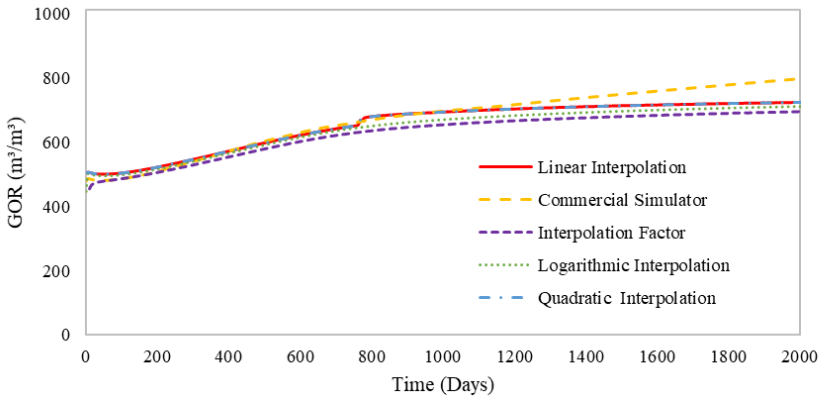

As can be observed in Fig. 1288, the GOR curve obtained with interpolation factor (see blue curve in Figure 7.58) has increased because of the higher injection gas rate.

GOR is also the only parameter, where the logarithmic interpolation function of the UTCOMPRS and the commercial simulator differ by a minor amount (88 m3/m3). This difference is due to a difference of 100 kPa in BHP values between the logarithmic interpolation function of UTCOMPRS and the commercial simulator. This information is inline the findings of Bigdeli et al. [**BIGDELI et. al., 2020, BIGDELI et. al., 2021**], whom found that the GOR is the greatest indication for simulator comparison due to its dimensionless power. However, here, the acquired results were sufficient to meet the requirements of the UTCOMPRS simulator's implemented framework.

Finally, Fig. 129 compares the results of CPU run time of case study 8 including logarithmic, quadratic and interpolation factor methods, while Fig. 130 compares the logarithmic interpolation function with commercial simulator in order to show more details on the developed framework for the UTCOMPRS simulator.

Fig. 129 - CPU time of different interpolation functions implemented in the UTCOMPRS.

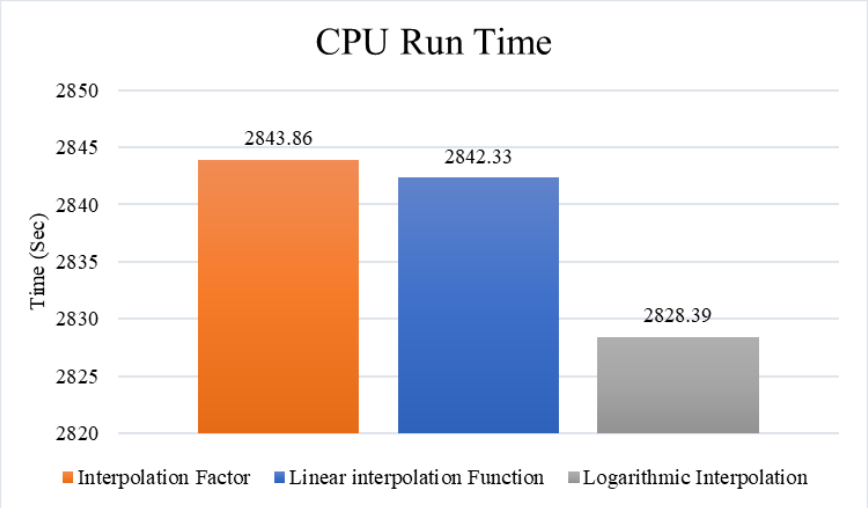

Figure 130 - Comparison of the CPU run time obtained with the logarithmic interpolation function of the UTCOMPRS with the commercial simulator

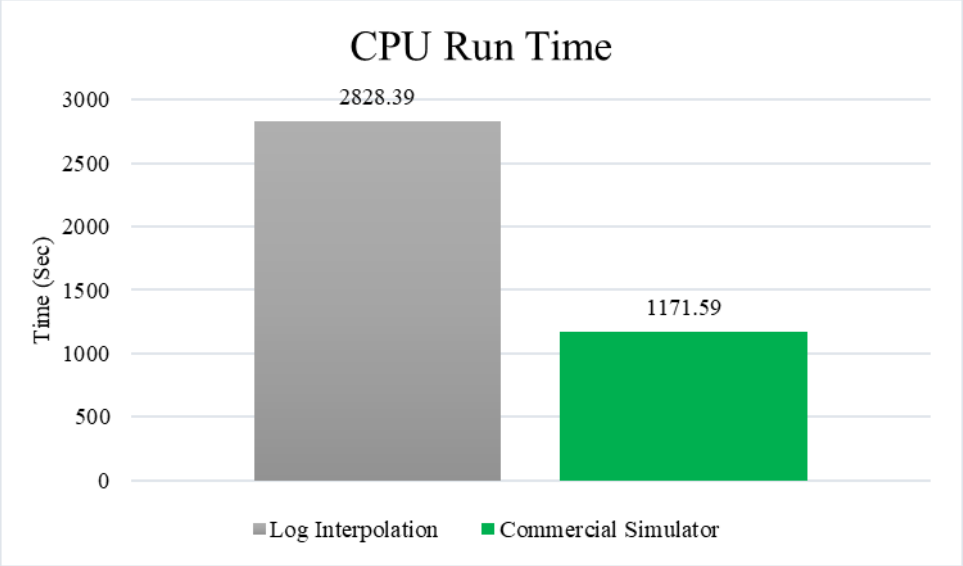

7.1.9. Case 9 – CFT-Pseudo-component case.

After comparing the UTCOMPRS results to those of a commercial simulator using the logarithm interpolation function, the case ninth was performed with an actual reservoir fluid obtained from the Petrobras company, whose composition and characteristics contained eight pseudo components. It should be emphasized that in order to account for more realistic conditions, this case study contains a mobile water phase, as well.

Table 22 shows the information of this case study.

Table 22 - The reservoir details, hydrocarbon components and injection fluid for Case 9.

Properties	**Value**
number of grid blocks in x,y,z direction	10x10x5
size of grid blocks in x,y,z directions	50x50x20 m (164x164x65 ft)
Porosity	0,15
Permeability in x, y, z directions	100x100x10 mD
Initial reservoir pressure	10342.13 kPa (7252 psi)

Components	"PC1","PC2","PC3","PC4","PC5","PC6”,"PC7”,"PC8”
Initial concentration	0.1, 0.5, 0.12, 0.06, 0.07, 0.06, 0.06, 0.03
Injection fluid concentration	Water injection
Type of producing well	CFT
Injection rate	Constant rate, 6289.82 STB/d
AWCO for injector and limited Pressure	No
Operating wellhead pressure	47573.83 kPa (6900 psi)
Coupling point	bottom hole
LFG	0.0 (no gas lift condition)
Phase Type (for comparing function)	Multiphase Table
Simulation Run Time	2000 days

Also, Fig. 131 shows the shape of the reservoir and location of the producer and injector wells.

Figure 131: Reservoir configuration used in Case 9.

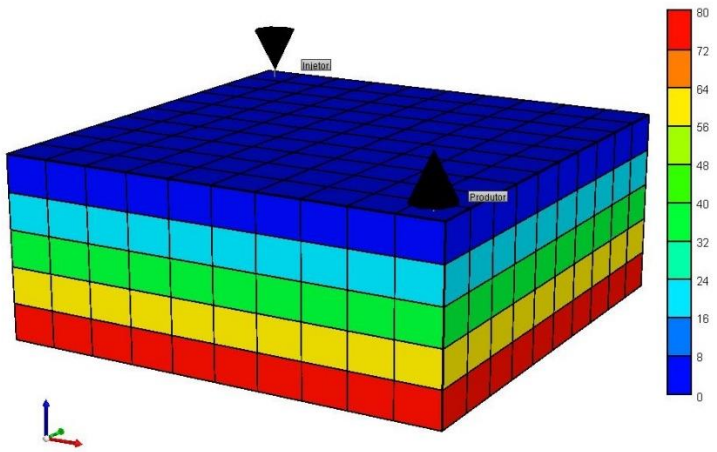

The BHP profile for the nineth case study is shown in Fig. 132. As can be observed, the logarithmic interpolation function was able to adequately represent the BHP trends

for real fluids. The pressure difference between two simulators is currently 38 kPa (5.5 psi).

Figure 132: BHP profile of the UTCOMPRS and commercial simulator for Case 9.

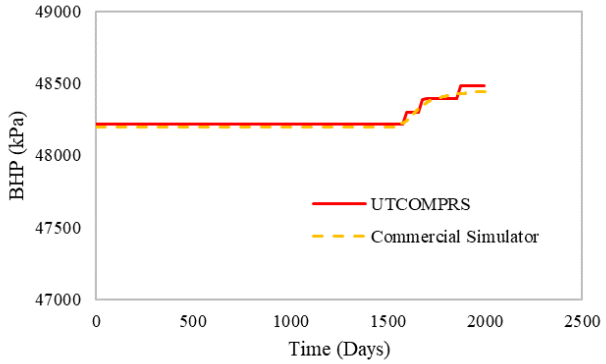

Figs 133-135 show the water, oil and gas rate profiles for case study nine.

Figure 133: Water rate plot of the UTCOMPRS and commercial simulator for Case 9.

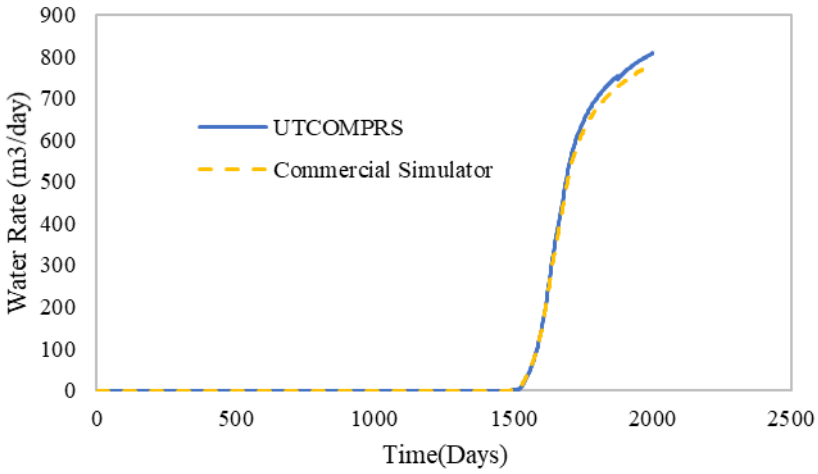

Figure 134 - Oil rate profile of the UTCOMPRS and commercial simulator for Case 9.

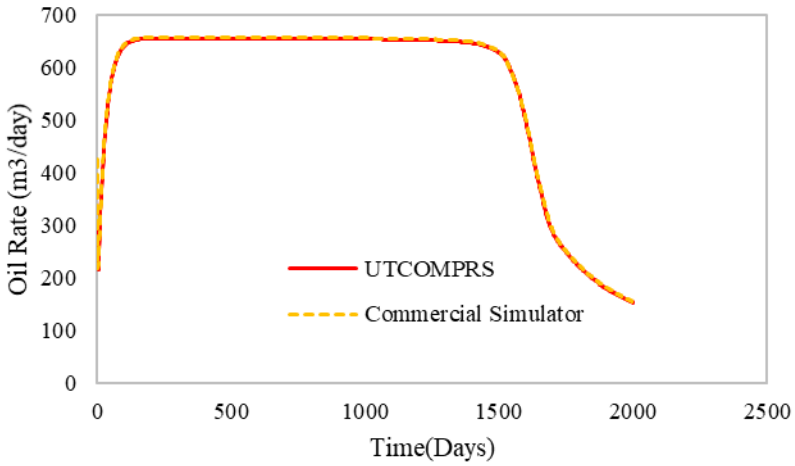

Figure 135 - Gas rate profile of the UTCOMPRS and commercial simulator for Case 9.

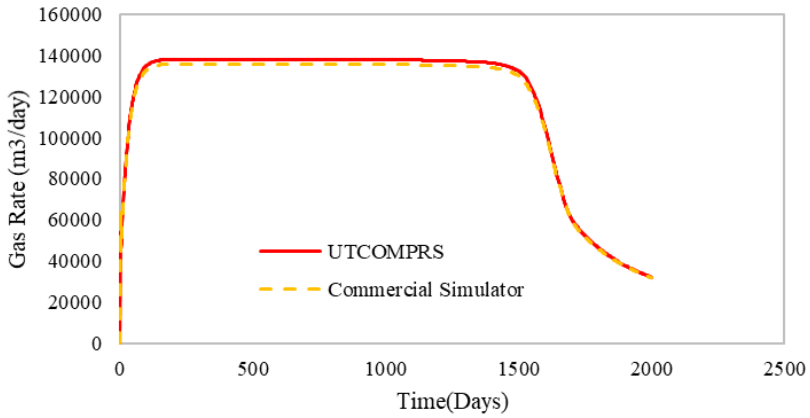

All three graphs of water, oil and gas rates presented above demonstrated a very good agreement between UTCOMPRS and the commercial simulator. The small discrepancy in the final days for the water rate in Fig 134 is due to the effect of relative permeabilities from the original case that was run and validated with constant BHP option; and it has nothing to do with the UTCOMPRS simulator's developed framework for Flow Tables.

Fig. 136 shows the injection pressure profile for case nineth.

Fig. 136 – Injection pressure profile of the
UTCOMPRS and commercial simulator for Case 9.

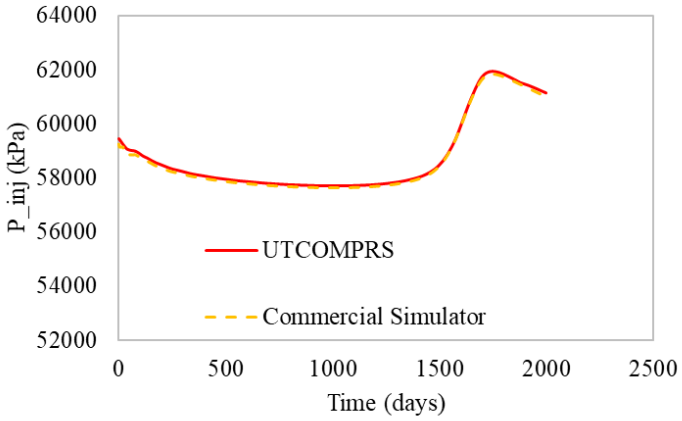

As can be seen form Fig. 136, the profile of injection pressure is in good agreement between two simulator, and as expected, after the break through, the injector responded to change of BHP and increased accordingly.

Figs. 137-139, present the GOR, WOR and water cut profile for case nineth.

Figure 137 - GOR profile of the UTCOMPRS
and commercial simulator for Case 9.

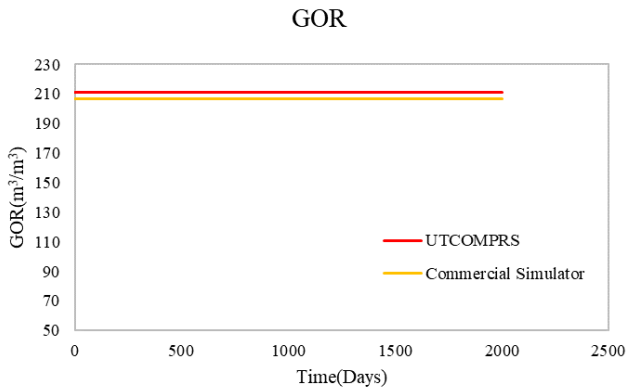

Figure 138 - WOR profile of the UTCOMPRS
and commercial simulator for Case 9.

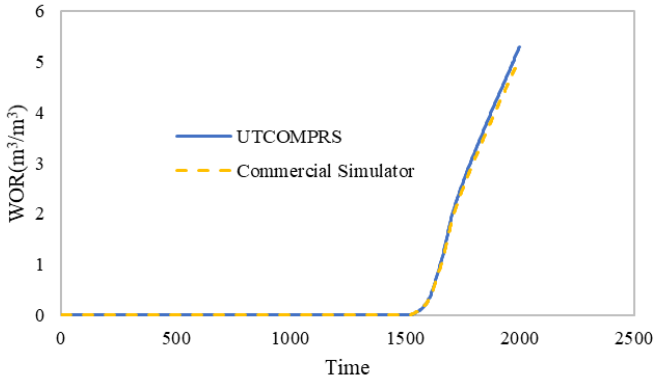

Figure 139 - Water cut profile of the UTCOMPRS
and commercial simulator for Case 9.

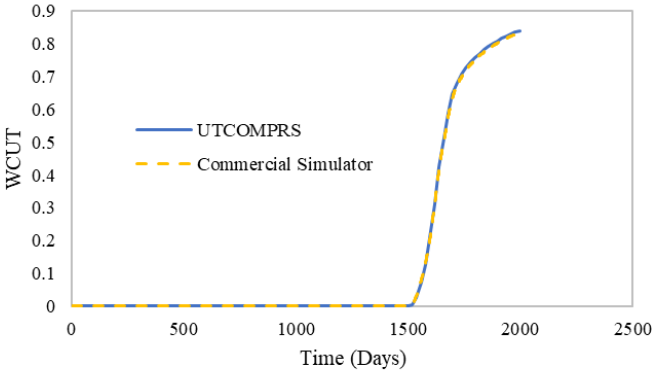

GOR and WOR are still the strongest indicators for comparing the developed with commercial simulator, as shown in Figs. 138 and 139. Also, by comparison Figs. 138 and 139 reveals that WOR is a better predictor than water cut, despite the fact that both numbers are dimensionless. This information was not previously available because the previous case studies did not include the water phase. Regardless, the most recent case study demonstrates that the developed framework, in combination with the logarithmic interpolation function, allows the simulator to represent more realistic conditions, such as real reservoir fluid from Petrobras.

7.1.10. Case 10 – CFT- Five-spot case with water variation

The final scenario is set up to look into the impact of water variations on the framework that has been developed. As a result, the same reservoir fluid of case study nine was employed, but now a five-spot reservoir was examined with a producer in the center and four injectors at the corners as shown in Fig. 140.

Figure 140 - The reservoir structure for case tenth

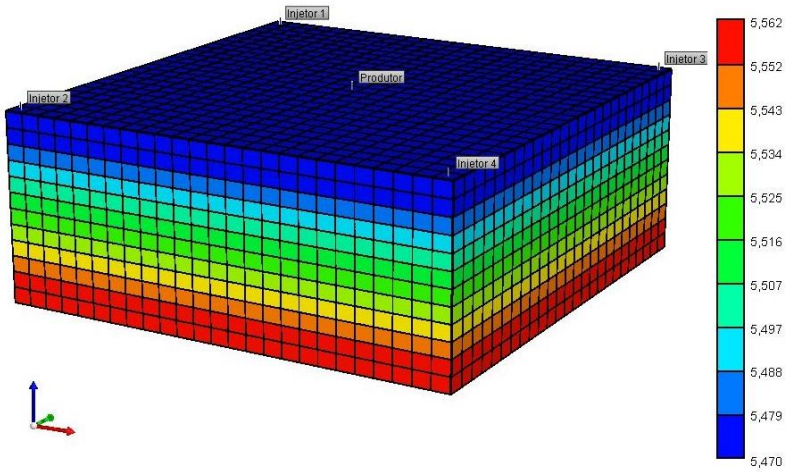

The number of grid blocks has been modified to 25x25x12, and the size of the gridblocks were equal to 20x20x8.33 m (65.6168x65.6168x27.3403 ft) in x-, y-, and z-directions, respectively. The reservoir and tube depths were estimated to be 17946 ft (5469.94 m), which are close to the Brazilian pre-salt fields. As a result, the wellhead pressure was set to 20000 kPa (2900.7548 psi). Water was injected at the rate of 250 m3/day and the simulation run time was set to 2000 days. In this example, the variance of the water cut would rise once the water breakthrough occurred, and the resilience of the developed framework would be assessed as a result. To improve the table's resolution, two sets of tables were investigated: one with 11 points for water cut and another with 20 points for all parameters (LIQ, GLR, WCUT, WHP). The greatest number of values that a commercial simulator could receive was 20, hence 20 points were chosen. Tables 23 and 24 show the 10 and 20 points tables.

Table 23 – The 11-point table and its information

```
LIQ
 10.0 500.0 1000.0 2000.0 3000.0 4000.0 5000.0 6000.0 7000.0
GLR
 0.0 100.0 200.0 400.0 500.0 600.0 800.0 1000.0 1200.0 1400.0 1500.0
WCUT
 0.0 0.1 0.2 0.3 0.4 0.5 0.6 0.7 0.8 0.9 0.99
LFG
 0.0
WHP
 100.0 145.0 2900.0 4351.0 5801.0 7251.0
BHP
**iflo  igfr  iwfr  iadd     bhp(1st whp).....bhp(nth whp)
   1     1     1     1      6496.64387      6541.65068      9296.77183      10747.7946      12197.8099
13647.8211
   1     1     2     1      6619.15258      6664.22805      9424.84976      10879.7789      12334.3951
13789.7072
   1     1     3     1      6742.26677      6787.41575      9553.90582      11012.9981      12472.5237
13933.5046
   1     1     4     1      6866.00999      6911.23755      9683.97971      11147.5043      12612.2638
14079.3027
   1     1     5     1      6990.40684      7035.71828      9815.11319      11283.3524      12753.6878
14227.1968
```

Table 24 – The 20 points table and its information

```
LIQ
350.0 700.0 1050.0 1400.0 1750.0 2100.0 2450.0 2800.0 3150.0 3500.0 3850.0 4200.0 4550.0 4900.0 5250.0 5600.0 5950.0 6300.0 6650.0 7000.0
GLR
75.0 150.0 225.0 300.0 375.0 450.0 525.0 600.0 675.0 750.0 825.0 900.0 975.0 1050.0 1125.0 1200.0 1275.0 1350.0 1425.0 1500.0
WCUT
0.0 0.05 0.1 0.15 0.2 0.25 0.3 0.35 0.4 0.45 0.5 0.55 0.6 0.65 0.7 0.75 0.8 0.85 0.9 0.95
LFG
0.0
WHP
362.55 725.1 1087.65 1450.2 1812.75 2175.3 2537.85 2900.4 3262.95 3625.5 3988.05 4350.6 4713.15 5075.7 5438.25 5800.8 6163.35 6525.9 6888.45 7251.0
BHP
   1     1     1     1      6646.57277      7025.46332      7393.12981      7758.90104      8123.75638      8488.06066      8852.00199      9215.68935      9579.19031      9942.55018      10305.7999      10668.9621      11032.0556
11395.0918      11758.0786      12121.0235      12483.9326      12846.8107      13209.6617      13572.4887
   1     1     2     1      6705.43376      7084.90414      7453.01858      7819.1378      8184.35558      8549.03908      8913.37786      9277.481      9641.41693      10005.2312      10368.955      10732.6111      11096.2159
11459.7838      11823.3251      12186.8449      12550.3493      12913.8431      13277.3304      13640.8144
   1     1     3     1      6764.36605      7144.4141      7513.02131      7879.50146      8245.09479      8610.17087      8974.92027      9339.45318      9703.83835      10068.1219      10432.3354      10796.5015      11160.637
11524.7549      11888.8649      12252.9786      12617.098      12981.2282      13345.3732      13709.5365
   1     1     4     1      6823.36446      7203.98895      7573.13214      7939.98724      8305.96963      8671.45197      9036.62605      9401.60296      9766.45259      10131.2207      10495.9397      10860.6323      11225.316
11590.0033      11954.7045      12319.4272      12684.1801      13048.9678      13413.7927      13778.6582
   1     1     5     1      6882.42252      7263.62328      7633.34371      8000.58846      8366.97452      8732.87722      9098.49057      9463.92644      9829.25545      10194.5243      10559.7651      10925.0015      11290.2509
11655.5262      12020.8378      12386.1939      12751.6007      13117.0637      13482.5902      13848.1816
   1     1     6     1      6941.53152      7323.30884      7693.64577      8061.29623      8428.10095      8794.43911      9160.50667      9526.41706      9892.2416      10258.0272      10623.807      10989.6047      11355.438
11721.3205      12087.2624      12453.2722      12819.3567      13185.5212      13551.7705      13918.1082
   1     1     7     1      7000.68103      7383.03586      7754.02451      8122.09793      8489.33741      8856.12712      9222.66499      9589.06591      9955.40219      10321.7217      10688.0581      11054.4354      11420.8716
11787.3807      12153.9735      12520.6583      12887.4424      13254.3316      13621.3304      13988.4433
   1     1     8     1      7059.85766      7442.79117      7814.44386      8182.97632      8550.66831      8917.92642      9284.95132      9651.85981      10018.7252      10385.5964      10752.5074      11119.483      11486.5419
11853.6979      12220.9625      12588.3444      12955.8512      13323.4887      13691.262      14059.176
   1     1     9     1      7119.04436      7502.55802      7874.8629      8243.90797      8612.07158      8979.81632      9347.34631      9714.78045      10082.1931      10449.6345      10817.1393      11184.733      11552.4344
11920.2585      12288.2168      12656.3185      13024.5714      13392.9819      13761.5556      14130.2973
```

Fig. 141 shows BHPs, curves of case tenth.

Figure 141 - Comparison of BHP's values for 11 points (top) and 20 points (down) between UTCOMPRS and commercial simulator.

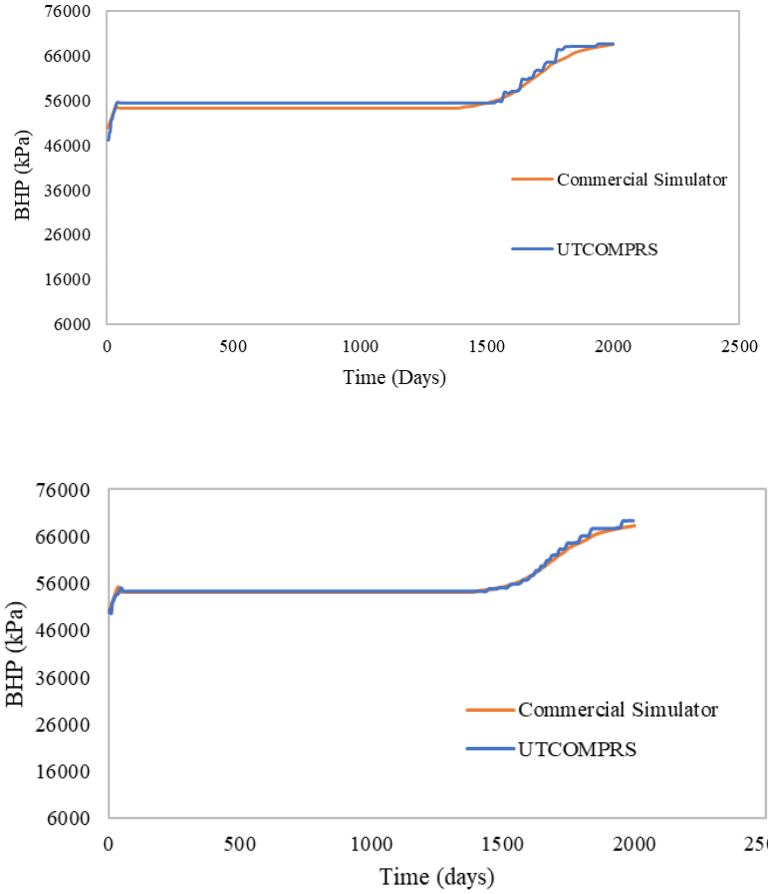

As shown in Fig. 141, the proposed framework was able to capture the behavior of the BHP in both cases; however, for the table with higher resolution, result was better represented similar to commercial simulator.

Figs. 142-145 shows the water, oil, liquid, and gas rates. As it can be seen in all of the presented figures, the oscillations after the breakthrough increase, but for the 20 parameters table the oscillations in the production profiles are reduced. Also, as it can be seen in Figs. 142-145, both simulators have the same trend before the breakthrough, but once the breakthrough occurs, the oscillations of the production profile of UTCOMPRS are large increased. Although the oscillations of the production profiles of the UTCOMPRS was improved by increasing the resolution of the table, it is still not comparable to the commercial simulator. This data shows three things: first, the table's resolution is a major factor in the correctness of the established framework when the

variation of table's parameters (Liq, GLR, WCUT) are high. Second, the multi-step wise behavior of BHP's is related to variations in production profiles. Third, because the liquid contains both oil and water values, the variations are more intense for both the 10 and 20 point tables (see Fig. 144).

Figure 142 - Comparison of water rate profile for 11 points (top) and 20 points (down) tables between UTCOMPRS and commercial simulator.

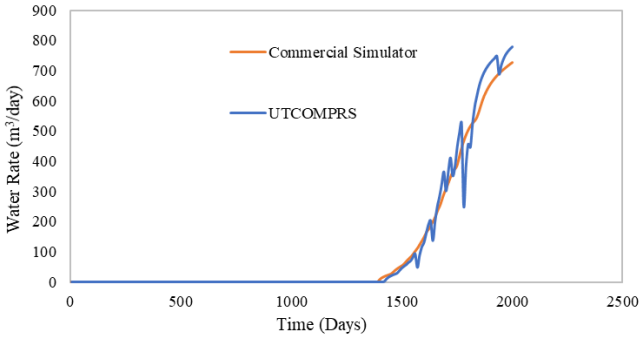

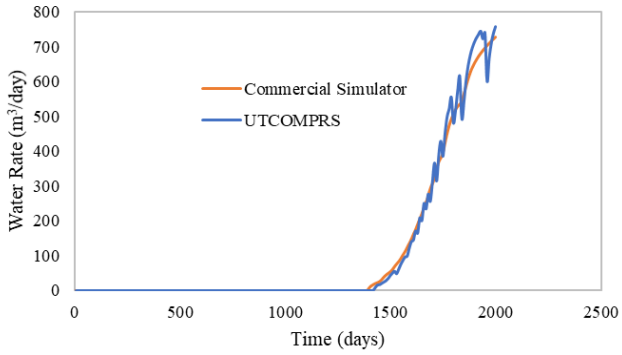

Figure 143 - Comparison of the oil rate profile for 11 points (top) and 20 points (down) between UTCOMPRS and commercial simulator.

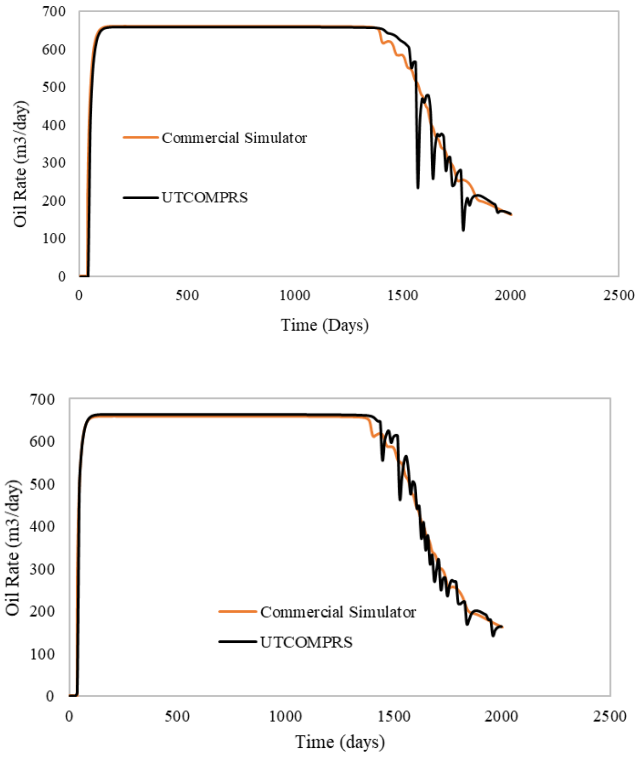

Figure 144 - Comparison of liquid rate profile for 11 points (top) and 20 points (down) between UTCOMPRS and commercial simulator

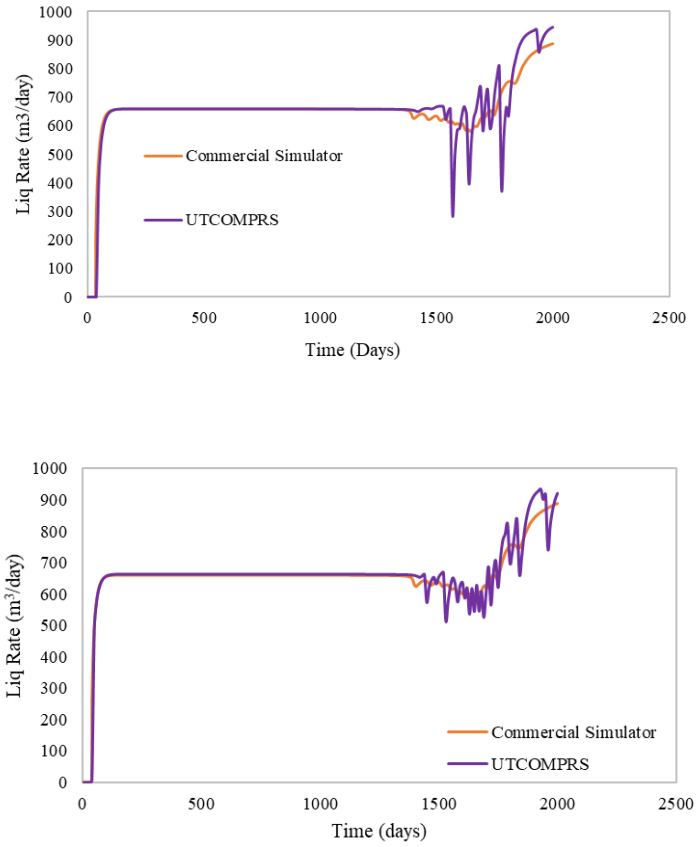

Figure 145 - Comparison of gas rate profile for 11 points (top) and 20 points (down) between UTCOMPRS and commercial simulator

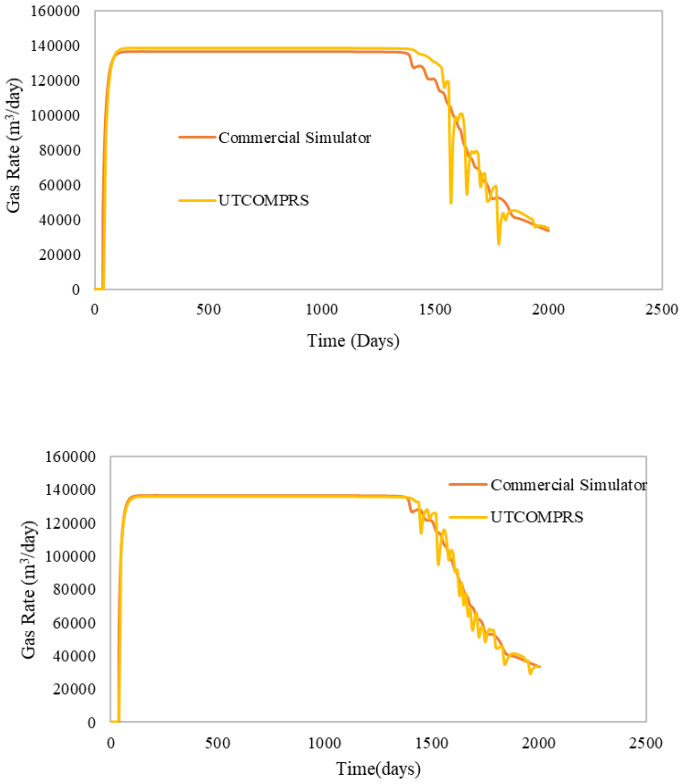

Fig. 146 shows the injection pressure and again the results of 20 points tables are smoother.

Figure 146 - Comparison of injection pressure for 11 points (top) and 20 points (down) between UTCOMPRS and commercial simulator.

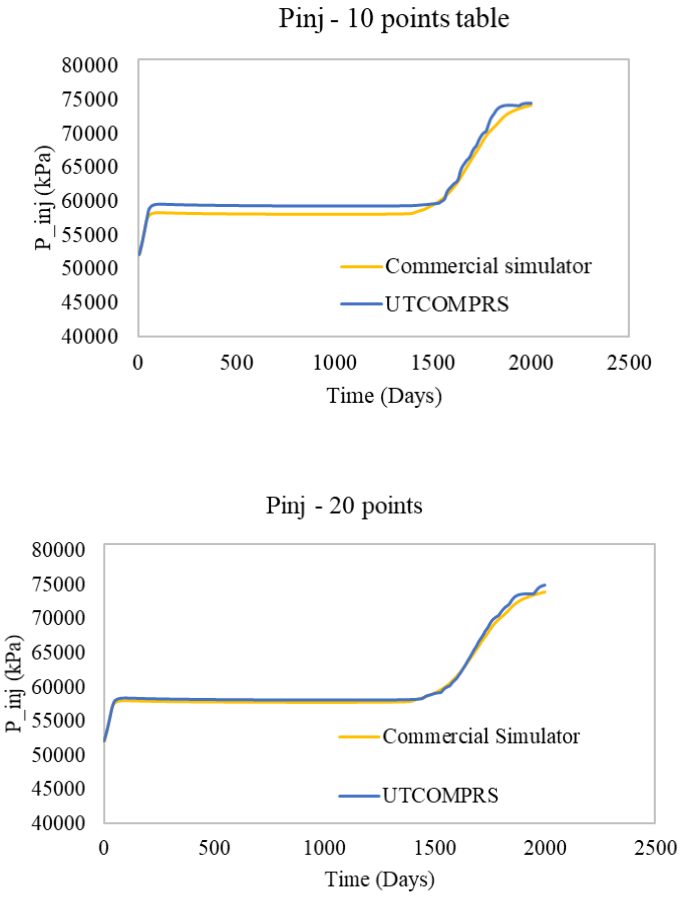

In comparison to BHP profiles, the change in injection pressure following breakthrough for both cases was smoother, as seen in Fig. 145. This is one of the reasons why the injector will respond to the BHP in the absence of any restriction on the injector. In addition, the injector pressure profile matched better in the case of the 20 points table, as expected.

Figs. 147 and 148 shows GOR and WOR plots for case tenth.

Figure 147 - Comparison of GOR for 11 points (top) and 20 points (down) between UTCOMPRS and commercial simulator

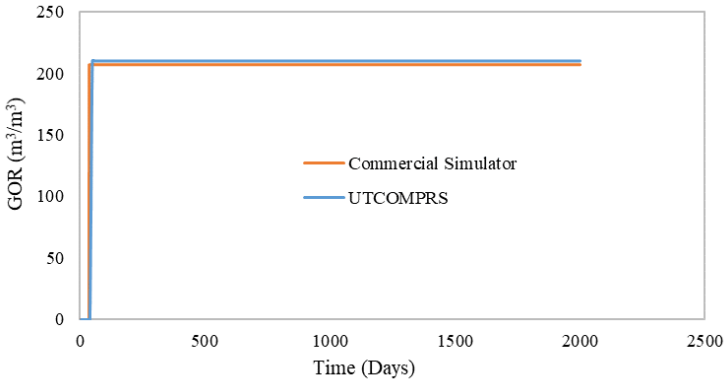

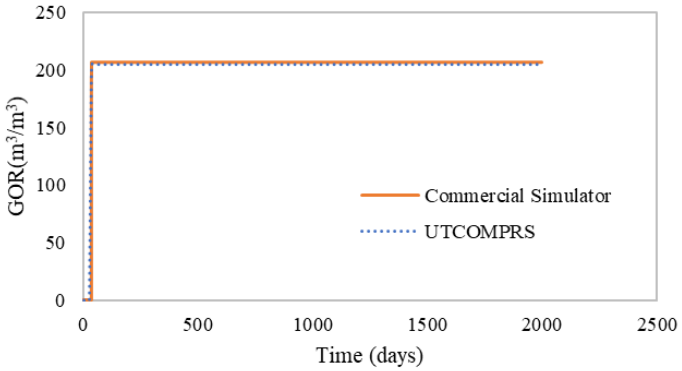

Figure 148 - Comparison of WOR for 11 points
(top) and 20 points (down) between
UTCOMPRS and commercial simulator

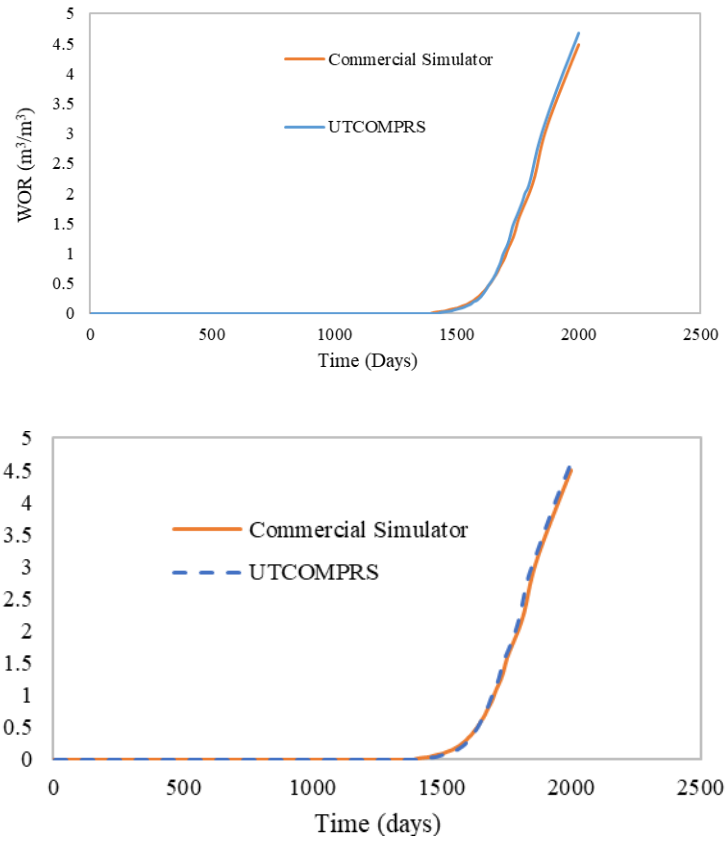

Despite the fact that the profile variance of oil, gas, and water was extensive, the behavior of GOR and WOR in case tenth is similar. As a result, GOR and WOR should be explored in conjunction with production profiles for appropriate comparison.

The logarithmic interpolation function was able to produce good results for UTCOMPRS in terms of BHP evaluation, but it may not accurately predict the production profile in the case of extensive table parameter fluctuation. Although the table's resolution may close the gap, and this research produces more accurate results, the UTCOMPRS framework needs to include more issues such as heterogeneity, lumped fluids, and a real field rather than merely a shoebox model.

What has been shown here was the results of sequential explicit coupling of the reservoir, multiple-wells and surface facility. With this tool, the UTCOMPRS simulator can simulate more realistic conditions although the accuracy of the developed model is intensely dependent on the interpolation function and value of BHP.

7.2. Sequential implicit coupling of the reservoir, well and surface facility

Sequential implicit coupling of the UTCOMPRS is under development and here we only show one example to check the connection table and a new method solving flow tables. Let us consider the same surface network that is presented in section 4.6.3.2, shown in Fig. 149.

Figure 149 - Single well connected to wellhead and separator. From (WATTS et al, 2010)

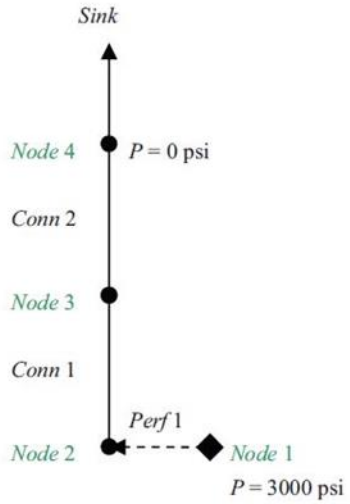

Previously, Watts *et al.* (**WATTS et al., 2009**) reported three methods of solving this system, *i.e.*, (1) linear pressure assumption, (2) rate constraint, (3) pressure constrain. The nodes are numbered one and four. We repeat the last approach, but instead of the flow equation, we used a flow table. Since their original development was reported in the field units, here we are reporting the results of this study in the field unit for comparison, but taking into account that this approach is still under development. Fig. 150 shows the connection table that represents Fig. 149.

Figure 150 - An example of a table connection from Watts *et al.* (**WATTS et al., 2009**)

#_Connection_Nodes
3
#_Pressure_Nodes
4
#_Boundry_Conditions
2
!Vec_Unknown
1 2 3 4 5 6 7
#_ROW_FOR_SURFACE_TABLE
7

nodes	upstream	downstream	Condition
1	0	0	1
2	1	3	2
3	4	5	3
4	2	0	4
5	6	7	3
6	4	0	4
7	0	0	5

Fig. 151 shows the obtained results of Watts *et al.* with the newly developed tool of the UTCOMPRS simulator.

Figure 151 - Single well pressure profile, with the reported results of Watts *et al.* compared to those of UTCOMPRS.

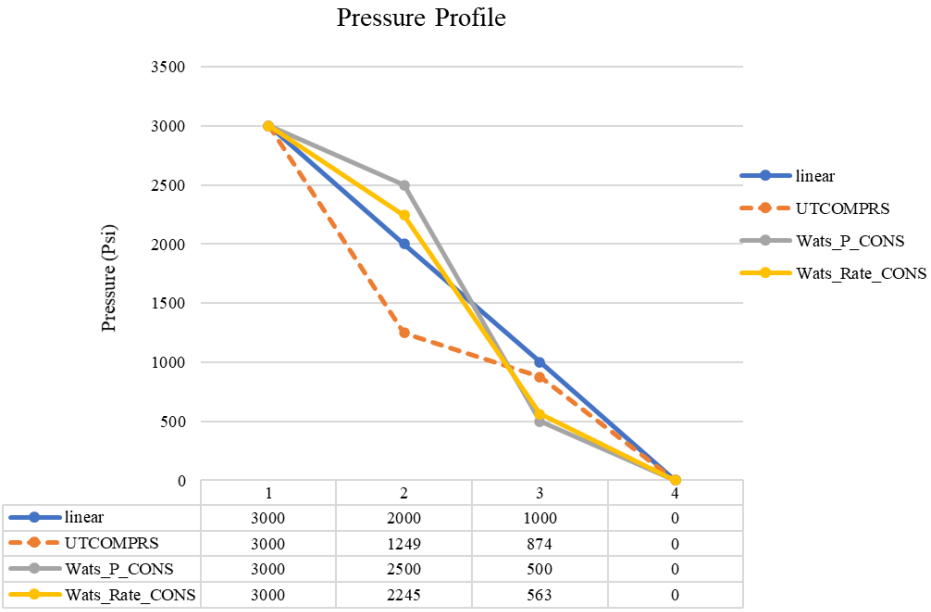

For the wellhead pressure the obtained results 874 psi were in the range of Watts *et al.* report. However, the BHPs (pressure at node two) is lower than all of the BHPs. This difference may be caused because the generated flow table of the UTCOMPRS simulator,

while the calculated result of Watts *et al.* were not informed precisely. The generated flow table for this study is may not representing the exact length and diameter that were used by Watts *et al*. This method of surface facility modeling is still under development and requires additional computational effort to generate the most reliable results. The important outcome of this case study is that with the connection table tool, the UTCOMPRS simulator can recognize the configuration of surface facility without the need of a third-party simulator. The connection table can be consistent with as many as unknown that the user requires and the condition of each segment, whether it needs to be a flow equation, or a flow table, is also included. As shown in Fig. 71's flowchart, this part should be completed with the reservoir. This investigation, however, is beyond the scope of the current Ph.D. thesis.

CHAPTER 8

CONCLUSIONS AND RECOMMENDATIONS

8.1. Conclusions

Compositional modeling of integrated surface and sub-surface facility requires a robust and flexible simulator. The main objective of this work was the development of a new framework that can include a surface facility modeling for the UTCOMPRS simulator by considering flow tables as an option for the well hydraulics. Hence, we developed a series of flow tables named simplified, advanced and commercial. Some numerical features were designed and implemented. It was validated for reading, comparing, and printing the information of surface facility and location of coupling point for UTCOMPRS. The outcome of this study is summarized as follows:

1- The surface facility option was included in the well input files of UTCOMP; and the corresponding keywords added to the simulator

2- All SFT, AFT, CFTs were implemented successfully, although SFT has been inactivated;

3- AFT enables the simulator to compute, current GOR and WOR, based on BHP WHP and PSEP, dynamically. As a result, the effect of the separators is only included with this form of table;

4- Simulation results of integrated models were sensitive to information of tables, so that when values are not suitable for the model, the old table should be replaced with a new table;

5- The presented framework enabled us to understand the behavior of the integrated system and identify the main factors that affect production operations, with results showing that GOR, and WOR are better indicating factors between two simulators;

6- For CFTs, different interpolation parameters were checked and based on the logarithmic interpolation functions, the pressure of the wellhead from the lower index, seems a better candidate, and the interpolation of the BHP proved to be the most determining factor for this study;

7- A new feature (AWCO) was added to the simulator to manage the injector well's pressure limit, preventing the reservoir from being over pressurized;
8- The CFT algorithm was extended for multiple wells and 3D reservoirs;
9- Although the accuracy of the developed framework was acceptable, there is still improvements to be made in terms of CPU run time;
10- The simulator was able to successfully manage Petrobras' real reservoir fluids, demonstrating that the built framework is capable of dealing with actual reservoir fluids, assuming correct table compilated, However, in situations when table parameters (LIQ, GLR, and WCUT) have a lot of fluctuation, there is still room for improvement;
11- Based on the experiences of developing flow tables, the connection table as a new tool was developed and successfully tested, but still requires additional validation efforts.

In general, this study shows the comparability of the new framework that was designed for our in-house simulator UTCOMPRS with the one from a commercial simulator. In our future studies, we will extend the sequential implicit framework to implement more advanced features for surface facility.

8.2. Recommendations

The following are some recommendations for the future work:

1. Include reservoir heterogeneity and anisotropy, while examining the performance and efficiency of the developed model, and parallelization;
2. Instead of using the connection table, the surface facility can be coupled with other surface facility simulators such as GAP, CoFlow, or SurfNet for performance comparison of each coupling method;
3. Include an optimization software to determines the effect of each parameter on the production;
4. Include data-related science, such as machine learning and artificial intelligence, for a more intelligent coupling approach;
5. Test the developed model with field data; and fractured reservoirs;
6. Coupling the developed framework to a deformable reservoir, whether through geomechanics, local grid refinement, or unstructured grids.

REFERENCES

AGBI, B. The Development, Testing And Application of an Efficient Steady State Gas Field Performance Evaluation Model. Journal of Canadian Petroleum Technology, v. 20, n. 03, 1 jul. 1981.

AHMED, T. H. Reservoir engineering handbook. Amsterdam ; Boston: Gulf Professional Pub, 2010.

ALEXIS, D. A.; AYALA, L. Assessment of Deliverability of a Natural-Gas-Gathering and -Production System: Development of an Integrated Reservoir/Surface Model. Oil and Gas Facilities, v. 1, n. 04, p. 55–63, 1 ago. 2012.

ARSLAN, O.; WOJTANOWICZ, A. K.; WHITE, C. D. Inflow Performance Methods for Evaluating Downhole Water Sink Completions vs. Conventional Wells in Oil Reservoirs With Water Production Problems. Canadian International Petroleum Conference, 2003.

BARROUX, C. C. et al. Linking reservoir and surface simulators: how to improve the coupled solutions. Society of Petroleum Engineers, 24 out. 2000

BARTOLOMEU, M.; ABDRAKHMANOV, A. Integrated Production Modelling of Gas Condensate Field. Society of Petroleum Engineers, 14 out. 2014.

BIGDELI, A. et al. Investigation of different interpolation functions for a newly developed framework for sequential coupling of the reservoir, wells, and surface facilities. [s.l: s.n.]. Disponível em: <https://cilamce.com.br/anais/arearestrita/apresentacoes/187/8552.pdf>. Acesso em: 6 abr. 2022.

BIGDELI, A. et al. Application of Sequential Explicit Coupling of Reservoir, Well, and Surface Facilities for 3D Compositional Simulation Models. [s.l: s.n.]. Disponível em: <https://repositorio.ufc.br/bitstream/riufc/63687/1/2021_eve_abigdeli.pdf>. Acesso em: 6 abr. 2022.

BIGDELI, A. et al. DEVELOPMENT OF A NOVEL FRAMEWORK FOR SEQUENTIAL COUPLING OF RESERVOIR, WELLS, AND SURFACE FACILITIES. [s.l: s.n.]. Disponível em: <https://cilamce.com.br/anais/arearestrita/apresentacoes/88/5746.pdf>.

BISWAS, D. Assisted History Matching for Surface Coupled Gas Reservoir Simulation. Society of Petroleum Engineers, 11 set. 2006.

BOOGAART, E. Coupling between a reservoir and a surface facilities network. repository.tudelft.nl, 2016.

BRAVO, C. et al. Applying Analytics to Production Workflows: Transforming Integrated Operations into Intelligent Operations. Society of Petroleum Engineers, 1 abr. 2014.

BREAUX, E. J. et al. Application of a Reservoir Simulator Interfaced With a Surface Facility Network: A Case History. Society of Petroleum Engineers Journal, v. 25, n. 04, p. 397–404, 1 jun. 1985

BRILL, J. P.; HEMANTA MUKHERJEE. Multiphase flow in wells. [s.l.] Richardson, Tex. Henry L. Doherty Memorial Fund Of Aime, Society Of Petroleum Engineers, 1999.

BROWN, K. E. The technology of artificial lift methods. Editorial: Tulsa: Pennwell Books, 1977.

BUILDER USER MANUAL, computer modeling group. 2019.

BYER, T. Preconditioned Newton methods for simulation of reservoirs with surface facilities. Sandford University

Canas, J.; Pop, J.;, Francois, X.; Elshahawi, Hani. "Advanced Compositional Gradient Analysis." Paper presented at the SPE Annual Technical Conference and Exhibition, Denver, Colorado, USA, September 2008

CANAS, J. A. et al. Advanced Compositional Gradient Analysis. Society of Petroleum Engineers, 21 set. 2008.

CHANG, Y.-B. Development and Application of an Equation of State Compositional Simulator, Ph.D. Dissertation. University of Texas at Austin, 1990

COATS, B. K. et al. A Generalized Wellbore and Surface Facility Model, Fully Coupled to a Reservoir Simulator. SPE Reservoir Evaluation & Engineering, v. 7, n. 02, p. 132–142, 1 abr. 2004.

DE SWAAN, A.; BERUMEN, S.; RODRIGUEZ, F. Reservoir and Surface-Network Simulation of Tight Gas Reservoirs in the North of Mexico. Society of Petroleum Engineers, 10 fev. 2002.

DEMPSEY, J. R. et al. An Efficient Model for Evaluating Gas Field Gathering System Design. Journal of Petroleum Technology, v. 23, n. 09, p. 1067–1073, 1 set. 1971.

ECONOMIDES, M. J. Petroleum production systems. Upper Saddle River, Nj: Prentice Hall, 2013.

Economist, Sheikhs v shale. Disponível em: <https://www.economist.com/leaders/2014/12/04/sheikhs-v-shale>.

EMANUEL, A. S.; RANNEY, J. C. Studies of Offshore Reservoir With an Interfaced Reservoir/Piping Network Simulator. Journal of Petroleum Technology, v. 33, n. 03, p. 399–406, 1 mar. 1981

FARIAS, M. COMPARISON OF STRUCTURED AND UNSTRUCTURED GRIDS FOR COMPOSITIONAL RESERVOIR SIMULATION, Master Thesis, UFC, 2020

FERNANDES, B. R. B. Implicit and semi-implicit techniques for the compositional petroleum reservoir simulation based on volume balance. repositorio.ufc.br, 2014.

FLEMING, G.;MA, J. MANAGING A NETWORK OF WELLS AND SURFACE FACILITY BY FINDING A STEADY - STATE FLOW SOLUTION FOR A PIPE SUB – NETWORK, Patent,2019

FLEMING, G.; WONG, T. "Fully Coupled Simulation of Multiple Compositional Reservoirs with a Shared Surface Facility Network." Paper presented at the SPE Reservoir Simulation Symposium, The Woodlands, Texas, USA, February 2013

FLEMING, G.; WONG, Q.. SYSTEM AND METHOD FOR USING AN ARTIFICIAL NEURAL NETWORK TO SIMULATE PIPE HYDRAULICS IN A RESERVOIR SIMULATOR, Patent, 2012

FOSSMARK, M. G. Multiphase-flow correlations' ability to model vertical lift performance. uis.brage.unit.no, 2011.

GAO, M. Reservoir and Surface Facilities Coupled Through Partially and Fully Implicit Approaches. Master's thesis, Texas A & M University 2014.

GHORAYEB, K. et al. A General Purpose Controller for Coupling Multiple Reservoir Simulations and Surface Facility Networks. Society of Petroleum Engineers, 3 fev. 2003

GILLBERT, W. E. “Flowing and Gas-Lift Well Performance,” Drilling and Production Practice, Vol. 13, 1954, pp. 126-157.

GOLAN, M.; WHITSON, C. H. Well performance. Norway: Tapir, 1996.

HAMEDI SHOKRLU, Y. et al. Integrated Production System Modelling and Optimization for Advanced EOR Application in Pre-Salt Offshore Carbonate Reservoir. Day 4 Thu, May 07, 2020, 4 maio 2020.

HAYDER, E. M.; DAHAN, M.; DOSSARY, M. N. Production Optimization through Coupled Facility-Reservoir Simulation. Society of Petroleum Engineers, 11 abr. 2006.

HOLMES, J. A.; BARKVE, T.; LUND, O. Application of a Multisegment Well Model to Simulate Flow in Advanced Wells. Society of Petroleum Engineers, 20 out. 1998.

HÖÖK, M. et al. The Evolution of Giant Oil Field Production Behavior. Natural Resources Research, v. 18, n. 1, p. 39–56, 5 fev. 2009.

ISLAMOV, R. et al. Maximising Asset Value through Implementation of Dynamic Well Operating Envelop. Day 8 Tue, March 30, 2021, 16 mar. 2021.

JAHN, F.; COOK, M.; GRAHAM, M. Hydrocarbon exploration & production. Amsterdam: Elsevier, 2009.

JAN DIRK JANSEN. Nodal analysis of oil and gas production systems. Richardson, Tx: Society Of Petroleum Engineers, 2017.

JIANG, Y. TECHNIQUES FOR MODELING COMPLEX RESERVOIRS AND ADVANCED WELLS. PhD thesis, Stanford University, 2007

KALAYDJIAN, F.; BOURBIAUX, B. Integrated Reservoir Management: a Powerful Method to Add Value to Companies’ Assets. a Modern View of the Eor Techniques. Oil & Gas Science and Technology, v. 57, n. 3, p. 251–258, maio 2002.

KILLOUGH, J.; FLEMING, G.; ENGLE, C.; BROCK, N. Surface Facility and Reservoir Modeling of a Middle Eastern Multi-Reservoir Complex. International Journal of Engineering and Applied Science. Vol. 1, n. 04, pp. 165- 183, 2013

KUMAR, K. et al. Integrated Production Optimization using Implicitly Coupled Multi–Reservoirs and Facility Modeling with Miscible Gas Injection EOR in South Oman. Day 4 Thu, November 12, 2020, 9 nov. 2020.

LITVAK, M. L.; DARLOW, B. L. Surface Network and Well Tubinghead Pressure Constraints in Compositional Simulation. Society of Petroleum Engineers, 12 fev. 1995.

LOHRENZ, J.; BRAY, B. G.; CLARK, C. R. Calculating Viscosities of Reservoir Fluids From Their Compositions. Journal of Petroleum Technology, v. 16, n. 10, p. 1171–1176, 1 out. 1964.

LU, Q.; FLEMING, G. Parallel network simulation apparatus, methods, and systems. Disponível em: <https://patents.google.com/patent/CA2876583C/en>. Acesso em: 8 abr. 2022.

MCAFEE, R. V. The Evaluation of Vertical-Lift Performance in Producing Wells. Journal of Petroleum Technology, v. 13, n. 04, p. 390–398, 1 abr. 1961.

MIRZAEI-PAIAMAN, A.; SALAVATI, S. A New Empirical Correlation for Sonic Simultaneous Flow of Oil and Gas through Wellhead Chokes for Persian Oil Fields. Energy Sources, Part A: Recovery, Utilization, and Environmental Effects, v. 35, n. 9, p. 817–825, maio 2013.

MONCORGÉ, A. Unified Reservoir / Well / Network Model for Advanced Processes. Society of Petroleum Engineers, 23 maio 2011.

NeXus: User Manual — nexus v2020.10 documentation. Disponível em: <https://manual.nexusformat.org/user_manual.html>. Acesso em: 8 abr. 2022.

OLGA User Manual. Disponível em: <https://pdfcoffee.com/olga-user-manual-3-pdf-free.html>. Acesso em: 8 abr. 2022.

VALBUENA OLIVARES, E. Production Performance Modeling Through Integration of Reservoir and Production Network with Asphaltene Deposition. Disponível em: <https://hdl.handle.net/1969.1/155139>. Acesso em: 8 abr. 2022. PhD thesis, Texas A&M University, 2015.

PATHAK, V. et al. Quantifying Geological Uncertainty for Complex Integrated Production Systems with Multiple Reservoirs and Production Networks. Day 4 Thu, June 06, 2019, 3 jun. 2019

PEACEMAN, D. W. Interpretation of well-block pressures in numerical reservoir simulation. Society of Petroleum Engineers Journal, v. 18, n. 1, p. 183–194, 1978

PEACEMAN, D. W. Interpretation of well-block pressures in numerical reservoir simulation with nonsquare grid blocks and anisotropic permeability. Society of Petroleum Engineers Journal, v. 23, n. 03, 1983.

PENA, O.; USE OF SUBSEA TECHNOLOGIES FOR PRODUCED WATER MANAGEMENT IN OFFSHORE FIELDS USING INTEGRATED ASSET MODELING CAMPINAS 2018. [s.l: s.n.]. Disponível em: <https://www.unisim.cepetro.unicamp.br/publicacoes/OSCAR_JULIAN_PENA_PIRANEQUE.pdf>. Acesso em: 8 abr. 2022. State university of Campinas, 2018.

Pipesim User Guide. Disponível em: <https://pdfcoffee.com/pipesim-user-guide-2-pdf-free.html>. Acesso em: 8 abr. 2022.

PUCHYR, P. J. A general gas reservoir and gathering system simulator. Journal of Canadian Petroleum Technology, v. 30, n. 03, p. 53–60, 1 maio 1991.

ROBINSON, D. B.; PENG, D.-Y.; CHUNG, S. Y-K. The development of the Peng - Robinson equation and its application to phase equilibrium in a system containing methanol. Fluid Phase Equilibria, v. 24, n. 1-2, p. 25–41, jan. 1985.

RODRIGUEZ VERA, R. A. et al. Integration of Subsurface, Surface, and Economics Under Uncertainty in Orocual Field. Society of Petroleum Engineers, 15 abr. 2007.

ROSSI, R. . et al. Simplified Network Simulation Vs. Integrated Asset Modelling for Management and Development of Offshore Gas Fields. **Day 3 Wed, September 16, 2015**, 14 set. 2015.

SANKARAN, S. et al. Creating Value by Implementing an Integrated Production Surveillance and Optimization System – An Operator's Perspective. Day 2 Tue, October 10, 2017, 9 out. 2017.

SAPUTELLI, L. .; RUDOLPH, S. .; EMBSER, J. . Integrated Production Model Calibration Applied to a Gulf of Mexico Sub-sea Field. Society of Petroleum Engineers, 23 mar. 2010.

SCHIOZER, D. J.; STANFORD UNIVERSITY. Simultaneous simulation of reservoir and surface facilities. Disponível em: <https://searchworks.stanford.edu/view/2861882>. Acesso em: 8 abr. 2022. PhD thesis, Stanford University, 1994

SCHIOZER, D. J.; AZIZ, K. Effect of Chokes on Simultaneous Simulation of Reservoir and Surface Facilities. SPE Latin America/Caribbean Petroleum Engineering Conference, 1994.

SETH, G. et al. Integrated Reservoir-Network Simulation Improves Modeling and Selection of Subsea Boosting Systems for a Deepwater Development. SPE Production & Operations, v. 34, n. 03, p. 485–497, 10 abr. 2019.

SHAMIR, U. Y.; HOWARD, C. D. D. Water Distribution Systems Analysis. Journal of the Hydraulics Division, v. 94, n. 1, p. 219–234, jan. 1968.

SHIRALKAR, G. S.; WATTS, J. W. An Efficient Formulation for Simultaneous Solution of the Surface Network Equations. All Days, 31 jan. 2005.

SHIRDEL, M. Development of a coupled wellbore-reservoir compositional simulator for damage prediction and remediation. repositories.lib.utexas.edu, PhD dissertation, University of Texas at Austin, Austin, Texas, August 2013

STACKEL, A. W.; BROWN, H. M. An Example Approach to Predictive Well Management in Reservoir Simulation. Journal of Petroleum Technology, v. 33, n. 06, p. 1087–1094, 1 jun. 1981.

STANKO, M. Petroleum Production Systems Compendium. [s.l: s.n.]. Disponível em: <http://www.ipt.ntnu.no/~stanko/files/Files/Compendium/Petroleum_Production_systems_V1.5.2_Stanko.pdf>. Acesso em: 8 abr. 2022.

STONE, H. L. Estimation of Three-Phase Relative Permeability And Residual Oil Data. Journal of Canadian Petroleum Technology, v. 12, n. 04, 1 out. 1973.

TANG, H. et al. A Unified Gas/Liquid Drift-Flux Model for All Wellbore Inclinations. SPE Journal, v. 24, n. 06, p. 2911–2928, 1 dez. 2019.

TINGAS, J.; FRIMPONG, R.; LIOU, J. Integated Reservior and Surface Network Simulation in Reservoir Management of Southern North Sea Gas Reservoirs. All Days, 20 out. 1998.

Tnavigator Manual, ROCK FLOW DYNAMICS. Disponível em: <https://pdfcoffee.com/how-to-use-tnavigator-pdf-free.html>. Acesso em: 8 abr. 2022.

TORRENS, R. et al. Modeling from Reservoir to Export: A Compositional Approach for Integrated Asset Model of Different Gas Fields in North Kuwait Jurassic Carbonate Reservoirs. Day 1 Mon, February 23, 2015, 23 fev. 2015.

TRICK, M. D. A Different Approach to Coupling a Reservoir Simulator with a Surface Facilities Model. All Days, 15 mar. 1998.

TRINA, S. .; JOHANSEN, T. . An Integrated Horizonal and Vertical Flow Simulation with Application to Wax Precipitation. All Days, 22 out. 2012.

WANG, Y. Integrated production modeling to assess the effect of subsea water separation. pantheon.ufrj.br, Rio de Janeiro, 2019

WANG, P. DEVELOPMENT AND APPLICATIONS OF PRODUCTION OPTIMIZATION TECHNIQUES FOR PETROLEUM FIELDS. Stanford University 2003 [s.l: s.n.]. Disponível em: <https://pangea.stanford.edu/ERE/pdf/pereports/PhD/Wang03.pdf>. Acesso em: 8 abr. 2022.

WANG, Q.; FLEMING, G.; LU, Q. A New Approach to Improve Linear Solver Performance for a Fully Implicit Coupled System of Reservoir and Surface Network. All Days, 18 fev. 2013.

WATTS. W.; FLEMING, G.; LU, Q. Systems and Methods for the Determination of Active Constraints in a Network Using Slack Variables. Disponível em: <https://patents.google.com/patent/US20100131257>. Acesso em: 8 abr. 2022.

WATTS, J. W. . W.; FLEMING, G. C. . C.; LU, Q. . Determination of Active Constraints in a Network. SPE Journal, v. 17, n. 02, p. 441–454, 29 mar. 2012.

WYLIE, E. B.; STONER, M. A.; STREETER, V. L. Network: System Transient Calculations by Implicit Method. Society of Petroleum Engineers Journal, v. 11, n. 04, p. 356–362, 1 dez. 1971.

YOONM, P.; THODOS, G. Viscosity of Nonpolar Gaseous Mixtures at Normal Pressures. AIChE Journal. v. 16, n. 2, p. 300–304. 1970.

YouTube - Schlumberger Software . Disponível em: <https://www.youtube.com/user/SchlumbergerSoftware>. Acesso em: 8 abr. 2022.

ZAPATA, V. J. et al. Advances in Tightly Coupled Reservoir/ Wellbore/Surface-Network Simulation. SPE Reservoir Evaluation & Engineering, v. 4, n. 02, p. 114–120, 1 abr. 2001.

ZAYDULLIN, R. et al. A New Framework for the Integrated Reservoir and Surface Facilities Modeling. Day 2 Thu, April 11, 2019, 29 mar. 2019.

ZHOU, J. et al. Coalbed Methane Production System Simulation and Deliverability Forecasting: Coupled Surface Network/Wellbore/Reservoir Calculation. International Journal of Chemical Engineering, v. 2017, p. 1–13, 2017.

Appendix One – MATLAB file for IMEX tubing tables generation[4]

```
% Script file Imex_lift_table
%
% Computes a lift table in Eclipse format for a deviated multi-phase gas-oil-water well, using
% the Hagedorn and Brown (1965), Mukherjee_and_Brill (1985) or Beggs and Brill (1973) pressure
% drop correlation.
%
% Has the possibility to "regularize" the curves by replacing the part to the left of the
% minimum FBHP (the "severe slugging regime") by a horizontal line. Regularization may avoid
% convergence problems in the reservoir simulator.
%
% Note: All flow rates have negative values, because the flow is from bottom to surface,
% whereas the positive s co-ordinate runs from surface to bottom.
%
% JDJ, 20-10-03, last revised 26-05-17

clear variables
close all

% ----------------------------------------------------------------------------------------
% Input data:
% ----------------------------------------------------------------------------------------

% Well and fluid property input in SI units:
alpha_deg = 0; % wellbore inclination with respect to vertical, degrees
d = 0.1397; % tubing inside diameter, m
e = 3e-5; % tubing roughness, m
fluid = 4; % fluid = 1: single-phase oil flow
%          fluid = 2: single-phase gas flow
%          fluid = 3: multi-phase gas-oil-water flow, Hagedorn and Brown correlation
%          fluid = 4: multi-phase gas-oil-water flow, Mukherjee and Brill correlation
%          fluid = 5: multi-phase gas-oil-water flow, Beggs and Brill correlation
%          fluid = 6: multi-phase gas-oil-water flow, Shi et al. drift flux model (exercise)
oil = 1; % parameter to select black oil model or volatile oil table, -. Not relevant for
%         fluids 1 and 2
%         oil = 1: black oil; parameters computed with the aid of Standing correlations
%         oil = 2: black oil; parameters computed with the aid of Glaso correlations
%         oil = 3: volatile oil; parameters read from file 'vol_oil_table_01'
%         Note: When using a volatile oil table, the input parameters R_sb and rho_sc should
%         be consistent with those used to generate the tabulated values. For
%         vol_oil_table_01: rho_g_sc = 0.80 kg/m^3, rho_o_sc = 800 kg/m^3, R_sb = 450 m^3/m^3.
rho_g_sc = 0.98; % gas density at standard conditions, kg/m^3
rho_o_sc = 876; % oil density at standard conditions, kg/m^3
rho_w_sc = 1030; % water density at standard conditions, kg/m^3
T_wf = 118; % bottomhole temperature, deg. C
T_tf = 43; % tubing head temperature, deg. C

% Flag to indicate if regularization is to be used:
regularize = 1; % 0 = no, 1 = yes

% Lift table input in 'allowable' SI units:
q_o_sc_ASI = [-100 -500 -900 -1300 -1700 -2100 -2500]; % oil rate, m^3/d
% Note: negative value, because oil flows from bottom to surface, whereas
% positive s co-ordinate runs from surface to bottom.
R_go = [20 60 100]; % producing gas-oil ratio, m^3/m^3
f_w_sc = [0.0 0.4 0.8]; % water cut (note: expressed as fraction), -
```

[4] All rights belongs to JAN DIRK JANSEN. Nodal analysis of oil and gas production systems

```
% p_tf_ASI = [500 1000]; % tubing head pressure, kPa. Note: always put in TWO
% % pressures. No more, no less!
p_tf_ASI = [500 5000 10000]; % tubing head pressure, kPa.
z_tvd = 2500; % true-vertical depth, m

% ------------------------------------------------------------------------
% End of input data
% ------------------------------------------------------------------------

% Compute auxiliary variables and convert to SI units:
alpha = from_deg_to_rad(alpha_deg); % wellbore inclination , rad
p_tf = 1000 * p_tf_ASI; % flowing tubing head pressure, Pa
q_o_sc = q_o_sc_ASI/(24*3600); % oil rate, m^3/s
s_tot = z_tvd/cos(alpha); % total along-hole well depth, m

rho_sc = [rho_g_sc,rho_o_sc,rho_w_sc];
n_f_w_sc = length(f_w_sc);
n_q_o_sc = length(q_o_sc);
n_R_go = length(R_go);

fid = fopen('Imex_lift_table.txt','w');
fprintf(fid,'*PTUBE');
fprintf(fid,' *LIQ 1\n');
fprintf(fid,'*DEPTH');
fprintf(fid,' %6.2f\n',s_tot);
fprintf(fid,'*GOR');
for k=1:n_R_go
   fprintf(fid,' %6.2f',R_go(k));
end
fprintf(fid,'\n*WCUT');
for j=1:n_f_w_sc
   fprintf(fid,' %6.4f',f_w_sc(j));
end
fprintf(fid,'\n*QO');
for i=1:n_q_o_sc
   fprintf(fid,' %6.2f',-q_o_sc(i)*24*3600);
end
fprintf(fid,'\n*WHP');
for m=1:2
   fprintf(fid,' %6.1f',p_tf(m)/1000);
end
fprintf(fid,'\n*BHPTO\n');

% Compute FBHP values:
data = zeros(n_q_o_sc,n_f_w_sc,n_R_go,3);
for i=1:n_q_o_sc
   for j=1:n_f_w_sc
      for k=1:n_R_go
         [i j k]
         q_g_sc = R_go(k) * q_o_sc(i);
         q_w_sc = (f_w_sc(j)/(1-f_w_sc(j))) * q_o_sc(i);
         q_sc = [q_g_sc,q_o_sc(i),q_w_sc];
         p_wf(1) = pipe(alpha,d,e,fluid,oil,p_tf(1),q_sc,rho_sc,0,s_tot,T_tf,T_wf);
         p_wf(2) = pipe(alpha,d,e,fluid,oil,p_tf(2),q_sc,rho_sc,0,s_tot,T_tf,T_wf);
         data(i,j,k,1:3)= [-q_o_sc(i) p_wf(1) p_wf(2)];
      end
   end
end

% Regularize:
```

```
if regularize == 1
   for i=n_q_o_sc-1:-1:1
      for j=1:n_f_w_sc
         for k=1:n_R_go
            if data(i,j,k,2) > data(i+1,j,k,2)
               data(i,j,k,2) = data(i+1,j,k,2);
            end
            if data(i,j,k,3) > data(i+1,j,k,3)
               data(i,j,k,3) = data(i+1,j,k,3);
            end
         end
      end
   end
end

% Print to file:
for i=1:n_q_o_sc
   for j=1:n_f_w_sc
      for k=1:n_R_go
         p_wf(1) = data(i,j,k,2);
         p_wf(2) = data(i,j,k,2);
         fprintf(fid,'%1.0f ', k);
         fprintf(fid,'%1.0f ', j);
         fprintf(fid,'%1.0f ', i);
         fprintf(fid,'%6.1f ', p_wf(1)/1000);
         fprintf(fid,'%6.1f \n', p_wf(2)/1000);
      end
   end
end
status = fclose(fid);

% Plot to screen:
subplot(1,2,1);
for j=1:n_f_w_sc
   for k=1:n_R_go
      plot(data(:,j,k,1)*24*3600,data(:,j,k,2)/1e6); hold on
   end
end
xlabel('Oil Flow Rate,\it -q_{o,sc}\rm (m^3/d)')
ylabel('FBHP,\it p_{wf}\rm (MPa)')
grid on

subplot(1,2,2);
for j=1:n_f_w_sc
   for k=1:n_R_go
      plot(data(:,j,k,1)*24*3600,data(:,j,k,3)/1e6); hold on
   end
end
xlabel('Oil Flow Rate,\it -q_{o,sc}\rm (m^3/d)')
ylabel('FBHP,\it p_{wf}\rm (MPa)')
grid on
```

Appendix Two – Phase Envelopes

- Two-phase envelope (3Comp)

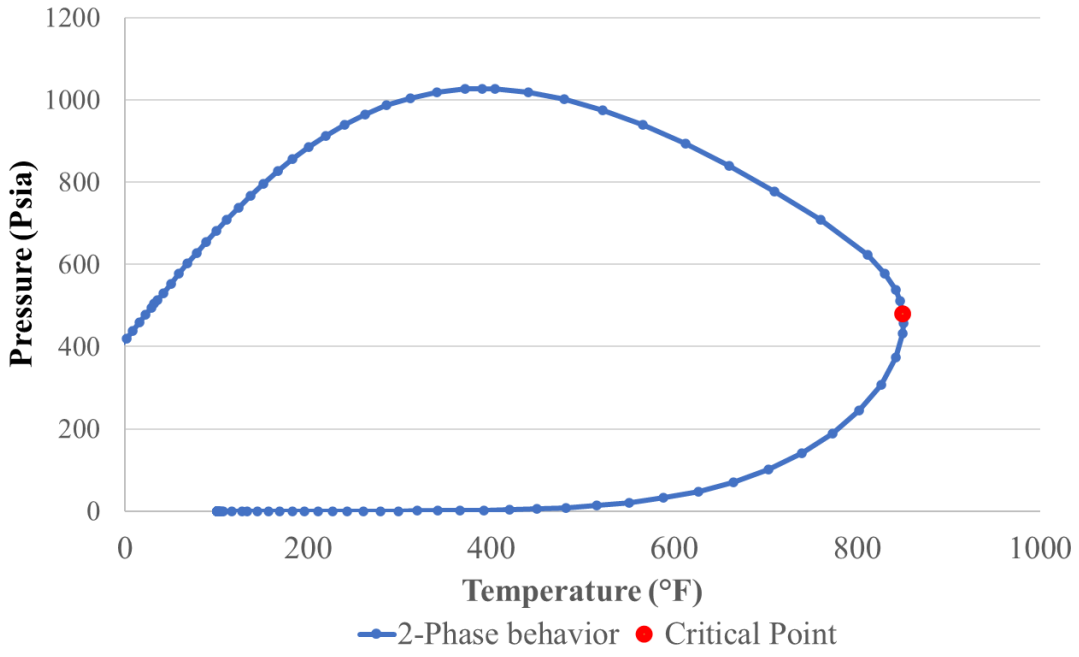

- Two-phase envelope (6Comp)

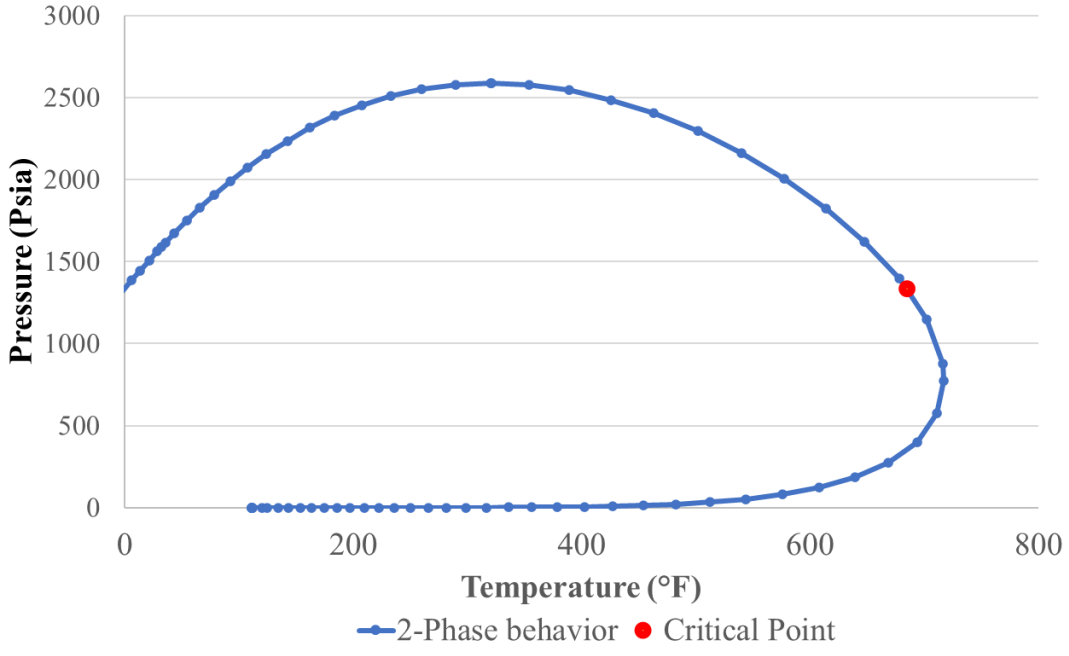

- Two-phase envelope (8Comp)

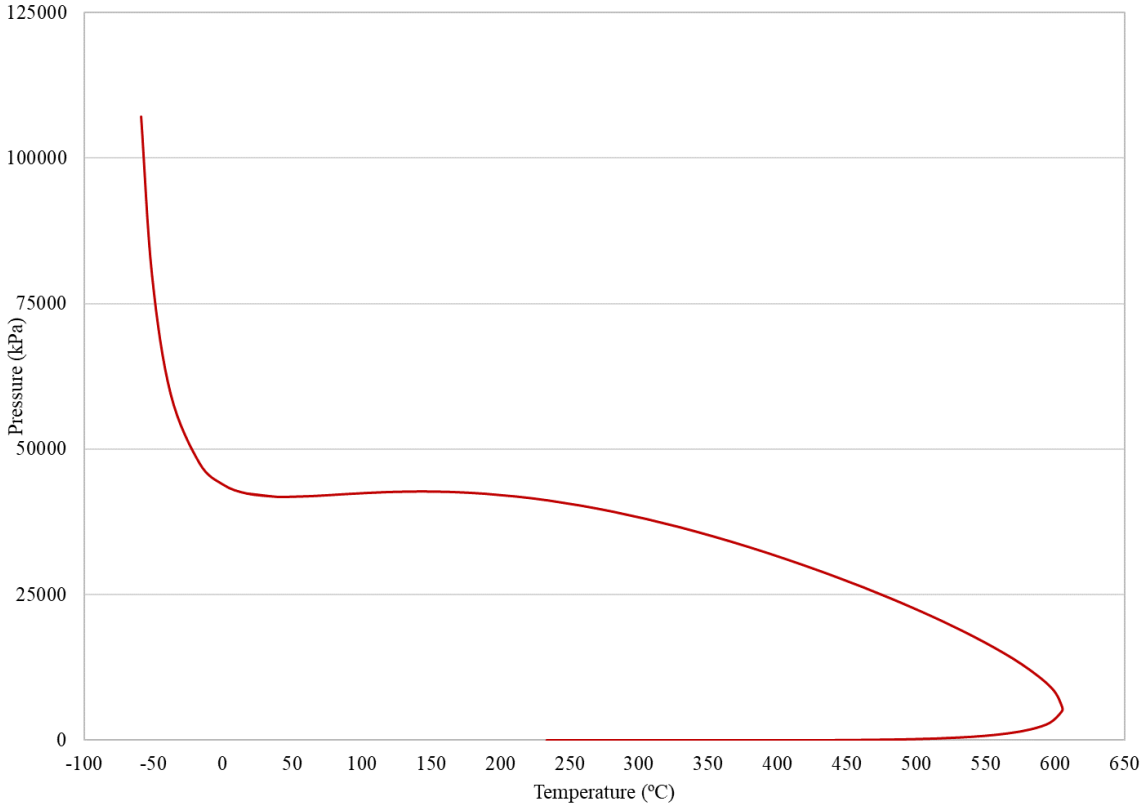

Appendix Three - An example of flow table for Case 3

12 7 3 3 5

LIQ

50.0 100.0 400.0 700.0 900.0 1300.0 2000.0 2500.0 5000.0 7000.0 11000.0 13000.0

GLR

50.0 1000.0 4000.0 10000.0 20000.0 50000.0 100000.0

WCUT

0.0 0.4 0.7

LFG

0.0 5000.0 10000.0

WHP

15.0 700.0 1500.0 2000.0 2500.0

				BHPs				
1	1	1	1	979.706685	1674.86153	2475.56929	2975.79484	3475.94935
1	1	1	2	937.246483	1655.07381	2458.19517	2959.14127	3459.77852
1	1	1	3	907.744313	1633.14874	2438.08111	2940.10161	3441.45231
1	1	2	1	1078.90733	1774.20335	2575.53259	3076.17014	3576.77525
1	1	2	2	1042.15617	1748.02566	2551.72549	3053.40966	3554.70724
1	1	2	3	1013.4961	1739.02365	2523.17826	3026.58598	3529.01914
1	1	3	1	1154.21393	1848.05582	2650.18119	3151.25658	3652.31064
1	1	3	2	1121.93412	1832.90969	2619.17934	3119.50237	3621.8228
1	1	3	3	1093.90683	1825.70264	2615.27591	3104.33743	3592.27791

.

.

.

.

.

.

.

12	7	3	1	12481.2926	12481.2941	12499.8458	12591.34	12747.2671
12	7	3	2	12481.3571	12481.3585	12499.9098	12591.4034	12747.33
12	7	3	3	12481.4215	12481.423	12499.9738	12591.4668	12747.3928